JUNE 1955

A.I.Ch.E. JOURNAL

UNIVERSITY OF MICHIGAN
JAN 31 1956
EAST ENGINEERING LIBRARY

Published by the American Institute of Chemical Engineers

CONTENTS

Gas Absorption and Oxidation in Dispersed Media
L. B. ANDERSEN AND H. F. JOHNSTONE

Development of an Equation of State for Gases
YU-CHUN HOU AND J. J. MARTIN

Operating Characteristics of Membranes
D. H. HAGERBAUMER AND KARL KAMMERMEYER

A Technique for Contacting Gases with Coarse Solid Particles
K. B. MATHUR AND P. E. GISHLER

Critical Constants of Unsaturated Aliphatic Hydrocarbons
GEORGE THODOS

Critical Constants of Saturated Aliphatic Hydrocarbons
GEORGE THODOS

Surface Tension and the Principle of Corresponding States
JAMES R. BROCK AND R. BYRON BIRD

Turbulence in Falling Liquid Films
CLIFFORD STIRBA AND D. M. HURT

Perforated-plate Extraction-column Performance and Wetting Characteristics
F. H. GARNER, S. R. M. ELLIS, AND J. W. HILL

Heat and Mass Transfer in Packed Beds
D. A. PLAUTZ AND H. F. JOHNSTONE

Performance of Vaned-disk Atomizers
W. M. HERRING, JR. AND W. R. MARSHALL, JR.

Thermodynamic Properties of 1-Butene
J. H. WEBER

Membrane Separations in the Liquid Phase
KARL KAMMERMEYER AND D. H. HAGERBAUMER

Dehydration of Hydrazine by Azeotropic Distillation
R. Q. WILSON, W. H. MINK, H. P. MUNGER, AND J. W. CLEGG

Gas Absorption in Beds of Rings and Saddles
MAX LEVA

Liquid Films in Viscous Flow
M. L. JACKSON

Vapor-liquid Equilibrium Relations Predicted by Thermodynamic Examination of Activity Coefficients
A. H. WEHE AND JESSE COATES

Performance of Packed Columns
Total, Static, and Operating Holdups
H. L. SHULMAN, C. F. ULLRICH, AND N. WELLS

Wetted and Effective-interfacial Areas, Gas- and Liquid-phase Mass Transfer Rates
H. L. SHULMAN, C. F. ULLRICH, A. Z. PROULX, AND J. O. ZIMMERMAN

Holdup for Aqueous and Nonaqueous Systems
H. L. SHULMAN, C. F. ULLRICH, N. WELLS, AND A. Z. PROULX

Correlation of Diffusion Coefficients in Dilute Solutions
PIN CHANG AND C. R. WILKE

Foote
LITHIUM HYDROXIDE

The basic lithium salt for industrial use, Foote lithium hydroxide provides chemically unique properties which are being applied to a host of products ranging from ceramic formulations to multi-purpose grease manufacture. Many other industrial uses of lithium are in the development stage.

Foote's integrated lithium facilities—raw material, production, research—are your assurance of an abundant supply of lithium for you and all industry.

We invite you to investigate and apply the unusual properties of lithium hydroxide and its derivatives in your products or processes.

Write for technical data sheets.

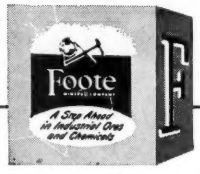

LITHIUM HYDROXIDE FOR INDUSTRY

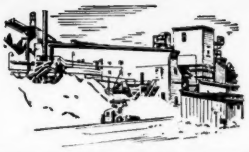

Kings Mountain, N.C... where Foote is mining large deposits of spodumene.

Sunbright, Va. ... the world's largest lithium chemical plant.

FOOTE MINERAL COMPANY

448 Eighteen West Chelten Building, Philadelphia 44, Pa.

RESEARCH LABORATORIES: Berwyn, Pa. • PLANTS: Exton, Pa.; Kings Mountain, N.C.; Sunbright, Va.

JUNE
1955

A.I.Ch.E. JOURNAL

Vol. 1
No. 2

ADVISORY BOARD

C. M. Cooper, O. E. Dwyer,
W. C. Edmister, E. R. Gilliland,
A. N. Hixson, W. R. Marshall, Jr.,
R H. Newton, R. L. Pigford,
J. M. Smith, Theodore Vermeulen,
R. R. White, R. H. Wilhelm

PUBLISHER

F. J. Van Antwerpen

EDITOR

Harding Bliss

The A.I.Ch. E. Journal, an official publication of the American Institute of Chemical Engineers, is devoted in the main to theoretical developments and research in chemical engineering and allied branches of engineering and science. Manuscripts should be submitted to the New York office.

A Second Glance 133

Gas Absorption and Oxidation in Dispersed Media ..... L. B. Andersen and H. F. Johnstone 135

Development of an Equation of State for Gases .....J. J. Martin and Yu-Chun Hou 142

Operating Characteristics of Membranes ..... D. H. Hagerbaumer and Karl Kammermeyer 152

A Technique for Contacting Gases with Coarse Solid Particles ..K. B. Mathur and P. E. Gishler 157

Critical Constants of Unsaturated Aliphatic Hydrocarbons .....George Thodos 165

Critical Constants of Saturated Aliphatic Hydrocarbons .....George Thodos 168

Surface Tension and the Principle of Corresponding States .....
James R. Brock and R. Byron Bird 174

Turbulence in Falling Liquid Films .....Clifford Stirba and D. M. Hurt 178

Perforated-plate Extraction-column Performance and Wetting Characteristics .....
F. H. Garner, S. R. M. Ellis, and J. W. Hill 185

Heat and Mass Transfer in Packed Beds .....D. A. Plautz and H. F. Johnstone 193

Performance of Vaned-disk Atomizers ..... W. M. Herring, Jr., and W. R. Marshall, Jr. 200

Thermodynamic Properties of 1-Butene .....J. H. Weber 210

Membrane Separations in the Liquid Phase .....Karl Kammermeyer and D. H. Hagerbaumer 215

Dehydration of Hydrazine by Azeotropic Distillation .....
R. Q. Wilson, W. H. Mink, H. P. Munger, and J. W. Clegg 220

Gas Absorption in Beds of Rings and Saddles .....Max Leva 224

Liquid Films in Viscous Flow .....M. L. Jackson 231

Vapor-liquid Equilibrium Relations Predicted by Thermodynamic Examination of Activity Coefficients .....A. H. Wehe and Jesse Coates 241

Performance of Packed Columns

I. Total, Static, and Operating Holdups ..... H. L. Shulman, C. F. Ullrich, and N. Wells 247

II. Wetted and Effective-interfacial Areas, Gas- and Liquid-phase Mass Transfer Rates..
H. L. Shulman, C. F. Ullrich, A. Z. Proulx, and J. O. Zimmerman 253

III. Holdup for Aqueous and Nonaqueous Systems .....
H. L. Shulman, C. F. Ullrich, N. Wells, and A. Z. Proulx 259

Correlation of Diffusion Coefficients in Dilute Solutions ..... C. R. Wilke and Pin Chang 264

Communications to the Editor 271

Books 272

Publication Office, Orange, Connecticut. Published quarterly in March, June, September, and December by the American Institute of Chemical Engineers, 25 West 45 Street, New York 36 New York. Manuscripts and other communications should be sent to the New York office. Correspondence with the editor may be addressed to him at Yale University, 225 Prospect Street, New Haven 11, Connecticut. Statements and opinions in the *A.I.Ch.E. Journal* are those of the contributors, and the American Institute of Chemical Engineers assumes no responsibility for them. Subscriptions: one year, member $4.50, nonmember $9.00; two years, member $7.50, nonmember $16.00; additional yearly postage, Canada 50 cents, Pan American Union $1.50, other foreign $2.00 (foreign subscriptions payable in advance). Single copies: $3.00. Application for second-class mail privilege is pending at Orange, Connecticut. Copyright 1955 by the American Institute of Chemical Engineers.

WILMAD TUBING...

Product of Pride and Precision

• PRECISION BORE TUBING

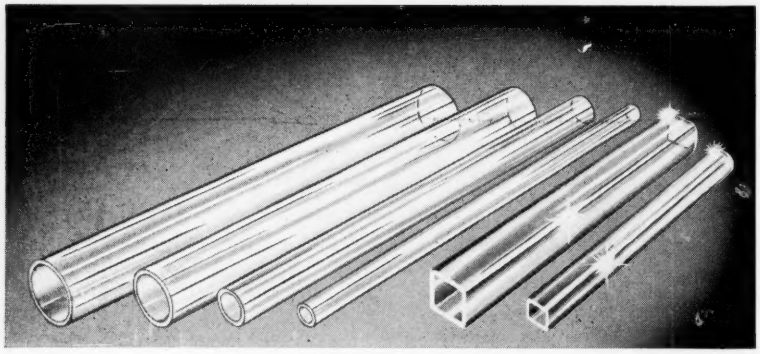

Many industrial and electronic engineers who need extreme accuracy in glass tubing use Wilmad Precision Bore Tubing exclusively. Ideal for use in barometers, bearings, dashpots, manometers, voltage regulators, capacitors, rotameter tubes, burettes, viscosimeters, wave guide tubes, UHF tuners and cavities, and hundreds of other applications.

Made in various shapes and sizes . . . square, rectangular, hexagonal, and tapered up to 7" ID. Fluted and other special shapes can be made to meet individual requirements. Available in Pyrex Brand, Vycor Brand and most of the electronic glasses.

• PRECISION BORE CAPILLARY TUBING

Our claim of consistently achieving an accuracy and uniformity hitherto considered impossible is no idle boast. In a size range that runs from .004" ID to .100" ID, our tolerance limits are set at ±.0002".

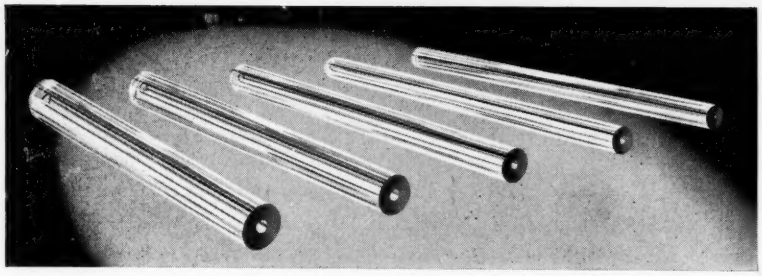

Send for this free catalog TODAY

We welcome the opportunity of discussing with your Engineering Department any particularly difficult problems they might have in the precision glass field. We will be glad to help you find a solution.

WILMAD GLASS COMPANY, INC.

DEPT. A

LANDISVILLE • NEW JERSEY

SPECIALISTS IN RESEARCH LABORATORY GLASSWARE

CHEMICAL · LABORATORY W GLASSWARE

A SECOND GLANCE

It is a pleasure to observe in the second issue of the *A.I. Ch. E. Journal* that a rather wide coverage of the field of chemical engineering has been accomplished. Thermodynamics and unit operations are the preponderant subjects, but kinetics and new techniques and theories are also encountered. The continuing expansion of chemical engineering is such that many more fine articles may be expected in the future. The literature in this field seems to behave like the circumference of a circle (or perhaps rather like the surface of a sphere) in that each development breeds new opportunities for further exploration and publication. There is no shortage of excellent papers coming to the editorial offices; and we have a substantial back log from which to select. This aspect of the editor's job is both pleasing and easy.

Mere quantity, of course, does not represent a particularly suitable aim or publication policy unless it is matched with quality. High standards in this regard have been set for us in the former *Transactions of the American Institute of Chemical Engineers* and in *Chemical Engineering Progress*, and we intend to maintain them. One can list easily many distinguished and significant papers appearing in those publications in past years which have opened up whole new fields of inquiry. Such papers bring in their train a series of solid observations and generalizations of great value. It is our hope that the *A.I.Ch.E. Journal* will be as fortunate in bringing to the readers so many original and pioneering contributions.

The geographical distribution of the authors in this issue is also worthy of attention. As was to be expected, most of the articles originated in the American universities, and certainly the prize for this issue must go to the Midwestern ones. It is disappointing that so few papers have come to us from industrial groups, and we hope for much more representation from them in the future.

Our expanded publishing program which has brought forth the *A.I.Ch.E. Journal* will also bring many problems. Chief among these is, of course, the financial one. The editor's constant insistence on paring and eliminating must sometimes be disappointing to authors, and he fears greatly for whatever personal popularity he may have once had. One of the main concerns is the problem of original data. Such data have been made available at the American Documentation Institute, and great economy results thereby because tabulations of data are very expensive to print. Treatment of the data and correlations and generalizations about them are ordinarily to be published in the magazine. Such correlations, however, also involve tabular presentations with consequent high printing costs. The editor feels that there might be much merit in confining the author's treatment thereof to graphs, which are less expensive, and to the text. There are exceptions to this dictum, of course, particularly when the manner of interpretation is clearly established. An example is *PVT* data, where presentation as "smoothed" compressibility factors or residuals is universal. In many fields, however, improvements in interpretation are constantly being made, and one of the aims of the Journal is to present these, both for application and for further refining. As this matter of economy is at present of paramount interest in the presentation of new developments in chemical engineering, observations on this matter would be welcomed from readers.

H. B.

PHOENIX FACILITIES AND PERSONNEL

AVAILABLE FOR

- **CONSULTATION**
- **ENGINEERING**
- **RESEARCH**
- **DEVELOPMENT**
- **DESIGN**
- **AND MANUFACTURE OF**

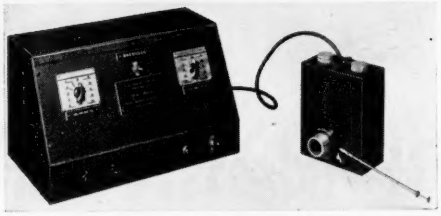

new instruments and automatic control systems for industrial, laboratory, pilot plant, and other special applications. We invite your inquiries on specialized instrumentation and automatic control systems.

OTHER PHOENIX PRODUCTS

Universal Light Scattering Photometers
Dual Photomultiplier type photometers
Electron Multiplier Photometers
Turbidimeters
Colorimeters
Visual Differential Refractometers
Automatic Recording Mass Collecting Differential Refractometers
Regulated High Voltage Power Supplies
D. C. Amplifiers
Maple Sirup and Honey Comparators
Optical Benches
Monochromatic Light Sources
Color Standards
Ultraviolet transmitting glasses
Lenses, prisms, mirrors, and reticles
Colorimetric Absorption Cells
Precision Electro-phoresis Cells
Precision Bore Glass tubing—round, square, rectangular, and conical (from .002" I.D. to 6" I.D.) tolerance plus or minus .0002"
Flanged glass pipe (¼" I.D. to 6" I.D.)
Flow meters and tubes
Manometers
Glass Venturi tubes and nozzles
Glass pumps and valves
Glass sheet, plate, rod, and balls

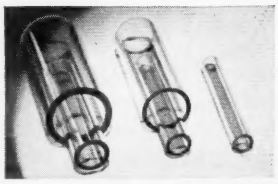

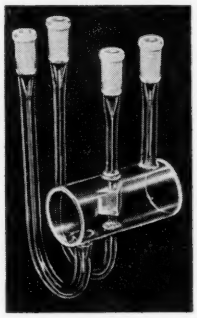

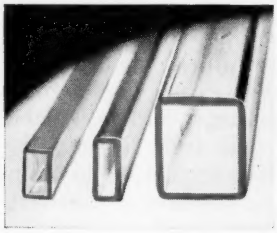

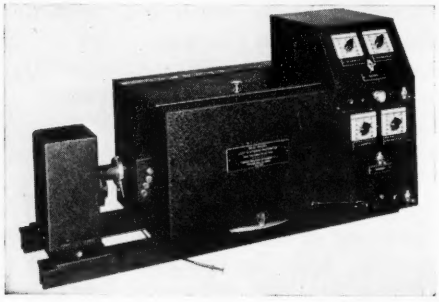

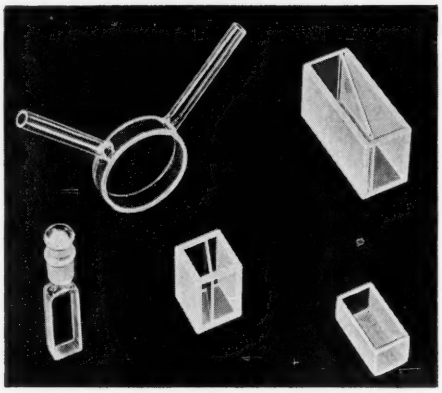

PHOENIX PRECISION INSTRUMENT COMPANY

3803-05 N. 5TH STREET • PHILADELPHIA 40, PA.

GAS ABSORPTION AND OXIDATION IN DISPERSED MEDIA

L. B. ANDERSEN and H. F. JOHNSTONE
University of Illinois, Urbana, Illinois

The absorption and subsequent liquid-phase reaction of oxygen was studied with two types of dispersion apparatus, the Venturi atomizer and the fritted-glass disperser. The systems studied in both devices included the absorption of atmospheric oxygen by catalyzed sodium sulfite solutions and the simultaneous absorption of atmospheric oxygen with nitrogen dioxide and with sulfur dioxide by water.

Very large values of the liquid-film mass transfer coefficient for oxygen absorption were measured in the atomization zone of the Venturi atomizer. Over-all recovery efficiencies were less than 2.3% for nitrogen dioxide but reached as much as 22% for sulfur dioxide. Oxidation efficiencies for sodium sulfite solutions ranged up to 80%, depending on the operating conditions.

The fritted-glass disperser gave recovery efficiencies of nitrogen dioxide as high as 90% from air containing 10% of the gas. The recovery efficiency decreased at low concentrations of nitrogen dioxide for both the Venturi atomizer and the fritted-glass disperser.

Fine dispersion of either the gas or liquid phase produces a large interfacial area for gas absorption and relatively high rates of mass transfer. Large mass transfer coefficients have been reported for the finely dispersed liquid phase in the Venturi atomizer(*3*). In this work, measurements were reported on the rates of absorption of sulfur dioxide and oxygen and the rate of desorption of carbon dioxide in the atomization zone. For carbon dioxide and oxygen the values of the liquid-film mass transfer coefficient were very large in the vicinity of the liquid injection and decreased rapidly with distance within the atomization zone. The high rates of carbon dioxide desorption suggested the present work, in which an attempt was made to define further the absorption process in the Venturi atomizer. The work was confined to processes involving oxygen absorption and subsequent chemical reaction in the liquid phase. If the oxygen in solution reacts chemically as rapidly as it is absorbed, the rate of absorption should be substantially increased.

Results are presented for two methods of dispersion: atomization in a Venturi throat and aeration through a porous fritted-glass cylinder. For the former, measurements are reported on rates of absorption of oxygen by pure water and by sodium sulfite solutions, as well as on the rates of oxygen absorption during the simultaneous absorption of nitrogen dioxide and sulfur dioxide. Mass transfer coefficients for oxygen were determined in each case as functions of distance near the point of liquid injection. This is the region of highest transfer rate. Over-all oxidation efficiencies for sodium sulfite solutions and recovery efficiencies for nitrogen dioxide and sulfur dioxide in the Venturi atomizer were also determined.

With the fritted-glass disperser, the gas phase is finely divided in the bulk liquid phase. This produces a large interfacial area per unit volume of gas and ensures intimate contact of all the gas with the liquid absorbent. Recovery efficiencies for nitrogen dioxide were determined for gas compositions up to 10% nitrogen dioxide. In addition, brief studies were made on sulfur dioxide recovery and sodium sulfite oxidation with this type of contactor.

EXPERIMENTAL

Two venturi sections were used in the work. The data for oxygen absorption by pure water were obtained in the Lucite venturi used previously for studies of carbon dioxide desorption (*8*). The throat diameter was approximately 1-1/8 in. and the throat length was 3 in. All other measurements were made in a Lucite venturi with a throat diameter of 1/4 in. and a throat length of 1/2 in. The gas velocity was 327 ft./sec. in the larger venturi throat and 300 ft./sec. in the smaller throat. Gas flow rates were measured upstream of the liquid injection venturi by a standard venturimeter. Nitrogen dioxide or sulfur dioxide was injected sufficiently far upstream to ensure a uniform composition at the gas-analysis point. Liquid was injected axially with a single stainless-steel hypodermic needle which had an inside diameter of 0.13 cm. Samples of the spray were collected with an impact tube at 0.45, 1.10, and 2.84 in. from the point of liquid injection in the larger venturi and at 0.25, 0.50, and 1.00 in. from injection in the smaller venturi.

The fritted-glass disperser was a relatively simple apparatus. The contacting element was a standard coarse-porosity Pyrex fritted-glass cylinder. The dimensions of the cylinder were 4 mm. I.D., 12 mm. O.D., and 19 mm. high. The base of the cylinder was sealed and gas passed only through the sides. The cylinder was located at the bottom of a liquid-filled column 43 in. high and 2-3/8 in. in diameter. The gas passed through the interstices in the fritted glass and bubbled up through two liters of liquid. It then passed to a column filled with standard sodium hydroxide and hydrogen peroxide for removal of any nitrogen dioxide or sulfur dioxide not absorbed in the first column.

Analytical Procedures. The gas phase in the venturi atomizer was analyzed for nitrogen dioxide, or sulfur dioxide, by passing a sample through a standard solution of sodium hydroxide containing hydrogen peroxide and measuring the remaining gas in the sample with a wet test meter. All the nitrogen dioxide, or sulfur dioxide, was absorbed in the sodium hydroxide and the excess hydroxide was determined by titration with standard hydrochloric acid. Total acid concentration in the liquid phase was determined by titration with standard sodium hydroxide. Nitrous acid was found by addition of an excess of potassium permanganate followed by back-titration with standard sodium thiosulfate. In the absorption of sulfur dioxide by water and of oxygen by sodium sul-

Complete data are found in the Ph. D. thesis of L. B. Andersen, obtainable on microfilm from University Microfilms, Inc., Ann Arbor, Michigan.

L. B. Andersen is at present at Lehigh University, Bethlehem, Pennsylvania.

fite solutions, sulfite ion was determined by addition of an excess of standard iodine solution and back-titration with standard sodium thiosulfate. Similar procedures, where applicable, were used with the fritted-glass absorber.

The quantity of oxygen absorbed in the atomization zone of the venturi atomizer with simultaneous absorption with nitrogen dioxide was found from the difference between the concentration of nitric acid and nitrous acid. In the over-all reaction of oxygen with nitrogen dioxide and water

$$n\ NO_2 + \frac{n}{2} H_2O + x\ O_2 = \left[\frac{n}{2} - 2x\right] HNO_2 + \left[\frac{n}{2} + 2x\right] HNO_3 \qquad (1)$$

and

$$\text{moles oxygen absorbed} = x = \frac{\text{moles } HNO_3 - \text{moles } HNO_2}{4} \qquad (2)$$

This calculation assumes that there is no escape of nitric oxide formed by decomposition of nitrous acid in the very short time in the atomization zone. This is reasonable, since decomposition of the acid in the liquid phase is slow (*1*) and oxygen can be absorbed sufficiently rapidly to oxidize any nitric oxide formed. The oxygen absorbed with sulfur dioxide was found from the amount of sulfuric acid formed. The oxygen absorbed by sodium sulfite solutions was found from the difference between the initial and final sulfite concentrations.

The Spray Zone. In order to calculate values for the liquid-film mass transfer coefficient in the venturi atomizer, it was necessary to determine the absorption volume occupied by the spray. The dimensions of the spray zone at a gas velocity of 300 ft./sec. were measured visually with calipers from the outside of the transparent throat. Within 1 in. of liquid injection the spray zone was found to be a straight-sided truncated cone. The cross-sectional diameter at the injection point was 0.051 in., and at 1 in. from injection it was 0.22 in. The shape of the spray zone should depend on the properties of the liquid, the size and shape of the injection nozzle, and the relative velocity between the liquid and the gas. It should be independent of the size of the venturi throat, so long as no wall impingement occurs. The absorption volume determined in this manner is not analogous to the absorption volume in conventional absorption equipment. It is useful, however, in calculating the absorption coefficient for comparison of the systems studied.

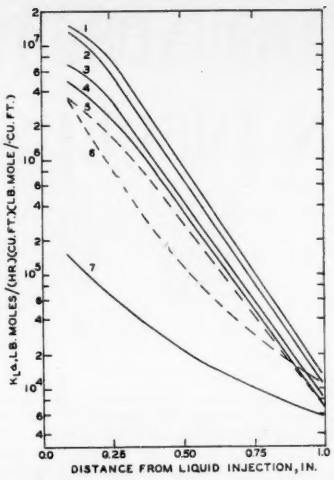

FIG. 2. COEFFICIENT K_La FOR OXYGEN ABSORPTION BY SODIUM SULFITE SOLUTIONS: CATALYST, 0.01*M* $CoSO_4$; GAS VELOCITY, 300 FT./SEC. EXCEPT AS NOTED.

	Solution	Liquid rate, ml./min.
1	0.0100*M* Na_2SO_3	300
2	0.0100*M* Na_2SO_3	200
3	0.0100*M* Na_2SO_3	100
4	0.0100*M* Na_2SO_3	50
5	0.050*M* Na_2SO_3	50
6	0.025*M* Na_2SO_3	50
7	Pure water	95.2, velocity, 327 ft./sec.

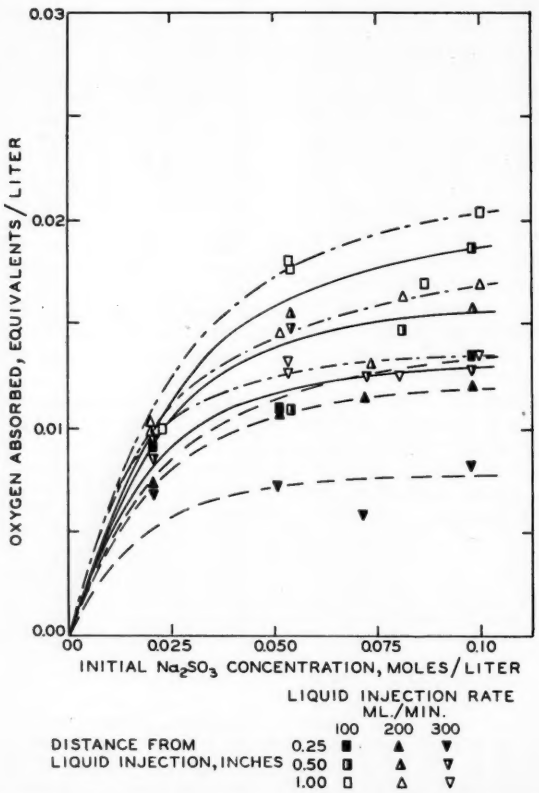

FIG. 1. EFFECT OF SULFATE CONCENTRATION ON RATE OF OXYGEN ABSORPTION IN THE VENTURI ATOMIZER.

ABSORPTION IN THE VENTURI ATOMIZER

Nukiyama and Tanasawa(*5*) describe the mechanism of atomization of a liquid when it is injected into a high-velocity air stream. At the gas velocities used in this work, the liquid is atomized by the formation and subsequent shattering of attentuated, twisted filaments and thin, cuplike films. These filaments and films are initially available for absorption. Subsequently more or less spherical droplets are formed which have less surface area per unit volume of liquid than the attenuated films and filaments.

The mass transfer coefficient was calculated(*3*) from the slope of the curve of oxygen absorbed as a function of the absorption volume, which was determined from the original data of oxygen absorbed as a function of distance from injection, illustrated in Figure 1. This slope, measured in gram-moles/(liter)(cubic inch), was multiplied by the liquid injection rate

and divided by the driving force across the liquid film to give the liquid-film mass transfer coefficient, K_La. The driving force is the difference between interfacial oxygen concentration and the bulk concentration. The interfacial concentration was assumed to be in equilibrium with the oxygen in the gas. The bulk concentration was taken as zero, since the chemical reaction consumed all the oxygen. The coefficient is the transfer rate per unit absorption volume per unit driving force.

The scatter of the data can be attributed to variations in the spray under otherwise identical conditions. The present measurements were all made within 1 in. of the point of injection, closer than in any of the previous work. The values of the coefficient K_La for oxygen absorption by catalyzed sodium sulfite solutions, shown in Figure 2, are initially much larger than those for absorption of the gas by pure water. The values for sodium sulfite decrease rapidly with distance until they are nearly equal to those for pure water at 1 in. from liquid injection.

Curves similar to those in Figure 1 were drawn through the original data for oxygen absorption with nitrogen dioxide and with sulfur dioxide. The data scattered like those for sodium sulfite. The values of the coefficient K_La for oxygen absorption with nitrogen dioxide are shown in Figure 3 and for oxygen absorption with sulfur dioxide, in Figure 4.

The high initial mass transfer coefficients for oxygen absorption by pure water can be attributed to the large initial interfacial area, high relative gas-liquid velocity, and great liquid turbulence. The rapid decrease in the absorption rate is caused by the decrease in interfacial area as the films and filaments shatter into spherical droplets, to the decrease in the relative velocity as the droplets are accelerated to the gas velocity, and to the decrease in liquid turbulence as the droplets pass downstream. When oxygen reacts in solution, the rate of chemical reaction is another factor to be considered. If the reaction is sufficiently rapid, there will be no build-up of dissolved oxygen and the absorption rate will be at a maximum. For slower reactions, a combination of diffusion and reaction rate will determine the rate of absorption. Slow reactions result in the same rate of absorption as when no chemical reaction occurs in the short time available in the Venturi apparatus.

In the oxidation of sodium sulfite solutions, the rapid removal of dissolved oxygen by reaction produces much larger values for the coefficient K_La than in the case of absorption by pure water. The value of K_La for oxygen absorption by a 0.025 M sodium sulfite solution at 0.1 in. from liquid injection is 5,200,000 lb. moles/(hr.)(cu. ft.)(lb. mole/cu. ft.) for a liquid rate of 100 ml./min. This is to be compared with K_La for absorption by pure water of 160,000 at aproximately the same liquid and gas rates. An additional factor influences the decrease in oxygen absorption rate by sodium sulfite solutions. As the sodium sulfite is oxidized, its concentration decreases and the rate of chemical consumption of oxygen consequently decreases. In the ultimate case all the sodium sulfite is oxidized, and the final absorption rate would approach that for absorption by pure water. Thus the value of the mass transfer coefficient for 0.025 M sodium sulfite solution is only twice as great as that in water at 1.0 in. from the point of injection. The values of the coefficient K_La decrease similarly for other initial sodium sulfite concentrations. Thus apparently the same factors which operate to decrease the rate of oxygen absorption by pure water also control the rate of absorption by sodium sulfite solutions. Such a situation can be explained by postulating that initially during atomization, in the region of filaments and films there is no significant physical resistance to absorption and therefore the absorption rate is controlled by the chemical reaction. Later, when the droplets have been formed, the diffusional resistance controls. This transition must occur rapidly, within 1 in. of the point of liquid injection.

This mechanism also affects the results of the oxygen–nitrogen dioxide absorption. The nitrogen dioxide must diffuse into the liquid before it reacts with dissolved oxygen. Thus the rate of oxygen absorption will depend on the rate of nitrogen dioxide absorption, as well as on the rate of intermediate reactions:

$$2\,NO_2\,(aq.) + H_2O = HNO_3\,(aq.) + HNO_2\,(aq.) \qquad (3)$$

$$2\,HNO_2\,(aq.) = NO\,(aq.) + NO_2\,(aq.) + H_2O \qquad (4)$$

$$NO\,(aq.) + \tfrac{1}{2}\,O_2\,(aq.) = NO_2\,(aq.) \qquad (5)$$

In dilute solutions nitrogen dioxide reacts immediately once it enters

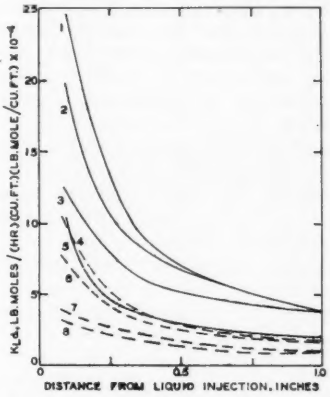

FIG. 3. COEFFICIENT K_La FOR OXYGEN ABSORBED SIMULTANEOUSLY WITH NITROGEN DIOXIDE.

	Gas composition	Liquid rate, ml./min.
1	10% NO_2	300
2	10% NO_2	200
3	10% NO_2	100
4	10% NO_2	50
5	8% NO_2	50
6	6% NO_2	50
7	4% NO_2	50
8	2% NO_2	50

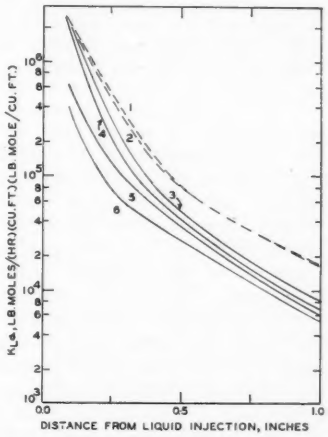

FIG. 4. COEFFICIENT K_La FOR OXYGEN ABSORBED SIMULTANEOUSLY WITH SULFUR DIOXIDE: CATALYST, 0.01M MANGANOUS SULFITE.

	Gas composition	Liquid rate, ml./min.
1	0.2% SO_2	300
2	0.3% SO_2	300
3	0.1% SO_2	300
4	0.1% SO_2	200
5	0.1% SO_2	100
6	0.1% SO_2	50

the liquid phase. The values for the coefficient K_La for oxygen absorption vary more with initial nitrogen dioxide concentration than they do with initial sodium sulfite concentration, an indication that the rate of oxygen absorption depends in part on the rate of nitrogen dioxide absorption. In general, the values in this case are lower than for sodium sulfite oxidation. The method of calculation of K_La is based on an assumed zero concentration of oxygen in the liquid phase because of rapid chemical reaction. Where the values of K_La for oxygen absorption with nitrogen dioxide fall below those for pure water under otherwise similar conditions, the assumption is no longer

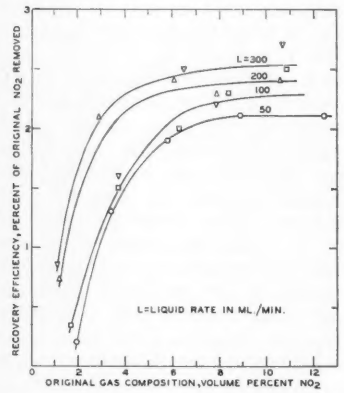

FIG. 5. EFFECT OF GAS COMPOSITION ON RECOVERY EFFICIENCY FOR NITROGEN DIOXIDE IN THE VENTURI ATOMIZER.

correct, because the value of K_La for oxygen absorption into pure water should be the minimum. Thus if the chemical reaction is slow, the oxygen concentration in the bulk of the liquid is not zero, because oxygen does not react as fast as it is absorbed. Since the values for the coefficient K_La for oxygen absorption with nitrogen dioxide actually fall below those for absorption by pure water, the reactions involved must be too slow to use the oxygen as rapidly as it is absorbed. The rate of nitrogen dioxide absorption does not completely control the rate of oxygen absorption, since there is still an oxygen deficiency. Apparently the nitrous acid decomposition and oxidation are the controlling reactions for oxygen absorption. This discussion assumes that there is no appreciable reaction between oxygen, nitrogen dioxide, and water vapor in the gas film, a reasonable assumption considering the short time available for the reaction and subsequent diffusion of nitric acid into the liquid.

A case where the chemical reactions are less complex, the absorption of oxygen with sulfur dioxide in the presence of a catalyst, should provide further information on this point. Sulfur dioxide dissolves in water to give sulfurous acid in solution. Here the chemical reaction is rapid, but the sulfur dioxide must be absorbed before the oxygen can react in solution. The values for the coefficient K_La for oxygen absorption with sulfur dioxide are initially between those for sodium sulfite and for nitrogen dioxide. The mass transfer coefficients fall off rapidly with distance to the same magnitude as those for sodium sulfite solutions. Initially the rate of reaction requires more oxygen than in the nitrogen dioxide

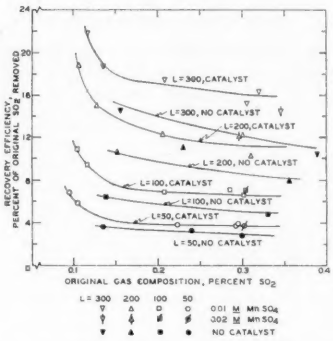

FIG. 6. EFFECT OF GAS COMPOSITION AND CATALYST ON THE OVER-ALL RECOVERY EFFICIENCY FOR SULFUR DIOXIDE IN THE VENTURI ATOMIZER.

case, but less oxygen is consumed than in the absorption by sodium sulfite solutions. For sodium sulfite oxidation the solute must diffuse outward to react with the oxygen diffusing inward from the surface if mixing is not complete within the droplet. For sulfur dioxide–oxygen absorption, both constituents must be absorbed by the liquid, but they can react immediately without further diffusion through the liquid. In this case, if the liquid droplet lacks circulation, the diffusion of sodium sulfite becomes controlling for a fast reaction.

Recovery of Gases. The application of the venturi atomizer to the removal of a constituent from the gas phase may now be considered. In the present work the recovery efficiencies for nitrogen dioxide and for sulfur dioxide were determined, based on the composition of the effluent from the cyclone following the atomizer. The recovery efficiency for nitrogen dioxide was low, as shown in Figure 5. The efficiencies decreased from approximately 2.3% for 10% nitrogen dioxide in the gas phase to less than 1% for 1% nitrogen dioxide. This decrease is expected on the assumption that the chemical reaction controls the absorption rate (*6*). Use of the venturi atomizer for the recovery of a substantial portion of nitrogen dioxide from the gas phase does not appear feasible because the reaction is too slow. The use of an oxidation catalyst gave no improvement in recovery efficiency. Apparently the oxidation reaction does not control the absorption of nitrogen dioxide in dilute solution.

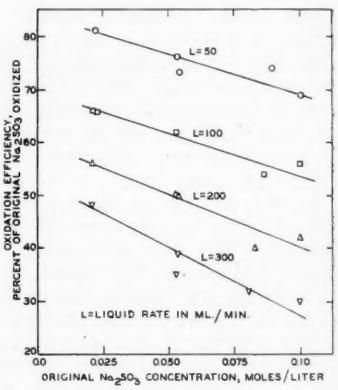

FIG. 7. EFFICIENCY OF OXIDATION OF SODIUM SULFITE SOLUTION IN THE VENTURI ATOMIZER.

The recovery efficiencies for sulfur dioxide were substantially higher than those for nitrogen dioxide, as shown in Figure 6. The efficiency increased at lower sulfur dioxide concentrations; the recovery increased in the presence of an oxidation catalyst, 0.01 *M* manganous sulfate. An increase in the concentration of the catalyst to 0.02 *M* had no appreciable effect. Efficiencies varied from 4 to 22% with liquid rate and sulfur dioxide concentration in the gas. These are sufficient to make the method of some commercial interest.

A number of factors contribute to the low recovery efficiencies in the venturi atomizer. In order to achieve fine atomization it is necessary to maintain a high gas velocity in the throat. In the present work the liquid supplied to contact the gas varied from 2.1 to 12.8 gal./1,000 cu. ft. of gas. Some of the droplets impinged on the wall

TABLE 1.—COMPARISON OF ABSORPTION IN THE ATOMIZATION ZONE WITH OVER-ALL ABSORPTION IN THE VENTURI ATOMIZER

Oxygen Absorption

Initial Na_2SO_3 concentration, moles/liter	Liquid rate, ml./min.	Oxygen absorbed, equiv./liter: Atomization zone	Oxygen absorbed, equiv./liter: Cyclone effluent	Ratio of atomization zone to over-all absorption
Pure H_2O	95.2	4.2×10^{-4}	5.6×10^{-4} (saturated)	0.75
0.021	100	0.0099	0.0141	0.70
0.054	100	0.0176	0.0292	0.60
0.054	300	0.0127	0.0209	0.61
0.100	100	0.0204	0.0555	0.31
0.100	200	0.0170	0.0418	0.41
0.099	300	0.0137	0.0297	0.46

Simultaneous Nitrogen Dioxide—Oxygen Absorption

Initial gas composition, vol. $\%NO_2$	Liquid rate, ml./min.	Oxygen absorbed, equiv./liter: Atomization zone	Oxygen absorbed, equiv./liter: Cyclone effluent	NO_2 absorbed, moles/liter: Atomization zone	NO_2 absorbed, moles/liter: Cyclone effluent	Ratio of atomization zone to over-all absorption: O_2	Ratio of atomization zone to over-all absorption: NO_2
1.7	100	0.0004	0.0010	0.0016	0.0042	0.40	0.38
1.1	300	0.0003	0.0016	0.0003	0.0022	0.19	0.14
6.3	100	0.0029	0.038	0.0083	0.090	0.08	0.09
6.5	300	0.0020	0.015	0.0027	0.037	0.13	0.07
8.4	100	0.0020	0.052	0.0116	0.132	0.04	0.09
7.9	300	0.0007	0.012	0.0037	0.040	0.02	0.09
10.9	100	0.0063	0.083	0.0171	0.191	0.08	0.09
10.7	300	0.0010	0.018	0.0048	0.068	0.06	0.07

Simultaneous Sulfur Dioxide—Oxygen Absorption

Initial gas composition, vol. $\%SO_2$	Liquid rate, ml./min.	Oxygen absorbed, equiv./liter: Atomization zone	Oxygen absorbed, equiv./liter: Cyclone effluent	SO_2 absorbed, moles/liter: Atomization zone	SO_2 absorbed, moles/liter: Cyclone effluent	Ratio of atomization zone to over-all absorption: O_2	Ratio of atomization zone to over-all absorption: SO_2
0.104	100	0.0017	0.0024	0.0034	0.0080	0.71	0.43
0.117	300	0.0013	0.0015	0.0026	0.0060	0.87	0.43
0.116	100	0.0021	0.0023	0.0036	0.0077	0.91	0.47
0.135	300	0.0011	0.0013	0.0019	0.0059	0.85	0.32
0.286	100	0.0020	0.0026	0.0070	0.0144	0.77	0.49
0.320	300	0.0010	0.0019	0.0039	0.0123	0.53	0.32

as they passed downstream and some settled out. The higher liquid rates necessary to ensure thorough contact of all the gas with the liquid resulted in greater wall impingement, with resultant decrease in interfacial area. Very low liquid rates gave little impingement, but not all the gas was brought into contact with the liquid. Because of the high linear velocities in the throat, the time of contact with the liquid is very short and the time of contact in the zone of high interfacial area and turbulence is even less. These difficulties of course do not exist in large venturi atomizers where impingement on the wall and settling do not occur.

Oxidation Processes. Although complete removal of a constituent from the gas phase appears to be impossible with the venturi atomizer, its use for absorbing oxygen from an air stream to oxidize an oxygen-deficient solution appears feasible. In this case it is not necessary to remove all or even a substantial part of the oxygen from the gas, nor must all the gas necessary for atomization come into contact with the liquid. Figure 7 shows the oxidation efficiencies of sodium sulfite solutions containing an oxidation catalyst. In this case the liquid rate is a major factor. Lower liquid rates give higher initial surface-volume ratios, less impingement, and higher oxidation efficiencies. Efficiencies as high as 80% were obtained with 0.025 *M* sodium sulfite original concentration.

Absorption in the Atomization Zone Compared with Over-all Absorption. It is of interest to compare with the over-all absorption the absorption that occurs in the very short time in the atomization zone up to 1 in. from liquid injection. In this way the effectiveness of the unique feature of the venturi atomizer can be determined for gas absorption. The remainder of the apparatus other than the atomization zone resembles a spray chamber. If the atomization zone does not accomplish a large share of the absorption, there is little point in using the venturi atomizer. Table 1 gives representative ratios of the absorption at 1 in. from injection to the over-all absorption. It is not possible to calculate the relative times, because of the unknown acceleration characteristics of the liquid particles and because of ultimate wall impingement, but there is certainly a factor of at least two hundred between the over-all time and that up to 1 in. In the case of the absorption of oxygen by pure water 75% of saturation was reached within 1 in. of liquid injection. For oxygen absorption into sodium sulfite solutions, from 30 to 70% of the total absorption occurs in the atomization zone. The solutions with lower initial concentrations give a higher proportion of oxidation in the atomization zone, because of the approach to complete oxidation in the atomization zone by the dilute solutions.

For nitrogen dioxide absorption, the atomization zone contributes much less to the total absorption. In general, less than 10% of the total absorption occurs within 1 in. of the liquid injection; thus, the unique characteristics of the venturi are of little use in nitrogen dioxide absorption. In sulfur dioxide–oxygen absorption the atomization zone is again significant. From 50 to 90% of the total oxygen is absorbed within 1 in., and from 30 to 50% of the sulfur dioxide is absorbed in the same region. It is interesting to note that in the atomization zone a greater proportion of oxygen is absorbed than of sulfur dioxide. This indicates the value of the venturi for the absorption of slightly soluble gases.

ABSORPTION IN THE FRITTED-GLASS DISPERSER

The fritted-glass disperser was studied as another means of obtaining phase dispersion and large interfacial absorption area. The high recovery efficiencies for nitrogen dioxide with this device indicate possible industrial applications in place of the conventional bubble-cap trays. The unique feature of the fritted-glass absorber is the high rate of gas absorption during bubble formation.

In the absorption of nitrogen dioxide from a gas containing 2.7% nitrogen dioxide in the fritted-glass disperser, an eightfold decrease in liquid volume causes only a 10% decrease in the amount of nitrogen dioxide absorbed in a 2-hr. period, as shown in Figure 8. This decrease is caused in part by the higher concentrations of acid in the smaller liquid volume. Thus most of the nitrogen dioxide absorption occurs during the bubble formation in or near the fritted-glass surface. Only a small portion occurs as the bubbles rise through the liquid. The rate of absorption

of nitrogen dioxide is nearly constant when air is the diluent, as shown in Figure 9. An increase in air rate decreases the recovery efficiency only slightly. A fourfold increase from 0.05 to 0.2 cu.ft./min. reduces the recovery efficiency by only 2%, as shown in Figure 10, and yet allows only one fourth the contact time for the gas within the

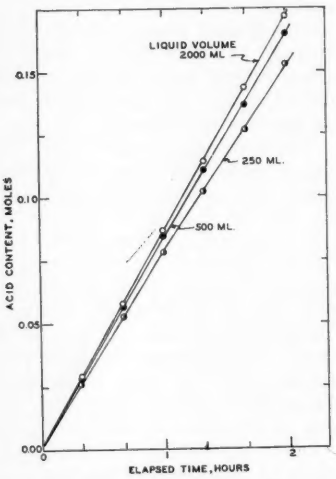

FIG. 8. EFFECT OF LIQUID VOLUME ON NITROGEN DIOXIDE ABSORPTION IN THE FRITTED-GLASS DISPERSER; GAS RATE, 0.05 CU.FT./MIN.; GAS COMPOSITION, 2.7% NO_2.

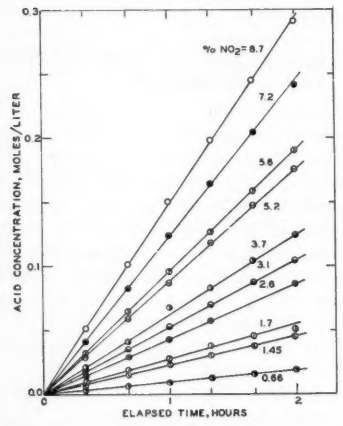

FIG. 9. ABSORPTION OF NITROGEN DIOXIDE FROM AIR IN THE FRITTED-GLASS DISPERSER AT A GAS RATE OF 0.05 CU.FT./MIN.

fritted glass. The substitution of pure oxygen for air improves the recovery of nitrogen dioxide in a 2-hr. period by 6%. Absorption of nitrogen dioxide with nitrogen as the diluent is 18% less than with air. Thus oxidation has some influence on absorption but is not the controlling factor.

The recovery efficiencies for nitrogen dioxide in the fritted-glass absorber, shown in Figure 11, are substantially higher than those for a bubble-cap column at atmospheric pressure, as reported by Peters(*6*). The efficiency decreases from 90% at a gas composition of 10% nitrogen dioxide in air to 89% at 3% nitrogen dioxide and then falls off to 80% at 1% nitrogen dioxide. This decrease with concentration agrees with the theory proposed by Peters(*6*). The high concentrations of nitrous acid found here were not found in the bubble-cap column. About 20% of the total acid was in the form of nitrous acid, but in the bubble-cap column the concentration of nitrous acid was negligible. With nitrogen as the diluent gas, the same concentration of nitrous acid was found. The decrease in efficiency at higher gas concentrations with nitrogen as the diluent, as shown in Figure 11, is not readily explained. It may be caused in part by a greater build-up of nitrous acid which retards the reaction of nitrogen dioxide with water. This would also explain the substantially lower recovery efficiencies when nitrogen is the diluent instead of air. There was no difference between nitrogen and air in the bubble-cap column.

The differences between the fritted-glass absorber and the bubble-cap column may be explained on the basis of gas- and liquid-film reactions. Peters made a theoretical analysis of the kinetics of the bubble-cap absorber, assuming that chemical reactions controlled, and concluded that the gas-film reaction predominates. The nitrogen dioxide reacts in the gas film with water vapor and oxygen and gives nitric acid and some nitrous acid. The nitric acid condenses into a mist and diffuses into the liquid. Any nitrous acid formed may decompose and react with oxygen; a small portion may diffuse into the liquid. This nitrous acid and any formed in solution will be oxidized by dissolved oxygen so that the nitrous acid concentration in the liquid is negligible.

In the fritted-glass absorber, on the other hand, because of the greater interfacial area and more complete contact of the gas with the liquid, the rate of absorption of nitrogen dioxide is greater; therefore the liquid-film reactions are more important. Nitric and nitrous acids form in the liquid phase, and oxygen must be absorbed to oxidize the nitrous acid. Decomposition of nitrous acid is slower in the liquid phase than in the gas phase, and the concentration of nitrous acid remains at a high value.

The higher over-all rate of absorption of nitrogen dioxide in the fritted-glass absorber compared with that in the bubble-cap column can be attributed to the more rapid reaction of nitrogen dioxide in the liquid phase compared with that in the gas phase.

Effect of Liquid-Phase Additives on Nitrogen Dioxide Absorption. Catalysts or inhibitors for nitrous acid de-

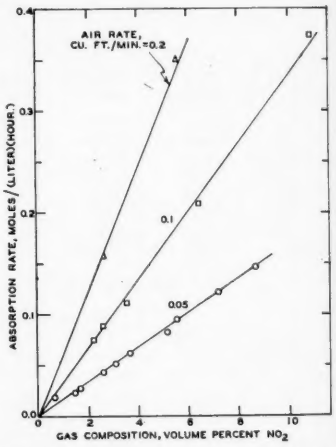

FIG. 10. EFFECT OF GAS RATE AND GAS COMPOSITION ON THE ABSORPTION RATE OF NITROGEN DIOXIDE IN THE FRITTED-GLASS DISPERSER.

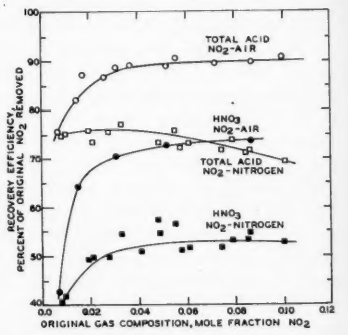

FIG. 11. RECOVERY EFFICIENCY FOR NITROGEN DIOXIDE IN THE FRITTED-GLASS DISPERSER: GAS RATE, 0.05 CU.FT./MIN.

composition, as well as oxidation catalysts, have no appreciable effect on the over-all acid content or nitrogen dioxide recovery. There is a slight effect on the nitrous acid concentration, as shown in Figure 12. Boric acid and potassium nitrate were used as the catalysts for nitrous acid decomposition(*4*). Manganous sulfate is an oxidation catalyst and phenol is both an oxidation and decomposition inhibitor. In the presence of these agents the

total acid curves are essentially the same as in their absence. The nitrous acid concentration is lower in the presence of the catalysts and higher in the presence of phenol, as expected. Thus, although a catalyst has some effect on the nitrous acid content of the solution, it has no effect on the total acid content or over-all recovery of nitrogen dioxide from air mixtures. With nitrogen as a diluent, however, the decomposition and oxidation of nitrous acid does have an effect on the over-all recovery. Above a critical minimum rate the decomposition of nitrous acid apparently does not influence the over-all recovery of nitrogen dioxide from dilute gases in the fritted-glass disperser.

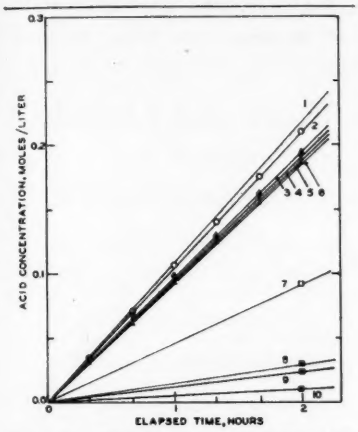

FIG. 12. EFFECT OF CATALYSTS AND SODIUM HYDROXIDE ON THE ABSORPTION OF NITROGEN DIOXIDE FROM AIR IN THE FRITTED-GLASS DISPERSER: GAS RATE, 0.05 CU.FT./MIN.; GAS COMPOSITION, 5.8% NO_2.

Total acid	Nitrous acid
1 With excess NaOH, 100% recovery	7 For phenol
2 With a stoichiometric quantity of NaOH	8 For H_3BO_4
3 With no catalyst	9 For KNO_3
4 Two runs: 0.01*M* KNO_3; 0.01*M* H_3BO_3	10 For $MnSO_4$
5 With 1*M* $CaCl_2$	
6 Two runs: 0.01*M* phenol, 0.01*M* $MnSO_4$	

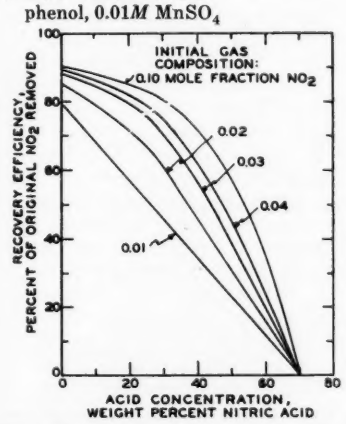

FIG. 13. EFFECT OF ACID CONCENTRATION ON RECOVERY EFFICIENCY FOR NITROGEN DIOXIDE AT VARIOUS GAS COMPOSITIONS IN THE FRITTED-GLASS DISPERSER; GAS RATE, 0.05 CU.FT./MIN.

Effect of Nitric Acid Concentration on Nitrogen Dioxide Recovery. As the nitric acid concentration of the solution increases, the reversibility of the reactions of nitrogen dioxide with water becomes important, until, at 15.4 *M* (69.6%) nitric acid, the rate of the forward reaction [Equation (3)] becomes insignificant compared with the reverse reaction, and no more nitrogen dioxide reacts with water at atmospheric pressure. The recovery efficiency thus becomes zero in 15.4 *M* nitric acid. This was verified experimentally, and the curves of Figure 13 show the decrease in recovery efficiency with acid concentration in the fritted-glass absorber. These efficiency data were used to calculate an over-all efficiency for a multistage absorber by the method of Sherwood and Pigford(*7*). For a four-stage countercurrent fritted-glass absorber with 10% nitrogen dioxide gas entering at the bottom of the tower and water entering at the top, assuming that all the nitric oxide is oxidized between stages, the over-all recovery efficiency for nitrogen dioxide is 99.7%. If the entering gas is 1% nitrogen dioxide, the over-all efficiency is 98.6%. With 30% acid entering at the top and 10% nitrogen dioxide in the gas, the over-all efficiency is 96.9%. These efficiencies are higher than those reported for bubble-cap columns at atmospheric pressure.

Other Reactions. In the absence of a catalyst in the absorption of 2 to 17% sulfur dioxide from air, the oxidation in solution is not rapid enough to prevent build-up of sulfur dioxide to the saturation point where no more sulfur dioxide is absorbed. At higher concentrations of sulfur dioxide in the gas, saturation is reached more readily. When an oxidation catalyst is present, the build-up is less pronounced. Previous work at very low sulfur dioxide concentrations (0.325%) in the gas showed that the catalyzed oxidation of sulfur dioxide is sufficiently rapid to prevent any build-up in solution.

The absorption of nitrogen dioxide by a solution containing an excess of sodium hydroxide over the amount necessary to react with all the nitrogen dioxide supplied in a 2-hr. period resulted in 100% recovery. The gas rate was 0.05 cu.ft./min. and the composition was 5.8% nitrogen dioxide. Chambers and Sherwood found a decrease in absorption by sodium hydroxide solutions in a wetted-wall column compared with absorption by pure water(*2*). In such a device the gas-film reaction predominates and the sodium hydroxide in solution lowers the vapor pressure of water. In the fritted-glass absorber the liquid-film reaction predominates because of the high interfacial area available for absorption.

COMPARISON OF THE VENTURI ATOMIZER AND THE FRITTED-GLASS DISPERSER

The two methods of gas-liquid contact used in this work cannot be compared in all respects. The initial rate of absorption is higher in the venturi atomizer, but the time of contact during which high absorption rates exist is much greater for the fritted-glass disperser. The over-all contact of the gas with the liquid is better in the disperser; consequently it is more effective for the recovery of a constituent from the gas phase. The shorter contact time in the venturi atomizer may be advantageous in a case where it is desired to stop a specific reaction after a short time. The use of a fritted disperser for nitrogen dioxide absorption appears to be promising.

Further work is planned on other fritted materials suitable for commercial absorbers of this type, such as sintered stainless steel. While the studies reported here were all made at atmospheric pressure, even higher recovery efficiencies for nitrogen dioxide would be expected at elevated pressures.

LITERATURE CITED

1. Abel, E., and H. Schmid, *Z. physik. Chem.*, 132, 55 (1928).
2. Chambers, F. S., and T. K. Sherwood, *Ind. Eng. Chem.*, 29, 1415 (1937).
3. Johnstone, H. F., R. B. Feild, and M. C. Tassler, *Ind. Eng. Chem.*, 46, 1601 (1954).
4. Mukerji, K. B., and N. P. Dhar, *Z. Elektrochem.*, 31, 255 (1925).
5. Nukiyama, S., and Y. Tanasawa, *Trans, Soc. Mech. Engrs. (Japan)*, 5, No. 18, 68 (1939).
6. Peters, M. S., C. P. Ross, and J. E. Klein, *A.I.Ch.E. Journal*, 1, No. 1, 105 (1955).
7. Sherwood, T. K., and R. L. Pigford, "Absorption and Extraction," 2 ed., Mc-Graw-Hill Book Company, Inc., New York (1953).
8. Tassler, M. C., Ph.D. thesis, Univ. Illinois (1952).

Presented at the A.I.Ch.E. New York meeting.

DEVELOPMENT OF AN EQUATION OF STATE FOR GASES

JOSEPH J. MARTIN and YU-CHUN HOU
University of Michigan, Ann Arbor, Michigan

I. Pressure-Volume-Temperature Behavior of Pure Gases and Liquids

More than a hundred equations of state relating the pressure, volume, and temperature of gases have been proposed according to Dodge(*7*), but only a very few of them have attained any practical importance as the majority do not represent the data with sufficient accuracy. In this work the significant pressure-volume-temperature (hereafter referred to as *PVT*) characteristics of pure gases have been examined in detail, and an equation has been developed to fit precisely the characteristics common to different gases.

PVT data may be plotted on different types of graphs, of which probably the oldest is that of pressure vs. volume with temperature as a parameter, as shown in Figure 1. From this graph van der Waals deduced two properties of the critical isotherm namely, that at the critical point the slope is zero and an inflection occurs.* Van der Waals expressed these two properties algebraically in the following well-known manner:

$$(dP/dV)_T = 0 \text{ at the critical point} \tag{1}$$

$$(d^2P/dV^2)_T = 0 \text{ at the critical point} \tag{2}$$

where P is pressure, V is volume, and T is temperature, as indicated above. Van der Waals employed these two conditions to evaluate the two arbitrary constants in the equation of state he proposed.

A number of other two-constant (exclusive of the gas constant) equations of state have been proposed, the best known being those of Berthelot and Dieterici. None of them, however, actually represent the *PVT* data over a wide range with any great degree of precision and not one of them is considered suitable for the calculation of accurate thermodynamic diagrams. This does not imply, however, that these two-constant equations have not been extremely useful. Van der Waals' equation was of the greatest value in leading to the principle of corresponding states.

In one form the corresponding-state principle suggests that the compressibility factor, $z = PV/RT$, depends only on the reduced temperature and pressure, which are defined respectively as $T_r = T/T_c$ and $P_r = P/P_c$. On a generalized compressibility chart for many different compounds single average lines are drawn for each isotherm; however, to demonstrate that the principle is approximate, Figure 2 has been constructed to emphasize the differences which actually exist among compounds.

From the compressibility chart it is noted that all gases follow the ideal-gas law as the pressure approaches zero, regardless of the temperature. This may be expressed as

$$Z = PV/RT = 1 \text{ at } P = 0 \text{ for all temperatures} \tag{3}$$

A curious corollary of this is the seemingly contradictory fact that in general V does not equal RT/P at $P = 0$. By definition of a derivative at any point (P_o, Z_o) on the compressibility chart,

$$(dZ/dP_r)_{Tr} = \lim (Z - Z_o)/(P_r - P_o) \text{ as } P_r \to P_o \tag{4}$$

With any isotherm taken at

$$P_o = 0,\ Z_o = 1.0,$$

$$(dZ/dP_r)_{Tr} = \lim (Z-1)/(P_r - 0) \text{ as } P_r \to 0$$

$$= \lim RT\,(Z-1)/RTP_r \text{ as } P_r \to 0$$

$$= (P_c/RT) \lim (ZRT/P - RT/P) \tag{5}$$

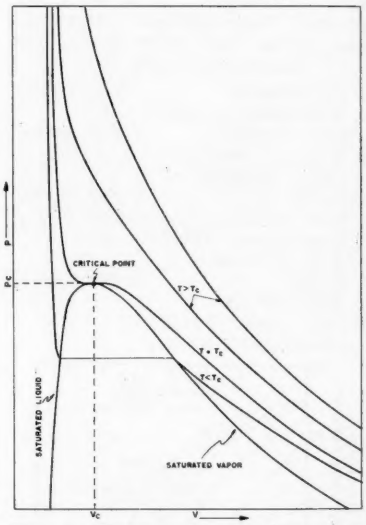

FIG. 1. PRESSURE-VOLUME DIAGRAM.

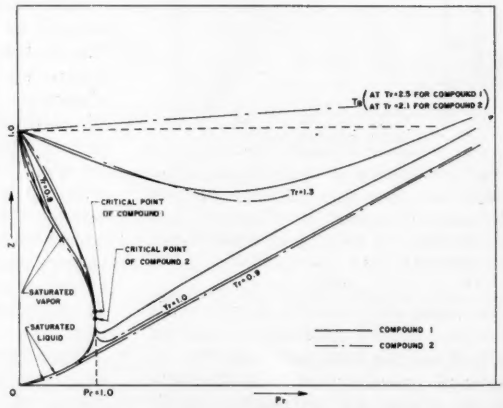

FIG. 2. COMPRESSIBILITY CHART.

*Some investigations (*13*) indicate that the critical isotherm is not the smoothly inflected curve shown in Figure 1. This result seems to be attributed to the indefiniteness of the critical state and possibly to the lack of attainment of true equilibrium.

or from by definition $Z = PV/RT$, or

$$ZRT/P = V, (dZ/dP_r)_{T_r} =$$

$$(P_c/RT) \lim (V - RT/P) \text{ as } P_r \to 0$$

$$= -(P_c/RT)(\alpha)_{P_r \to 0} \quad (6)$$

where α is defined as the residual volume, $(RT/P\text{-}V)$.
If Equation (6) is rewritten,

$$\text{at 0 pressure } \alpha$$

$$= -(RT/P_c)(dZ/dP_r)_{T_r} \quad (7)$$

which relates α to the slope of an isotherm on the compressibility chart. Since in general this slope is not zero at zero pressure, α is a finite quantity. The one isotherm for which the slope is zero is known as the Boyle point.

Most generalized compressibilty charts show the Boyle point occurring at a T_r of about 2.5. This is probably true only for such compounds as nitrogen, carbon monoxide, and methane, which were considered in making the plots. These compounds all have critical temperatures of approximately the same magnitude. For hydrogen with a much lower critical temperature the data indicate that the Boyle point is around a T_r of 3.3. For compounds with higher critical temperatures there are no experimental data at the required high temperatures. However, by extrapolation of the experimental data on isometric plots (*see* Figure 6), it appears that the Boyle-point reduced temperature goes down as the critical temperature goes up and that many compounds have Boyle points much lower than a T_r of 2.5. Figure 3 is a plot of the Boyle point vs. critical temperature, prepared by consideration of the measured points wherever possible and utilization of extrapolations to higher temperatures where necessary, as just mentioned.

A characteristic of gas behavior noted on both the compressibility chart and the pressure-volume plot is the straightness of the critical isotherm for a considerable range on either side of the critical point. The length of the straight portion indicates the possibility that derivatives of pressure with respect to volume higher than the two of van der Waals may be zero or at least very small. Examination of experimental data to prove whether any derivatives higher than the second are zero is difficult, since the data are often not too accurate. The higher derivatives cannot be assumed indiscriminately either, or the essential inflection at the critical point may not be preserved.

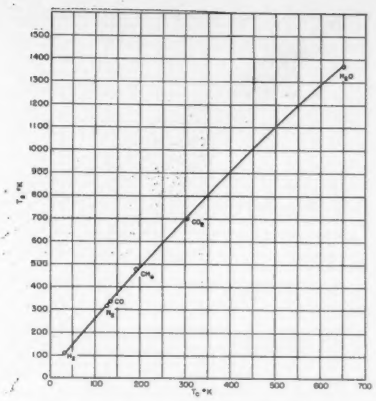

FIG. 3. T_B AS FUNCTION OF T_C.

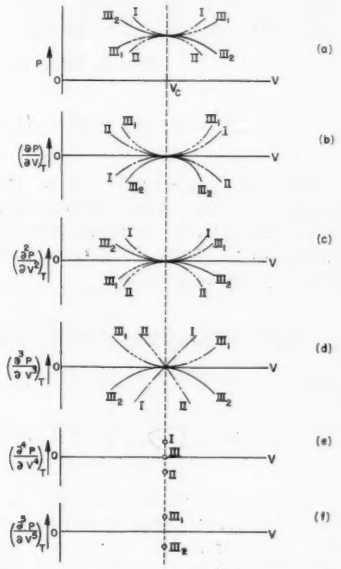

FIG. 4. PRESSURE-VOLUME DERIVATIVES WHEN $\left(\frac{\partial^3 P}{\partial V^3}\right)_T = 0$ AT CRITICAL POINT. [IT IS TAKEN FOR GRANTED THAT $\left(\frac{\partial P}{\partial V}\right)_T = 0$, AND $\left(\frac{\partial^2 P}{\partial V^2}\right)_T = 0$ AT CRITICAL POINT.]

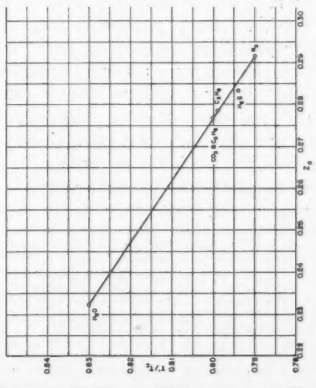

FIG. 5. T'/T_c AS FUNCTION OF Z_c.

In Figure 4 the necessary implications of the assumption that the third derivative is zero are considered. In Figure 4*d* four possible curves have been drawn, all of which go through zero according to the assumption. If the true situation is similar to curve I, the fourth derivative must be positive, as shown in Figure 4*e;* the second derivative will pass through a minimum, as shown in Figure 4*c;* the first derivative will have an inflection, as shown in Figure 4*b;* and the primary pressure vs. volume curve will exhibit a minimum, as shown in Figure 4*a*. As the primary curve must show an inflection, it is obvious that curve I cannot be correct. A similar analysis of curves II and III_1 shows that they cannot be used; however, curve III_2 does give the required character of the pressure vs. volume curve and therefore one concludes that if the third derivative is assumed to vanish, then the fourth must also vanish, as shown in Figure 4*e*, and the fifth must be negative or zero, as shown in Figure 4*f*.

Another assumption which can be made is that the fourth derivative vanishes while the third remains. An analysis similar to that above shows that for this case the third derivative must be negative in order to preserve the correct inflection at the critical point. The hypothesis which is advanced here is that in addition to the vanishing of the first two derivatives, as suggested by van der Waals, the third derivative is either zero or a small negative number and the fourth derivative is zero. Assumptions regarding the derivatives higher than the fourth might be made, but these derivatives would have much smaller effects. In current studies the fifth and sixth derivatives are being given some attention.

Another characteristic of gas behavior noted on the compressibility chart is that for compounds with different values of $Z_c (PV/RT$ at the critical point) lines which connect the critical point to the point $Z = 1.0$, $P_r = 0$ are tangent to isotherms whose reduced temperature is about 0.8. Algebraically this condition is

$$(dZ/dP_r)_{T_r} = -(1 - Z_c)$$

$$\text{at } T' \cong 0.8 T_c \quad (8)$$

The meager data available indicate that T' varies slightly from

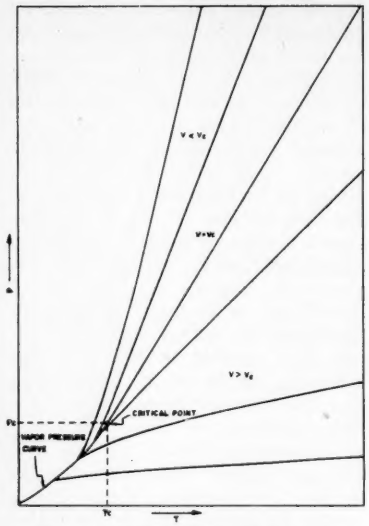

FIG. 6. PRESSURE-TEMPERATURE DIAGRAM.

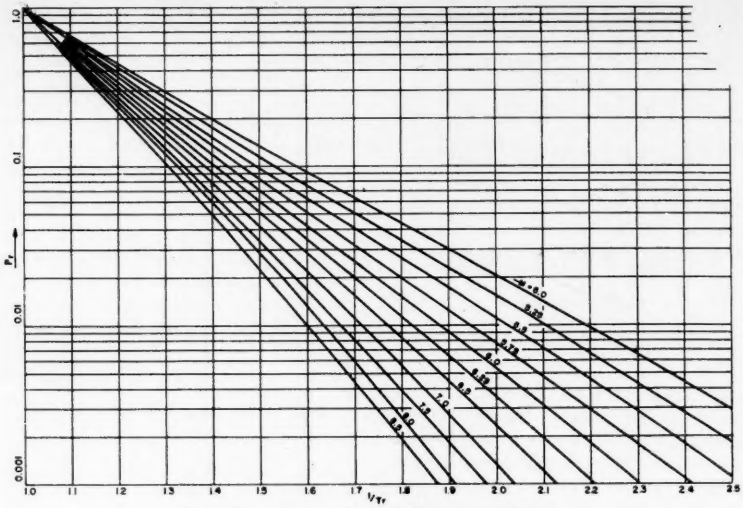

FIG. 7. REDUCED VAPOR-PRESSURE PLOT.

0.8 according to the value of Z_c. Figure 5 is a plot of the relation between T' and Z_c, and it is seen that were it not for the low Z_c of water, it would be difficult to draw any curve. Of course, there are other compounds with low Z_c's, but their data at a T_r of 0.8 are insufficient to warrant their use.

There are other characteristics of gas behavior indicated on the compressibility chart that seem to be of lesser importance than those previously mentioned. Some isotherms not only go through a minimum point but also exhibit inflections, notably those between a T_r of 1.0 and about 1.3. Isotherms above the Boyle point are almost straight. The compressibility factor is approximately 1.1 to 1.2 for all isotherms at a reduced pressure of about 10. Although these conditions are not utilized in this paper for the obtaining of an equation of state, they have been given some consideration.

Another important diagram of PVT data is the pressure-temperature (isometric) plot shown in Figure 6. The most important fact noted here is that the isometrics are almost straight. In fact there are three places where the lines can be considered straight: one is for large volumes at low pressures, another is for the critical volume, and the third is for all volumes at high temperatures. The three conditions can be expressed as

$$(d^2P/dT^2)_V = 0 \text{ as } P \longrightarrow 0 \quad (9)$$

$$(d^2P/dT^2)_V = 0 \text{ at } V = V_c \quad (10)$$

$$(d^2P/dT^2)_V = 0 \text{ for high } T \quad (11)$$

Also the isometrics below the critical density curve down, and those above the critical density curve up.* These conditions are given by the equations

$$(d^2P/dT^2)_V < 0 \text{ at } V > V_c \quad (12)$$

and

$$(d^2P/dT^2)_V > 0 \text{ at } V < V_c \quad (13)$$

A final observation on the isometric chart is that the slope of the vapor-pressure curve at the critical point is identical with the slope of the critical-density isometric. The experimental verification of this fact is difficult because the slope of the vapor-pressure curve is changing very rapidly. Usually the slope obtained by differentiating a vapor-pressure equation at the critical point is slightly less than the slope of the critical isometric. This may be attributed to the fact that in many cases the vapor-pressure equation may not reflect the slight upward curvature of the vapor-pressure curve on a log P vs. $1/T$ plot in the region near the critical, as emphasized by Thodos (*23*). Also the critical volume is difficult to determine accurately, and any error in its value would result in an error in its slope. From a thermodynamic point of view, the equality of the slope of the vapor-pressure curve and the critical isometric has been justified by the following analysis. From the Clapeyron equation the slope of the vapor-pressure curve is $dP/dT = \Delta S/\Delta V$ at any temperature. At the critical point $\Delta S/\Delta V$ becomes $(dS/dV)_T$, but from the Maxwell relation this is $(dP/dT)_{V_c}$. Therefore, the vapor pressure slope $dP/dT = (dP/dT)_{V_c}$, which is the desired equality.

Another important graph is the reduced-vapor-pressure plot of log P_r vs. $1/T_r$, as shown in Figure 7. The different curves are for a number of different compounds. Implication of the plot is that if two compounds fall on the same curve at any point, they tend to lie together over the whole range of temperature. The plot is extremely useful in filling in unexplored ranges of vapor pressure, provided that the critical temperature and pressure and one other point on the vapor-pressure curve are known. The plot is also useful for predicting the slope of the vapor-pressure curve at the critical point. Each curve approaches the critical point $(T_r = 1, P_r = 1)$ with a unique slope, $d \log P_r/d(1/T_r)$. This is called M and is designated on each curve. If a compound is known to follow one of the curves, then M is known. From this $(dP/dT)_{V_c}$ may be obtained as follows:

$$dP_r/P_r = -M dT_r/T_r^2 \quad (14)$$

from the definition of M. Since P_r and T_r are both 1,

$$dP_r/dT_r = -M \quad (15)$$

*Data on hydrogen indicate that the isometrics above the critical density may curve up for a while, but at the highest reduced temperatures they start to curve down. Since these high reduced temperatures are not encountered with other compounds, the negative curvature of all isometrics at such high temperatures is not important. Also at very high densities indications are that all isometrics curve down for all reduced temperatures. This means that at some very high density the isometrics for moderate temperatures are straight.

or from the definitions of P_r and T_r,

$$dP/dT = -MP_c/T_c = (dP/dT)_{V_c} = m \quad (16)$$

This fact is of great value because it means that vapor pressure determines the *PVT* behavior along the critical isometric.

A study of the interdependency of the characteristic properties of gases, as here presented, has led to a consideration of the minimum number of conditions or facts necessary to characterize the *PVT* behavior of any given compound. A new hypothesis is advanced that four properties are necessary to give the complete characterization for any compound. These are the critical temperature, critical pressure, critical volume, and one point on the vapor-pressure curve. The one point on the vapor-pressure curve determines the slope m of the critical isometric, as given above. Mathematically this hypothesis is written as

$$f(P, V, T, P_c, T_c, V_c, m) = 0 \quad (17)$$

or in terms of Z_c,

$$f(P, V, T, P_c, T_c, Z_c, m) = 0 \quad (18)$$

If this hypothesis is compared with previous work, it is seen that it is not so simple as van der Waals', which states that the compressibility is dependent only upon the critical temperature and pressure, or as that which says that the critical temperature, pressure, and volume determine the compressibility; however, accurate data show that neither of these latter hypotheses is correct.

It is the primary objective of this work to develop an equation which will represent the function implied by Equations (17) and (18). One might also develop graphical representations of those equations, which could be in the form of compressibility plots (Z vs. P_r with T_r as a parameter) for various values of Z_c, T_c, and M. Probably a number of plots would be required to cover the widest ranges, but such plots might prove sufficiently useful to justify their preparation. Part II considers only the equation and not the graphs.

II. Derivation of the Equation

Although there have been a number of attempts to develop an equation of state from kinetic theory and statistical mechanics, only token results have been obtained to date. The important practical equations which are in use today, such as the Benedict, Webb, and Rubin (*5*) and the Beattie and Bridgeman (*1*), are empirical. The equation about to be developed is also empirical; however, it is believed that this equation fits more of the known behavior characteristics of gases than does any previous equation.

The form of equation representing empirically the *PVT* behavior is chosen so that the data are represented as nearly as possible within the precision of the experiment. The equation should also be reasonably simple in order to be useful in thermodynamic calculations. Obviously, more terms may be put into an equation to get better agreement with the data, but complexity is the penalty. In this study various polynomial and exponential equations were considered. In view of the fact that it is the derivatives of pressure which are given by the van der Waals analysis and that pressure is almost a linear function of temperature at constant volume, equations explicit in pressure were preferred.

Because of its symmetry and the ease of differentiation and integration, the following equation was chosen over the others:

$$P = f_1/(V-b) + f_2/(V-b)^2 + f_3/(V-b)^3 + f_4/(V-b)^4 + f_5/(V-b)^5 \quad (19)$$

where f's are functions of temperature and b is a constant.

In choosing the temperature functions for Equation (19), one first considers the character of the isometrics of Figure 6. Since these are straight at the high-temperature ends and curve only at the low ends near the saturation curve, any equation to represent the isometrics must become linear at high temperatures. Beattie and Bridgeman (*1*) suggested the form

$$P = A + BT + C/T^2 \quad (20)$$

where A, B, and C are functions of volume. Benedict, Webb, and Rubin employed the same form. The last term, which is the curvature term, was considered carefully in the more general form C/T^n. It was found that to represent the experimental data for many different compounds n varied from about 2 to 5, depending largely upon the critical temperature of the substance in question. For most compounds with critical temperatures near room temperature n was about 3, and for compounds with high critical temperatures, such as water, n was about 5. In view of this variation, a different form of equation was selected:

$$P = A + BT + Ce^{-kT/T_c} \quad (21)$$

Equation (21) was found to represent the curvature of isometrics of many different compounds with only one value of k, this value being 5.475. (This could be rounded off, but as with other constants will be carried to preserve internal consistency.) If Equation (21) is compared with Equation (19), it is seen that the temperature functions, f_1 to f_5, must be of the form

$$f_1 = A_1 + B_1T + C_1e^{-5.475T/T_c}$$

$$f_2 = A_2 + B_2T + C_2e^{-5.475T/T_c}$$

etc. (22)

where A_1, B_1, C_1, A_2, etc., are constants which may be finite or zero. Thus, with the selection of the complete form of the equation of state through Equations (19) and (22), the problem now is to find a method of evaluating the constants.

By virtue of the hypothesis given in Part I that the *PVT* behavior of a given compound depends only upon P_c, T_c, V_c, and m, one must have recourse to the general properties of gas behavior to see just how many arbitrary constants can be determined. The general properties to be used are restated in the following summary:

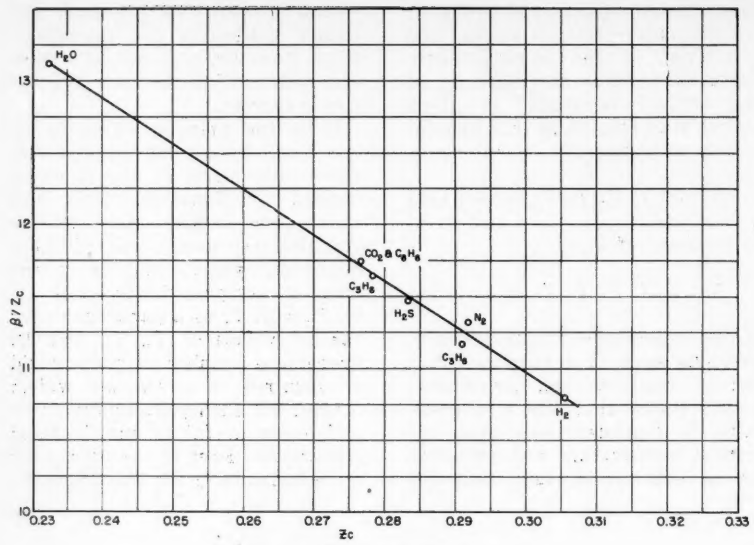

FIG. 8. β/Z_c AS FUNCTION OF Z_c.

$$PV = RT \text{ as } P \rightarrow 0 \quad (23)$$

$$(dP/dV)_T = 0 \text{ at critical} \quad (24)$$

$$(d^2P/dV^2)_T = 0 \text{ at critical} \quad (25)$$

$$(d^3P/dV^3)_T = 0 \text{ at critical} \quad (26)$$

$$(d^4P/dV^4)_T = 0 \text{ at critical} \quad (27)$$

$$\left[(dZ/dP_r)_{T_r}\right]_{P_r=0} = -(1-Z_c) \text{ at } T' \cong 0.8T_c \quad (28)$$

$$\left(dZ/dP_r\right)_{T_r}\Big]_{P_r=0} = 0 \text{ at Boyle-point temperature } T_B \quad (29)$$

$$(d^2P/dT^2)_V = 0 \text{ at } V = V_c \quad (30)$$

$$(dP/dT)_V = m = -MP_c/T_c \text{ at } V = V_c \quad (31)$$

By use of the foregoing nine conditions plus the PVT relation at the critical point (since P_c, T_c, and V_c are to be given) determination of an equation of state with ten arbitrary constants might be expected. Equation (26) however is not determinate as it stands, and so a total of only nine constants can be obtained from the conditions listed.

Equation (23) is utilized by multiplying through Equation (19) by V-b and letting P approach zero while V, and therefore V-b, approaches infinity:

$$PV = f_1 \text{ as } P \rightarrow 0 \quad (32)$$

and in the light of Equation (23),

$$f_1 = RT \quad (33)$$

The equation of state now becomes

$$P = RT/(V-b) + f_2/(V-b)^2 + f_3/(V-b)^3 + f_4/(V-b)^4 + f_5/(V-b)^5 \quad (34)$$

Next are employed the four derivative conditions, (24) to (27), and the condition that the equation of state must be satisfied at the critical point. There are five equations containing five unknowns, $f_2(T_c)$ through $f_5(T_c)$, and b, where $f(T_c)$ means the temperature function evaluated at the critical temperature. However, Equation (26) cannot be used directly until the inequality is removed. The solution of the remaining four equations in terms of b is

$$f_2(T_c) = 9P_c(V_c-b)^2 - 3.8RT_c(V_c-b) \quad (35)$$

$$f_3(T_c) = 5.4RT_c(V_c-b)^2 - 17P_c(V_c-b)^3 \quad (36)$$

$$f_4(T_c) = 12P_c(V_c-b)^4 - 3.4RT_c(V_c-b)^3 \quad (37)$$

$$f_5(T_c) = 0.8RT_c(V_c-b)^4 - 3P_c(V_c-b)^5 \quad (38)$$

If $(d^3P/dV^3)_T$ in Equation (26) is assumed to be zero, Equations (35) through (38) may be substituted into Equation (26) to determine b as*

$$b = V_c - 3RT_c/15P_c \quad (39)$$

or in terms of Z_c,

$$b = V_c - 3V_c/15Z_c \quad (40)$$

The equation of state is now determined along the critical isotherm; however, a comparison of the equation with the data for a number of different gases showed that the equation predicted pressures too high for volumes greater than the critical volume. Previous comparisons using only the two van der Waals derivatives and a correspondingly shorter equation of state (i.e., one terminating at f_4 and with $b = 0$) showed that pressures in this region were predicted too low. In another trial the third derivative condition was completely neglected when an equation terminating with f_4, but otherwise the same as Equation (19), was utilized. This implies that f_5 is arbitrarily set equal to zero; therefore, from Equation (38),

$$b = V_c - 4RT_c/15P_c = V_c - 4V_c/15Z_c \quad (41)$$

This assumption predicted pressures too low; therefore, some in-

*Sometime after working out the analysis of the derivatives at the critical point, it was found that Plank and Joffe (*20, 11*) had studied equations similar to Equation (19). They assumed five equal roots at the critical point, which is the same as assuming the first four derivatives to be zero. This equality may be shown by considering the meaning of five equal roots at the critical point. Let P be a function of V, with five equal roots at the critical point. Then $P = f(V)$ at $T = T_c$ and $P - P_c = f(V) - P_c$. At $P = P_c$ the $f(V) - P_c$ must be zero, and because of the equality of five roots this must be equivalent to another function $F(V)(V-V_c)^5$ set equal to zero or $P - P_c = F(V)(V-V_c)^5$, where $F(V_c) \neq 0$. Differentiating with respect to V gives

$$dP/dV = 5(V-V_c)^4 F(V) + (V-V_c)^5 F'(V)$$

Since $V = V_c$, this is zero. Carrying on three more differentiations will continue to give factors of $V - V_c$, which will cause the derivatives to vanish, until one comes to the fifth derivative, where at least one term will not have $V - V_c$, i.e., $120F(V)$. Then the derivative is not zero.

termediate value between Equations (40) and (41) is required. For this purpose let

$$b = V_c - \beta V_c/15Z_c \qquad (42)$$

where β is a constant for a given compound. It can be shown that β cannot be less than 3.0 or more than 4.0.

By trial with the data of a number of different compounds along the critical temperature line, it was found that β depended upon Z_c. Use of the varying values of β permitted very accurate representation of the data up to densities about 1.5 times the critical density.

Figure 8 is a plot which gives β as a function of Z_c*.

Since one of the original ten conditions was used to evaluate f_1 as RT and since one condition was indeterminate but can be satisfied by setting the magnitude of the third pressure-volume derivative through the term β, there are eight conditions left to evaluate the temperature functions f_2 to f_5. Each temperature function may contain a maximum of three constants, A, B, and C, and so a total of twelve constants must be fixed. In view of the eight conditions, four constants must be set equal to zero. As mentioned earlier, more conditions might be utilized, in which case all twelve constants might be finite. However, it has been found that some constants are much less important than others and that dropping four of them still leaves an equation which represents the data with a high order of accuracy.

When the eight constants to remain in the temperature functions were chosen, it was felt that the slope constants, B, and the intercept constants, A, were most important, the curvature constants, C, being of less significance. In order to apply Equation (30), however, it is necessary that there be at least two C terms in the equation. The six constants left were divided equally between A's and B's. The following was decided upon as being at least as good as any other arrangement:

$$f_1 = RT \qquad (43)$$

$$f_2 = A_2 + B_2T + C_2e^{-5.475T_r} \qquad (44)$$

$$f_3 = A_3 + B_3T + C_3e^{-5.475T_r} \qquad (45)$$

$$f_4 = A_4 \qquad (46)$$

$$f_5 = B_5T \qquad (47)$$

The problem of evaluating these eight constants is now mathematical manipulation of the eight conditions. From Equation (46) f_4 is a constant independent of temperature and directly equal to A_4. Therefore, from Equation (37),

$$A_4 = f_4(T_c) = 12P_c(V_c-b)^4 - 3.4RT_c(V_c-b)^3 \qquad (48)$$

Since Equation (47) sets $f_5 = B_5T$, $f_5(T_c) = B_5T_c$ and from Equation (38),

$$B_5 = f_5(T_c)/T_c = 0.8R(V_c-b)_4 - 3P_c(V_c-b)^5/T_c \qquad (49)$$

The derivation of the remaining six constants is a little more involved. Starting with Equation (19), one multiplies through by $V-b$, substitutes $PV = ZRT$ to eliminate variable V, and then differentiates partially with respect to pressure at constant temperature, to obtain

$$\begin{aligned}(dZ/dP)_TRT-b = &\left\{(ZRT-bP)f_2 - f_2P[(dZ/dP)_TRT-b]\right\}/(ZRT-bP)^2 \\ &+\left\{(ZRT-bP)f_3P(2) - 2f_3P^2[(dZ/dP)_TRT-b]\right\}/(ZRT-bP)^3 \\ &+\left\{(ZRT-bP)f_4P^2(3) - 3f_4P^3[(dZ/dP)_TRT-b]\right\}/(ZRT-bP)^4 \\ &+\left\{(ZRT-bP)f_5P^3(4) - 4f_5P^4[(dZ/dP)_TRT-b]\right\}/ZRT-bP)^5\end{aligned} \qquad (50)$$

Since at $P_r = 0$, $Z = 1.0$, Equation (50) simplifies to

$$f_2 = \left\{\left[(dZ/dP_r)_{P_r=0}\right](RT)^2/P_c\right\} - bRT \qquad (51)$$

Combining Equations (28) and (51) at $T_r = T'/T_c$ gives

$$f_2(T') = A_2 + B_2T' + C_2e^{-5.475T'/T_c} = [(RT')^2(Z_c-1)/P_c] - bRT' \qquad (52)$$

From Equation (29) $[(dZ/dP_r)_T]_{T=T_B,\ P_r=0} = 0$, and inserting this into Equation (51) gives

$$f_2(T_B) = A_2 + B_2T_B + C_2e^{-5.475T_B/T_c} = -bRT_B \qquad (53)$$

Equations (52) and (53) with

$$f_2(T_c) = A_2 + B_2T_c + C_2e^{-5.475} \qquad (54)$$

which is known by Equation (35) in terms of P_c, T_c, V_c, and b, form a set of simultaneous equations with three unknowns, A_2, B_2, and C_2. The solution of this set of simultaneous equations is

$$C_2 = \frac{[f_2(T_c)+bRT'+(RT')^2(1-Z_c)/P_c](T_B-T_c)+[f_2(T_c)+bRT_B](T_c-T')}{(T_B-T_c)\left\{e^{-5.475}-e^{-5.475T'/T_c}\right\}-(T_c-T')\left\{e^{-5.475T_B/T_c}-e^{-5.475}\right\}} \qquad (55)$$

$$B_2 = [-f_2(T_c) - bRT_B - C_2(e^{-5.475T_B/T_c}-e^{-5.475})]/(T_B-T_c) \qquad (56)$$

$$A_2 = f_2(T_c) - B_2T_c - C_2e^{-5.475} \qquad (57)$$

Substituting Equations (43) to (47) into Equation (19), rearranging in the form of Equation (21), and differentiating twice with respect to volume give, by use of Equation (30),

$$C_3 = -C_2(V_c-b) \qquad (58)$$

Applying Equations (31) and (58) gives

$$B_3 = m(V_c-b)^3 - R(V_c-b)^2 - B_2(V_c-b) - B_5/(V_c-b)^2 \qquad (59)$$

From Equation (45), with $T = T_c$, one obtains

$$A_3 = f_3(T_c) - B_3T_c - C_3e^{-5.475} \qquad (60)$$

This now completes the solution for all the constants in the equation of state. If the critical temperature, critical pressure, critical volume, and one point on the vapor-pressure curve are known for a given compound, appropriate graphs will give slope m of the critical isometric; the Boyle point, T_B; the T' point (about $0.8T_c$); and β, the determinant of the value of the third derivative of pressure

*It will be noted on Figure 8 that β never exceeds a value of 3.35 for the gases which have been studied so far. One might wonder about the nature of the five roots of the equation at the critical point for β lying between 3.0 and 3.35, since for $\beta = 3.0$, it has been shown that the five roots are equal. Further analysis shows that there are three real equal roots and two complex roots for β greater than 3.0 and less than 3.5.

with respect to volume at the critical point.

When gases were chosen to test the new equation, two considerations were paramount: first, the *PVT* data for any gas had to be fairly complete and accurate, and, second, the gases had to be as different as possible. Seven gases have been studied so far, and it is felt that the selection of CO_2, H_2O, C_6H_6, N_2, C_3H_6, H_2S, and C_3H_8 is sufficiently broad to test the versatility of the equation. The application of this new equation of state will be discussed and the calculated results for the seven gases studied will be presented in Part III.

III. Application and Discussion of the Equation

In the two foregoing parts of this paper *PVT* behavior of gases is considered in some detail and appropriate algebraic equations are given to represent that behavior. A new hypothesis is stated concerning the minimum amount of information necessary to characterize any given gas and an equation of state with nine constants is developed which requires only the minimum information according to the hypothesis for evaluation of the constants. This equation has been applied to seven different gases within a maximum error of 1%, and usually much less, for densities up to about 1.5 times the critical density.* Table 1 gives the constants that were calculated from the required P_c, T_c V_c, and m information for each of the gases. Tables have been made of comparisons of the pressures predicted from the equation of state with the experimentally measured pressures reported in the literature.

The points which are compared in these tables have been selected at places where the equation would represent the data least well. It is probable that the average deviation for the equation if compared at regularly spaced intervals over all ranges of temperature and pressure would be less than the average of the deviations listed in the tables. which is about 0.4%.

The precision of experimental data was important in the equation of state at almost every turn in its development. It was necessary in many cases to decide which data points of different investigators and which data points in different ranges were the most reliable, an especially necessary decision because of the desire to hold the maximum deviation under 1%. Data taken in the region of the critical point are more inconsistent than those from anywhere else. This reflects the inherent experimental difficulties in this region. The critical volume is the most unreliable measurement, and it is not uncommon to find differences of 5% in this value. Naturally slope m inherits any error in the determination of critical volume when fitting the equation to specific data is attempted.

The procedures used in developing the equation of state might well be of value in helping to determine a better value of critical volume. Usually this value is not measured experimentally but is determined by a rectilinear diameter plot, wherein the mean saturated liquid and vapor density is extrapolated to the critical temperature, which has been determined by disappearance of the meniscus. Another procedure which has been used is to determine the critical temperature as the lowest temperature at which a measured pressure-volume line undergoes a smooth inflection, the point of the inflection being the critical volume. These

TABLE 1.—CONSTANTS EVALUATED FOR THE EQUATION

	CO_2	H_2O	C_6H_6	N_2	C_3H_6	H_2S	C_3H_8
T_c	547.5°R.	1165.1°R.	562.66°K.	126.1°K.	364.92°K.	672.4°R.	666°R.
P_c	1069.4 lb./sq. in.	32062 lb./sq. in.	48.7 atm.	33.5 atm.	45.61 atm.	1,306.0 lb./sq. in.	618 lb./sq. in.
V_c	0.03454 cu. ft/lb.	0.0503 cu. ft./lb.	3.36 cc./g.	90.1 cc./g. mole	0.191 liter/g. mole	1.565 cu. ft./lb. mole	3.220 cu. ft./lb. mole
Z_c	0.27671	0.23246	0.27683	0.29171	0.290932	0.28329	0.278465
m	14.0	22.6	0.625	1.647	0.81	12.8	6.47
β	3.25	3.05	3.25	3.30*	3.25	3.25	3.25
T_B/T_c	2.3	2.1	2.15	2.5	2.3	2.3	2.3
T'/T_c	0.80	0.83	0.80	0.79	0.791	0.794	0.799
b	0.007495	0.0063101	0.730231	22.1466*	0.0487575	0.368095	0.714598
R	0.24381	0.59545	1.05052	82.055	0.082055	10.73	10.73
A_2	−8.9273631	−85.7394396	−4104.138	−1592238.2	−10.2233898	−21206.0776	−44105.1544
B_2	0.005262476	0.0312961744	2.62510	3,221.616	0.0081804454	9.7631723	21.127023
C_2	−150.97587	−2590.5815	−59333.234	−22,350,930	−153.061055	−318,608.803	−736,929.321
A_3	0.18907819	3.09248249	8553.304	89,845,367	1.219453756	21133.013	88,025.6002
B_3	−0.0000704617	−0.00082418321	−3.89165685	−134,024.05	0.00074168283	−7.41557245	−28.1649342
C_3	+0.0831424	113.95968	156032.7	1,518,821,653	21.7717909	381,344.629	1,846,304.2
A_4	−0.002112459	−0.0567185967	−8599.2791	−2,467,297,480	−0.068940713	−9897.9772	−89,907.6635
B_4	1.9565593×10^{-8}	4.2388378×10^{-7}	7.53651	244,915,183	5.0385878×10^{-8}	3.3036675	63.416365

All the constants for the equation of state are given in units of T_c, P_c, and V_c for that compound.

*β for N_2 could be 3.25 depending upon the manner by which the checked points on the critical isotherm are interpolated from experimental data reported.

*Calculations performed after the writing of this paper indicate that at about one and one half times the critical density the equation predicts too much curvature of the isometrics. It has been found that this may be improved by adding a C_5 term to the equation and utilizing the condition stated in the first paper, that at some very high density (approximately twice the critical density) the isometric is straight. With this condition the only changes in the equations for the constants are

$$C_3 = \frac{C_2\left[(V_c-b)^3 - \left(\frac{V_c}{n}-b\right)^3\right]}{\left[\left(\frac{V_c}{n}-b\right)^2 - (V_c-b)^2\right]}$$

$$C_5 = -C_2(V_c-b)^3 - C_3(V_c-b)^2$$

$$B_5 = \frac{f_5(T_c) - C_5 e^{-5.475}}{T_c}$$

Here n is approximately 2.

procedures do not agree too well in many cases, and two alternatives are suggested here. First, one can plot the vapor-pressure data on Figure 7 to determine slope m. Then referring to the experimental data, he can establish the critical volume as that volume whose slope agrees with the m so selected. This, of course, means that he is relying on the inherent accuracy of the slopes of the generalized vapor-pressure curves. An alternative to this is to differentiate the vapor-pressure curve directly for the compound and use that slope m as the determining factor in picking the critical volume. However, as mentioned in the first paper, this must be done with care for often the slight increase in the slope of the vapor-pressure curve near the critical is overlooked. Second, one may fix the critical volume by fitting the data points on the critical isotherm as in step 5 in the procedure, which will be described later, for obtaining an equation of state to fit data. When the best possible fit of the critical isotherm has been obtained by adjusting the critical volume and β, one may say that the critical volume has been determined by analytical means. This is equivalent to fixing the critical volume by a study of graphs of the isotherms and noting the lowest temperature and point at which a pressure-volume line undergoes a smooth inflection.

The Boyle-point temperature is worthy of further discussion in this work. In the estimation of Boyle points for most compounds, the procedure was simply to extrapolate a large volume isometric to the point where $Z = PV/RT = 1$. This has two drawbacks: first, the extrapolated isometric instead of being straight may have a slight negative curvature, which will be important when the extrapolation is carried over a wide range of temperature; second, the Boyle point should be determined at zero pressure. It is seen on the compressibility chart, however, that the Boyle-point isotherm follows $Z = 1$ up to fairly appreciable pressures, so that the procedure seems justified. Furthermore, as the equation is not very sensitive to the Boyle point except at high temperatures, it seems that Figure 3, which correlates these extrapolated Boyle points with the critical temperature, is sufficiently accurate for most purposes.

As better critical data become available, it is expected that some of the correlations will change. Possibly new ones will be developed; for example, even now there is a tendency for the reduced slope M of the critical isometric to be a function of Z_c. Several compounds seem to fall out of line, but if future experimental work were to change some of the critical values for these compounds the correlation might be good.

In general it is claimed that the equation reproduces the experimental data within 1% up to densities of about 1.5 times the critical density and up to temperatures of about 1.5 times the critical temperature. At about 1.5 times the critical density the isotherms become so steep that a 1% error in volume may cause 5% or more error in pressure. Therefore, it is not to be expected that the equation will predict closely above 1.5 times the critical density. This region, which is really the compressed-liquid region, has been given some consideration, and it is believed that to represent it properly either the term b in the equation will have to become a function of volume or more terms will have to be added to the equation. That b might change with volume seems reasonable when one recalls that the b in van der Waals' equation accounts for the effective volume of the molecules themselves, and the effective volume of the molecules might become smaller as the gas is compressed. This is, in fact, the direction of the necessary change in b to get agreement at very high densities, for the equation at present tends to predict pressures too high. Decreasing b will increase the denominators of the higher power positive terms and thus decrease the pressure.

An interesting application of the question is contemplated for mixtures. Ordinarily when one wishes to get an equation of state for mixtures, he averages the constants in the equation of state for the pure gases involved according to some method of averaging such as arithmetical mean or geometrical mean. This process may be applied to the proposed equation; however, an alternate process is permitted here. The fundamental constants that determine the equation, P_c, T_c, V_c, and m, may be averaged at the start and the equation of state for the mixture determined by the same process as would be used for a pure component. It is expected to try this out in the near future.

Comparison of this equation with other equations has been deliberately avoided, largely because of the misinterpretation of the term *average deviation*. Although it may be generally accepted that the average deviation of the Beattie-Bridgeman and Benedict-Webb-Rubin equations is 0.18 and 0.34% respectively (*7, 10*), experience in applying the equations within the density limits claimed showed these values to be misleading, because deviations over 1% were found in certain places. Therefore, this work did not try to compare different equations but tried to determine maximum errors between the equation proposed and the data.

This new equation is valuable when applied to a compound whose experimental data are limited to only the critical temperature, pressure, and volume and one point on the vapor-pressure curve. Table 2 gives a summary of the formulas for evaluation of the constants in the equation of state, together with the procedure for application to any gas for which the P_c, T_c, V_c, and m can be obtained.

Another situation often arises when it is desired to fit an equation of state to a rather complete set of PVT data for a specific compound. The procedure of application can be modified. Of course, to start, one may obtain the equation by using only the P_c, T_c, V_c, and m; however, it is possible that a better fit may be obtained by utilizing all the data in the following procedure:

1. Select the best values of P_c, T_c, V_c, as would be done when the generalized equation, is developed.
2. Calculate Z_c and read off from Figure 8 a value of β/Z_c *or* $\beta = -31.883Z^2_c + 20.533Z_c$.
3. Calculate the temperature functions along the critical isotherm, i.e., $f_2(T_c)$, $f_3(T_c)$, etc.
4. With the equation established from 3, at the critical temperature calculate a series of pressures for different densities along this isotherm. The maximum density to which this calculation should be carried should not exceed about 1.5 times the critical density, as above this density it is known that the error becomes large.
5. If the agreement of the calculated and experimentally measured pressures is not considered satisfactory in step 4 (it ought to be within 1% if the data are reliable), it is likely that an improvement can be made by adjusting V_c and β. This may not seem quite right to adjust a data point such as V_c to get an equation of state; however, usually V_c cannot be determined experimentally with a very high degree of accuracy and it is quite possible that the value first chosen is somewhat in error. As usually the critical temperature and pressure are known with greater precision than the critical volume, it

TABLE 2.—SUMMARY OF THE FORMULAS AND PROCEDURES FOR EVALUATING THE ARBITRARY CONSTANTS IN THE EQUATION OF STATE

Equation of state

$$P=\frac{RT}{V-b}+\frac{A_2+B_2T+C_2e^{-5.475T/T_c}}{(V-b)^2}+\frac{A_3+B_3T+C_3e^{-5.475T/T_c}}{(V-b)^3}$$

$$+\frac{A_4}{(V-b)^4}+\frac{B_5T}{(V-b)^5}$$

Formulas (in order of evaluation)

$$b = V_c - \frac{\beta V_c}{15Z_c} \text{ where } Z_c = \frac{P_cV_c}{RT_c} \quad (42)$$

$$f_2(T_c)=9P_c(V_c-b)^2-3.8RT_c(V_c-b) \quad (35)$$

$$f_3(T_c) = 5.4RT_c(V_c-b)^2 - 17P_c(V_c-b)^3 \quad (36)$$

$$f_4(T_c) = 12P_c(V_c-b)^4 - 3.4RT_c(V_c-b)^3 \quad (37)$$

$$f_5(T_c) = 0.8RT_c(V_c-b)^4 - 3P_c(V_c-b)^5 \quad (38)$$

$$C_3 = -(V_c-b)C_2 \quad (58)$$

$$A_2 = f_2(T_c) - B_2T_c - C_2e^{-5.475} \quad (57)$$

$$A_4 = f_4(T_c) \quad (48)$$

$$B_5 = \frac{f_5(T_c)}{T_c} \quad (49)$$

$$B_3 = m(V_c-b)^3 - R(V_c-b)^2 - B_2(V_c-b) - \frac{B_5}{(V_c-b)_2} \quad (59)$$

$$A_3 = f_3(T_c) - B_3T_c - C_3e^{-5.475} \quad (60)$$

$$= \frac{[f_2(T_c)+bRT'+\frac{(RT')^2}{P_c}(1-Z_c)](T_B-T_c)+[f_2(T_c)+bRT_B](T_c-T')}{(T_B-T_c)(e^{-5.475}-e^{-5.475\,T'/T_c})-(T_c-T')(e^{-5.475\,T_B/T_c}-e^{-5.475})} \quad (55)$$

$$B_2 = \frac{-f_2(T_c) - bRT_B - C_2(e^{-5.475\,T_B/T_c}-e^{-5.475})}{T_B-T_c} \quad (56)$$

Procedure for application of the foregoing formulas to obtain the equation of state for a given compound

1. Select the best values of T_c, P_c and V_c. In case any of these are not known or are in doubt, refer to Hougen and Watson (*10*) for procedures for estimating.
2. Calculate $Z_c = P_cV_c/RT_c$.
3. Read off the Boyle temperature T_B from Figure 3.
4. Read off the T' temperature from Figure 5, or $\frac{T_c}{T'} = -0.6751Z_c + 0.9869$.
5. Read off the third derivative characteristic β from Figure 8, or $\beta = -31.883Z_c^2 + 20.533Z_c$.
6. Calculate the reduced temperature and pressure of a vapor-pressure point and place on Figure 7. By interpolation estimate the value of M. and from this calculate $dp/dT = m = -MP_c/T_c$.
7. With P_c, T_c, V_c, m, T_B, T', and β now fixed, substitute in the foregoing formulas.

is not recommended that these be changed unless the experimental values have been determined or presented with a considerable lack of precision. Also as V_c is changed, the value of Z_c will change and a different β will be predicted from Figure 8. One need not limit the values of β to this graph, however, for if the selection of another β value which does not fit the graph will give a better fit of the data, that is the one to use. From the nature of the equation β must lie between 3 and 4 to retain the correct inflection at the critical point. As a guide in predicting the effects of adjusting β and V_c, it has been found by trial that increasing β tends to decrease all pressures on the critical isotherm except at the critical point itself; whereas, increasing V_c tends to increase all pressures on the critical isotherm.

6. When the critical isotherm is represented accurately by the equation, read off a value of T_B and T'/T_c from Figures 3 and 5, or $T'/T_c = -0.6751Z_c + 0.9869$
7. Obtain slope m by reference to the data for the critical isometric. Usually this can be done easily by reading off one high temperature point on the critical isometric and calculating $m = (P-P_c)/(T-T_c)$.
8. Evaluate all the constants in the temperature functions so that the equation is completely determined.
9. Calculate a few points at high temperatures and low temperatures (near the saturation curve) for several isometrics, the latter being taken for example at densities about 25% greater than the critical density, about two thirds the critical density, about one quarter the critical density, and about one tenth or one twentieth the critical density. Of course, the exact densities will be those available from the data.
10. If the calculated points do not agree with the data with the desired degree of precision, the values of m, T_B, and T' may be adjusted. The effect of changing these values is approximately as follows. Increasing m increases the pressure at higher temperatures for densities near the critical. Increasing the Boyle temperature T_B decreases the pressure at higher temperatures for low densities. Increasing T' increases the pressure at higher temperature for medium densities at about half the critical density while it decreases the pressure for temperatures near the saturation curve. There is one other parameter which may be changed in the equation, the constant in the exponential term, which is given as 5.475, but it might be shifted a little in a particular case. In general increasing this constant has about the same effect as increasing T'.
11. It is good practice to check on the calculation of the constants by substituting V_c into the equation obtained at the end of step 3 to see whether it produces the critical pressure. The procedure should be re-

peated at the end of step 8. These are not considered complete checks on the work, but they reveal most of the errors which might be introduced into the calculations.

In conclusion the new equation should have some value where one wishes accurate PVT representation from a minimum of data or where one wishes to represent some data with an empirical equation. Even at this time the equation is being employed to calculate the thermodynamic properties of a compound for which the PVT data are meager. The equation permits all the usual differentiations and integrations required for such thermodynamic treatment. For example, the changes in enthalpy and entropy may be given in terms of the ideal-gas heat capacities and the equation of state.

$$\Delta H = \int_{T_1}^{T_2} C_v^o\, dT + \Bigg| PV + \frac{A_2 + \left(1 + \frac{5.475T}{T_c}\right) C_2\, e^{-5.475T/T_c}}{(V-b)} + \frac{A_3 + \left(1+\frac{5.475T}{T_c}\right) C_3\, e^{-5.475T/T_c}}{2\,(V-b)^2} + \frac{A_4}{3\,(V-b)^3} \Bigg|_{V_1,\,T_1}^{V_2,\,T_2} \qquad (61)$$

and

$$\Delta S = \int_{T_1}^{T_2} C_v^o\, dT + \Bigg| R \ln (V-b) - \frac{B_2}{V-b} - \frac{B_3}{2\,(V-b)^2} + \left(\frac{C_2}{V-b} + \frac{C_3}{2\,(V-b)^2}\right) \left(\frac{5.475}{T_c}\right) e^{-5.475\,T/T_c} \Bigg|_{V_1,\,T_1}^{V_2,\,T_2} \qquad (62)$$

ACKNOWLEDGMENT

The authors wish to express their gratitude to the following persons, who assisted with many of the calculations: H. F. Barry, R. A. Farran, K. H. Gharda, G. A. Gryka, H. A. O'Hern, I. P. Patel, R. G. Reimus, R. B. Roof, and P. P. Vora. Appreciation is also expressed to the Rackham Graduate School of the University of Michigan for financial assistance in the form of a Faculty Research Grant.

NOTATION

A, B, and C = functions of specific volume

A_2, B_2, C_2, A_3, B_3, C_3, A_4, and B_5 = characteristic constants

C_p = heat capacity at constant pressure

H = enthalpy

M = slope of reduced vapor pressure curve at critical point = $\frac{dP_r}{dT_r} = -m\,\frac{P_c}{T_c}$

P = pressure

R = universal gas constant

S = entropy

T = temperature in absolute scale

T_B = absolute temperature at Boyle point

T' = absolute temperature for which the slope at $P_r = 0$ of the isotherm on the compressibility chart equals the slope of the line joining the critical point and ($Z = 1$, $P_r = 0$)

V = specific volume or mole volume

Z = compressibility factor = $\frac{PV}{RT}$

b = a characteristic constant for a given substance

e = base of natural logarithm, 2.71828

f_1, f_2, f_3, f_4, f_5 = temperature functions

$f_1(T_c), f_2(T_c), f_3(T_c), f_4(T_c)$, and $f_5(T_c)$ = temperature functions evaluated at $T = T_c$

m = slope of the critical isometric on pressure-temperature diagram

$$\left(\frac{dP}{dT}\right)_{V=V_c} = -M\,\frac{P_c}{T_c}$$

Greek Letters

α = residual volume = $\frac{RT}{P} - V$

β = a characteristic constant in $V_c - b = \frac{\beta V_c}{1.3\alpha_2}$

μ = Joule-Thompson coefficient = $\left(\frac{dT}{dP}\right)_H$

Subscripts

c = the value at critical point, e.g., T_c, P_c, V_c, and Z_c

r = reduced property, $T_r = \frac{T}{T_c}$, $P_r = \frac{P}{P_c}$, etc.

LITERATURE CITED

1. Beattie, J. A., and O. C. Bridgeman, *Proc. Am. Acad. Arts Sci.*, **63**, 229-308 (1928).
2. Beattie, J. A., N. Poffenberger, and C. H. Hadlock, *J. Chem. Phys.*, **3**, 96-7 (1935).
3. Beattie, J. A., W. C. Kay, and J. Kaminsky, *J. Am. Chem. Soc.*, **59**, 1589-90 (1937).
4. Benedict, M., *J. Am. Chem. Soc.*, **59**, 2224-33 (1937).
5. Benedict, M., G. B. Webb, and L. C. Rubin, *J. Chem. Phys.*, **8**, 334 (1940); **10**, 747 (1942).
6. Deschner, W. W., and G. G. Brown *Ind. Eng. Chem.*, **32**, 836-40 (1940).
7. Dodge, B. F., "Chemical Engineering Thermodynamics," McGraw-Hill Book Company, Inc., New York (1944).
8. Farrington, P. S., and B. H. Sage, *Ind. Eng. Chem.*, **41**, No. 8, 1734-7 (1949).
9. Gornowski, E. J., E. H. Amick, and A. N. Hixson, *Ind. Eng. Chem.*, **39**, No. 10, 1348-52 (1947).
10. Hougen, O. A., and K. M. Watson, "Chemical Process Principles," Part II, John Wiley & Sons, Inc., New York (1947).
11. Joffe, J., *J. Am. Chem. Soc.*, **69**, No. 3, 540 (1947).
12. Keenan, J. H., and F. G. Keyes, "Thermodynamic Properties of Steam," John Wiley & Sons, Inc., New York (1936).
13. Maass, O., and S. N. Naldrett, *Can. J. Res.*, **B18**, 103, 108 (1940).
14. Marchman, H., W. Prengle, Jr., and R. L. Motard, *Ind. Eng. Chem.*, **41**, No. 11, 2658-60 (1949).
15. Michels, A., and C. Michels, *Proc. Roy. Soc.*, **A153**, 201-24 (1935).
16. Michels, A., B. Blaisse, and C. Michels, *Proc. Roy Soc.*, **A160**, 358 (1937).
17. Myers, *J. Research Natl. Bur. Standards*, **29**, 168 (1942).
18. Onnes, H. K., and A. T. Van Urk, *Commun. Kamerlingh Onnes Lab., Univ. Leiden*, No. 169d (1924).
19. Perry, J. H., "Chemical Engineers' Handbook," 3 ed., McGraw-Hill Book Company, Inc., New York (1950).
20. Plank, R., *Forsch. Gebiete Ingenieurw.*, **7**, 161 (1936).
21. Reamer, H. H., B. H. Sage, and W. N. Lacey, *Ind. Eng. Chem.*, **41**, No. 3, 482-4 (1949).
22. Reamer, H. H., B. H. Sage, and W. N. Lacey, *Ind. Eng. Chem.*, **42**, No. 1, 140-3 (1950).
23. Thodos, G., *Ind. Eng. Chem.*, **42**, No. 8, 1514-26 (1950).

Presented at A.I.ChE. San Francisco meeting, 1953.

OPERATING CHARACTERISTICS OF MEMBRANES

DONALD H. HAGERBAUMER and KARL KAMMERMEYER

State University of Iowa, Iowa City, Iowa

It appears inevitable that membrane research will eventually lead to the establishment of the gaseous-diffusion process as one of industry's basic unit operations. This process permitted successful large-scale separation of isotopic uranium hexafluorides and was thus of paramount importance in the atomic bomb program; it continues to play just as important a role in peacetime developments of atomic energy. Industry has at its disposal literally hundreds of different porous materials which ultimately will be investigated and may be used as membranes for the separation of gases and vapors.

During the past two years a number of studies have been reported which utilized strictly microporous as well as plastic membranes for the separation of gases and vapors (*1, 2, 5, 8, 11, 13*). One of the microporous membranes of more than passing interest is porous glass (*3, 4, 5, 7, 8, 9, 12*), because the pore diameters of this material are in the range of 20 to 60 Å. and therefore are considerably smaller than the mean free paths of most gases at atmospheric temperature and pressure [about 500 to 3,000 Å. (*6*).] Five porous-glass membranes were studied, four of which were prepared at different times by the Corning Glass Works. Two of the membranes were taken from the same group of samples. Average wall thicknesses, that is, membrane thicknesses, were determined by a mercury - displacement method. Actual measurements of wall thicknesses would have required breaking of the membranes. The average value for the thicknesses of the five membranes is 0.114 cm. Thickness measurements on five other broken membranes which were available averaged 0.114 ± 0.017 cm.

Equilibrium time, rates of permeation, and ratios of the permeability rates which indicate the direction and degree of separation to be expected were determined for the five membranes at the same time and under identical conditions. The gases used were oxygen, nitrogen, and carbon dioxide at 25°C. over a range of 3.72 to 7.80 atm. absolute upstream and atmospheric downstream pressure.

D. H. Hagerbaumer is with The Chemstrand Corporation, Decatur, Alabama.

APPARATUS AND PROCEDURE

The diagram of the apparatus is presented in Figure 1, and photographs are shown in Figures 2 and 3. The test gases were obtained from commercial sources and were not further purified. However, each gas was dried by being passed through silica gel before it entered the testing unit. The purity of the gases, as quoted by the suppliers, was 99.6% for oxygen, 99.0% for nitrogen, and 99.5% for carbon dioxide. Before the five membranes were installed in the top flange, they were "normalized" at 510°C. for 12 hr. to remove adsorbed organic vapors and water vapor. This procedure was rigidly followed before each run even though the same gas was being used. To determine the time required for membrane equilibrium at different pressures, it was necessary to desorb the membrane of the gas which had been passing through it during the previous run. All runs were made at essentially 25°C. Porous glass is normally consolidated to Vycor at 1,100° to 1,200°C. (*10*), which is far enough above the normalizing temperature for the pores to be assumed unaltered during the normalizing operation. Rates of permeation through the membranes were essentially the same before and after normalizing. Before a run was started, the valve in the top flange was opened and the system was purged at approximately 1.3 atm. abs. (5 lb./sq.in. gauge) for 2 min. The valve was then closed and the system immediately subjected to the desired operating pressure. The gas which permeated the membrane was discharged into the atmosphere except when a sample was collected in the burette to determine the rate of permeation, which was measured by displacement of a saturated sodium chloride solution from a 100-cc. gas burette, connected to the membrane by a rubber tube. The time required to collect samples was determined with a stop watch which could be read to within ± 0.25 sec. Atmospheric pressure was maintained on the downstream side of the membranes by means of a leveling bulb connected to the bottom of the gas burette. After a run was completed, either the rubber tubing leading to the gas burette was removed from the membrane or the three-way stopcock in the collection line was opened to the atmosphere. Diffusion of gas through the rubber tubing was considered negligible, as essentially atmospheric pressure was maintained on both sides of the tubing, the wall of which was 2 mm. thick. The time required for runs was quite short, namely, about 20 to 200 sec. The temperature of the room in which the experiments were conducted was constant within ± 0.5°C. during each run, and consequently it was not considered necessary to place the unit in a constant-temperature bath.

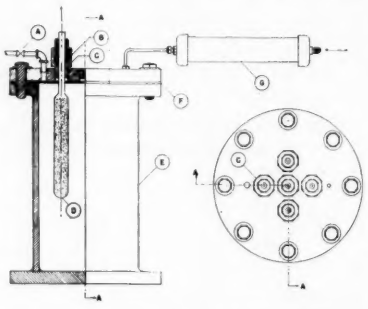

FIG. 1. DIAGRAM OF APPARATUS:

A, ⅛-in. stainless steel needle valve; *B*, ¾-in. O.D. by ¼-in. I.D. by ¾-in. rubber gasket; *C*, brass packing-gland-type adapter to hold porous-glass membrane; *D*, porous-glass membrane; *E*, standard pipe 6-in.-diam. by 12-in. long with 8-in.-diam. by ½-in. long steel flanges welded to both ends; the top flange, which contains the five adapters, was bolted on with eight ⅝-in. S.A.E. hexagonal bolts; *F*, ⅛-in. Garlock rubber gasket; *G*, 1½- by 10-in. standard pipe, silica-gel–filled gas drying unit.

DISCUSSION OF RESULTS

The dimensions of the five porous-glass membranes studied are presented in Table 1. Typical rates of permeation at equilibrium, G_{eq}, and the time required for equilibrium to be established within the membranes, t_{eq}, under various operating conditions for nitrogen, oxygen, and carbon dioxide are presented in Tables 2 through 4. The equilibrium rate of permeation, G_{eq}, is defined as the number of standard cubic centimeters of

TABLE 1.—DIMENSIONS OF POROUS-GLASS MEMBRANES TESTED

Sample*	Length, mm.	Outside area, sq. cm.	Thickness, cm.
1	145	78.57	0.109
2	47	21.0	0.107
3	84	39.8	0.122
4	143	75.4	0.112
5	141	75.87	0.121
			Avg. 0.114

*Membranes 1 and 5 were from the same group of samples received from the Corning Glass Works.

also the final operating pressure. In the second case the initial operating pressure was higher than the final operating pressure. When essentially constant rates of permeation were established for all the membranes at the initial operating pressure, the final operating pressure was produced by suddenly decreasing the pressure on the membranes to the desired value. This

TABLE 2.—NITROGEN EQUILIBRIUM PERMEABILITY DATA

G_{eq} = rate of permeation at equilibrium, std. cc./(sec.) (sq. cm.) -10^3
t_{eq} = time required for equilibrium to be established, hr.
p = 1.0 atm. abs. downstream pressure

Porous glass				1		2		3		4		5	
Upstream pressure conditions, π, atm. abs.				G_{eq}	t_{eq}	G_{eq}	t_{eq}	G_{eq}	t_{eq}	G_{eq}	t_{eq}	G_{eq}	t_{eq}
							A						
≈1.3	to	3.72		7.70	57.9	7.33	51.5	12.47	57.9	8.81	67.6	6.97	57.9
≈1.3	to	3.72		6.94	56.0	6.46	45.6	10.9	15.9	7.87	45.7	6.56	51.1
≈1.3	to	3.72		7.17	55.7	6.67	49.8	11.19	49.8	8.27	49.8	6.81	55.9
≈1.3	to	3.72		6.84	61.0	6.44	58.0	10.78	34.6	7.84	58.2	6.53	63.0
≈1.3	to	5.08	to 3.72	7.02	0.25	6.56	2.22	10.82	13.7	8.10	0.25	6.64	0.25
≈1.3	to	5.08	to 3.72	6.98	0.25	6.50	0.25	10.77	0.25	8.01	0.25	6.60	0.25
≈1.3	to	7.80	to 3.72	7.07	0.92	6.47	0.92	10.81	0.25	7.96	0.92	6.62	0.92
≈1.3	to	7.80	to 3.72	7.25	0.87	6.61	1.5	10.98	0.87	8.18	0.25	6.75	0.25
							B						
≈1.3	to	5.08		10.28	43.5	9.71	51.1	16.15	17.0	11.78	34.8	9.73	38.4
≈1.3	to	5.08		10.47	34.3	9.66	36.8	16.05	13.3	11.78	27.6	9.73	25.2
≈1.3	to	3.72	to 5.08	10.28	0.25	9.62	0.25	15.92	2.25	11.78	0.25	9.73	0.25
							C						
≈1.3	to	6.44		14.36	3.50	13.39	7.67	22.29	1.06	16.34	5.50	13.74	7.67
≈1.3	to	3.72	to 6.44	14.31	0.25	13.21	2.47	22.22	0.25	16.48	0.25	13.43	0.25
							D						
≈1.3	to	7.80		17.94	1.0	16.23	0.25	27.86	4.0	20.31	4.0	17.10	1.0
≈1.3	to	3.72	to 7.80	17.94	0.25	16.53	0.25	27.86	0.25	21.04	0.25	17.18	0.25
≈1.3	to	6.44	to 7.80	17.94	0.25	17.61	0.25	28.47	0.25	20.74	0.25	16.93	0.25

TABLE 3.—OXYGEN EQUILIBRIUM PERMEABILITY DATA

G_{eq} = rate of permeation at equilibrium, std. cc./(sec.) (sq. cm.) - 10^3
t_{eq} = time required for equilibrium to be established, hr.
p = 1.0 atm. abs. downstream pressure

Porous glass				1		2		3		4		5	
Upstream pressure conditions, π atm. abs.				G_{eq}	t_{eq}	G_{eq}	t_{eq}	G_{eq}	t_{eq}	G_{eq}	t_{eq}	G_{eq}	t_{eq}
							A						
≈1.3	to	3.72		6.30	25.3	5.92	42.7	9.86	6.0	7.27	49.5	5.98	31.0
≈1.3	to	3.72		6.53	20.5	6.17	35.5	10.13	5.5	7.46	20.5	6.21	5.5
≈1.3	to	3.72		6.50	23.5	6.10	23.5	10.04	23.5	7.46	23.5	6.21	27.2
≈1.3	to	7.80	to 3.72	6.57	1.75	6.19	1.25	10.22	0.25	7.65	5.0	6.35	3.5
≈1.3	to	7.80	to 3.72	6.57	1.5	6.12	1.5	10.13	0.25	7.55	0.25	6.21	0.25
							B						
≈1.3	to	5.08		9.78	11.8	9.24	20.3	15.10	6.5	11.10	22.6	9.26	12.8
≈1.3	to	3.72	to 5.08	9.92	2.5	9.04	1.0	15.06	2.5	11.11	1.0	9.27	1.0
≈1.3	to	3.72	to 5.08	9.83	0.5	9.20	2.5	15.06	0.5	11.33	0.5	9.34	0.5
≈1.3	to	3.72	to 5.08	9.72	1.4	9.03	2.5	15.00	2.5	11.11	0.5	9.27	0.5
							C						
≈1.3	to	6.44		13.46	2.25	12.59	5.0	20.78	5.0	15.29	2.25	12.70	14.75
≈1.3	to	5.08	to 6.44	13.46	1.25	12.37	1.25	20.44	1.25	15.31	1.25	12.70	1.25
≈1.3	to	5.08	to 6.44	13.46	1.50	12.30	2.25	20.64	2.25	15.31	2.25	12.70	0.5
							D						
≈1.3	to	7.80		16.62	2.5	15.58	4.5	25.90	4.25	19.26	2.0	16.17	8.5
≈1.3	to	7.80		16.78	2.3	15.60	3.75	25.90	4.0	19.31	1.75	16.25	6.75
≈1.3	to	6.44	to 7.80	16.87	1.12	15.61	0.25	26.22	0.25	19.31	0.25	16.07	0.25
≈1.3	to	6.44	to 7.80	16.87	1.50	15.67	1.5	25.92	1.5	19.31	0.25	16.22	0.50

gas per second per square centimeter passing through the membrane. The time, t_{eq}, required for equilibrium to be established within the membrane is in hours.

The membranes were operated in three ways. In the first case after the system was purged (at 5 lb./sq.in. gauge) the membranes were brought rapidly from purging pressure to the initial operating pressure, which in this case was

type of operation was initiated to save time in establishing membrane equilibrium, because during several trial runs it was observed that the membrane came to equilibrium considerably faster at higher than

TABLE 4.—CARBON DIOXIDE EQUILIBRIUM PERMEABILITY DATA

G_{eq} = rate of permeation at equilibrium, std. cc./(sec.) (sq. cm.) -10^3
t_{eq} = time required for equilibrium to be established, hr.
p = 1.0 atm. abs. downstream pressure

Porous glass	1		2		3		4		5	
Upstream pressure conditions, π atm. abs.	G_{eq}	t_{eq}	G_{eq}	t_{eq}	G_{eq}	t_{eq}	G_{eq}	t_{eq}	G_{eq}	t_{eq}
				A						
≈1.3 to 3.72	10.09	47.6	7.12	53.1	11.81	53.1	9.35	53.1	8.52	57.6
≈1.3 to 6.44 to 3.72	9.74	2.75	6.96	2.75	11.60	2.75	9.28	2.75	8.34	2.75
≈1.3 to 7.80 to 3.72	10.47	0.5	7.20	0.5	11.85	0.5	9.50	8.5	8.59	6.00
≈1.3 to 7.80 to 3.72	10.66	0.75	7.35	0.75	12.11	0.75	9.82	0.75	8.98	0.75
				B						
≈1.3 to 5.08	15.6	38.2	10.8	46.3	17.80	34.6	14.40	46.3	13.10	40.5
≈1.3 to 3.72 to 5.08	15.70	4.25	10.91	9.25	17.83	0.25	14.36	0.75	12.98	0.50
				C						
≈1.3 to 6.44	20.55	32.2	14.49	42.2	24.22	25.7	19.00	42.2	16.68	28.9
≈1.3 to 5.08 to 6.44	20.9	0.5	14.69	18.25	24.5	18.25	19.63	4.75	17.70	7.0
				D						
≈1.3 to 7.80	26.9	10.1	18.72	10.1	30.5	8.58	24.5	10.1	22.46	10.08
≈1.3 to 7.80	26.9	9.08	18.89	9.08	30.9	9.08	24.5	9.08	22.9	9.08
≈1.3 to 6.44 to 7.80	26.9	0.42	18.4	3.42	30.9	0.42	24.5	0.42	22.46	4.67

at lower operating pressures. In the third case the initial operating pressure was greater than atmospheric, but less than the final operating pressure. When the rates of permeation through all the membranes were nearly constant, the pressure was increased rapidly to the final operating level.

The upstream pressure side conditions, represented by II, in Tables 2 through 4, have been arranged so that the first pressure listed corresponds to the purging pressure on the membrane. After the system was purged, the pressure was suddenly increased to the second pressure listed and equilibrium was established within the membranes at this pressure. In cases where a third pressure is given, the pressure was rapidly changed from the second to the third value and equilibrium was again attained. All tables list G_{eq} and t_{eq} only for the last upstream pressure condition.

In all instances the rate of permeation through membrane 3 was definitely greater than through the other membranes. To some extent this is also true for membrane 4. The membrane thicknesses, listed in Table 1, differ by less than 14% and therefore the differences in flow cannot be explained by thickness variations. Previous investigations (*3, 9, 12*) have repeatedly demonstrated that the average pore size of porous glass is at most about 60 Å. and also that the pore-size distribution is rather sharp; therefore, it is unlikely that a difference in pore size or in distribution was responsible for the different flow rates. Support for this contention is given by the data in Table 5, where average permeability are shown to be essentially constant for all five porous-glass membranes. This is proof that all flow experiments were made in the molecular flow region.

Table 5 also gives ratios of permeabilities of N_2 and O_2. These ratios were found to be constant for the individual runs, and therefore only average values are reported. This fact signifies that all membranes behaved exactly alike in molecular flow. Consequently the conclusion is justified that the differences in flow rates were due to variations in the number of pores per unit surface area, that is, differences in void volume. This is a perfectly logical explanation.

In designing industrial diffusion units, it is important that the variation in flow rates per unit area and the variation in separation characteristics for different membranes constructed of the same basic material should be well defined. Without such knowledge, the design engineer faces the possibility of over- or underdesigned units.

The data presented in Tables 2 through 4 are pertinent to the start up of a diffusion process. Probably

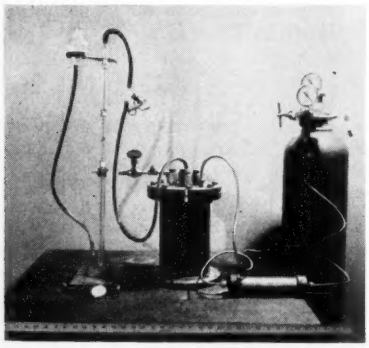

FIG. 2. ASSEMBLED TESTING APPARATUS.

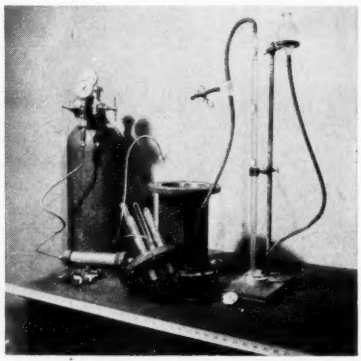

FIG. 3. MEMBRANES AND DISASSEMBLED TESTING APPARATUS.

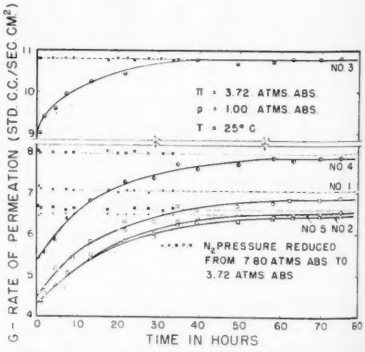
G - RATE OF PERMEATION (STD. C.C./SEC CM²) × 10³
TIME IN HOURS
NO. 3
π = 3.72 ATMS. ABS.
p = 1.00 ATMS. ABS.
T = 25° C
NO. 4
NO. 1
NO. 5 NO. 2
N₂ PRESSURE REDUCED FROM 7.80 ATMS ABS TO 3.72 ATMS ABS

FIG. 4. NITROGEN PERMEATION RATES × 10^3 THROUGH POROUS-GLASS MEMBRANES.

all membranes require a certain length of time to reach membrane equilibrium. The data indicate that equilibrium can be obtained in anywhere from a fraction of an hour to several hours at high pressures, compared with as much as several days or more at low pressures. One would expect that similar phenomena would be exhibited by ceramic and metallic membranes which have pore diameters up to approximately 500 Å. For pore diameters greater than 500 Å., the adsorbed molecular layers should not contribute appreciably to the total rate of flow through the capillary. It would be expected that the smaller the pore diameter, the greater would be the length of time required for membrane equilibrium. Very slow adsorption of gas within the pores is believed to account for the time lag observed in attaining membrane equilibrium; therefore, the smaller the pore diameter, the greater would be the influence of the adsorbed layers on the effective pore diameter and the greater would be the effect which adsorption contributed to the flow and separation mechanism.

Some variation in reproducibility of t_{eq} was observed (Tables 2 through 4) when the membranes were studied under the same conditions. It was definitely established, however, that t_{eq} is always smaller at higher upstream pressures than at the lower upstream pressures. In all cases it was consistently found that on reducing the upstream pressure to a lower final operating pressure, the time required for membrane equilibrium was considerably reduced. It is recommended that membrane equilibrium be attained by initially subjecting the membrane to a high upstream pressure for a short period of time and then either suddenly or slowly decreasing it to the final operating pressure. The typical data presented in Figure 4 justify this recommendation.

For the data presented in Figure 4, nitrogen was placed on the outside of membranes at 7.80 atm. abs. (100 lb./sq. in. gauge) for just 1/2 hr. and the membranes did not necessarily reach equilibrium before the pressure was suddenly decreased to 3.72 atm. abs. (40 lb./sq.in. gauge). When the membranes were operated in this manner, it was found that reduction of the upstream pressure resulted in very rapid establishment of flow equilibrium as compared with the approximately 2 days needed when the pressure was increased from the purging pressure to 3.72 atm. abs. Similar results were obtained for oxygen and carbon dioxide under identical operating conditions, and the rates of permeation were of the same order of magnitude as the G_{eq} values obtained when the upstream pressure was increased from purging pressure (about 1.3 atm. abs.) to 3.72 atm. abs.

The experimental data in Tables 2 through 4 are also significant in that t_{eq} was observed to be greater in all cases when the upstream pressure was increased from essentially atmospheric conditions to the intermediate rather than to the higher final pressures.

Consequently, the lower the upstream operating pressure, the more important it becomes to direct attention to the best method for obtaining membrane equilibrium as rapidly as possible.

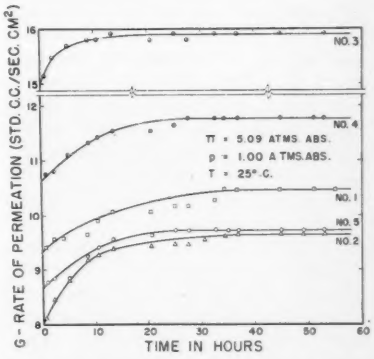

FIG. 5. NITROGEN PERMEATION RATES $\times 10^3$ THROUGH POROUS-GLASS MEMBRANES.

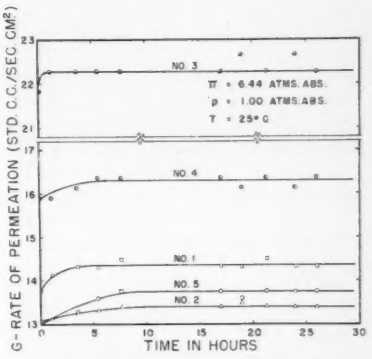

FIG. 6. NITROGEN PERMEATION RATES $\times 10^3$ THROUGH POROUS-GLASS MEMBRANES.

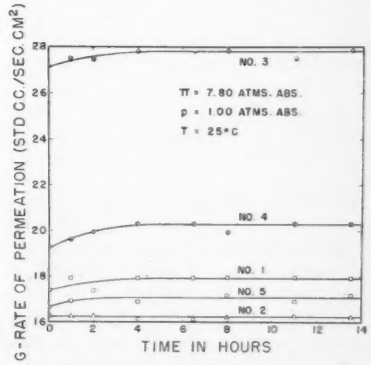

FIG. 7. NITROGEN PERMEATION RATES $\times 10^3$ THROUGH POROUS-GLASS MEMBRANES.

TABLE 5.—AVERAGE PERMEABILITIES AND PERMEABILITY RATIOS

Gas	Average permeability*: $P \times 10^3$ Membrane number 1	2	3	4	5
Nitrogen	0.285	0.260	0.494	0.334	0.297
Oxygen	0.265	0.242	0.461	0.310	0.279
Carbon dioxide					
Δp: 2.72 atm.	0.411	0.282	0.531	0.392	0.382
: 4.08 atm.	0.417	0.285	0.532	0.394	0.385
: 5.44 atm.	0.415	0.287	0.545	0.398	0.386
: 6.80 atm.	0.430	0.293	0.552	0.403	0.402
Based on N_2 and O_2 the CO_2 flow should be	0.227	0.207	0.394	0.266	0.237
	Actual permeability ratios α values				Theoretical ratio†
N_2/O_2	1.076	1.076	1.070	1.077	1.065	1.069
N_2/CO_2‡	0.688	0.916	0.922	0.848	0.773	1.253
O_2/CO_2‡	0.635	0.852	0.860	0.787	0.727	1.172

* Permeability $P = \dfrac{\text{(Std. cc.) (cm. thickness)}}{\text{(sq. cm. area) (sec.) } (\Delta p \text{ atm. pressure drop})}$

†Theoretical ratio: $\dfrac{P_{N_2}}{P_{O_2}} = \sqrt{\dfrac{M_{O_2}}{M_{N_2}}} = \sqrt{\dfrac{32}{28}} = 1.069$

‡Average P_{CO_2} values at Δp of 2.72, 4.08, 5.44 atm. are used. At 6.80 atm. condensed flow begins to increase noticeably with pressure.

For the sake of simplicity, the G_{eq} and t_{eq} data have been presented in tabular form in Tables 2 through 4. To show typical detailed rates of permeation data obtained, one complete set of data has been presented for nitrogen at various upstream pressures in Figures 4 through 7. It is seen in Figure 4 that the initial rate of permeation may vary by as much as 30% from the rate of permeation at equilibrium, G_{eq}. As the upstream pressure was increased (Figures 5, 6 and 7), the initial rates of permeation more closely approached the rates at equilibrium, G_{eq}. This should be expected, for adsorption takes place much more rapidly at the higher pressures. Membranes 2 and 3 diverged the most in regard to rates of permeation. On increase of the upstream pressure, the percentage variation in rates of permeation remained approximately the same for all membranes, but when it is interpreted as difference in actual flow rates the higher the upstream pressure, the greater the difference in actual flow rates.

Uniform separation characteristics of individual membranes are just as important as uniform flow rates through the membranes. Similarly, the effect of pressure on establishing membrane equilibrium and the time required for membrane equilibrium is of paramount importance. It would indeed be undesirable to construct a number of diffusion stages without knowing whether all the membranes used possessed identical separation characteristics.

The separation factor, α, for ideal gases through ideal membranes is equal to the square root of the inverse ratio of the molecular weights of the individual components. This is in accordance with the separation predicted by Graham's equation(*5*), which is

$$\frac{y_A}{1-y_A} = \sqrt{\frac{M_B}{M_A}}\left[\frac{\pi x_A - p y_A}{\pi\,(1-x_A) - p\,(1-y_A)}\right]$$

where y_A and y_B are the mole fractions of the components on the low-pressure side of the membrane, x_A and x_B are the mole fractions of the components on the high-pressure side, M_A and M_B are the molecular weights, and Π and p are the upstream and downstream pressures, respectively. Graham's equation in this form assumes that the feed composition remains virtually constant. When experimental permeability data for individual components and for identical operating conditions are available, they may be used in place of $\sqrt{M_B/M_A}$, usually expressed in terms of $\alpha = G_A/G_B$. The α values are an index to the direction and degree of separation of the components. The separation characteristics of the five membranes studied are presented in Table 5 in terms of α values which were computed from observed rates of permeation data, and the α values are also compared with $\sqrt{M_B/M_A}$ values. As stated previously, the constancy of the α values for N_2-O_2 is proof that the separation characteristics of all five membranes for nitrogen-oxygen separation were quite uniform even though the equilibrium rates of permeation through the five membranes varied as much as 30% under identical operating conditions. The consistent α values for nitrogen-oxygen indicate that the pore diameters of the five membranes are relatively uniform, but the number of pores per unit area probably varied.

This accounts for the marked difference in the observed rates of permeation at equilibrium. The α values for nitrogen-oxygen also were in good agreement with the theoretical values.

When the carbon dioxide data in Table 5 are analyzed, it is obvious that carbon dioxide permeated at a much higher rate than would be predicted from N_2 and O_2 flow. At 25°C. oxygen and nitrogen are considerably above their critical temperatures, which are —118.8° and —147.1°C. respectively. The critical temperature of carbon dioxide is 31.1°C.; consequently, oxygen and nitrogen were actually gases at 25°C., whereas carbon dioxide could be considered a vapor. Experimental evidence has been reported which shows that vapor mixtures and gas-vapor mixtures cannot be expected to separate in the direction predicted by the square root of the inverse ratio of the component molecular weights(*5, 8*), and the α values calculated here for nitrogen–carbon dioxide and oxygen–carbon dioxide indicate that these gas-vapor mixtures do not separate in inverse proportion to the square root of the molecular weights.

The flow rates of carbon dioxide were found to be greater than predicted by Graham's law. The anomalous flow behavior of carbon dioxide through various membranes has also been reported by other investigators(*8*). This observation is in accordance with the concept that "condensed" flow rates of vapors are generally greater than flow rates of gases. Substantiating evidence of condensed flow phenomena was reported in the separation study of azeotropic vapors (*5*). It is of further interest to note that the α values for the gas-vapor mixtures studied showed considerable variation between the five different membranes. The membranes which gave the highest flow rates, that is 3 and 4, also exhibited a greater proportion of condensed flow, a result that agrees with the contention that these membranes possessed a higher void volume, or pore surface.

ACKNOWLEDGMENT

The authors gratefully acknowledge the support of the United States Atomic Energy Commission, which sponsored the investigation, and also wish to express their appreciation to Dr. Martin Nordberg of the Corning Glass Works for his cooperation and valuable suggestions. Dr. C. J. Major solved the problem of determining membrane thicknesses without destroying the specimens.

LITERATURE CITED

1. Brubaker, D. W., and Karl Kammermeyer, *Ind. Eng. Chem.*, **45**, 1148-52 (1953).
2. *Ibid.*, **46**, 733-9 (1954).
3. Emmett, P. H., and T. W. DeWitt, *J. Am. Chem. Soc.*, **65**, 1253-62 (1943).
4. Emmett, P. H., and M. Cines, *J. Phys. & Colloid Chem.*, **51**, 1248-62 (1947).
5. Hagerbaumer, D. H., and Karl Kammermeyer, *Chem. Eng. Progr. Symposium Ser.* No. 10, **50**, 25-44 (1954).
6. Hodgman, C. D., "Handbook of Chemistry and Physics," 30th ed., p. 2627, Chem. Rubber Publishing Co., Cleveland, Ohio (1947).
7. Hood, H. P., and M. E. Nordberg, U. S. Patent 2,106,744 (1938).
8. Huckins, H. E., Jr., and Karl Kammermeyer, *Chem. Eng. Progr.*, **49**, 180-4, 294-8, 517 (1953).
9. Nordberg, M. E., *J. Am. Ceram. Soc.*, **27** (10), 299-305 (1944).
10. Nordberg, M. E., private communication.
11. Osburn, J. O., and Karl Kammermeyer, *Ind. Eng. Chem.*, **46**, 739-42 (1954).
12. Schwertz, F. A., *J. Am. Ceram. Soc.*, **32**, 390 (1949).
13. Weller, S., and W. A. Steiner, *J. Appl. Phys.*, **21**, 279-83 (1950).

A TECHNIQUE FOR CONTACTING GASES WITH COARSE SOLID PARTICLES

K. B. Mathur and P. E. Gishler
National Research Council of Canada, Ottawa

Although coarse, uniformly sized particles are not amenable to fluidization, it has been found possible by use of either gases or liquids to impart a regular cycling motion to a bed of this type of material in which the solids are rapidly carried upward by the fluid in a central well-defined core within the bed. The particles move uniformly downward in the annular space surrounding the core, thus providing dense-phase countercurrent contact between the fluid and the solids. There is no wall separating the core from the annulus. This method is called the spouted-bed technique. The effect of column diameter, fluid inlet diameter, bed depth, and physical properties of solids and fluids on spouting behavior has been investigated. The minimum fluid velocity required for spouting has been correlated, and the flow pattern of the fluid and of the solids has been studied. The technique has been applied to the drying of wheat.

Fluidization of solids has proved to be a useful technique for vapor-solid contact. The reasons for its wide acceptance and application are certain unique characteristics which are inherent in the system, viz., ease of transferring solids to and from vessels, uniformity of conditions such as temperature, etc., within the bed, and high heat and mass transfer rates associated with the system. Application has, however, been limited to relatively fine solids because coarse materials when subjected to fluidization show a marked tendency toward slugging (*4, 7*). This paper describes a technique—called the spouted-bed technique—which has been developed for effectively handling coarse particles. The mechanism of flow of solids as well as of gas in this technique is different from fluidization, but it appears to achieve the same purpose for coarse particles as fluidization does for fine materials. Whereas the major application of the technique is believed to be for coarse particles, it was found to work effectively for solids as fine as 20 to 35 mesh which are also capable of being fluidized. Thus there is a slight overlap between spoutable and fluidizable sizes.

DESCRIPTION OF THE SPOUTED-BED TECHNIQUE

If coarse solid material is poured into a cone-bottomed column having a small central opening for air inlet at the base of the cone and subjected to an increasing upward air flow, the following steps will occur. At low air velocities the air will simply pass upward through the solids bed without disturbing the particles; however, as the air velocity is increased, a point will be reached when there is a noticeable readjustment of the particles. A further increase in air flow causes a stream of solids to rise rapidly as a central core, or spout, within the bed. The solids in the spout, having reached somewhat above the bed level, fall back onto the annular space around the spout and travel downward uniformly as a packed bed. Thus a spouted bed is a composite of a central air spout carrying the solids upward and a downward-moving annulus with a countercurrent flow of air. A considerable cross flow of solids from the annulus into the spout takes place all along the bed height. Figure 1 illustrates a spouted bed of wheat in a sectional column; Figure 2 indicates the solids-flow pattern schematically.

The effect of air flow on bed condition is illustrated by the pressure drop across the bed. A typical pressure-drop curve is shown in Figure 3. With increasing air velocities the pressure drop rises directly to point *B*, as would be expected in a packed bed. Increasing the air flow beyond this causes a sharp decrease in pressure drop to the point at which the air velocity at the inlet becomes high enough to lift the particles at the base of the cone and thus form a short internal spout in that region. With further increase in air flow this spout increases in height until at point *C* enough solids have been displaced from the central core to cause a noticeable expansion of the bed. At an air-flow rate corresponding to point *D*, movement of particles at the top of the bed is observed, but the spout is still confined to the lower part of the bed. Increasing the air flow beyond this point causes a sharp decrease in the pressure drop to point *E*, where the spout breaks through the top of the bed and steady spouting sets in. Beyond this point the pressure drop decreases only slightly with an increase in air flow.

If the air flow is then decreased, the bed stays in the spouted con-

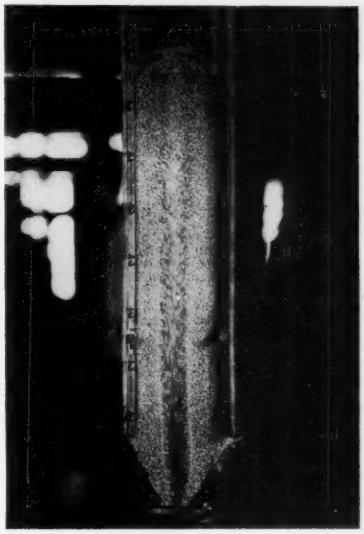

FIG. 1. SPOUTED WHEAT BED IN A 6-IN. SECTIONAL COLUMN.

dition until an air velocity corresponding to point E' is reached, which is somewhat lower than the velocity at point E. This is made possible because the energy for breaking interparticle contacts in the central core is no longer necessary as is the case with increasing air flow. Point E' represents the minimum air flow for spouting; a slight reduction in air flow at this stage results in a sharp rise in the pressure drop owing to the collapse of the spout. The bed behaves like a packed bed beyond this point, the curve for decreasing air flow being lower because the particles are loosely packed.

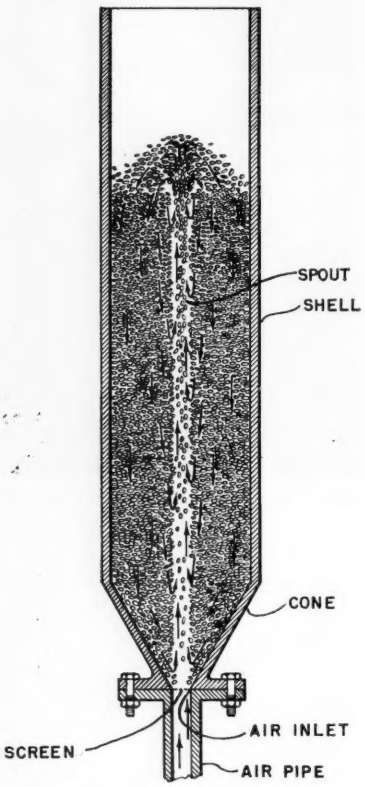

FIG. 2. SCHEMATIC DIAGRAM OF A SPOUTED BED.

CONDITIONS NECESSARY FOR SPOUTING

Conditions, viz., inlet-air diameter, air-flow rate, bed depth, and particle size, necessary for spouting are critical. For a certain particle size and column diameter there is a maximum inlet-air size beyond which spouting does not take place. The maximum bed depth to which a certain material can be made to spout is also limited and depends upon the column diameter and the size of the inlet-air opening.

Figures 4 and 5, which are phase diagrams for —20+35-mesh Ottawa sand, quantitatively illustrate the critical nature of the inlet-air diameter, air flow, and bed depth on spouting. For the data represented in Figure 4, a 1/2-in. standard pipe was used for the inlet air at the bottom of an 85° (included) angle cone, which formed the base of a 6-in. glass column. An increase in air flow caused the transition of the sand bed from packed to fluidized with further increase resulting in slugging. However, when the size of the air inlet was reduced to a 3/8-in. standard pipe (Figure 5), a bed as deep as 27.0 in. could be made to spout. Good spouting was achieved only over a narrow range of air flow; increasing the air rate above a certain value resulted in fluidizing and finally slugging. A bed deeper than 27 in. did not spout but changed directly from a packed to a fluidized bed with increasing air flow.

A similar phase diagram for wheat, in a 6-in. column with a 3/8-in. standard pipe for air inlet, is depicted in Figure 6. The range of air flow for spouting is considerably wider with wheat than with sand.

SCOPE OF INVESTIGATION

This work was conducted with two main objects in view: (1) to gain an insight into the mechanism of gas and solids flow in a spouted bed and (2) to study the effect of the major variable of the system on spouting behavior.

MECHANISM OF GAS AND SOLIDS FLOW

The flow characteristics of such a system are of importance in understanding and properly applying the technique. In order to arrive at a complete picture of the flow mechanism, the following characteristics have to be studied: flow of gas through annulus and through spout, flow of solids through annulus and through spout, void space in annulus and in spout.

EXPERIMENTAL

Considerable data have been taken for different solids with varying column diameters, bed depths, and air-inlet sizes. For explaining the flow mechanism, a 25-in.-deep wheat bed in a 6-in.–diam. column with a 3/8-in. standard pipe for air inlet at the base of an 85° cone has been chosen as a typical spouted bed. The choice of this system is arbitrary, and a study of the effect of column design, solids properties, and fluid properties on flow mechanism has not been attempted. The following discussion is confined to the typical system described above.

Flow of Air. The data taken to establish the flow pattern of air in a spouted bed consist of vertical static-pressure-drop profiles. The radial pressure-drop gradient was found to be negligible. A single pressure probe consisting of 1/8-in. Shelby tubing with 1/64-in. static pressure holes, and a water-air manometer were used for taking the pressure-drop data. Readings were usually taken every 4 in. along the bed height; all observations were taken above the cone, which extends 5 in. above the air inlet. Pressure-drop measurement, as an indication of air flow, was considered preferable to direct measurement of air velocity because of the usual difficulties encountered as a result of solids interference (*6*).

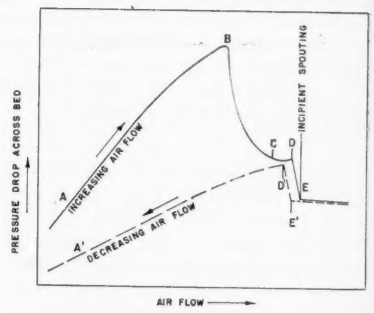

FIG. 3. EFFECT OF AIR FLOW ON PRESSURE DROP IN A BED OF SOLIDS USING A SMALL CENTRAL AIR INLET.

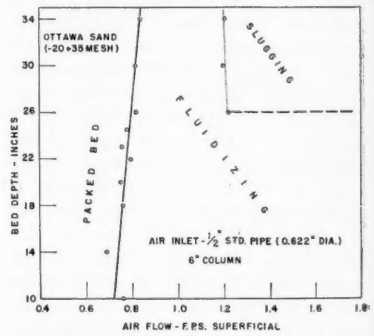

FIG. 4. PHASE DIAGRAM FOR SAND, 1/2-IN. STANDARD PIPE FOR AIR INLET.

Flow of Solids. It is not possible to obtain information on the upward velocity of particles in the spout in the circular column because the spout is not open to view. A sectional 6-in.–diam. Plexiglass column was built in which the spout is visible along the flat side (Figure 1). The inlet-air opening for this column was a 0.493-in.–diam. (equivalent to a 3/8-in. standard pipe) half circle.

It is doubtful whether the half column is a true representation of the full column, as interference is caused by the introduction of a flat wall; however, the relative flow behaviors in the half column should be comparable to those in the full column. This view is supported by the fact that the shapes of the particle velocity-at-wall and pressure-drop profiles for the half and full columns are identical (Figures 7 and 8). While use has been made of the information obtained on the half column for flow explanations in the full column, it has been kept in mind that only the relative behaviors in the half column are significant.

To obtain data on particle velocity in the spout in the half column, high-speed motion picture technique was employed. A Western Electric Fastax 16-mm. camera was used to take motion pictures of the spout at 3,000 frames/sec. Colored wheat particles were dropped in the bed to serve as indicators. Close-up shots from about 5 ft. were taken on 100 ft. rolls so that the movement of the particles might be distinctly traced. Projecting the movies in slow motion made it possible to measure particle velocities in the spout at different levels. Data were also taken to measure vertical profiles of the particle velocity at the column wall. This was done simply by timing the particles across 4-in. increments along the bed height. The observations were fairly reproducible; an average of a dozen readings across each increment of height has been reported. The particle velocities did not vary along the column periphery.

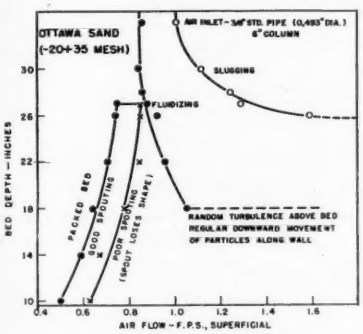

FIG. 5. PHASE DIAGRAM FOR SAND, 3/8-IN. STANDARD PIPE FOR AIR INLET.

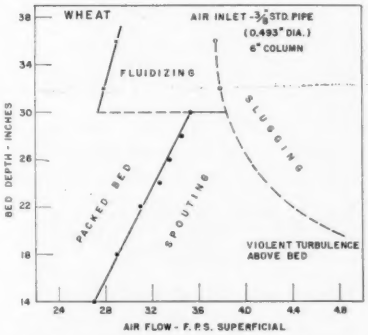

FIG. 6. PHASE DIAGRAM FOR WHEAT, 3/8-IN. STANDARD PIPE FOR AIR INLET.

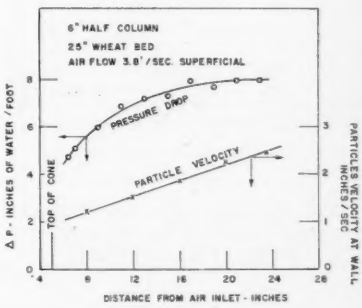
6" HALF COLUMN
25" WHEAT BED
AIR FLOW 3.8 /SEC. SUPERFICIAL
PRESSURE DROP
PARTICLE VELOCITY
TOP OF CONE
ΔP - INCHES OF WATER / FOOT
PARTICLES VELOCITY AT WALL INCHES / SEC
DISTANCE FROM AIR INLET - INCHES

FIG. 7. PRESSURE DROP PER FOOT AND PARTICLE VELOCITY AT WALL VS. BED LEVEL (HALF COLUMN).

RESULTS AND DISCUSSION

Flow of Air. *Annulus.* The annulus in a spouted bed is a downward-moving bed of solids. The expansion in the bed was observed to be about 6%, which is roughly equivalent to the volume of the solids displaced from the spout, and indicates that the annulus is substantially a packed bed. Visual observation verifies this. The pressure drop along the bed height is, therefore, a measure of the loss of energy of the air flowing through it, and the situation is similar to the flow of gas through a loosely packed bed.

In order to arrive at the air flow through the annulus, a pressure-drop vs. airflow curve for a packed bed was first determined experimentally. These data were obtained in a 6-in. glass column by use of a sintered stainless steel grid as an air distributor. Static pressure-drop readings were taken at different air-flow rates including rates high enough to cause agitation of the bed.

Figure 9 gives ΔP as a function of superficial air velocity; the lower curve is for loose packing. Figure 8 is the vertical pressure-drop profile in a spouted bed. For a certain value of pressure drop in the spouted bed, the superficial air velocity in the annulus is equal to that indicated by the curve for a loosely packed bed.

The air velocity in the annulus has been worked out on this basis and plotted in Figure 11 against bed level. To obtain the volumetric air flow from the superficial velocity, the cross-sectional area of the annulus and therefore the diameter of the spout along the bed height must be known. This was measured in a 25-in. spouted bed of wheat in the half-sectional column. The spout diameter was 1.1 in. at a level of 2 in. from the inlet; it increased rapidly to 1.4 in. at the 6-in. level and then gradually to 2 in. at the top of the 25-in.-deep bed. In the full column it was possible to estimate the spout diameter at the bed top as 2 in. which agrees with the spout diameter at bed top in the half column; hence it is assumed that the spout diameters at different bed levels in the half and full columns are identical. Since the variation in spout diameter along bed height is relatively small, the over-all flow picture would not be significantly affected even if this assumption were not strictly true. The volumetric flow in the annulus as a percentage of total flow is also contained in Figure 10. From this it can be seen that the air steadily flares out from the spout into the annulus as it rises up the bed; this tendency is much more pronounced in the lower part of the bed, as is evident from the rapid change in slope of the curve for this region. Near the top of the bed almost two thirds of the total air flows through the annulus.

It is interesting to note that the maximum air velocity in the annulus at the top of the bed is approximately the velocity required to fluidize wheat, as indicated in Figure 9.

Spout. The air flow through the spout has been worked out for different bed levels by taking differences between the total air flow and the air flow through the annulus. Results are plotted in Figure 11 as the percentage of total flow through the spout against bed level. Based on the diameters of the spout, the superficial air velocity through the spout has been calculated and plotted in the same figure. The air enters the bed at a high linear velocity; about 30% of it flares out into the annulus during its travel through the cone, and at the same time the core diameter increases to about 1.4 in., reducing the velocity through the spout at the top of the cone to 50 ft./sec. The lateral flow of air from the spout to the annulus is gradual

above the cone, the velocity falling off to 13.5 ft./sec. at the top of the bed.

Flow of Solids. *Annulus.* The particle velocity at the column wall should be an indication of the downward flow of solids in the annulus. The particles gradually slow from 2.62 in./sec. at the top of the bed to 1.74 in./sec. at a level of 10 in. from the base of the column (Figure 8), indicating that there is a steady cross flow of solids from the annulus into the spout along the bed height. Observations made on the flat side of the half column show that the radial gradient of particle velocity in the annulus is not appreciable; in other words, the solids in the annulus as a whole are moving downward at velocities indicated at the column wall. The flow of solids in the annulus, worked out on this basis, is plotted in Figure 12.

Spout. Data obtained from high-speed motion pictures of the spout for the half column are shown in Figure 13. The particles which enter the spout at the bottom receive a sudden impulse from the high-velocity stream of air and accelerate rapidly from rest to a maximum velocity of about 25 ft./sec. at a level of 7 in. from the air inlet. As they travel further up the bed, they transfer part of their kinetic energy to the particles which enter the spout from the annulus, thereby accelerating them from rest to the average particle velocity in the spout at that level. Owing to this constant transfer of energy along the bed height, the over-all particle velocity in the spout rapidly falls off until it reaches zero at a level of 28 in. from the air inlet, a point 1 1/2 in. above the bed level, at which the particles reverse their direction. Superimposed on this effect is the lifting action caused on the particles by the upflowing air in the spout. However, since the air velocity in the spout drops off sharply above the cone, this is estimated to be small compared with the initial energy imparted to the particles by the air in the cone. The experimental points on Figure 13 are for the half column with a total superficial air velocity of 3.8 ft./sec. In the full column the air velocity used was 3.72 ft./sec. Theoretical considerations based on drag coefficients indicate that the rising part of the particle-velocity curve for the full column should be slightly lower than the curve for the half column (*1*). The falling part of the curve would not be significantly altered by differences in air-flow rates used in the half and full columns.

Void Space. *Annulus.* The annulus in a spouted bed is considered similar to a loosely packed bed. The void space for such a bed of wheat, calculated from the measured bulk and absolute densities, equals 43.2%.

Spout. The downward solids flow in the annulus should equal the upward solids flow in the spout at any bed level since spouting is a

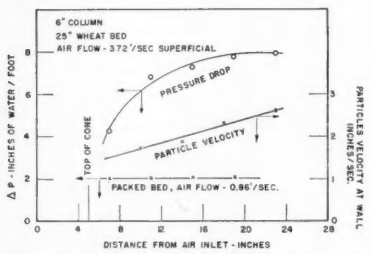
6" COLUMN
25" WHEAT BED
AIR FLOW - 3.72'/SEC SUPERFICIAL
PRESSURE DROP
PARTICLE VELOCITY
TOP OF CONE
PACKED BED, AIR FLOW - 0.86'/SEC.
Δ P - INCHES OF WATER / FOOT
PARTICLES VELOCITY AT WALL (INCHES/SEC.
DISTANCE FROM AIR INLET - INCHES

FIG. 8. PRESSURE DROP PER FOOT AND PARTICLE VELOCITY AT WALL VS. BED LEVEL (FULL COLUMN).

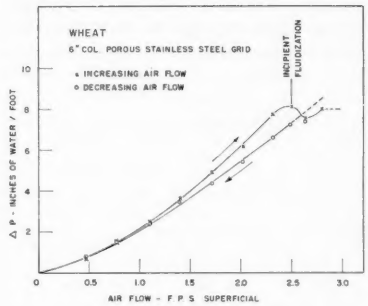
WHEAT
6" COL. POROUS STAINLESS STEEL GRID
INCREASING AIR FLOW
DECREASING AIR FLOW
INCIPIENT FLUIDIZATION
Δ P - INCHES OF WATER / FOOT
AIR FLOW - F P S SUPERFICIAL

FIG. 9. PRESSURE DROP PER FOOT VS. AIR FLOW USING A UNIFORM AIR DISTRIBUTOR.

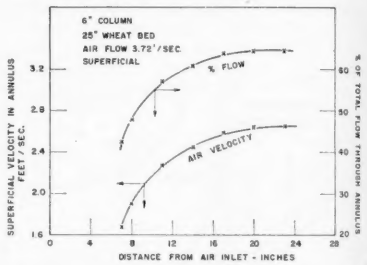

FIG. 10. AIR FLOW THROUGH ANNULUS VS. BED LEVEL.

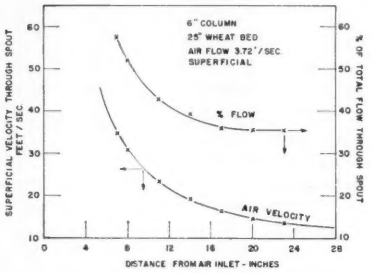

FIG. 11. AIR FLOW THROUGH SPOUT VS. BED LEVEL.

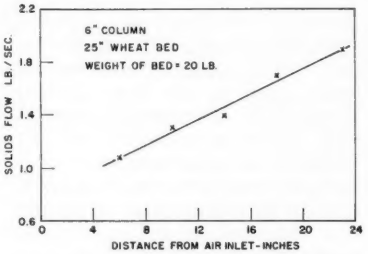

FIG. 12. SOLIDS FLOW IN ANNULUS VS. BED LEVEL.

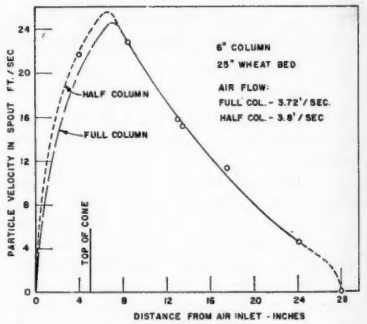

FIG. 13. PARTICLE VELOCITY IN SPOUT VS. BED LEVEL.

steady-state flow system. The solids flow in the annulus has been worked out from the data on particle velocity at wall. Knowing the upward linear velocity of the particles in the spout, the authors calculated the bulk density and void space in the spout, the latter being plotted in Figure 14.

It has been found possible to calculate the void space in the spout from the pressure drop data as well. The spout can be compared to a vertical riser through which

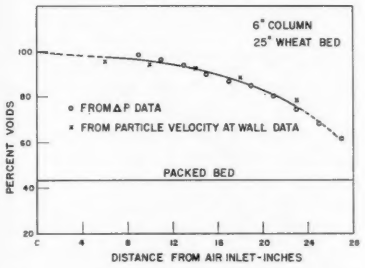

FIG. 14. VOID SPACE IN SPOUT VS. BED LEVEL.

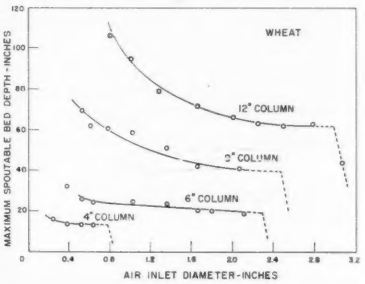

FIG. 15. EFFECT OF AIR INLET DIAMETER ON MAXIMUM SPOUTABLE BED DEPTH.

solids are being transported by a stream of air. The pressure drop under such conditions is composed of (2, 7) (*a*) a solids static head equivalent to the dispersed-solids density, (*b*) a solids friction loss due to contact of particles with air and with the pipe wall (the pipe in this case may be visualized as made of wheat particles), and (*c*) an acceleration pressure drop. In mathematical terms

$$dP_{total} = dP_{friction} + dP_{acceleration} + dP_{weight}$$

$$dP_T = dP_{f+a} + dP_w \qquad (1)$$

When an incremental height of spout dh is considered, one may let the solids flow across $dh = m$ lb./sec., the solids velocity across $dh = v_p$ ft./sec., the cross-sectional area of the spout $= A$ ft.; then kinetic energy associated with the solids at any point

$$= \frac{1}{2g} \cdot m v_p^2 \qquad (2)$$

Change in kinetic energy across $dh =$

$$d\left(\frac{1}{2g} \cdot m v_p^2\right) = \frac{1}{2g} \cdot d(m v_p^2) \qquad (3)$$

If the average air velocity through the spout across $dh = v_a$ ft./sec. then the energy loss from air to solids across $dh =$

$$d\,(v_a \cdot A \cdot P_{f+a}) = v_a \cdot A \cdot dP_{f+a} \qquad (4)$$

when air velocity and spout diameter are assumed to be constant across dh and substantially equal to the average values for the increment; dh has been taken small enough so that this assumption is valid.

Energy gained by the solids = energy lost by the air or

$$\frac{1}{2g} \cdot d\,(m v_p^2) = -\,v_a A \cdot dP_{f+a} \qquad (5)$$

changes in heat energy, potential energy, etc., being neglected.

$$dP_{f+a} = -\frac{1}{2g \cdot v_a \cdot A} \cdot d\,(m v_p^2) \qquad (6)$$

It is known that

$$dP_w = d\,(\rho_b \cdot h) \qquad (7)$$

where $\rho_b =$ bulk density in spout, lb./cu.ft.

Dividing Equation (6) by Equation (7) gives

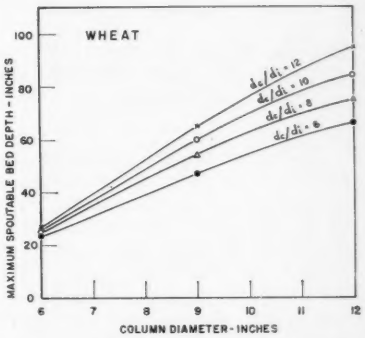

FIG. 16. EFFECT OF COLUMN DIAMETER ON MAXIMUM SPOUTABLE BED DEPTH.

$$\frac{d.P_{f+a}}{dP_w} = -\frac{d(m v_p^2)}{d(\rho_b . h)} \cdot \frac{1}{2g . v_a . A} \qquad (8)$$

$$m = v_p \cdot A \cdot \rho_b \qquad (9)$$

Substituting Equation (9) in (8) gives

$$\frac{dP_{f+a}}{dP_w} = -\frac{d(v_p^3 \cdot \rho_b)}{d(\rho_b \cdot h)} \cdot \frac{1}{2g \cdot v_a} \qquad (10)$$

TABLE 1.—SPOUTING BEHAVIOR OF VARIOUS MATERIALS, 6-IN.-DIAM. GLASS COLUMN, 3/8-IN. STANDARD AIR INLET

No.	Material	Size, in.	Absolute density, lb./cu. ft.	Maximum spoutable bed depth, in.	Minimum air flow for spouting, F.P.S. superficial
1	Brucite	0.0232	156.5	27.5	0.56
2	Coffee beans	0.3×0.45	39.5	20.0	3.22
3	Lima beans	0.5×0.75	83.0	11.4	4.43
4	Mustard seeds	0.0855	75.7	34.0	2.57
5	Rape seeds	0.0691	68.9	30.0	2.01
6	Sunflower seeds	0.315×0.473	....	15.0	3.06
7	Oats	0.118×0.394	....	19.0	2.42
8	Wheat	0.125×0.25	85.9	30.0	3.53
9	Peas	0.25	86.6	12.0	5.31
10	Ottawa sand (−20+35)	0.0232	145.0	27.0	0.75
11	Shale (−14+20)	0.0390	128.8	36.0	1.21
12	Gravel (−4+8)	0.139	166.6	25.0	4.31
13	Gravel (−8+14)	0.0695	164.0	46.0	3.27

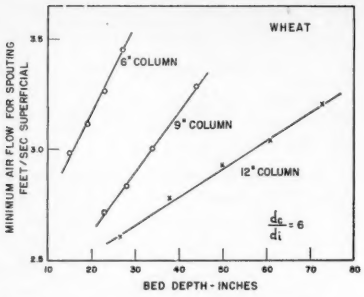

FIG. 17. EFFECT OF BED DEPTH ON MINIMUM AIR FLOW REQUIRED FOR SPOUTING.

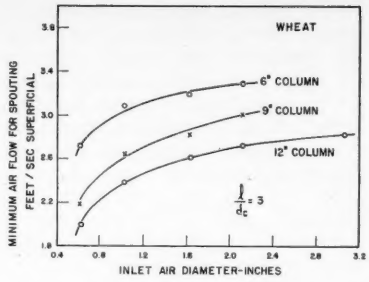

FIG. 18. EFFECT OF AIR INLET DIAMETER ON MINIMUM AIR FLOW REQUIRED FOR SPOUTING.

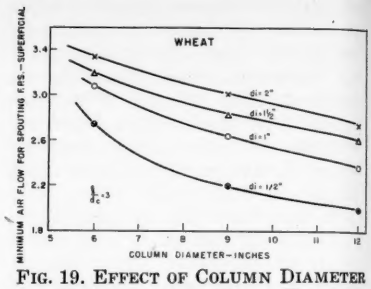

FIG. 19. EFFECT OF COLUMN DIAMETER ON MINIMUM AIR FLOW REQUIRED FOR SPOUTING (VARYING AIR INLET DIAMETER).

The value of the preceding expression for each 2-in. increment of the spout has been worked out by use of v_p from Figure 13 and v_a from Figure 11. This value, on substitution in Equation (1), gives the pressure drop per foot due to the solids density in the spout from which the voidage in the spout has been calculated. The results are included in Figure 14 and check fairly well with the voidage obtained from the solids flow in the annulus.

EFFECT OF MAJOR VARIABLES ON SPOUTING BEHAVIOR

The effect of such variables as column design and physical properties of the solids and the fluid on spouting behavior has been investigated.

EXPERIMENTAL

To study the effect of column design, wheat was chosen as a typical solid material, and air was used as the spouting medium. The experimental work was conducted in 4-, 6-, 9-, and 12-in.-diam. columns. The 4- and 6-in. columns were made of glass with metal cones; the two larger columns were of sheet iron. In each case an 85° cone was used at the base of the column. Data were taken on the maximum spoutable bed depth and the air requirement for spouting by use of varying air-inlet sizes for each of the foregoing columns. Some preliminary work has been conducted in a 2-ft.-diam. Plexiglas column.

For investigating the effect of the physical properties of solids on spouting behavior, a 6-in.-diam. glass column with a 3/8-in. standard pipe for air inlet at the base of an 85° (included) angle cone was used. A variety of solid materials of different sizes, densities, shapes and, surface characteristics were studied, air being used as the spouting fluid.

The major part of the work was done on air-solids spouting; however, to obtain an idea of the variation of fluid density on the flow required for spouting, experiments were also conducted with water as the spouting medium. Data were taken on 3-, 4-, and 6-in.-diam. glass columns using different water inlet sizes (1/16 to 1/2 in.) for a variety of solid materials. With water the circulation of solids has some resemblance to that in a "teeter"(*8*).

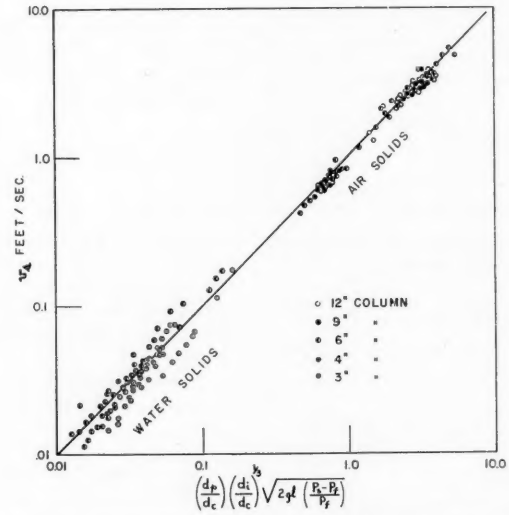

FIG. 20. CORRELATION OF DATA ON MINIMUM FLUID FLOW REQUIRED FOR SPOUTING.

RESULTS AND DISCUSSION

Maximum Spoutable Bed Depth. The maximum bed depth which can be made to spout has been found to depend upon the air-inlet diameter, the column diameter, and the physical properties of the solids.

Data on maximum spoutable bed depth as a function of air-inlet diameter for the 4-, 6-, 9-, and 12-in.-diam. columns, reported in Figure 15, indicate that deeper beds can be spouted with smaller air-inlet size. The curves, however, tend to flatten out for higher values of d_i until a sharp break occurs. This break represents the point at which the air-inlet diameter has become too large to cause a spout; at this point the bed would tend to fluidize. No experimental observations have been made in this region for wheat, and the dotted lines merely indicate the expected behavior.

The effect of column diameter on bed depth is clearly brought out by the series of curves in Figure 16, which shows λ_{max} against d_c for different ratios of d_c/d_i. Larger diameter columns permit higher spoutable bed depths; for example, in the 6-in. column the spoutable bed depth is limited to 26 in., and a bed as deep as 95 in. can be spouted in the 12-in.-diam. column.

Data on the maximum spoutable bed depths for a variety of solids in the 6-in.-diam. column is reported in Table 1. The factors governing the maximum spoutable

bed depth are complex and possibly include the interparticle friction of the solids besides their size, shape, and density. A correlation of the data on maximum spoutable bed depth was not found possible at this stage.

Air Flow Required for Spouting. The minimum air flow required for spouting has been studied as a function of bed depth, column diameter, air-inlet diameter, and physical properties of the solids. Data were taken with the wheat-air system to establish the effect of bed depth, column diameter, and air-inlet diameter, and the resultant significant trends are presented in Figures 17 to 19.

Minimum air required for spouting is plotted against bed depth in Figure 17 for the 6-, 9-, and 12-in.-diam. columns. The curves indicate that the air flow for spouting increases with bed depth, in contrast with the results in a fluidized bed, where the air flow is relatively independent of bed depth. The effect of column diameter on air flow for spouting is shown in Figure 19, which gives the superficial air velocity required for spouting as a function of column diameter. The series of curves in Figure 19 is for different values of air-inlet diameters and for a fixed λ/d_c ratio, indicating that lower superficial velocities are necessary for spouting in larger diameter columns. The air required for spouting increases with air-inlet diameter, as is indicated by Figure 18, which shows data plotted for the 6-, 9-, and 12-in. columns for an λ/d_c ratio of 3. The curve for the 12-in.-diam. column indicates that a sixfold increase in the air-inlet size caused an increase of about 35% in the air requirement.

The data plotted in the foregoing figures were obtained using 85° (included) angle cones for all the columns. Preliminary work on the 24-in.-diam. column by use of a 45° cone indicates that spouting is much more stable, and the air flow required for spouting is considerably lower with the steeper cone. For a 60-in.-deep bed of wheat in the 24-in. column, the air requirement was about 25% lower with a 45° cone than with an 85° cone. In the 6-in. column, however, the cone angle (85°, 60°, and 45°) did not show any marked influence on either the spouting behavior or the minimum air flow required for spouting. Further work is being conducted to establish the effect of cone angle on spouting behavior in different-sized columns.

TABLE 2.—DATA ON MINIMUM AIR REQUIREMENT FOR SPOUTING OF VARIOUS MATERIALS, 6-IN.-DIAM. COLUMN, ⅜-IN.-DIAM. AIR INLET

		Physical properties			
No.	Material	Effective particle diam., in.	Absolute density, lb./cu. ft.	Bed depth, in.	Air flow, ft./sec. superficial
1	Peas	0.2500	86.6	12	5.33
				10	4.76
				8	4.15
2	Wheat	0.1250	85.9	30	3.52
				24	3.21
				18	2.88
				12	2.44
3	Mustard seeds	0.0855	75.2	30	2.54
				24	2.19
				18	1.82
				12	1.44
4	Rape seeds	0.0691	68.9	30	2.02
				24	1.72
				18	1.44
				12	1.15
5	Ottawa sand (−20+35 mesh)	0.0232	145	24	0.74
				20	0.68
				16	0.61
				12	0.55
6	Gravel (−4+8 mesh)	0.1390	166.6	24.5	4.67
7	Gravel (−8+14 mesh)	0.0695	164.0	35.6	3.18
8	Gravel (−14+20 mesh)	0.0394	160.0	48.5	1.72
9	Gravel (−4+8) 1, (−8+14) 1	0.1320	165.3	31.7	3.14
10	Gravel (−8+14) 1, (−14+20) 1	0.0463	162.0	42.4	2.04
11	Gravel (−14+20) 1, (−20+35) 1	0.0240	158.0	26.5	0.82
12	Wheat 1, Mustard 1	0.0977	80.8	27.7	2.60
13	Wheat 1, Mustard 1, Peas 1	0.0997	82.7	22.3	2.91

TABLE 3.—SOLID MATERIALS USED WITH WATER AS THE SPOUTING MEDIUM

		Particle size		Absolute density,
No.	Material	Tyler mesh	d_p, in.	lb./cu. ft.
1	Quartz (crushed)	20/35	0.0232	164
2	Quartz (crushed)	14/20	0.0394	164
3	Catalyst (spheres)	6/8	0.124	219
4	Catalyst (spheres)	4/6	0.1504	219
5	Alundum	10/14	0.0555	242
6	Ottawa sand	20/35	0.0232	145
7	Gravel	8/14	0.0695	164
8	Gravel	14/20	0.0394	160
9	Gravel	20/35	0.0232	159
10	Galena	20/35	0.0232	464
11	Brucite	8/14	0.0695	156.5
12	Brucite	14/20	0.0394	156.5

Data on minimum air requirement for a variety of solid materials are given in Table 1. The air requirement was determined as a function of bed depth also for relatively spherical particles; the results are tabulated in Table 2, which also includes the air-requirement data at single bed depth for three sizes of gravel and a number of mixtures.

The solid materials used with water as the spouting medium are listed in Table 3, which also gives the physical properties. The results of this investigation are reported in Table 4.* The effect of the solids-particle size and density and of fluid density on fluid requirement for spouting has been established in the form of a dimensionless correlation. The correlation also includes bed depth, air-inlet diameter, and column diameter;

*Table 4 may be obtained from the American Documentation Institute, Photoduplication Service, Library of Congress, Washington 25, D. C., as document 4562 for $1.25 for microfilm or photoprints.

the individual effect of these on air flow requirement has already been discussed.

$$v_s = \left(\frac{d_p}{d_c}\right)\left(\frac{d_i}{d_c}\right)^{1/3}\sqrt{\frac{2g.\lambda.(\rho_s-\rho_f)}{\rho_f}}$$

The correlation has been derived empirically on the basis of the data in Tables 2 and 4*; however, the groups used may have theoretical significance. The plot of the data, based on the foot, pound, second system of units, is shown in Figure 20 for the following range of variables:

d_p = 0.023-0.25 in.
d_i = 1/16-2 1/8 in.
ρ_s = 69-464 lb./cu.ft.
d_c = 3-12 in.
λ = 3 1/2-106 in.
ρ_f = 0.073 and 62.4 lb./cu.ft.

For wheat, the smaller diameter was taken as the particle size since in the spout the particles would have a tendency to align themselves so as to offer a maximum resistance to the frictional drag of the air. This would be achieved when the smaller diameter of the wheat particle was normal to the flow of air. Visual observations in the spout justify this assumed orientation. The particle diameter used in the correlation for other materials is equivalent to the average screen opening, as these particles are essentially isometric in shape. For mixtures, the arithmetic average diameter and an average value of density weighted according to the mass fraction has been used.

APPLICATION TO WHEAT DRYING

The spouting-bed technique provides good contacting of gases with coarse solid particles in a cycling bed and should therefore be applicable to continuous drying. Wheat was used as the material tested.

A small pilot plant was built consisting of a 12-in.-diam. dryer column and a 9-in.-diam. cooler column each about 6 ft. high, connected by a series of overflow pipes so that different bed depths might be studied. Steam was used to preheat the air to the dryer, into which wheat of a known moisture content was fed at a predetermined rate. From here it overflowed into the cooler, average retention time being dependent on feed rate and bed volume.

The variables studied included inlet-air temperature (210° to 350°F.), initial moisture content of wheat (16 to 26%, wet basis), feed rate (240 to 600 lb./hr.), and bed depth (12 to 48 in.). The highest inlet-air temperature used without causing damage to the wheat was 350°F., which resulted in a bed temperature of 118°F. Under these conditions 600 lb./hr. of wheat were dried through a moisture range of 4%.

The cycling motion of the bed, coupled with the continuous mixing of fresh feed with the bed wheat, resulted in quite low (100° to 118°F.) bed temperatures despite the high inlet-air temperatures. A substantial amount of the sensible heat of the wheat entering the cooler was available for further moisture removal. Over-all heat efficiencies of 65% were obtained.

The drying behavior of the wheat indicated that this method should be particularly applicable to the drying of thermally sensitive coarse particles.

COMPARISON WITH OTHER TECHNIQUES

Spouting appears not to be just a special form of fluidizing. It can be applied to materials that are either too coarse or of too uniform a particle size for good fluidization. In fluidizing there is a net vertical upward motion of particles in the center of the bed and a net downward motion of particles at the wall, but the local effect is one of an apparently random motion of fine solid particles, with the entire bed expanded. In spouting, the upward motion is very rapid and is restricted to a well-defined central core. In the remainder of the bed there is never any upward motion of particles; rather, a packed bed is moving steadily downward and, to some extent, inward. This steady motion eliminates back mixing (*3, 9*). At the same time the fairly rapid bed turnover tends to eliminate the temperature differences usually associated with conventional packed-bed systems.

Studies on heat and mass transfer in a spouted bed are being conducted in order to compare the effectiveness of the technique with packed- and fluidized-bed systems.

SUMMARY

A study was made of the contacting of coarse solid particles and gases in a bed in which the gases forced the solids to cycle in a regular fashion. The flow pattern of both the gas and solids has been described, and the effect of column design and physical properties of solids and fluids on the flow rates required to produce spouting have been correlated.

ACKNOWLEDGMENT

The authors wish to acknowledge with thanks the contribution of data on water spouting by John Klassen and the assistance in experimental work by Gerald Crawford. Patent applications on this technique have been assigned to the Canadian Patent Development Corporation, National Research Council, Ottawa.

NOTATION

A = cross-sectional area of spout, sq. ft.
d_c = column diameter
d_i = fluid-inlet diameter
d_p = particle diameter
dP_f = change in static pressure due to friction
dP_a = change in static pressure due to acceleration
dP_w = change in static pressure due to solids density
g = acceleration due to gravity
h = spout level
λ = bed depth, in.
λ_{max} = maximum spoutable bed depth, in.
m = solids flow, lb./sec.
v_p = particle velocity in spout, ft./sec.
v_s = minimum superficial fluid velocity for spouting, ft./sec.
v_a = superficial air velocity through spout, ft./sec.
ρ_s = absolute density of solids, lb./cu.ft.
ρ_f = fluid density, lb./cu.ft.
ρ_v = density of solids in spout, lb./cu.ft.
ΔP = static pressure drop, in. of water

LITERATURE CITED

1. Brown. G. G., "Unit Operations," p. 74. John Wiley and Sons, Inc., New York (1950).
2. Gasterstadt, J., *Forsch. Gebiete Ingenieurw.*, 265, 3 (1924).
3. Gilliland, E. R., and E. A. Mason, *Ind. Eng. Chem*, 41, 1191 (1949).
4. Matheson, G. L., W. A. Herbst, and P. H. Holt, *Ind. Eng. Chem.*, 41, 1099 (1949).
5. Mathur, K. B., and P. E. Gishler, "A Study of the Application of the Spouted Bed Technique to Wheat Drying," presented to Society of Chemical Industry, London (Dec. 14, 1954).
6. Schwartz, C. E., and J. M. Smith, *Ind. Eng. Chem.* 45, 1209 (1953).
7. Sittig, M., *Chem. Eng.*, 60, 219 (1953).
8. Taggart, A. F., "Handbook of Mineral Dressing," pp 8-47, John Wiley and Sons, Inc., New York (1950).
9. Van Heerden, C., *J. Appl. Chem. (London)*, 2 Supplementary Issue No. 1, S7 (1952).

Presented at A.I.Ch.E. Glenwood Springs meeting.

* See footnote on page 163.

CRITICAL CONSTANTS OF UNSATURATED ALIPHATIC HYDROCARBONS

GEORGE THODOS

Northwestern Technological Institute, Evanston, Illinois

The van der Waals' constants *a* and *b* evaluated from structural considerations of the unsaturated aliphatic hydrocarbons are used to calculate the critical constants for these types of compounds. For these unsaturated hydrocarbons, both van der Waals' constants are calculated through the additive contribution of unsaturated bonds to the van der Waals' constants of the corresponding saturated aliphatic hydrocarbons calculated according to a method previously proposed (*6*).

With both van der Waals' constants available, the critical temperatures, pressures, and volumes for these types of compounds can be obtained.

By use of this approach, the critical temperatures, pressures, and volumes of several olefins, diolefins, and acetylenes have been calculated. These calculated values have been compared whenever possible with values reported in the literature to produce an average percentage deviation of 1.3 for the critical temperature, 3.0 for the critical pressure, and 1.5 for the critical volume. In this comparison questionable literature values have been included, and consequently the reported deviations present the worst possible expectation.

The prediction of the critical constants of the unsaturated aliphatic hydrocarbons is a subject that has received little attention in the past, primarily because of the lack of sufficient information from which a generalized approach could be established for the estimation of these critical values. Critical constants for a limited number of olefins, diolefins, and acetylenes are reported in the literature survey of Kobe and Lynn (*3*) and constitute the only data used in this study. From this information a method is developed that can be applied for the prediction of critical constants for the unsaturated aliphatic hydrocarbons only from a knowledge of the chemical structure of these compounds.

In a similar investigation dealing with saturated aliphatic hydrocarbons, Thodos (*6*) presents a method for estimating for this type of compound the pressure and volume van der Waals' constants a and *b*, respectively, which in turn are used to define the critical temperature and pressure of these substances through the relationships

$$T_c = \frac{8a}{27\,Rb} \qquad (1)$$

$$p_c = \frac{a}{27b^2} \qquad (2)$$

The evaluation of the van der Waals' constants for the saturated paraffins becomes possible by taking into account the additive contribution of these constants involved in the successive replacement of hydrogen by methyl groups until the desired saturated hydrocarbon structure is obtained. In this connection the contributions of both van der Waals' constants *a* and *b* were found to be additive with $a^{0.626}$ and $b^{0.76}$. The extension of this approach into the field of the unsaturated aliphatic hydrocarbons considers the removal of hydrogen atoms for the formation of unsaturated double and triple bonds from the corresponding saturated paraffins to produce the van der Waals' constants *a* and *b* for these unsaturated compounds.

From the screened literature critical constants of Kobe and Lynn (*3*) the critical temperatures and pressures of all the olefins, diolefins, and acetylenes for which values were available were used to calculate the pressure and volume van der Waals' constants *a* and *b* from the expressions

$$a = \frac{27R^2T_c^2}{64p_c} \qquad (3)$$

$$b = \frac{RT_c}{8p_c} \qquad (4)$$

Both van der Waals' constants resulting from Equations (3) and (4) are unique for the calculation of the critical temperatures and pressures; however, the use of the volume van der Waals' constant *b* in the theoretical relationship

$$v_c = 3b \qquad (5)$$

produces critical volumes for these unsaturated aliphatic hydrocarbons that are not in agreement with the values reported in the literature (*3*). A similar behavior has been found for the saturated aliphatic hydrocarbons by Thodos (*6*), who modified Equation (5) in order to produce critical volumes consistent with those reported in the literature. Thus introduction of the empirical volume factor β enables Equation (5) to assume the modified form

$$v_c = 3\beta b \qquad (6)$$

Equation (6) when applied to the normal paraffins produced volume factors β that were found to depend only on the number of carbon atoms present in the molecule. Furthermore, it was also found (*6*) that the ratio of the volume factors for the isomeric paraffins to those of the corresponding normal paraffins maintained the approximate value of 1.032 and proved to be independent of the degree of branching.

Volume factors for the limited number of monoolefins for which critical volumes are available have been calculated with Equation (6). These volume factor values β_u when referred to those of the corresponding saturated aliphatic hydrocarbons produced the following ratios:

	$\frac{\beta_u}{\beta_s}$
Ethene	0.9429
Propene	0.9919
1-Butene	1.0090
2-Butene	0.9990
2-Methylpropene	0.9725
	0.9931

The average value of the ratio β_u/β_s with the exclusion of the value for ethene was found to be 0.9931 and is recommended for monoolefins. A similar treatment of the data for 1,3-butadiene and ethyne produced ratios of 0.9863 and 0.9609, respectively. As a result of this study,

the following values for the volume factor ratios β_u/β_s are recommended:

	$\frac{\beta_u}{\beta_s}$
Monoolefins	0.9931
Diolefins	0.9863
Acetylenes	0.9609

TREATMENT OF VAN DER WAALS' CONSTANTS

By means of an approach parallel to that carried out for the saturated aliphatic hydrocarbons (*6*), values of $a^{0.626}$ and $b^{0.76}$ were produced for the unsaturated hydrocarbons used in this investigation and were compared with the values of the corresponding saturated aliphatic hydrocarbons. This comparison was made in order to establish contributions involved in the removal of hydrogen atoms to produce unsaturated double and triple bonds. Contribution values $\Delta a^{0.626}$ and $\Delta b^{0.76}$ involved in the removal of hydrogen atoms to form unsaturated bonds were found to depend primarily on the nature of the carbon atoms involved before the removal of the hydrogen atoms. To differentiate between the different types of carbon atoms, the designation of Andersen, Beyer and Watson (*1*) has been used. Their method associates directly the type of carbon atom with the number of carbon-to-carbon bonds present in the saturated aliphatic hydrocarbon. Thus the following structures constitute the types of carbon atoms occurring with saturated paraffins:

Type	1	2	3	4
Structure	$-CH_3$	$-CH_2-$	$-CH-$	$-C-$

and represent the types of carbon atoms always encountered in the introduction of the first double or triple bond. The contribution values $\Delta a^{0.626}$ and $\Delta b^{0.76}$ associated with the introduction of a second double bond have been found to depend on the nature of the carbon atoms directly involved in the formation of the bond and the nature of the carbon atoms adjacent to them. The adjacent carbon atoms may be attached to a double bond that influences the contribution value associated with the introduction of the second unsaturated bond. This condition necessitates a somewhat different classification of carbon atoms, and consequently the following designation has been adopted:

Type	$\dot{3}$	$\dot{4}$
	H	
Structure	$=C-$	$=C=$

The contribution values $\Delta a^{0.626}$ and $\Delta b^{0.76}$ resulting from the literature data are limited in number and do not as such represent all the possible cases that can arise. In order to present a larger number of combination types, the available information was extrapolated and interpolated as well as possible to produce the average contribution values reported in Table 1.

CALCULATION OF CRITICAL CONSTANTS

To illustrate the use of the method proposed in this investigation, the critical temperatures, pressures, and volumes of 1-butene, 1, 3-butadiene, and 1-butyne will be considered. For each of these substances, van der Waals' constants a and b must be produced, from which the critical temperature, pressure, and volume can be calculated. The van der Waals' constants for these unsaturated hydrocarbons can be calculated from the van der Waals' constants of the corresponding saturated paraffins. Thus from the work of Thodos (*6*) for n-butane, $a^{0.626} = 29{,}379$, $b^{0.76} = 37.137$, and $\beta_s = 0.7314$.

1-Butene

n-butane	29,379	37.137
from Table 1, first double bond (1-2)	— 1,518	— 1.940
	$a^{0.626} = 27{,}861$;	$b^{0.76} = 35.197$

$a = 12.603 \times 10^6$ (cc./g.mole)^2 atm., $b = 108.36$cc./g. mole

$$T_c = \frac{8a}{27\,Rb} = \frac{8\,(12.608 \times 10^6)}{27\,(82.055)\,(108.36)} = 420.1°\text{K.}$$

$$p_c = \frac{a}{27\,b^2} = \frac{12.608 \times 10^6}{27\,(108.36)^2} = 39.77 \text{ atm.}$$

for monoolefins: $\beta_u/\beta_s = 0.9931$; therefore, $\beta_u = 0.9931\,(0.7314) = 0.7264$

$$v_c = 3\beta_u = 3\,(0.7264)\,(108.36) = 236.1 \text{ cc. g. mole}$$

Kobe and Lynn (*3*) report for 1-butene critical values of 419.6°K., 39.7 atm., and 239.7 cc./g. mole.

1,3-Butadiene

n-butane	29,379	37.137
from Table 1,; first double bond (1-2)	— 1,518	— 1.940
second double bond (1-2→$\dot{3}$)	— 792	— 1,549
	$a^{0.626} = 27{,}069$;	$b^{0.76} = 33.648$

$a = 12.041 \times 10^6$ (cc./g. mole)^2 atm., $b = 102.13$ cc./g. mole

$$T_c = \frac{8a}{27\,Rb} = \frac{8\,(12.041 \times 10^6)}{27\,(82.055)\,(102.13)} = 425.7°\text{K.}$$

$$p_c = \frac{a}{27\,b^2} = \frac{12.041 \times 10^6}{27\,(102.13)^2} = 42.76 \text{ atm.}$$

for diolefins: $\beta_u/\beta_s = 0.9863$; therefore, $\beta_u = 0.9863\,(0.7314) = 0.7214$

$$v_c = 3\beta_u b = 3\,(0.7214)\,(102.13) = 221.0 \text{ cc./g. mole}$$

Kobe and Lynn (*3*) report for 1, 3-butadiene critical values of 425.2°K., 42.7 atm. and 220.8 cc./g. mole.

1-Butyne

n-butane	29,379	37.137
from Table 1, triple bond (1-2)	— 942	— 3.260
	$a^{0.626} = 28{,}437$;	$b^{0.76} = 33.877$

$a = 13.027 \times 10^6$ (cc./g. mole)^2 atm., $b = 103.04$ cc./g. mole.

$$T_c = \frac{8a}{27\,Rb} = \frac{8\,(13.027 \times 10^6)}{27\,(82.055)\,(103.04)} = 456.5°\text{K.}$$

$$p_c = \frac{a}{27\,b^2} = \frac{13.027 \times 10^6}{27\,(103.04)^2} = 45.44 \text{ atm.}$$

for acetylenes: $\beta_u/\beta_s = 0.9609$; therefore $\beta_u = 0.9609\,(0.7314) = 0.7028$

$$v_c = 3\beta_u b = 3\,(0.7028)\,(103.04) = 217.2 \text{ cc./g. mole.}$$

Kobe and Lynn (*3*) report for 1-butyne a critical temperature of 463.7°K. and no critical pressure and volume.

TABLE 2.—CALCULATED VAN DER WAALS' CONSTANTS AND COMPARISON OF CALCULATED AND REPORTED CRITICAL TEMPERATURES, PRESSURES AND VOLUMES FOR SOME OLEFINS, DIOLEFINS, AND ACETYLENES

TABLE 2.—CALCULATED VAN DER WAALS' CONSTANTS AND COMPARISON OF CALCULATED AND REPORTED CRITICAL TEMPERATURES, PRESSURES AND VOLUMES FOR SOME OLEFINS, DIOLEFINS, AND ACETYLENES

	Calculated van der Waals' Constants			Calculated			Literature (3)			Percentage deviation		
	$a^{0.626}$	$b^{0.76}$	a (cc./g. mole)^2 atm.	b cc./g. mole	T_c, °K.	p_c, atm.	v_c, cc./g. mole.	T_c, °K.	p_c, atm.	v_c, cc./g. mole	T_c	p_c	v_c
Olefins													
Ethene	14,633	21.742	4.507×10^6	57.49	283.1	50.51	129.9	283.1	50.5	123.6	0.00	−0.02	−5.10
2-Methylpropene	27,790	35.234	12.556	108.51	417.8	39.50	244.0	417.9	39.5	238.7	0.02	0.00	2.22
3-Methyl-1-butene	33,122	41.076	16.620	132.73	452.2	34.94	293.0	464.8	33.9	.....	2.71	−3.07	
1-Dodecene	79,197	88.685	66.898	365.56	660.8	18.54	680.2						
1-Eicosene	130,533	142.173	148.62	680.38	788.8	11.89	1049						
Diolefins													
1, 3-Butadiene	27,069	33.648	12.040	102.13	425.7	42.76	221.0	425.2	42.7	220.8	−0.12	−0.14	−0.11
1, 4-Pentadiene	32,760	39.943	16.330	127.98	460.7	36.92	271.9						
1, 5-Hexadiene	39,177	46.629	21.732	156.90	500.2	32.70	327.1	507.6	....	....	1.46		
Acetylenes													
Ethyne	14,431	19.992	4.408	51.48	309.2	61.61	112.5	309.2	61.6	112.7	0.00	−0.02	0.19
Propyne	22,020	27.191	8.658	77.16	405.2	53.86	165.7	401.2	52.8	....	−1.00	−2.01	
											1.30*	2.99*	1.50*
											0.78†	0.63‡	0.90**

*All deviations included in average value.
†Deviations of propadiene and 2-butyne not included.
‡Deviations of 1-pentene, 2-pentene, and 2-methyl-2-butene not included.
**Deviation of ethene not included.

Complete table is available from the American Documentation Institute, Photoduplication Service, Library of Congress, Washington 25, D. C., as document 4559, obtainable for $1.25 for microfilm or photoprints.

TABLE 1.—CONTRIBUTION VALUES, $\Delta a^{0.626}$ AND $\Delta b^{0.76}$, INVOLVED IN THE REMOVAL OF HYDROGEN ATOMS FROM SATURATED ALIPHATIC HYDROCARBONS TO PRODUCE UNSATURATED BONDS

	$\Delta a^{0.626}$	$\Delta b^{0.76}$
A. First double bond		
1–1	−1,941	−2.126
2–1	−1,518	−1.940
2–2	—1,204	—2.123
3–1	— 801	−1.692
3–2	— 561*	−1.858*
B. Second double bond		
3–1	— 610*	−1.158*
$\dot{3}$–1	— 713*	−1.814*
3–2	— 428*	−1.811*
$\dot{3}$–2	— 670*	−1.978*
$\dot{3}$–3	— 637*	−2.142*
$\dot{3}\leftarrow$–2–1	— 792	−1.549
$\dot{3}\leftarrow$–2–2	— 610*	−1.68*
$\dot{4}\leftarrow$–2–1	— 750*	−1.615
C. Triple bond		
1–1	−2,143	−3.876
1–2	— 942	−3.260
2–2	— 628*	−3.443*

*Estimated values.

Arrow points away from the carbon atoms involved in the formation of unsaturate bonds and toward the type of carbon atoms adjacent to them.

COMPARISON OF RESULTS

Following a similar approach, the critical temperatures, pressures, and volumes of forty-four unsaturated hydrocarbons, including olefins, diolefins, and acetylenes, have been calculated and appear in Table 2, where the calculated values are compared with those available in the literature(*3*) to produce average absolute deviations of 1.3% for the critical temperature, 3.0% for the critical pressure, and 1.5% for the critical volume. In these comparisons questionable literature values have been included and consequently the foregoing deviations present the worst possible expectation.

In order to compare the validity of the present method, critical values have been calculated by the methods of Riedel(*4, 5*) and Lydersen(*2*). Riedel utilizes a method involving group contributions and the molecular weight to calculate the critical pressure(*4*) and the normal boiling point to establish the critical temperature(*5*). Lydersen(*2*) refines the method of Rie-

del (4, 5) and extends his work to include the critical volume. Critical values for the unsaturated aliphatic hydrocarbons, for which literature data are available and appear in Table 2, have been calculated by these methods and compared to produce the following average percentage deviations:

Critical value	(4,5)	(2)	This work
Temperature	1.53	1.71	1.30
Pressure	3.58	3.70	2.99
Volume	....	1.97	1.50

The comparisons in the present investigation appearing in Table 2 point to significant deviations of critical temperature for propadiene and 2-butyne, of critical pressure for the pentenes and 2-methyl-2-butene, and of critical volume for ethene. If the deviations for these compounds are not included in the over-all average values, the deviations become 0.78% for the critical temperature, 0.63% for the critical pressure, and 0.90% for the critical volume.

NOTATION

a = pressure van der Waals' constant, (cc./g. mole)^2 atm.
b = volume van der Waals' constant, cc./g. mole
p_c = critical pressure, atm.
R = gas constant, 82.055 (atm.) (cc.) / (g. mole) (°K.)
T_c = critical temperature, °K.
v_c = critical volume, cm./g. mole
β_s = volume factor for saturated aliphatic hydrocarbons
β_u = volume factor for unsaturated aliphatic hydrocarbons

LITERATURE CITED

1. Andersen, J. W., G. H. Beyer, and K. M. Watson, *Nat. Petroleum News, Tech. Sec.*, 35, R476 (July 5, 1944).
2. Hougen, O. A., K. M. Watson, and R. A. Ragatz, "Chemical Process Principles," pp. 87-95, John Wiley and Sons, New York (1954).
3. Kobe, K. A., and R. E. Lynn, Jr., *Chem. Rev.*, 52, 117-236 (1953).
4. Riedel, L., *Z. Elektrochem.*, 53, 222-28 (1949).
5. Riedel, L., *Chem. Ing. Tech.*, 24, 353-7 (1952).
6. Thodos, G., *A.I.Ch.E. Journal*, 1, 168-173 (1955).

CRITICAL CONSTANTS OF SATURATED ALIPHATIC HYDROCARBONS

Through the use of group contributions the van der Waals' constants, a and b, were estimated for a number of saturated aliphatic hydrocarbons from a knowledge of the chemical structure of these compounds and were used to define the critical temperature and pressure of these substances.

By the use of methane as the base group, both van der Waals' constants were estimated for a number of saturated aliphatic hydrocarbons of considerable size and complexity through the additive contribution of methyl groups in the successive substitution of hydrogen until the desired structure of the substance was obtained. For the normal saturated hydrocarbons these contributions were found to be additive for the evaluation of $a^{0.626}$ and $b^{0.76}$ up through n-octane, and these exponents have been assumed to apply in the scaling up of larger normal and isomeric hydrocarbon molecules for which experimental data are lacking.

The volume van der Waals' constant b alone serves to define the critical volume of these compounds through the expression $v_c = 3\ \beta\ b$, where β represents a factor which has been found to depend on the size and arrangement of the molecule.

By following this procedure the critical temperatures, pressures and volumes of the normal saturated hydrocarbons through eicosane ($C_{20}H_{42}$), inclusive, and all the isomeric hydrocarbons up to and through the nonanes were calculated and compared, whenever possible, with values already available in the literature with an agreement of 0.43% for the estimation of the critical temperature, 0.69% for the critical pressure, and 0.86% for the critical volume. A combined consideration of these average deviations points to the estimation of the critical constants of the aliphatic saturated hydrocarbons with an average error of 0.7%.

George Thodos
Northwestern Technological Institute
Evanston, Illinois

The ever-present problem of the prediction of the critical constants of substances has received considerable attention from a number of investigators. For the estimation of the critical values some of the common physical properties of a substance such as density, normal boiling point, molecular weight, and surface tension have been used as correlating variables. When information is available, these properties prove satisfactory for estimating the critical constants for a

Complete tabular matter is available from the American Documentation Institute, Photoduplication Service, Library of Congress, Washington 25, D. C., as document 4563 for $1.25 for microfilm or photoprints.

number of compounds, but frequently the required information on the physical properties of substances is not readily available.

For the estimation of the critical temperature of a compound, Watson(*13*) proposed a method which uses the normal boiling point, liquid density at this temperature, and the molecular weight of the substance. For some normal saturated paraffins, Wan(*12*) was able to predict critical temperatures from molar refraction. Gamson and Watson(*4*) defined the critical pressure of hydrocarbons through a vapor-presure equation of the reduced state, Meissner and Redding (*8*) introduced the use of the parachor and normal boiling point, and

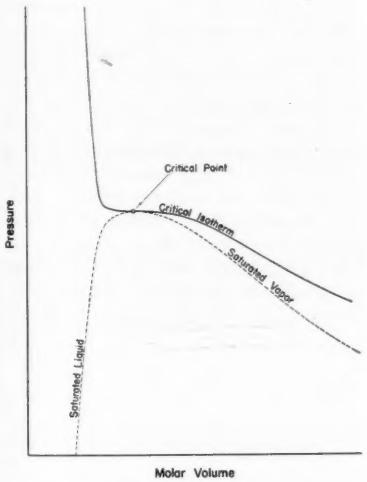

FIG. 1. TYPICAL PRESSURE-VOLUME RELATIONSHIP OF A SUBSTANCE AT ITS CRITICAL ISOTHERM.

Herzog(*5*) followed a similar procedure to present the critical constants for a number of hydrocarbons. Boas(*2*) used the Albertosi equation in reduced form to estimate the critical temperatures of organic compounds from liquid density data which when associated with viscosity data in the Souders equation also make possible the estimation of critical densities. Riedel(*10, 11*) through the use of group contributions, the normal boiling point, and molecular weight of a substance was able to predict the critical temperature and pressure of substances. The work of Riedel was refined and extended to include the critical volume by Lydersen(*6*). These methods, although valuable in themselves, are frequently inconvenient to apply because of the lack of some one needed physical property. Michael and Thodos(*9*) estimated the parachor from a knowledge of the chemical structure of hydrocarbons

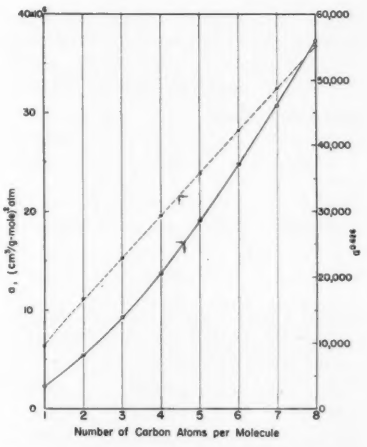

FIG. 2. RELATIONSHIPS OF PRESSURE VAN DER WAALS' CONSTANT *a* VS. NUMBER OF CARBON ATOMS PER MOLECULE FOR THE LIGHT NORMAL PARAFFINS.

and used it for the estimation of van der Waals' constants, which in turn define the critical temperature and pressure of these compounds. Although this method is capable of predicting critical constants with an absolute average error of 1.8%, its use for various types of hydrocarbons demands the determination of the parachor from which the van der Waals' constants can be calculated.

The present investigation was undertaken objectively to establish the van der Waals' constants directly from a knowledge of the chemical structure of the compound without any recourse to parachor evaluation.

RELATIONSHIPS OF CRITICAL CONSTANTS AND VAN DER WAALS' CONSTANTS

The pressure-volume relationship of real gases at isothermal conditions as expressed by the van der Waals' equation of state:

$$\left(p + \frac{a}{v^2}\right)(v - b) = RT \quad (1)$$

makes possible the development of fundamental expressions relating the critical temperature, pressure, and volume of pure substances with their van der Waals' constants. In this connection, use is made of the pressure-volume relationship at the critical isotherm which is continuous and exhibits an inflection point of zero slope at the critical pressure and volume of the substance. This behavior is illustrated for a typical case in Figure 1, from which it is apparent for this restricted case of isothermal conditions at the critical temperature that $[\partial p/\partial v]_{T_c} = 0$ and $[\partial^2 p/\partial v^2]_{T_c} = 0$. By application of these

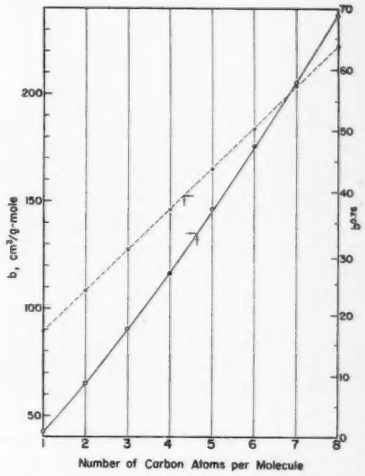

FIG. 3. RELATIONSHIPS OF VOLUME VAN DER WAALS' CONSTANT *b* VS. NUMBER OF CARBON ATOMS PER MOLECULE FOR THE LIGHT NORMAL PARAFFINS.

restrictions to the critical isotherm, it is possible to define the critical volume, temperature, and pressure of a substance in terms of the van der Waals' constants *a* and *b*. These developments have been presented by Dodge(*3*), the final results being summarized as follows:

$$v_c = 3b \quad (2)$$

$$T_c = \frac{8a}{27Rb} \quad (3)$$

and

$$p_c = \frac{a}{27b^2} \quad (4)$$

TABLE 1.—CRITICAL TEMPERATURES AND PRESSURES AND CALCULATED VAN DER WAALS' CONSTANTS FOR THE LIGHT NORMAL SATURATED HYDROCARBONS

	T_c, °K.	p_c, atm.	Van der Waals' Constants a (cc./g.-mole)² atm.	b cc./g.-mole
Methane	191.065	45.8	2.264×10^6	42.79
Ethane	305.465	48.2	5.499	65.00
Propane	369.965	42.0	9.257	90.35
n-Butane	425.165	37.5	13.692	116.29
n-Pentane	469.765	33.3	18.824	144.70
n-Hexane	507.865	29.9	24.503	174.22
n-Heptane	540.165	27.0	30.696	205.20
n-Octane	569.365	24.6	37.432	237.40

By use of Equations (2), (3), and (4), it is possible to define both van der Waals' constants in terms of the critical temperature and pressure of a substance:

$$a = \frac{27R^2T_c^2}{64p_c} \tag{5}$$

and

$$b = \frac{RT_c}{8p_c} \tag{6}$$

Equations (5) and (6) permit the evaluation of the van der Waals' constants from the critical temperature and pressure of the substance and conversely the critical temperature and pressure of a substance becomes possible of definition through a knowledge of the van der Waals' constants with the aid of Equations (3) and (4).

FUNDAMENTAL CONSIDERATIONS

The recent exhaustive literature survey of Kobe and Lynn(*7*) dealing with the critical constants of substances was used as the source of critical data from which van der Waals' constants were calculated with the aid of Equations (5) and (6). The critical values recommended by these authors represent the best constants available to date and consequently have been accepted as sufficiently reliable to evaluate from them the van der Waals' constants a and b, which were studied further in detail. For purpose of presentation, the critical constants of the normal saturated hydrocarbons from methane through *n*-octane have been presented in Table 1 along with the corresponding van der Waals' constants calculated from them. A study of these constants reveals that their variation with the number of carbon atoms is not linear but instead curved, as shown in Figures 2 and 3.

In order to obtain linear variations, both constants a and b were arbitrarily raised to different exponents, m and n respectively, until linear distributions of a^m and b^n were realized with the number of carbon atoms present in the chain length. A trial-and-error procedure revealed that values of $m = 0.626$ and $n = 0.76$ produced good linear relationships for all the normal saturated hydrocarbons from propane through *n*-octane. Since the critical values for the normal hydrocarbons used in this analysis are well established and represent considerable accuracy and since establishing a method applicable to hydrocarbons in general is desired, these exponents have been assumed to apply in the same manner to the isomeric hydrocarbons as well.

An exhaustive analysis of the calculated van der Waals' constants a and b raised to the 0.626 and 0.76 powers, respectively, indicated that there exists an additive contribution in the substitution of hydrogen by a methyl group. Changes in the values $a^{0.626}$ and $b^{0.76}$, designated as $\Delta a^{0.626}$ and $\Delta b^{0.76}$, appeared to be consistent as postulated by Andersen, Beyer, and Watson(*1*) for comparable substitutions in the evaluation of the thermodynamic properties of compounds. The classification of the types of carbon atoms involved in these studies has been arbitrarily selected to be that proposed by Andersen, Beyer, and Watson(*1*), summarized as follows:

Type	1	2	3	4
Structure	$-CH_3$	$-CH_2-$	$-CH-$	$-C-$

In the present study it was found that the values $\Delta a^{0.626}$ and $\Delta b^{0.76}$ were dependent not only on the type of carbon atom on which the methyl group substitution was made, but were also influenced by the nature of the carbon atoms adjacent to the carbon atom. Therefore, it became necessary to associate both the type of carbon atom directly involved in the substitution and also the nature of the carbon atoms immediately surrounding it. The results of a detailed analysis of the available data for all the saturated aliphatic hydrocarbons through the octanes produced the average group contributions for both $\Delta a^{0.626}$ and $\Delta b^{0.76}$ appearing in Table 2. In this table the designation given to the type of carbon atom involved in the substitution has been arbitrarily tagged as the one from which the

TABLE 2.—METHYL GROUP CONTRIBUTIONS $\Delta a^{0.626}$ AND $\Delta b^{0.76}$ IN THE REPLACEMENT OF HYDROGEN FROM SATURATED ALIPHATIC HYDROCARBONS

Base group values

	$a^{0.626}$	$b^{0.76}$
Methane	9509	17.371

Methyl Group Contributions in the Replacement of Hydrogen from Methane

$\Delta a^{0.626}$	$\Delta b^{0.76}$
7065	6.497

Methyl Group Contributions in the Replacement of Hydrogen from Saturated Aliphatic Hydrocarbons

	$\Delta a^{0.626}$	$\Delta b^{0.76}$
1 ← 1	6388	6.583
2 ← 1	6417	6.686
3 ← 1	5742	5.450
4 ← 1	5968	4.870
1 ← 2 → 1	5629	6.475
1 ← 2 → 2	5261	5.879
1 ← 2 → 3	5250	5.065
1 ← 2 → 4	5189	4.351
2 ← 2 → 2	4865	4.663
2 ← 2 → 3	4758	3.882
2 ← 2 → 4	4750	3.354
3 ← 2 → 3	5137	3.481
1 ← 3 → 1	4895	5.817
↓ 1		
1 ← 3 → 2	4575	4.455
↓ 1		
3 ← 3 → 1	4307	3.781
↓ 1		
1 ← 3 → 4	4087	3.471
↓ 1		
2 ← 3 → 2	4082	3.658
↓ 1		
3 ← 3 → 2	3814	2.984
↓ 1		
3 ← 3 → 3	3719	2.200
↓ 1		
2 ← 3 → 2	3770	2.401
↓ 2		

arrows point away and toward the types of carbon atoms adjoining it. For instance, the designation 3-←1 indicates the substitution of a hydrogen atom by a methyl group on a carbon atom of type 1 ($-CH_3$) adjoined to a carbon atom of type 3 ($-\overset{|}{\underset{|}{C}}H$). Thus, the following structures are representative of this kind of substitution:

$$\begin{array}{ccc} & & CH_3 \\ & & | \\ CH_3 & & CH_2 \\ | & & | \\ -CH_2-CH-CH_2- & \longrightarrow & -CH_2-CH-CH_2- \end{array}$$

The designation 2-←2→-2 indicates the substitution of a methyl group for hydrogen on a type 2 carbon atom ($-CH_2-$) adjoined on both sides by carbon atoms of similar type. For this case this type of substitution suggests the following structural transformation:

$$\begin{array}{ccc} & & CH_3 \\ & & | \\ -CH_2-CH_2-CH_2- & \longrightarrow & -CH_2-CH-CH_2- \end{array}$$

Furthermore, the designation

$$\begin{array}{c} 2 \leftarrow 3 \rightarrow 1 \\ \downarrow \\ 1 \end{array}$$

considers the methyl group substitution on the type 3 carbon atom ($-\overset{|}{\underset{|}{C}}H$) for its hydrogen atom to produce the resulting structure:

$$\begin{array}{ccc} & & CH_3 \\ & & | \\ -CH_2-CH-CH_3 & \longrightarrow & -CH_2-C-CH_3 \\ | & & | \\ CH_3 & & CH_3 \end{array}$$

Through this proposed method the evaluation of both $a^{0.626}$ and $b^{0.76}$ for the normal saturated hydrocarbons is direct and no ambiguity can arise, because the constructive process for building up molecules consists of successive methyl group substitutions for the hydrogen atoms present at the end of the hydrocarbon chain. However, considerable ambiguity can arise in the introduction of methyl groups to produce branched chain hydrocarbons because the order of these substitutions can be varied. For this reason the following sequence pattern has been adopted in the construction of molecular structures for branched hydrocarbons:

1. Construct the longest normal chain present in the hydrocarbon.
2. Produce only single methyl group substitutions directly on the normal chain beginning from the left end of the normal chain and moving always in a clockwise direction.
3. If necessary, continue methyl group substitutions on already substituted methyl groups by maintaining the previously established clockwise direction until the desired structure is realized.

In accordance with this approach van der Waals' constants for all the saturated aliphatic hydrocarbons were calculated and were found to agree closely with those obtained directly from the critical values of Kobe and Lynn (7).

Since Equations (5) and (6) utilize the critical temperature and pressure to define both van der Waals' constants, compatibility necessarily must exist between the critical temperature and pressure with both van der Waals' constants a and b. An extension of this background to consider the critical volume in this study produced results that were not consistent with the theoretical development presented in Equation (2). Van der Waals' constant b when divided into the critical volumes reported in the literature (7) produced ratios inconsistent with the value of 3 dictated by Equation (2) and varied from 2.314 for methane to 2.065 for n-octane. In view of this behavior Equation (2) has been modified in order to produce with the volume van der Waals' constant b, critical volumes that are consistent with those reported in the literature. With the introduction of the empirical volume factor, β, Equation (2) becomes

$$v_c = 3\beta b \qquad (7)$$

where β has been found to be a function of the number of carbon atoms in the hydrocarbon and to depend on the arrangement of the molecule. The volume factor, β_n, for the normal paraffins can be defined as

$$\beta_n = 0.7849 - 0.01337\, n_c \qquad (8)$$

where n_c represents the number of carbon atoms present in the normal paraffin. A review of volume factors, β, revealed that this factor remained essentially constant for isomeric paraffins having the same number of carbon atoms and decreased with increasing molecular weight of the hydrocarbon. The resulting average values of β_i for the isomers when divided by the volume factor of the corresponding normal paraffin produced essentially constant ratios as indicated:

	$\frac{\beta_i}{\beta_n}$
butanes	1.032
pentanes	1.000
hexanes	1.026
heptanes	1.032
octanes	1.039

By elimination of the value for the pentanes, the average value of the ratios β_i/β_n resulting from the value for butanes, hexanes, heptanes, and octanes becomes

$$\frac{\beta_i}{\beta_n} = 1.032 \qquad (9)$$

where β_i represents the volume factor for any isomeric paraffin and β_n is the volume factor of the corresponding normal paraffin as calculated by Equation (8). Combining Equations (8) and (9) results in an expression defining the volume factor of isomeric paraffins, β_i

$$\beta_i = 0.8100 - 0.0138\, n_c \qquad (10)$$

For the normal paraffins pentane through dodecane, critical volumes have been calculated by the present method and that of Boas (2), who utilized liquid density and viscosity data to estimate the critical density. The critical volumes produced by both methods are presented in Table 3 along with the available literature values. They

TABLE 3.—COMPARISON OF CALCULATED CRITICAL VOLUMES OBTAINED BY THE METHOD OF BOAS (2) AND THE PRESENT INVESTIGATION FOR SOME NORMAL PARAFFINS

	Calculated critical volumes, cc./g.-mole		
	Literature (7)	Boas (2)	This Investigation
Pentane	310.99	305.98	311.42
Hexane	368.25	366.68	368.47
Heptane	426.38	424.58	425.71
Octane	490.21	484.60	482.80
Nonane		544.59	539.56
Decane		604.67	595.59
Undecane		665.39	650.63
Dodecane		725.74	704.66

TABLE 4.—CALCULATED VAN DER WAALS' CONSTANTS AND COMPARISON OF CALCULATED AND REPORTED CRITICAL TEMPERATURES, PRESSURES, AND VOLUMES FOR THE LIGHT SATURATED ALIPHATIC HYDROCARBONS

	Calculated van der Waals' constants			Calculated critical constants			Literature values (7)			Percentage deviation		
	$a^{0.626}$	$b^{0.76}$	a (cc./g.-mole)² atm. / b cc./g.-mole	T_c, °K.	p_c atm.	v_c cc./g.-mole	T_c, °K.	p_c atm.	v_c cc./g.-mole	T_c	p_c	v_c
n-Pentane	35,796	43.823	18.816×10⁶ / 144.58	469.9	33.33	311.42	469.8	33.3	310.99	−0.02	−0.09	−0.14
2, 2-Dimethylpropane	33,486	42.743	16.914 / 139.92	436.5	32.00	311.04	433.8	31.6	303.15	−0.62	−1.27	−2.60
n-Hexane	42,213	50.509	24.486 / 174.29	507.3	29.86	368.47	507.9	29.9	368.25	0.12	0.14	−0.06
2, 2-Dimethylbutane	39,215	47.471	21.768 / 160.63	489.4	31.24	350.48	489.4	30.7	366.68	0.00	−1.76	4.42
n-Heptane	48,630	57.195	30.696 / 205.27	540.0	26.98	425.71	540.2	27.0	426.38	0.04	0.07	0.16
3-Methylhexane	47,078	55.172	29.147 / 195.77	537.6	28.17	418.99	535.6	28.1	417.50	−0.37	−0.25	−0.36
2, 2, 3-Trimethylbutane	44,197	51.862	26.350 / 180.46	527.3	29.97	386.22	531.5	29.75	394.49	0.79	−0.74	2.10
n-Octane	55,047	63.881	37.420 / 237.40	569.2	24.59	482.80	569.4	24.6	490.21	0.04	0.04	1.51
4-Methylheptane	53,495	61.858	35.747 / 227.57	567.2	25.56	477.62	563.2	25.6	475.92	−0.71	0.16	−0.36
2, 5-Dimethylhexane	52,735	62.267	34.940 / 229.55	549.6	24.56	481.78	550.0	24.6	481.94	0.07	0.16	0.03
2, 2, 4-Trimethylpentane	50,893	60.036	33.010 / 218.78	544.8	25.54	459.18	544.1	25.4	470.04	−0.13	−0.16	2.31

TABLE 5.—CALCULATED VAN DER WAALS' CONSTANTS AND CRITICAL TEMPERATURES, PRESSURES, AND VOLUMES FOR SOME OF THE HEAVIER SATURATED ALIPHATIC HYDROCARBONS

	Van der Waals' constants		Calculated critical constants		
	a (cc./g.-mole)² atm	b cc./g.-mole	T_c, °K.	p_c, atm.	v_c, cc./g.-mole
Nonanes					
n-Nonane	44.625×10⁶	270.62	595.4	22.57	539.6
3-Ethylheptane	42.069	254.31	597.3	24.09	523.2
2, 5-Dimethylheptane	41.526	256.44	584.7	23.39	527.6
4, 4-Dimethylheptane	40.200	245.44	591.4	24.72	505.0
2, 2, 3-Trimethylhexane	39.054	238.24	591.9	25.48	490.2
2, 3, 5-Trimethylhexane	40.109	248.55	582.7	24.04	511.4
2, 2, 4, 4-Tetramethylpentane	37.876	240.40	568.9	24.27	494.6
Normal saturated hydrocarbons					
n-Decane	52.298	304.87	619.4	20.84	595.6
n-Pentadecane	97.052	489.30	716.2	15.02	857.8
n-Eicosane	151.40	692.47	789.5	11.69	1075

show good agreement through *n*-octane. For the normal paraffins above *n*-octane, no absolute comparisons can be made with the calculated critical volumes because of the lack of literature values. The method of Boas (2) produces for these heavier hydrocarbons critical volumes that are somewhat higher than those predicted by the present method.

ILLUSTRATION A

In order to illustrate the utility of the proposed method, van der Waals' constants a and b are calculated for 2, 2, 4-trimethylpentane, from which all the critical constants are evaluated. Beginning with methane, the van der Waals' constants are calculated by the successive substitutions on methane to produce *n*-pentane, and then side chain substitutions are made in the order of 2, 4, and 2 as outlined below:

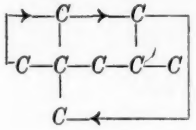

Methane-base group	9509	17.371
Primary methyl substitution	7065	6.497
Secondary methyl substitutions		
1 ← 1	6388	6.583
2 ← 1	6417	6.686
2 ← 1	6417	6.686
1 ← 2 → 2	5261	5.879
2 ← 2 → 1	5261	5.879
1 ← 3 → 2	4575	4.455
↓ 1	$a^{0.626}=50{,}893$	$b^{0.76}=60.036$

$a=33.010\times10^6$ (cc./g.-mole)² atm. $b=218.78$ cc./g.-mole

from Equation (3) $T_c=\dfrac{8a}{27Rb}=\dfrac{8\times33.010\times10^6}{17\times82.055\times218.78}=544.8°$ K.

and Equation (4) $p_c=\dfrac{a}{27b^2}=\dfrac{33.010\times10^6}{27\ (218.78)^2}=25.54$ atm.

The volume factor β_i for this hydrocarbon becomes through the use of Equation (10)

$$\beta_i=0.8100-0.0138\ (8)=0.6996$$

By use of Equation (7) the critical volume of this isometric paraffin becomes $v_c=3(0.6996)\ (218.78)=459.2$ cc./g.-mole.

Kobe and Lynn (7) report for 2, 2, 4-trimethylpentane critical values of 544.1°K., 25.4 atm., and 470.0 cc./g.-mole.

ILLUSTRATION B

The evaluation of van der Waals' constants a and b and the corresponding calculated critical temperature, pressure, and volume is presented for 2-methyl-3-ethylpentane in order to illustrate a case in which a methyl substitution is made on an already substituted methyl group. The order of methyl group substitutions will be along the following pattern:

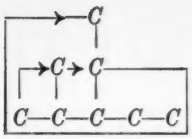

Methane—base group	9509	17.371
Primary methyl substitution	7065	6.497
Secondary methyl substitutions		
1 ← 1	6388	6.583
2 ← 1	6417	6.686
2 ← 1	6417	6.686
1 ← 2 → 2	5261	5.879
3 ← 2 → 2	4758	3.882
3 ← 1	5742	5.450
	$a^{0.626}=51{,}557$	$b^{0.76}=59.034$

$a=33.702\times10^6$ (cc./g.-mole)^2 atm. $b=214.00$ cc./g.-mole

$$T_c=\frac{8a}{27Rb}=\frac{8\times33.702\times10^6}{27\times82.055\times214.00}=568.6^\circ\text{ K.}$$

$$p_c=\frac{a}{27b^2}=\frac{33.702\times10^6}{27\ (214.00)^2}=27.26\text{ atm.}$$

The volume factor, β_i, for 2-methyl-3-ethylpentane is the same as that calculated for 2,2,4-trimethylpentane presented in illustration *A*. Therefore the critical volume of 2-methyl-3-ethylpentane becomes

$v_c=3(0.6996)\ (214.00)=449.12$ cc./g.-mole.

Kobe and Lynn (*7*) report for 2-methyl-3-ethylpentane critical values of 568.2°K., 27.4 atm., and 449.68 cc./g.-mole.

A direct comparison of critical temperatures, pressures, and volumes calculated by this method and those reported by Kobe and Lynn (*7*) is presented in Table 4.* In this table are also included the calculated van der Waals' constants a and b resulting from the present group contribution method and the $\Delta a^{0.626}$ and $\Delta b^{0.76}$ values appearing in Table 2. As a result of these comparative studies on thirty-eight saturated aliphatic hydrocarbons for which literature values are available, an average percentage deviation for the critical temperature of 0.43, for the critical pressure of 0.69, and for the critical volume of 0.86 was found to exist. In view of these percentage deviations, it is safe to assume that the critical temperature, pressure, and volume for the saturated aliphatic hydrocarbons can be estimated by the proposed method with an average deviation of 0.7%.

A comparison of the proposed method with a similar scheme of Riedel (*10, 11*) has been carried out. The method of Riedel (*11*) utilizes group contributions and the normal boiling point of the substance to predict the critical temperature. For the thirty-eight saturated aliphatic hydrocarbons studied, the average deviation for the prediction of the critical temperature amounts to 0.74%. For the estimation of the critical pressure Riedel (*10*) is able to treat adequately the normal paraffins, but because of inconsistencies is unable to account properly for the critical pressures of branched chain paraffins. Despite this limitation, Riedel proposes the use of a common group contribution for the different types of carbon atoms existing in the aliphatic saturated hydrocarbons to produce with the aid of the molecular weight, critical pressures for branched chain paraffins. For the thirty-eight compounds investigated, the critical pressures calculated by the method of Riedel gave an average deviation of 5.78%.

Hougen, Watson, and Ragatz (*6*) present the method of Lydersen which has been used to calculate all the critical constants of the paraffins for which literature data are available. Lydersen improves on the method of Riedel by producing refined group contributions to predict both the critical temperature and pressure of substances and extends this work to include the critical volume. A careful study of the thirty-eight paraffins treated above produced critical temperatures, pressures, and volumes that showed an average deviation of 0.50, 3.82 and 2.03% respectively. A review of the results produced by the method of Lydersen shows that the critical temperatures can be evaluated with a high degree of precision and the greatest uncertainty lies in the estimation of the critical pressure.

For completeness, the critical constants of all the saturated nonanes and the normal saturated hydrocarbons from *n*-decane through *n*=eicosane inclusive, have been calculated and are presented in Table 5* along with the corresponding calculated van der Waals' constants. For these hydrocarbons no comparisons can be made since the literature does not present the reliable experimental values needed.

* See footnote on page 168.

NOTATION

a = pressure van der Waals' constant, (cc./g.-mole)^2, atm.
b = volume van der Waals' constant, cc./g.-mole
m, n = arbitrary constants (m = 0.626, n = 0.76)
n_c = number of carbon atoms in saturated aliphatic hydrocarbon
p = pressure, atm.
p_c = critical pressure, atm.
R = gas constant, 82.055 (atm.) (cc.)/(K.°) (g.-mole)
T = temperature, °K.
T_c = critical temperature, °K.
v = molar volume, cc./g.-mole
v_c = critical volume, cc./g.-mole
β = volume factor
β_i = volume factor for isomeric paraffins
β_n = volume factor for normal paraffins
Δ = change in the substitution of hydrogen by a methyl group

LITERATURE CITED

1. Andersen, J. W., Beyer, G. H., and K. M. Watson, *Natl. Petroleum News*, **36**, R476 (July 5, 1944).
2. Boas, A., *Ind. Eng. Chem.*, **40**, 2202-3 (1948).
3. Dodge, B. F., "Chemical Engineering Thermodynamics," pp. 172-4, McGraw-Hill Book Company, Inc., New York (1944).
4. Gamson, B. W., and K. M. Watson, *Natl. Petroleum News*, **36**, R258-64 (1944).
5. Herzog, R., *Ind. Eng. Chem.*, **36**, 997-1001 (1944).
6. Hougen, O. A., Watson, K. M., and R. A. Ragatz, "Chemical Process Principles," pp. 87-95, John Wiley and Sons, New York (1954).
7. Kobe, K. A., and R. E. Lynn, Jr., *Chem. Revs.*, **52**, 117-236 (1953).
8. Meissner, H. P., and E. M. Redding, *Ind. Eng. Chem.*, **34**, 521-25 (1942).
9. Michael, G. V., and George Thodos, *Chem. Eng. Progr. Symposium Series No. 7*, **49**, 131-46 (1953).
10. Riedel, L., *Z. Elektrochem.*, **53**, 222-28 (1949).
11. Riedel, L., *Chem. Ing. Tech.*, **24**, 353-7 (1952).
12. Wan, S. W., *J. Phys. Chem.*, **45**, 903-7 (1941).
13. Watson, K. M., *Ind. Eng. Chem.*, **23**, 360-4 (1931).

SURFACE TENSION AND THE PRINCIPLE OF CORRESPONDING STATES

James R. Brock and R. Byron Bird, University of Wisconsin, Madison, Wisconsin

Experimental surface-tension data for pure substances have been correlated successfully by the use of two recent modifications of the principle of corresponding states. The results are expressed in terms of simple analytical relations which allow one to calculate the surface-tension curves either from the critical constants P_c, V_c, and T_c or from P_c, T_c, and the boiling point T_b and also provide a method for estimating critical properties from surface-tension measurements. In addition, a method for estimating the surface tension of molten metals is suggested.

There is at present considerable interest in fluid mechanics problems involving free surfaces in connection with the reexamination of the unit operations in terms of the fundamental transport processes taking place. It is therefore important to have experimental data on surface properties or in the absence of such data to be able to make intelligent predictions of them.

The current status of the experimental data and the theory of surface tension is not too satisfactory. Many of the data in the standard handbooks are more than thirty years old and have never been corroborated by subsequent investigators. Also the discrepancies between measurements on a given substance by two different methods have not been properly explained. Considerable progress has been made, however, in developing the theory of surface tension in terms of intermolecular forces by means of statistical mechanics (*10*). Two main approaches have been used: the *free-volume* theories, based on an approximate evaluation of the partition function (*5, 15*), and the *radial-distribution-function* method (*2, 3, 13*). Thus far these theories have been developed only for monatomic substances, and much more needs to be done before the statistical theories will be generally useful for predicting surface tensions of complex compounds.

Hence the methods presented here, based on the principle of corresponding states (hereinafter abbreviated P.C.S.), are offered as an aid for practical calculations pending further experimental and theoretical developments. The results given here also serve as an additional test for the two modifications of the P.C.S. which are used.

PRINCIPLE OF CORRESPONDING STATES AND ITS MODIFICATIONS

The P.C.S. in its original form as enunciated by van der Waals was applied specifically to the equation of state in the form

$$P_r = P_r(V_r, T_r) \qquad (1)$$

That is, for all substances the reduced pressure should be a universal function of the reduced volume and reduced temperature. This principle has been used in an alternate form by Hougen and Watson (*11*) in the preparation of their generalized compressibility chart, which is a graphical representation of the function

$$Z = Z(P_r, T_r) \qquad (2)$$

In addition to the generalized compressibility chart (and the derived charts for the thermodynamic functions) charts have been prepared for two of the transport coefficients: viscosity (*11, 24*), for which $\mu_r = \mu_r(P_r, T_r)$, and thermal conductivity (*8, 12*), for which $k_r = k_r(P_r, T_r)$.

All these charts have been of considerable use for purposes of instruction and rapid calculation. It is, however, inherently assumed in these generalized representations that the constituent molecules of all substances are mechanically similar. This drawback led Kamerlingh Onnes to modify the original P.C.S. by suggesting that each group of mechanically similar substances—for example, the halogens, the alcohols, the straight chain paraffins—should obey a separate P.C.S. characteristic of its own group.

Actually very little has been done to modify the P.C.S. by the introduction of additional parameters to characterize the chemical structure of the constituent molecules. The reason for this is that an enormous amount of very accurate experimental data is required in order to deduce the effects of dipole moments, quadrupole moments, polarizabilities, and molecular shape on the bulk physical properties. Because of the impracticality of any such attempt at the present time, one might well ask whether some sort of empirical correlating parameter can be found—one which could be expected to work for a large number of substances. Recently two such empirical methods have been suggested, in which a single additional "correlating parameter" has been introduced:

1. Meissner and Seferian (*20*) have suggested that all substances with the same value of the parameter $Z_c = P_c V_c / RT_c$ obey the same P.C.S., that is, that Equation (2) be replaced by

$$Z = Z(P_r, T_r; Z_c) \qquad (3)$$

indicating the explicit parametric dependence on Z_c. Similar expressions can be written for the transport coefficients and other properties. This modification of the P.C.S. has been used by Lydersen, Greenkorn and Hougen (*18*) to make a very extensive analysis of data on equation of state and thermodynamic properties of gases and liquids.

2. Riedel (*21*) has suggested that all substances with the same value of $Y_c = (d \ln P_V / d \ln T)_c$ follow the same P.C.S., that is, that Equation (2) be replaced by

$$Z = Z(P_r, T_r; Y_c) \qquad (4)$$

with analogous relations for the other physical properties. Riedel has achieved particularly good suc-

J. R. Brock is at present with Humble Oil and Refining Company, Houston, Texas.

cess with this method in the correlation of vapor-pressure data.*

The application of either of these methods raises the important question as to whether a single correlating parameter—such as Z_c or Y_c—can be expected to be sufficient for describing the behavior of many different physical properties. Recently Rowlinson(*23*) succeeded in showing theoretically that at least for certain types of molecular interactions a single correlating parameter is indeed adequate. To substantiate his theory he has studied the following properties of sixteen widely varying substances: second virial coefficients, vapor pressure of liquids, rectilinear diameters, Trouton's constants, heat capacities (at constant volume) of liquids, and surface tension. The success which the authors have had in correlating surface-tension measurements on the basis of methods 1 and 2 above can be regarded as an additional justification of Rowlinson's generalization of the P.C.S.

*The quantity here called Y_c, is given the symbol α_k by Riedel(*20*), but the present authors prefer not to use α since this letter is frequently used for the coefficient of expansion $(\partial \ln V/\partial T)_p$. Riedel has shown by a very careful analysis of vapor-pressure data that the quantity Y_c can be calculated from the boiling point T_b at a pressure P by means of the equation

$$\ln P_r = Y_c \ln T_{br} - 0.0364(Y_c - 3.75)[(36/T_{br}) + 42 \ln T_{br} - 35 - T_{br}^6]$$

in which T_{br} is the reduced boiling temperature corresponding to the reduced pressure P_r. If many values of Y_c are needed, they can be calculated quickly from tables prepared by Riedel(*21*).

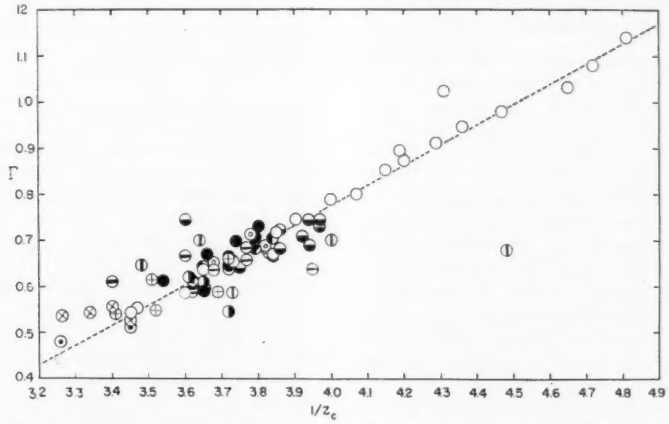

FIG. 1. DETERMINATION OF THE FUNCTION Γ (Z_c) IN EQUATION (8). THE VARIOUS TYPES OF CHEMICAL SUBSTANCES USED IN THE CORRELATION ARE INDICATED BY THE FOLLOWING SYMBOLS:

- ⊙ noble gases
- ⊗ diatomic molecules
- ⊕ simple inorganic molecules
- ○ straight-chain paraffins
- ◐ alkyl benzenes
- ◑ nitrogen-containing organic compounds
- ⊖ halogen-containing organic compounds
- ⊙ miscellaneous organic compounds
- ● branched paraffins
- ◒ esters
- ◑ unsaturated hydrocarbons

THE DOTTED LINE REPRESENTS THE LEAST SQUARE FIT, $\Gamma = -0.951 + (0.432/Z_c)$.

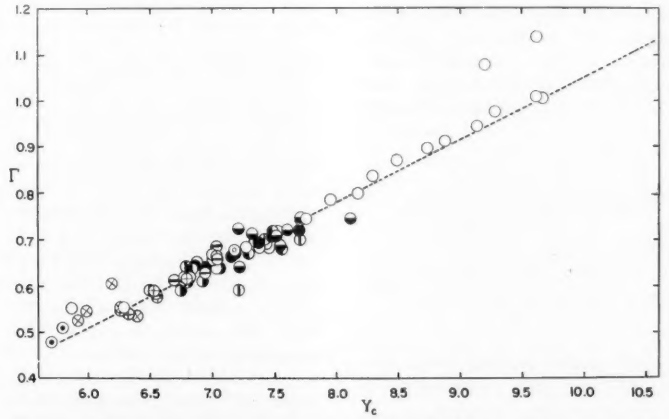

FIG. 2. DETERMINATION OF THE FUNCTION $\Gamma(Y_c)$ IN EQUATION (9). THE SYMBOLS USED FOR THE VARIOUS TYPES OF CHEMICAL SUBSTANCES ARE THE SAME AS THOSE GIVEN IN FIGURE 1. THE DOTTED LINE REPRESENTS THE LEAST SQUARE FIT, $\Gamma = -0.281 + 0.133 Y_c$.

APPLICATION OF THE MODIFIED P. C. S. TO SURFACE TENSION

Neither of the above discussed modifications of the P.C.S. has yet been fully examined as to how well various physical properties can be described. It is of interest to test these methods by applying them to the correlation of surface-tension data. For this property it is well known that the P.C.S. in its original form is definitely inadequate (*9*), probably because of the alignment effects at the interface, which are of course highly sensitive to the molecular shapes and molecular interactions. The surface tension of a pure substance is particularly easy to study, since it is a function of temperature but not of pressure.

For the purpose of this work a "reduced" surface tension has been defined by*

$$\gamma_R = \frac{\gamma}{P_c^{2/3} T_c^{1/3}} \qquad (5)$$

(It should be noted that the quantity $\gamma/P_c^{2/3}(\kappa T)^{1/3}$ is dimensionless but that quantity γ_R, defined in Equation (5), is not, because of the missing factor $\kappa^{\frac{1}{3}}$, which was omitted to simplify calculations.) According to the original P.C.S. one would expect γ_R to be a unique function of T_r for all substances.

*One might also define a reduced surface tension thus:

$$\gamma_R = \gamma V_c^{2/3}/\kappa T_c \qquad (5a)$$

This definition suffers from the disadvantage that V_c is not known accurately for many substances. Rowlinson(*23*) has, however, used this definition in his investigation.

According to the two modified P.C.S., however,

$$\gamma_R = \gamma_R(T_r; Z_c) \qquad (6)$$

$$\gamma_R = \gamma_R(T_r; Y_c) \qquad (7)$$

The temperature dependence of the surface tension for a great many substances has been shown(*9*) to be proportional to $(1-T_r)^{11/9}$. The assumption that this temperature dependence is universal allows one to rewrite Equations (6) and (7) thus

$$\gamma_R = \Gamma(Z_c)(1-T_r)^{11/9} \qquad (8)$$

$$\gamma_R = \Gamma(Y_c)\,(1-T_r)^{11/9} \qquad (9)$$

The experimental surface-tension data used for obtaining $\Gamma(Z_c)$ and $\Gamma(Y_c)$ are those given in Landolt-Börnstein's Physikalisch-Chemische Tabellen, the International Critical Tables, the Annual Table of Physical Constants, Tables Annuelles de Constantes et Données Numériques and the Tables of the American Petroleum Institute. For many substances it was not possible to find the surface tension of the pure substance against its own saturated vapor; it was necessary to use the value of surface tension against air or some inert gas. The error involved in the use of the latter data is believed to be quite small in comparison with the average deviation from the correlations based on the principle of corresponding states. The critical constants needed for the correlation were obtained from a recent compilation made by Lydersen(*17*) and from the extensive tabulation prepared by Kobe and Lynn(*14*). Eighty-four substances of widely differing **character were** selected for which both surface-tension and critical data were available. These included two noble gases, five diatomic molecules, seven simple polyatomic inorganic substances, the first twenty normal paraffins, ten branched paraffins, five alkyl benzenes, six unsaturated hydrocarbons, eight esters, eight organic halogen compounds, six organic nitrogen compounds, and seven other organic compounds. The experimental values of $\gamma_R/(1-T_r)^{11/9}$ were plotted against $1/Z_c$ (as shown in Figure 1) and against Y_c (as shown in Figure 2). Through the point so plotted, the best straight lines were drawn by means of a least-squares fit. These linear relations then allow Equations (8) and (9) to be rewritten as

TABLE 1.—ANOMALOUS DEVIATION OF EXPERIMENTAL SURFACE TENSIONS FROM GENERALIZED EQUATIONS

Substance	Average % deviation from Eq. (10)	Eq. 11
Polar inorganic substances		
Water	+ 90.6	+ 44.0
Ammonia	+ 35.5	+ 6.2
Hydrogen chloride	+ 31.4	+ 13.2
Hydrogen bromide	+ 13.4	+ 5.0
Alcohols		
Methanol	+179	+ 58.2
Ethanol	+ 89	+117
Butanol	+ 39.4	+ 87
Carboxylic acids		
Acetic acid	+166	+ 70
Propionic acid	+ 88	+ 91
Butyric acid	+ 21	+115

$$\gamma_R = (-0.951 + 0.432/Z_c)\,(1-T_r)^{11/9} \qquad (10)$$

$$\gamma_R = (-0.281 + 0.133\,Y_c)\,(1-T_r)^{11/9} \qquad (11)$$

which are the final generalized relations for surface tension based on the two modified P.C.S. described above.*

GENERALIZED RELATIONS FOR SURFACE TENSION

Applicability. Over the temperature range of the available data for the eighty-four substances considered, it was found that the average error for Equation (10) is 6.2% and for Equation (11, 3.0%. The smaller deviation for the Y_c correlation does not necessarily indicate that Y_c is fundamentally a better choice of correlating parameter than Z_c. Many of the deviations in the Z_c correlation are quite likely due to erroneous values of Z_c (which in turn frequently can be traced to faulty V_c values).

Equations (10) and (11) are sufficiently accurate for most engineering calculations and provide a quick method for estimating surface tension from critical data. If experimental critical data are not available, they can be estimated by the group-contribution methods devised by Riedel(*21, 22*) and extended by Lydersen(*17*). Lydersen has also given an empirical relation whereby Z_c may be estimated from heats of vaporization.

Equations (10) and (11) could be used for estimating critical constants from surface-tension measurements. If P_c and T_c are known, then V_c can be obtained from

$$V_c = 0.432\,(RT_c/P_c)\left[0.951 + \frac{\gamma/P_c^{2/3}T_c^{1/3}}{(1-T_r)^{11/9}}\right]^{-1} \qquad (12)$$

And if T_c and a boiling point are known, then P_c can be found from

*The constants in Equations (10 and (11) are slightly different from those given previously[1], since only 30 substances were used in the original correlation.

$$P_c = \left[\frac{\gamma/T_c^{1/3}}{(-0.281+0.133Y_c)(1-T_r)^{11/9}}\right]^{3/2} \qquad (13)$$

A trial-and-error method has to be used to obtain P_c, as Y_c depends on P_c. Equation (13) is probably about as good for estimating P_c as is the group-contribution formula given by Lydersen(*17*).

Limitations. The generalized relations for surface tension are reasonably successful for simple inorganic substances and for a wide variety of organic compounds. There are several groups of substances for which the correlations cannot be expected to hold: very light atoms and molecules (the isotopes of hydrogen and helium), molten metals, certain highly polar inorganic substances (H_2O, NH_3, HCl, HBr), associating substances (alcohols, carboxylic acids, etc.), and fused salts. The order of magnitude of the deviations of some of these substances from the generalized equations is indicated in Table 1.

The only class of substances listed above which has been successfully studied is the first one—the isotopes of hydrogen and helium—which exhibit quantum effects. These substances should always be excluded from generalized correlations inasmuch as there are other preferable ways to handle them. The first method was suggested by Byk(*4*), who proposed a quantum mechanical modification of the original van der Waals' principle of corresponding states. A theoretically sounder method is the use of a quantum mechanical P.C.S. based on the reduction of variables with molecular parameters (rather than critical parameters), as proposed by de Boer(*7*) and discussed extensively by Lunbeck(*19*). The application of this latter approach to surface tension has been carried out by one of the authors(*6*). In this way the surface tension of He^3 and the various heavy isotopes of hydrogen. Recently the surface tension of He^3 was measured by Lovejoy(*16*) in the range 1.0° to 2.5°K. Above about 1.8°K. the experimental values agree almost exactly with the predicted curve. The discrepancy below 1.8°K. is undoubtedly due to statistics effects, which were not taken into account in the P.C.S. prediction. As yet no experimental values of the surface tension for the heavy isotopes of hydrogen are available.

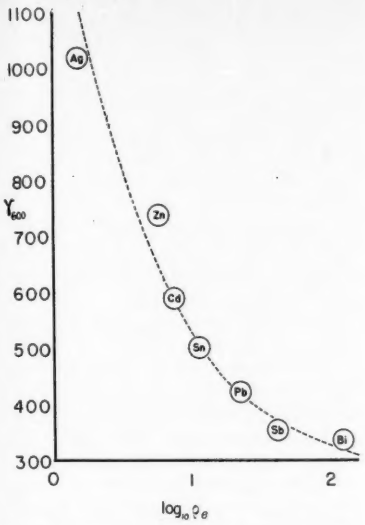

FIG. 3. SURFACE TENSION AT 600°C. IN DYNE CM.$^{-1}$ OF VARIOUS MOLTEN METALS PLOTTED AGAINST THE LOGARITHM OF THEIR ELECTRICAL RESISTIVITY AT 20°C. IN MICROHM CM.

Much needs to be done in connection with the other anomalous substances. For the molten metals there seems to be a relationship between the surface tension and the electrical resistivity, as can be seen in Figure 3. For the materials in the last three groups above, no workable generalizations have been obtained. It is not known at present whether Equations (10) and (11) apply generally to the fluorocarbons. The only one of these substances for which both surface-tension and critical data could be found was perfluoroheptane, for which the agreement was not particularly good. It will be interesting to see whether this class of compounds exhibits further deviations.

SURFACE TENSION AND THE PARACHOR

The calculation of the surface tension from the modified P.C.S. methods is not presented as a substitute for the method of calculating surface tension from the parachor. The latter calculation requires a knowledge of the liquid and vapor densities, whereas the former requires that one know either P_c, V_c, T_c or P_c, V_c, T_b. Thus the two schemes of estimating surface tension are complementary. Furthermore it is frequently useful to have two different methods available for estimating physical properties under unusual conditions. A P.C.S. approach to surface tension is in a sense more satisfying, in that the correlation is obtained by a general method, capable of being applied to a variety of properties as already discussed. The parachor, on the other hand, involves a specific method.

The parachor is far from being well understood theoretically. It was introduced as a useful empiricism by Sugden, and its use in structural determinations is well known. At the present time there is no satisfactory explanation of the fact that the parachor is very nearly constant over a wide range of temperature. Lennard-Jones and Corner(*13*) have shown that the parachor is given within about 4% for simple substances by the empirical relation:

$$[P] = (7.1 \times 10^3\ \epsilon^{1/4}\ \sigma^{5/2} \quad (14)$$

in which σ and ϵ are the parameters in the Lennard-Jones potential (σ is the low-energy collision diameter in Ångström units and ϵ is the maximum energy of intermolecular attraction in ergs). This relation shows that the parachor is almost proportional to σ^3, which is in agreement with Sugden's contention that the parachor is some sort of modified molecular volume.

ACKNOWLEDGMENT

The authors are indebted to Aksel Lydersen for numerous interesting discussions and for the use of some of his unpublished work. They also wish to thank Arthur Stroud for performing some of the calculations. In addition, R. B. Bird wishes to acknowledge the financial support of the National Science Foundation.

NOTATION

k = coefficient of thermal conductivity
P = pressure
P_V = vapor pressure
R = gas constant
T = temperature
V = molar volume
$Y = (d \ln P_V / d \ln T)$
Z = compressibility factor, PV/RT
γ = surface tension
γ_R = "reduced" surface tension [*see* Equation (5)]
Γ = quantity defined in Equations (8) and (9)
κ = Boltzmann's constant
μ = coefficient of shear viscosity
ρ_e = electrical resistivity

Subscripts

b = quantity evaluated at the boiling point
c = quantity evaluated at the critical point
r = quantity made dimensionless by division by the corresponding quantity at the critical point

LITERATURE CITED

1. Brock, J. R., MS. thesis, Univ. Wisconsin (1954).
2. Buff, F. P., and J. G. Kirkwood, *J. Chem. Phys.*, **17**, 338 (1949).
3. Buff, F. P., *J. Chem. Phys.*, **19**, 991 (1950).
4. Byk, A., *Ann. Physik*, **66**, 157 (1921); **69**, 161 (1922).
5. Corner, J., *Trans. Faraday Society*, **44**, 1036 (1948).
6. De Boer, J., and R. B. Bird, "Quantum Theory and the Equation of State," Chapter 6 in Reference *10*, p. 430.
7. de Boer, J., *Physica*, **14**, 139 (1948).
8. Gamson, B. W., *Chem. Eng. Progr.* **45**, 154 (1949).
9. Guggenheim, E. A., "Thermodynamics," 2 ed., North-Holland Publishing Company, Amsterdam (1950).
10. Hirschfelder, J. O., C. F. Curtiss, and R. B. Bird, "Molecular Theory of Gases and Liquids," John Wiley and Sons, New York (1954).
11. Hougen, O. A., and K. M. Watson, "Chemical Process Principles," John Wiley and Sons, New York (1947).
12. Hougen, O. A., *Chem. Eng. Progr. Monograph Series*, No. 1, 47, (1951).
13. Kirkwood, J. G., and F. P. Buff, *J. Chem. Phys.*, **17**, 338 (1949).
14. Kobe, K. A., and R. E. Lynn, Jr., *Chem. Revs.*, **52**, 117 (1953).
15. Lennard-Jones, J. E., and J. Corner, *Trans. Faraday Society*, **36**, 1156 (1940).
16. Lovejoy, D. R., *Can. J. Phys.*, **33**, 49-53 (1955).
17. Lydersen, A. L., "Estimation of Critical Properties of Organic Compounds by the Method of Group Contributions," *Univ. Wisconsin Eng. Expt. Sta. Rept.* (1955).
18. Lydersen, A. L., R. A. Greenkorn, and O. A. Hougen, "Thermodynamic Properties of Pure Fluids from the Theorem of Corresponding States," *Univ. Wisconsin Eng. Expt. Sta. Rept.* (1955).
19. Lunbeck, R. J., Doctoral dissertation, University of Amsterdam (1951).
20. Meissner, H. P., and R. Seferian, *Chem. Eng. Progr.*, **47**, 579 (1951).
21. Riedel, L., *Chem. Ing. Tech.*, **26**, 83 (1954).
22. *Ibid.*, p. 259.
23. Rowlinson, J. S., *Trans. Faraday Society*, **50**, 647 (1954).
24. Uyehara, O. A., and K. M. Watson, *Nat. Petroleum News*, **36**, 764 (October 4, 1944).

TURBULENCE IN FALLING LIQUID FILMS

Clifford Stirba and D. M. Hurt
E. I. du Pont de Nemours & Company
Wilmington, Delaware

On the basis of fluid dynamic and heat transfer studies on falling-film towers by various investigators, it has been commonly accepted by most workers that the liquid flow is essentially streamline in nature for liquid-film Reynolds numbers under 1,800 to 2,000; consequently it would be expected that the rate of physical gas absorption in such liquid films could be predicted directly from a knowledge of molecular diffusion rates.

Measurements of the absorption of pure gases in falling liquid films at low Reynolds numbers substantiated the findings of other investigators that the mass transfer rates were manyfold greater than could have been predicted if molecular diffusion were the only transfer process. Increased interfacial area due to rippling of the liquid films could not account for the large increase in mass transfer rates found, and experiments with the addition of a dye stream to the liquid at the free interface indicated turbulence.

Dissolution rates of slightly soluble solids coated on the tube wall to liquid films were measured and showed that the liquid film was not in laminar flow even for Reynolds numbers as low as 300.

An explanation is proposed which resolves these apparently conflicting results between momentum and heat and mass transfer, based on the fact that mass transfer measurements provide a more sensitive test for the presence of turbulence than do momentum or heat transfer measurements.

Existing theory for the design of gas-liquid reactors is not adequate at the present time owing to lack of knowledge as to what is taking place in the liquid phase near the phase boundary. This work was undertaken to study the physical system, without reaction, since an understanding of the mechanism of liquid-phase mass transfer is essential for the development and application of any fundamental theory for the combined diffusion-reaction case. A falling-film tower was selected for preliminary work primarily because of its relatively constant and known interfacial area. In addition, certain apparent anomalies exist between mass, heat, and momentum transfer data for falling-film towers, and it was believed that an explanation which could reconcile these differences would also shed light on the liquid-phase mass transfer process.

LIQUID-PHASE MASS TRANSFER DATA

A number of investigators have studied mass transfer in falling liquid films and have in general found that the measured absorption rates are considerably greater than would have been predicted by theory. For example, Johnstone and Pigford (*14*) reported values for the heights of liquid-film transfer units, H_L, for distillation in a wetted-wall column one half to one quarter those predicted by theory for liquid-film Reynolds numbers ranging from 100 to 500. In a paper on distillation of ethanol-water in a wetted-wall column, Surowiec and Furnas (*25*) reported

heights of liquid-film transfer units about 1/14 of those predicted from heat transfer equations in the Reynolds number range of 125 to 340. Data from the work of Hodson(*11*) and Hurlburt(*12*) on oxygen and carbon dioxide desorption in a 1.05- by 18.5-in. tower show desorption rates severalfold greater than theory in the laminar flow range. Runs made in this investigation on the absorption of carbon dioxide in water in roughly 3- and 6-ft. towers also indicated mass transfer rates 1 1/2- to 3-fold as great as the rate predicted by theory based on molecular diffusion below liquid-film Reynolds numbers of 1,800. The apparatus of all investigators differ somewhat in the types of calming sections used for liquid and gas introduction, but this detail does not appear to be significant in the relatively long towers used. One thing common to all the liquid-film work appears to be the presence of ripples in the liquid film, and this fact has been used by previous investigators to explain the higher than expected mass transfer results.

MOMENTUM-TRANSFER DATA

The equations for viscous flow in a falling-film tower with no drag at the free interface were first set up by Nusselt(*22*). The theory shows that the velocity distribution is parabolic, with the maximum velocity at the free interface equal to 1.5 times the average velocity. Friedman and Miller(*8*) have shown that the surface velocity is considerably greater than that predicted by theory at Reynolds numbers above 25, about the point they found rippling to begin. Experiments by Grimley(*10*), in which high-speed photographs of illuminated particles within the liquid film were taken to determine the velocity profile at different points, indicated that the liquid-velocity profile goes through a maximum about 1/10 of the film thickness from the gas-liquid interface. This resembles the velocity profile commonly encountered in open channel flow. Near the wall, however, the velocity profile measured by Grimley does not depart appreciably from that of a parabolic gradient. Although these experiments point out discrepancies between the theory and actual conditions, nevertheless a number of investigators have shown(*5, 7, 22*) that the liquid-film holdup checks the holdup predicted by the theoretical equations up to Reynolds numbers of 1,800 to 2,000. This range of Reynolds numbers has, therefore, been commonly used as the criterion for the presence or absence of turbulence; i.e., above this range the equations cease to hold because of the presence of turbulence.

HEAT TRANSFER DATA

In addition to work on momentum transfer, a number of workers have carried out experiments on the condensation of pure vapors on the outside surfaces of vertical tubes(*16, 19, 21*). In general, below a Reynolds number of 2,000, the data for heat transfer rates fall 25 to 50% higher than values predicted by the viscous-flow equations based on a parabolic velocity distribution.

Data have also been reported(*1*) for the heating of fluids in streamline flow in falling-film towers, where heat is transferred from a wall at constant temperature to the fluid, care being taken to avoid appreciable vaporization. For the streamline flow region (based on the criterion $4\ \Gamma/\mu \leq 1{,}800$) the data fall some 20 to 30% higher than predicted by theory.

DEVELOPMENT OF THEORY

The previous paragraphs present the experimental facts on hand at the start of this work. The question to be answered was why mass transfer rates were so much greater than those predicted by theory in the streamline region, while holdup measurements checked laminar-flow theory closely and heat transfer results, while slightly higher than theory, were nevertheless in fair agreement. The data for momentum and heat transfer are consistent with the postulation of laminar-flow conditions, and the data for the mass transfer case indicate the presence of turbulence in the liquid film.

The explanation used by previous investigators for the high rate of mass transfer in the streamline flow region has been associated with rippling of the liquid film, which could increase mass transfer results by increasing the interfacial area or by creating turbulence* in the liquid film. The maximum increase in surface caused by the presence of ripples as judged by visual observation and photographs is probably less than 50%, and this would not be adequate to explain the increased rates observed in the mass transfer experiments. The work of Friedman and Miller(*8*) indicated turbulence in the liquid at the free interface, and similar experiments were performed by the authors. A dye stream introduced on the surface of a water film was observed to spread out in the form of a cone downstream from the point of introduction. At no time was a laminar dye thread observed in the rippling film although the Reynolds number was reduced to as low as 200. Thus the evidence at hand indicated turbulence at the free interface, which would be expected to be present to some degree within the main liquid film. The question raised is whether or not turbulence can markedly increase mass transfer rates while not affecting to any major degree either momentum or heat transfer rates.

Equations of definition can be written for molecular transport of momentum, heat, and mass as

Momentum

$$\frac{1}{\rho}\frac{dP}{dL} = \frac{1}{yg_c}\frac{\mu}{\rho}\frac{dV}{dy}$$

Heat

$$\frac{1}{a}\frac{dT}{d\theta} = \frac{k}{\rho c_p}\frac{dT}{dy}$$

Mass

$$\frac{1}{a}\frac{dc}{d\theta} = D_L\frac{dc}{dy}$$

It will be noted that μ/ρ, $k/\rho c_p$, and D_L all have identical units and can be considered as rates per unit driving potential; i.e., per unit force, temperature, and concentration. For water at 31°C. these diffusivities have the following values:

Momentum transfer (kinematic viscosity) = $3{,}020 \times 10^{-5}$ sq.ft./hr.

Heat transfer (thermal diffusivity) = 569×10^{-5} sq.ft./hr.

Mass transfer (molecular diffusivity) $D_L CO_2$ in water = 9.3×10^{-5} sq.ft./hr.

D_L benzoic acid — water = 5.2×10^{-5} sq.ft./hr.

From the foregoing tabulations it can be seen that for water films the momentum diffusivity is about five times as large as the thermal diffusivity, which is in turn about sixty times as large as the molecular diffusivity. These values change slightly with temperature, but the ratios between them remain essentially the same. These significant differences in transfer rates

*The criterion for turbulence used throughout this paper is based upon whether or not experimental results check mass transfer theory based solely on molecular diffusion.

per unit driving force between momentum, heat, and mass transfer for liquid films are not surprising, since mass transfer is the transport of a specific molecular or ion, while heat and momentum may be transferred not only by physical transport, but also by collision. From this, it is apparent that if turbulence were present to any degree, it would have a greater effect upon the mass transfer rate than upon the rates of heat or momentum transfer; i.e., the slowest process would show a measurable effect first. With this assumption it then would be possible, within a given range of Reynolds numbers, to have equations based on laminar flow hold reasonably well for momentum and heat transfer and not correlate mass transfer data at all.

It is of interest to examine the diffusivities for gas films. For air at 0°C. and atmospheric pressure, the diffusivities have the following values:

Momentum transfer (kinematic viscosity) = 0.51 sq.ft./hr.

Heat transfer (thermal diffusivity) = 0.69 sq.ft./hr.

Mass transfer (molecular diffusivity) D_V CO_2 in air = 0.53 sq. ft./hr. D_V water in air = 0.85 sq. ft./hr.

It is immediately noted that the large differences in diffusivities for momentum, heat, and mass transfer disappear for gas films. It would thus be expected that correlations (*3, 9, 24*) between heat and mass transfer for gas systems in turbulent flow would be valid through the dip region, while similar correlations for liquid systems would not be expected to hold in this manner.

The foregoing explanation, although forming a logical explanation for the observed abnormalities in momentum, heat, and mass transfer rates in liquid films, needs proof. An experimental program was, therefore, set up to furnish data to prove or disprove the proposed explanation.

EXPERIMENTAL WORK

As it was desired to obtain mass transfer data under identical physical conditions employed by previous workers (*1*) in obtaining heat transfer data, the rate of solution of various materials from a solid wall to a falling liquid film was measured. In addition to enabling one to establish whether turbulence existed below Reynolds numbers of 1,800 to 2,000 in falling liquid films near the tube wall, these measurements would also give a quantitative picture of the diffusivity across the film from the wall side outward. Together with absorption measurements previously referred to, this would yield a rather clear picture of the extent of turbulence existing across the entire film.

The first three materials to be used as coatings were benzoic acid, adipic acid, and succinic acid. The tubes were coated internally by melting the crystalline acids and pouring molten liquid into the tubes via a funnel while rotating the tubes. In this simple manner a uniform and smooth coating was obtained. It was found that fine crystals and, therefore, smoother surfaces were obtained if cold water was circulated through a jacket surrounding the tubes so that rapid crystallization took place.

The falling-film tubes used in the experiments were jacketed glass with the inside diameter as measured with the solid coating in place varying from 0.77 to 1.13 in. Column lengths varied from 30 to 74.5 in. The liquid was introduced into a reservoir at the top of the columns and flowed over the top. Several layers of stainless steel screen held in place around the top of the column caused a slight head of liquid to build up in the reservoir above the tube inlet, and in this manner uniform liquid flow around the periphery of the tube was obtained. Although no definite calming section at the liquid entrance was provided, the solid coatings all started some 3 to 4 in. from the top of the column.

Distilled water was used in all the runs and this was heated to the operating temperature by means of a coil immersed in a constant-temperature water bath. In all runs the temperature change of the water between inlet and outlet was no more than ±0.2°C. Analysis of the effluent stream for benzoic acid, adipic acid, and succinic acid, was made by titrating with standard sodium hydroxide using phenolphthalein as indicator. The percentage saturation of the effluent as reported in the tables of data is believed to be accurate within 10%, the precision as measured by check samples being within 1%. The solubilities of the acids in the water used were measured and these figures were used in all calculations. A comparison of measured solubilities with values from the literature, where available, checked closely. Molecular diffusivities used for comparison with the measured apparent diffusivities were taken from the literature (*13, 15*).

It was found that water would not completely wet the benzoic acid surface below Reynolds numbers of about 3,400. A wetting agent, the sodium salt of an aliphatic sulfonate, was then added to the water (0.02 and 0.05% by weight) and runs were made down to a Reynolds number of about 950. Below this Reynolds number, incomplete wetting was again encountered and it was found that adding additional wetting agent did no further good.

When results of the runs at Reynolds numbers from 2,200 to 3,000 made with the wetting-agent-treated water were extrapolated to Reynolds numbers of 3,400 to 3,800, they were found to check closely results obtained in the latter Reynolds number range using pure water. Thus the addition of the small amount of wetting agent appeared to have a negligible effect upon the dissolution rate. All adipic and succinic acid runs were made with 0.05% by weight of wetting agent in water.

Since it was anticipated that there might be some question as to how smooth the coatings of benzoic, adipic, and succinic acids were, two other systems were run; i.e., paraffin wax—butanol and stearic acid—ethanol. Although both of these latter solids are crystalline, the crystals are small and an extremely smooth surface can be produced by the coating method used. In addition, no trouble was encountered with wetting of the solid surfaces by the liquids and no wetting agent was therefore employed. Analysis of the effluent in the paraffin wax–butanol system was made gravimetrically by evaporating the butanol. With the stearic acid–ethanol system the stearic acid in the effluent was determined volumetrically by direct titration with sodium methylate using phenolphthalein as indicator. Values of the molecular diffusivity were obtained from the literature (*13*) or estimated by the method of Wilke (*27*).

TREATMENT OF DATA

The differential equation set up by Nusselt (*22*) for the flow of heat from a wall at constant temperature to a falling liquid film is

$$-k\frac{\partial^2 T}{\partial y^2}c_p V\rho\frac{\partial T}{\partial L}=0 \quad (1)$$

Since V varies with y, Nusselt substituted the parabolic velocity distribution, shown to be accurate from holdup data, to obtain

$$k\frac{\partial^2 T}{\partial y^2}=\frac{C_p\rho^2}{\mu}\left(yB-\frac{y^2}{2}\right)\frac{\partial T}{\partial L} \quad (2)$$

Nusselt solved the foregoing equation by a difference method and tabulated his results as ϕ vs. S where

$$S=\frac{k\mu L}{C_p\rho^2 B^4 g} \text{ and } \phi=\frac{T_2-T_1}{T_o-T_1}$$

Nusselt also shows his results as a plot of ϕ vs. S, which is reproduced in Figure 1. The differential equation for mass transfer applica-

ble to the dissolution runs may be obtained by substituting concentration for temperature and D_L, the diffusivity, for $k/c_p\rho$.

The differential equation for absorption of a gas in a falling water film with a parabolic velocity distribution is

$$\left[1-\left(\frac{s}{B}\right)^2\right]\frac{\partial C}{\partial L}=\frac{D_L}{Vm}\frac{\partial^2 C}{\partial s^2} \quad (3)$$

Johnstone and Pigford(*14*) give the following solutions of the Equation (3):

$$\frac{C_2-C_i}{C_1-C_i}=0.786\,e^{-5.12\eta}+0.100\,e^{-39.3\eta}+0.036\,e^{-105.6\eta}+\ldots \quad (4)$$

where

$$\eta=\frac{D_L L}{B^2 Vm}$$

for low values of η the series may be expressed as

$$\frac{C_2-C_i}{C_1-C_i}=1-\frac{3}{\sqrt{\pi}}\sqrt{\eta} \quad (5)$$

The foregoing solutions were used together with the experimental data to calculate the apparent liquid-film diffusivities for the carbon dioxide absorption and solid dissolution runs. The equations were used throughout the Reynolds range studied, since the data of Grimley(*10*) indicate a maximum deviation of about 30% between measured and calculated velocities at various points within the film.

RESULTS

Experimental results for the solid dissolution runs and the CO_2 absorption runs referred to under Mass Transfer Data are shown plotted in Figure 2 as the apparent liquid diffusivity vs. Reynolds number. As can be seen, the apparent diffusivities for the CO_2 absorption and solid dissolution runs are considerably greater than the molecular diffusivities, which vary from about 0.5×10^{-5} sq.ft./hr. to 10×10^{-5} sq.ft./hr. This is so down to Reynolds numbers as low as 300 to 400.

It will be noted that the apparent eddy diffusivities have been plotted against Reynolds number in Figure 2. The usual equation of definition for turbulent mass transfer is

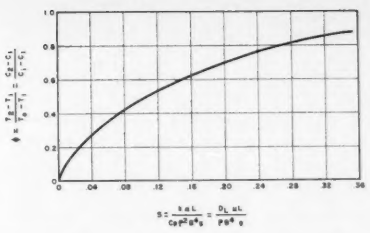

FIG. 1. PLOT OF ϕ VS. S, FROM NUSSELT (*22*) FOR TRANSFER OF HEAT OR MASS FROM A WALL TO A FALLING LIQUID FILM.

$$\frac{1}{a}\frac{dc}{d\theta}=(D_L+E_D)\frac{dc}{dy}$$

The equation states that the apparent diffusivity is the arithmetic sum of the molecular and eddy diffusivities. It is readily seen that if this is so the data indicate that the true eddy diffusivity is a function of the material being transferred, which does not appear at all reasonable. The authors prefer to believe that while the preceding equation holds with negligible error where D_L is much larger than E_D or vice versa, it is not valid where D_L and E_D are of the same order of magnitude.

It is apparent from the results that one is dealing with turbulent flow and that as far as mass transfer is concerned turbulence appears to persist throughout the flowing layer. The conclusion which may be drawn is that the assumption of turbulence throughout the liquid layer leads to negligible error in the calculation of mass transfer rates both for the absorption process and the solid solution process. This conclusion is not only in contrast to the usual assumption of turbulent, buffer, and completely laminar zones for fully developed turbulent flow(*2, 18, 23, 26*), but also differs somewhat from the assumption made for heat transfer

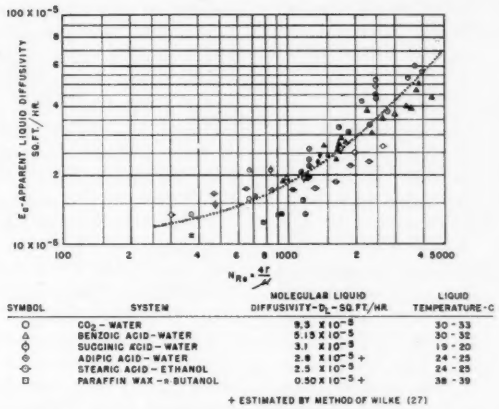

FIG. 2. VARIATION OF APPARENT LIQUID DIFFUSIVITY WITH REYNOLDS NUMBER.

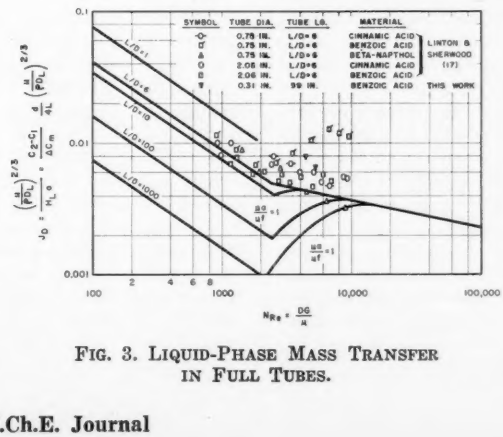

FIG. 3. LIQUID-PHASE MASS TRANSFER IN FULL TUBES.

by Murphree(*20*), who assumed that the thermal eddy diffusivity varied as the cube of the distance from the wall at small distances from the wall.

A comparison of the results of the mass transfer runs with those of the published heat transfer runs seems to prove that mass transfer rates are affected considerably more than heat transfer rates by small amounts of turbulence. Further, since holdup data for falling-film towers are correlated well up to a Reynolds number of 2,000 by use of the theoretical laminar flow equation, it is apparent that momentum transfer is not affected by turbulence to so great an extent as either mass or heat transfer. It is postulated that the presence of turbulence is not necessarily proved by measurements of any singular effect and that the transition of flow from laminar to turbulent is noted at decreasing Reynolds numbers when measurements of momentum, heat, and mass transfer rates are respectively used as criteria. It is of interest to recall that the experiments of Reynolds, using the diffusion of a dye as a criterion for turbulent flow, are visual measurements of mass transfer rates.

SURFACE TENSION EFFECTS

There is one more variable not mentioned up to this point which markedly affects film appearance and mass transfer rates in falling-liquid films. This variable is surface tension. Experiments were conducted in which a stream of dye was introduced into a water film through a 0.013-in. hole in the wall of a 1 1/2 in. I.D. Lucite tube, about 3 ft. long. The water film was found to ripple at all Reynolds numbers and the dye thread was dissipated within 12 to 14 in. from the point of introduction. Some of the wetting agent previously referred to was then added to the water. Not only did the dye thread become continuous throughout the entire tube length when the wetting agent was added, but also the physical appearance of the film changed, the ripples disappeared, and the film became physically laminar even up to Reynolds numbers of about 3,000. If the tube was tapped with the hand, ripples immediately appeared but in a few seconds were completely damped and the dye thread again became continuous. These observations indicate that if ripples are eliminated, mass transfer rates into the liquid should check theory. This has been shown to be the case in the work of Emmert and Pigford (*6*).

The possibility exists that the use of the wetting agent in most of the organic acid–water systems may have affected the dissolution results to some extent. Ripples were present in all the dissolution experiments. Since rippling of the water film was not visually affected in these systems and since the results check reasonably well the data for the systems where no wetting agent was used, it is believed that any correction necessitated by the use of the wetting agent is small.

MASS TRANSFER FROM A COATED WALL TO A LIQUID IN FULL PIPES

In full pipes the Reynolds number criterion is well defined, and up to the breakpoint, equations based on laminar flow correlate mass transfer data well(*17*). Linton and Sherwood(*17*) also have shown that mass transfer rates for liquid systems follow reasonably well the Chilton and Colburn correlation(*3*) both in the transition and turbulent flow ranges. (The exception to this would appear to be the benzoic acid–water system, which gave higher mass transfer rates than the other two systems studied by Linton and Sherwood; however, these authors attributed the higher rates to cracks which developed in the cast pieces which formed the tube wall.) Since the Chilton and Colburn correlation was developed from heat and mass transfer measurements with gases, the reasonable check of theory afforded by the Linton and Sherwood data would appear to refute the reasoning used previously which proposed that differences between heat and mass transfer for liquid systems should be evident.

Once the method of coating benzoic acid on the interior walls of tubes was developed, two runs were made on the transfer rates of benzoic acid to distilled water in a full tube 0.310 in. I.D. by 99 in. long. The Reynolds numbers at which the runs were made were intentionally selected just above the critical point so that turbulence, although not fully developed, would be present. The mass transfer rates predicted by the Chilton and Colburn correlation(*3* and *4*) in the dip region were originally taken from heat transfer measurements, to which a correction was added for free convection due to density and viscosity difference. In the light of the falling-film work, it would be expected that for full pipes the actual mass transfer rate would be higher than that predicted from heat transfer measurements at Reynolds numbers where turbulence had just started. The measured mass transfer rates for the two runs, calculated as j factors, were found to be 2 to 2 1/2 fold as great as those predicted by the Chilton and Colburn correlation (*see* Figure 3).

A possible explanation of the differences between the Linton and Sherwood results and the two runs made in this work is based on an analogy from heat transfer work with gases. When heat is transferred through a laminar boundary layer where there is a stepwise wall-temperature variation, a "starting-length correction factor" is introduced to correlate the data. In effect the heat transfer coefficient at a point along the heated surface is found to be lower when the heated section follows a surface which is not heated than when it does not. This decrease in heat transfer is a function of the ratio of the distance along the heated surface to the total distance along the surface and would be more pronounced for short heated sections. While calculations for a short heated length in a long tube (similar to mass transfer apparatus used by Linton and Sherwood) show that this type of correction would be small for gases, it is nevertheless in the right direction. If, as proposed above, the effect is more pronounced for mass transfer in liquid systems, then the differences between the mass transfer data may be reconciled.

SUMMARY

An explanation for the apparent conflict in the data for momentum, heat, and mass transfer in falling-liquid films below a liquid-film Reynolds number of 2,000 is proposed. The results obtained indicate that apparently a slight amount of turbulence exists throughout what has heretofore been thought to be a laminar film. While the increase in transfer rates due to turbulence in the film is slight for heat and momentum transfer, this increase is important for mass transfer. The apparent diffusivities herein reported for falling films can be used directly in the equations for the diffusion-reaction case, which have been predicated on the basis of a constant diffusivity throughout the

liquid. It is suggested that this technique be used as a means for studying turbulence close to walls and phase boundaries.

Although this work is confined for the most part to falling-liquid films, the effect of turbulence upon liquid-phase mass transfer rates would be expected to be qualitatively the same for liquid-phase diffusion in other types of equipment. Thus it is indicated that the assumption of a constant diffusivity from the phase boundary to the bulk of the liquid may be a much closer approximation of the true facts than the sharp demarcation between molecular and eddy diffusivities commonly used. Although this concept does not add measurably to present methods for handling liquid-phase physical diffusional problems, the simplification which may be possible would greatly aid in the solution of the diffusion and simultaneous reaction problem.

TABLE 1—PHYSICAL ABSORPTION RUNS, 100% CARBON DIOXIDE—WATER*

Run	$4\Gamma/\mu$	Liquid Temp.	Gas Temp.	% Saturation of exit liquid	Apparent diffusivity, sq. ft./hr. $\times 10^5$
		Tower: 1.0 in. I. D. $\times$ 76.5 in. long			
1	2500	30.4	30.0	44.0	48.4
2	1270	33.0	31.1	50.5	25.9
3	2500	31.3	31.2	42.2	44.5
4	3750	30.2	31.0	37.4	60.4
		Tower: 0.852 in. I. D. $\times$ 36 in. long			
5	380	32.0	30.4	56.8	13.2
6	690	31.2	30.5	41.5	15.5
7	690	31.5	30.5	48.1	20.9
8	1270	31.4	30.6	30.6	19.4

*Complete table may be obtained as document 4560 from the American Documentation Institute Auxiliary Publications Project, Photoduplication Service, Library of Congress, Washington 25, D. C., for $1.25 for photoprints or microfilm.

TABLE 2.—MASS TRANSFER OF BENZOIC ACID FROM A WALL TO A FALLING WATER FILM*

Run	$4\Gamma/\mu$	Avg. water temp.	Normality exit liquid, °C.	Normality saturated solution	% Saturation of exit liquid	Molecular diffusivity (lit. value), sq. ft./hr.	Apparent diffusivity (Nusselt Eq.) sq. ft./hr. $\times 10^5$	Weight % wetting agent added
			Tower: 74.5 in. coated length 0.91 in. I. D.					
1	2410	30.5	0.00475	0.0261	18.2	5.15×10^{5}	30.0	0.05
2	1670	31.0	0.0055	0.0261	21.1	5.15×10^{5}	23.1	0.05
3	1000	31.0	0.00765	0.0261	29.3	5.15×10^{5}	19.1	0.05
4	965	31.0	0.0079	0.0261	30.3	5.15×10^{5}	18.6	0.05

*See footnote to Table 1.

TABLE 3.—MASS TRANSFER OF BENZOIC ACID FROM WALL TO WATER, FULL PIPES

Run	DG/u	Avg. water temp., °C.	Normality exit water	Normality saturated water	% Approach	L/D	N_{SCH}, $\mu/\rho D_L$	j_D
			Pipe: 8 ft. 3 in. coated length $\times$ 0.310 in. I. D.					
1	4450	31.5	0.00419	0.0321	13.06	320	586	0.00782
2	5240	31.5	0.00350	0.0321	10.90	320	586	0.00638

TABLE 4.—MASS TRANSFER OF SUCCINIC ACID FROM A WALL TO A FALLING WATER FILM

Run	$4\Gamma/\mu$	Avg. water temp. °C.	Normality exit water	Normality saturated solution	% Approach	Molecular diffusivity (lit. value) D_L, sq. ft./hr.	Apparent diffusivity (Nusselt Eq.), sq. ft./hr. $\times 10^5$	Wt. % wetting agent added to water
			Tower: 34.5 in. coated length $\times$ 0.807 in. I. D.					
1	1730	19.3	0.1114	1.12	9.94	3.1×10^{-5}	25.7	0.05
2	1200	19.5	0.1264	1.12	11.3	3.1×10^{-5}	19.2	0.05
3	848	19.5	0.1826	1.12	16.3	3.1×10^{-5}	20.9	0.05
4	481	19.5	0.2406	1.12	21.45	3.1×10^{-5}	14.7	0.05

TABLE 5.—MASS TRANSFER OF ADIPIC ACID FROM A WALL TO A FALLING WATER FILM

Run	$4\Gamma/\mu$	Avg. water temp., °C.	Normality exit water	Normality saturated solution	% Approach	Molecular diffusivity*, D_L-sq. ft./hr.	Apparent diffusivity (Nusselt Eq.) sq. ft./hr. $\times 10^5$	Wt. % wetting agent added to water
			Tower: 38.5 in. coated length $\times$ 1.13 in. I. D.					
1	1250	24.8	0.0343	0.2603	13.2	2.95×10^{-5}	19.5	0.05
2	1373	24.8	0.0353	0.2603	13.6	2.59×10^{-5}	22.6	0.05
3	1423	24.6	0.0363	0.2603	14.0	2.59×10^{-5}	24.2	0.05
4	1530	24.5	0.0340	0.2603	13.1	2.59×10^{-5}	24.3	0.05
5	1680	24.5	0.0329	0.2603	12.65	2.59×10^{-5}	26.3	0.05
6	1703	24.3	0.0332	0.2603	12.78	2.59×10^{-5}	27.6	0.05

*Estimated by method of Wilke (27).

TABLE 6.—MASS TRANSFER OF STEARIC ACID FROM A WALL TO A FALLING ETHANOL* FILM

Tower: 30⅛ in. coated length×0.794 in. I. D.

Run	$4\Gamma/\mu$	Average Liquid temp., °C.	Normality exit	Normality Saturated solution	% Approach	Molecular diffusivity †, D_L, sq. ft./hr.	Apparent diffusivity (Nusselt Eq.), sq. ft./hr.×10^5
1	2700	24.8	0.00162	0.0458	3.54	2.48×10^{-5}	26.4
2	2340	24.7	0.00168	0.0458	3.68	2.48×10^{-5}	22.7
3	1980	24.7	0.00191	0.0458	4.16	2.48×10^{-5}	21.7
4	1675	24.7	0.00194	0.0458	4.24	2.48×10^{-5}	18.3
5	1350	24.5	0.00234	0.0458	5.10	2.48×10^{-5}	17.1
6	1070	24.7	0.00288	0.0458	6.28	2.48×10^{-5}	16.8
7	868	24.7	0.00354	0.0458	7.72	2.48×10^{-5}	17.0
8	665	24.7	0.00454	0.0458	9.91	2.48×10^{-5}	17.0
9	478	24.7	0.00588	0.0458	12.8	2.48×10^{-5}	16.2
10	308	24.7	0.00837	0.0458	18.3	2.48×10^{-5}	13.2

* Ethanol used was 2B alcohol.
† Diffusivity from I. C. T. (*13*) for stearic acid in absolute alcohol.

TABLE 7.—MASS TRANSFER OF PARAFFIN* WAX FROM A WALL TO A FALLING *n*-BUTANOL FILM

Tower: 35 in. coated length × 0.772 in. I. D.

Run	$4\Gamma/\mu$	Liquid temp. °C.	Wt. % paraffin in exit liquid	Wt. % paraffin in saturated solution	% Approach	Molecular diffusivity † D_L-sq. ft./hr.	Apparent diffusivity (Nusselt Eq.), sq. ft./hr.×10^5
1	376	38.3	0.124	1.50	8.27	0.503×10^{-5}	10.7
2	792	38.1	0.0718	1.50	4.79	0.503×10^{-5}	12.3
3	903	38.0	0.0676	1.50	4.51	0.503×10^{-5}	13.2
4	955	38.2	0.0655	1.50	4.37	0.503×10^{-5}	13.4
5	1220	38.0	0.0669	1.50	4.45	0.503×10^{-5}	19.2

* B. P. of paraffins correspond to C_{23}.
† Estimated acid to method of Wilke (27).

NOTATION

a = interfacial area per unit liquid volume, sq.ft./cu.ft.
B = total film thickness, ft.
C_p = specific heat
C = concentration of component in liquid
C_1 = initial mixed concentration at time zero or at top of tower
C_i = equilibrium concentration at interface
C_2 = mixed concentration in liquid, distance L from top of tower
ΔC_m = mean concentration driving force
D = tube diameter, ft.
D_L = molecular liquid diffusivity, sq.ft./hr.
E_a = apparent liquid diffusivity, sq.ft./hr.
E_D = eddy liquid diffusivity, sq.ft./hr.
G = mass velocity, lb./(sq.ft.) (hr.)
g = acceleration due to gravity, ft./sec.^{2}
g_c = conversion factor, lb. mass/(ft.) (lb. force) (sec.^{2})
H_L = height of liquid film transfer unit, ft.
j_D = mass transfer factor, dimensionless
k = thermal conductivity, P.cu./(hr.) (sq.ft.) (°C./ft.)
L = tube length, ft.
P = lb. force/sq.ft.
s = distance from gas-liquid interface to point in liquid film, ft.
T_o = temperature of wall, °C.
T_1 = initial temperature at time zero or at the top of the tower
T_2 = liquid temperature, distance L from top of tower
V = velocity, ft./hr.
V_m = maximum velocity, ft./hr.
y = distance from wall to point in liquid film
μ = viscosity, lb./(ft.) (hr.)
ρ = density, lb./cu.ft.
θ = time, hr.
Γ = liquid flow per unit periphery, lb./(hr.) (ft.)

LITERATURE CITED

1. Bays, G. S., Jr., and W. H. McAdams, *Ind. Eng. Chem.* **29**, 1240-46 (1937).
2. Boelter, L., R. C. Martinelli, and F. Jonassen, *Trans. Am. Soc. Mech. Engrs.*, **63**, 447-455 (1941).
3. Chilton, T. H., and A. P. Colburn, *Ind. Eng. Chem.* **26**, 1183 (1934).
4. Colburn, A. P., *Trans. Am. Inst. Chem. Engrs.* **29**, 174 (1933).
5. Cooper, C. M., T. B. Drew, and W. H. McAdams, *Ind. Eng. Chem.*, **26**, 428-431 (1934).
6. Emmert, R. E., and R. L. Pigford, *Chem. Eng. Progr.*, **50**, 87-93 (1954).
7. Fallah, R., T. G. Hunter, and A. W. Nash, *J. Soc. Chem. Ind.*, **53**, 368-79 (1934).
8. Friedman, S. J., and C. O. Miller, *Ind. Eng. Chem.*, **33**, 885-891 (1941).
9. Gilliland, E. R., and T. K. Sherwood, *Ind. Eng. Chem.*, **26**, 516 (1934).
10. Grimley, S. S., *Trans. Inst. Chem. Engrs. (London)* **23**, 228, (1945).
11. Hodson, J. R., thesis, Mass Inst. Technol. (December, 1949).
12. Hurlburt, H. Z., thesis, Mass. Inst. Technol. (1949).
13. International Critical Tables, vol. 5, McGraw-Hill Book Company, Inc., New York (1949).
14. Johnstone, H. F., and R. L. Pigford, *Trans. Am. Inst. Chem. Engrs.* **38**, 25 (1942).
15. King, C. V., and W. H. Cathcart, *J. Am. Chem. Soc.*, **59**, 63-7 (1937).
16. Kirkbride, C. G., *Trans. Am. Inst. Chem. Engrs.*, **30**, 170-86 (1933-34).
17. Linton, W. H., Jr., and T. K. Sherwood, *Chem. Eng. Progr.*, **46**, 258-64 (1950).
18. Martinelli, R. C., *Trans. Am. Soc. Mech. Engrs.* **69**, 947 (1947).
19. McAdams, W. H., "Heat Transmission," McGraw-Hill Book Company, Inc., New York (1942).
20. Murphree, E. V., *Ind. Eng. Chem.*, **24**, 726-36 (1932).
21. Nusselt, W. Z., *Z Ver. deut. Ing.*, **60**, 541, 569 (1916).
22. *Ibid.*, **67**, 206-210 (1923).
23. Prandtl, L., *Engineering*, **123**, 627 (1927).
24. Sherwood, T. K., and R. L. Pigford, "Absorption and Extraction," p. 75-86, McGraw-Hill Book Company, Inc., New York (1952).
25. Surowiec, A. J., and C. C. Furnas, *Trans. Am. Inst. Chem. Engrs.*, **38**, 53-89 (1942).
26. Von Karman, T., *Trans. Am. Inst. Mech. Engrs.*, **61**, 705-710 (1939).
27. Wilke, C. R., *Chem. Eng. Progr.*, **45**, 218-24 (1949).

Presented at the A.I.Ch.E. Glenwood Springs meeting.

PERFORATED-PLATE EXTRACTION-COLUMN PERFORMANCE AND WETTING CHARACTERISTICS

F. H. Garner, S. R. M. Ellis, and J. W. Hill, The University, Edgbaston, Birmingham, England

The type of surface of the perforated plate influences the performance of a perforated-plate column. Pilot plant data on a 4-in column for the system toluene-diethylamine-water at 20°C. show that when the water phase is dispersed and the direction of mass transfer is from the continuous toluene to the dispersed water phase polyethylene plates give a continuous stream of droplets and a higher efficiency, but that when the direction of mass transfer is from the dispersed water to the continuous toluene phase the metal plates give the higher efficiency.

The design of perforated plates for liquid-liquid extraction columns has been studied with reference to the number of plates in the column and their spacing and percentage of free area, but little information has appeared in the literature concerning the effects of the nature of the surface of the perforated tray and of its drop-releasing properties.

Usually the two phases in liquid-liquid extraction possess different characteristics; water is generally one of the phases, and some organic liquid the other phase, and it is usual to disperse the organic phase in the aqueous one. The surface tension of the two phases thus vary considerably, and in consequence each phase will have different wetting properties. The continuous water phase preferentially wets steel plates; the layer of organic liquid below the plate gives rise to droplets of regular size and shape which are formed very close to the plate surface, and the extraction column operates satisfactorily. If however the water phase is dispersed, it still preferentially wets the plate, and irregular droplet formation results unless some alteration is made to the plate to improve droplet formation. This is probably the reason why little use has been made in perforated-plate columns of systems with the water phase dispersed.

An application of the wetting theory has been made to the operation of a pulsed extraction column by use of a perforated plate divided into two layers of different material, each layer possessing different wetting properties (*3*). The selection of packings with correct wetting characteristics giving higher contacting efficiency in extraction columns has also received attention (*12*). Recently a successful attempt has been made to disperse the water phase efficiently by fitting sharp-edged jets to the plates and operating the column above the streaming velocity; the efficiency of operation was greatly increased (*13*). Another method of ensuring good droplet release is changing or altering the surface of the plate so that the organic phase instead of the water phase will wet the trays. This can be done in two ways: by selecting a material with suitable surface characteristics for all the plates or by coating the surface of the existing plates with a suitable compound that will be unaffected by the solvent action of the organic phase. The former method is by far the simpler.

In order to provide a method of selecting an appropriate metallic or nonmetallic surface for use in a perforated-tray column under certain conditions of phase dispersion, the contact angles made by the organic droplet in a water phase and by the water droplets in an organic phase have been measured for a number of different surfaces by use of the two liquid phases of the system under investigation. From an inspection of the results of these measurements a suitable material was chosen and a set of perforated plates made.

EXPERIMENTAL WORK

The experimental program investigated the wetting properties of different surfaces, leading to the selection of polyethylene for use as the perforated tray when the water phase is dispersed. Mild-steel plates have been found to be suitable for toluene dispersion in a continuous water phase (*5*).

The results obtained with a 4-in. pilot plant plate column provide a comparison of operation for polyethylene and metal plates with the water phase dispersed. The factors

which have been investigated are given below in order of importance:

1. Surface of plate—affecting droplet release.

2. Direction of solute transfer (in connection with 3).

3. Phase dispersed—whether that extracting or giving up the solute.

4. Upcomer height—affecting column operation.

Wetting Characteristics of Surfaces. The contact angles made by the droplets on a number of different materials in a surrounding continuous phase were measured by observing the sessile droplet through a traveling microscope, which contained cross wires that could be rotated and placed along the tangent to the droplet at the point of contact. The angle through which the cross wires had been turned was read from a scale fixed to the barrel of the microscope. Values of the vertical height of the drop were also recorded together with its base length. The latter measurements enabled a check to be made on the angle of contact by application of the equations of Talmud and Lubman(*19*). Samples of the surfaces investigated were made 1 5/8-in. long and 1/2 in. wide and by means of a special brass clipped holder were immersed in the continuous phase, contained in a $6 \times 6 \times 6$ cm. glass cell with plain plate sides.

It was considered necessary to measure both the contact angle made by the solvent droplet on the solid in water and also that made by the water droplet in the solvent. These typify instances when the water phase was receding and advancing, respectively. It can be shown(*7*) that the difference in the cosine value of the two contact angles when the water phase is receding and advancing is an empirical measure of the adhesive work between the fluids and the surface in question.

TABLE 1.—TOLUENE-WATER SYSTEM AT 20°C.

	Water receding θ_1, degrees	Water advancing θ_2, degrees	Cos θ_1 — cos θ_2
Glass	134	17	—1.66
Porcelain glazed	144	88	—0.88
Mild steel (rusted)	160	95	—0.77
Brass	135	130	—0.07
Porcelain unglazed	88	120	+0.85
Mild steel (clean)	58	141	+1.31
Mild steel cadmium plated	43	144	+1.54
Mild steel chromium plated	35	138	+1.56
Hostaflon	35	≅180	+1.82
Polyethylene	32	≅180	+1.85
Kel-F	32	≅180	+1.85
P.T.F.E. (Teflon)	23	≅180	+1.92

The results of these measurements are given in Table 1. The negative sign for cos θ_1 — cos θ_2 indicates that the surface is hydrophilic in nature, being preferentially wet by the water phase, whereas a positive value of cos θ_1 — cos θ_2 indicates that the surface is preferentially wet by the solvent phase (hydrophobic). When the water phase is dispersed, the more hydrophobic the nature of the surface, the more suitable is the material for a perforated tray. When the solvent phase is dispersed, a hydrophilic surface is more efficient with regard to droplet release.

From Table 1 polyethylene was chosen as the perforated-plate material in a 4-in. extraction unit using the system toluene-diethylamine-water, in order to observe the effect of water phase dispersion and at the same time to compare operation with the more conventional mild-steel plates. Polytetrafluoro ethylene (P.T.F.E.) would be a better material to employ, but its cost is at present restrictive. Polyethylene is relatively cheap and easy to machine, but it has a tendency to swell slightly in the presence of toluene. This was overcome to a large extent by machining the plates undersize and fitting gaskets to avoid buckling.

Polyethylene was used in a pulsed column as a perforated-plate material by Werning and Higbie(*24*), because of the need for resistance against attack in acid solutions. Teller(*20*) has also used polyethylene in the form of rosette rings in a packed ammonia absorption tower; this material was chosen in order to minimize any wetting contribution to transfer by the liquid phase and so to obtain higher interstitial holdup.

Apparatus. A flow diagram of the pilot plant used in this study is given in a previous paper(*5*). The column was constructed from two 2-ft. lengths of 4-in. nominal-bore glass pipe with flat ground joints connected to a 1-ft.-long 6-in. bore-head section by means of a steel-throat section. The base of the glass column was attached to a 21-in.-high conical sectional enlarged from 4 to 9 in. in diam. in a distance of 12 in.

TABLE 2.—DETAILS OF RUN TYPES OF THE 4-IN.-TRAY COLUMN

Series	No. of runs performed	Plate type	Upcomer height, in.	Phase dispersed	Transfer direction	Average continuous phase rate, cu. ft./(sq. ft.)(hr.)	Comments
E	3	Metal	4½	Water	$W \rightarrow T$	56.5	Eff. 2-3% poor dispersion
L	4	Metal	4½	Water	$W \rightarrow T$	21.0	Eff. 7-8% poor dispersion Low solute transfer, but extreme turbulence
K	5	Metal	4½	Water	$T \rightarrow W$	21.0	Eff. 8-11% poor dispersion Extreme turbulence of dispersed phase
F	4	Polyethylene	4½	Water	$W \rightarrow T$	{2@56.5 2@21.0}	Eff. 2-3% low solute transfer
I	4	Polyethylene	4½	Water	$T \rightarrow W$	21.0	Eff. 7-15% good droplet release
J	1	Polyethylene	4½	Water	$T \rightarrow W$	75.4	Good droplet release
G	15	Polyethylene	2	Water	$W \rightarrow T$	21.0	Eff. 3-7% low solute transfer
H	7	Polyethylene	2	Water	$T \rightarrow W$	21.0	Eff. 7-14% good droplet release

In series *A*, *B*, *C*, and *D*, metal plates were used with 4½-in.-high downcomers, and the toluene phase was dispersed. Transfer direction was mainly toluene to water (*5*).

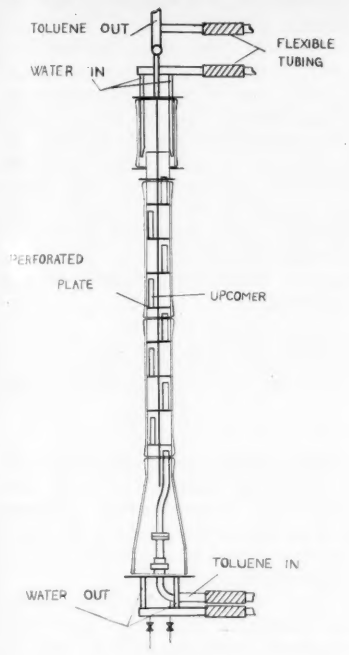

FIG. 1.

The interface was maintained at a constant height in the bottom conical section by adjustment of the back pressure on the column by means of control valves in the exit water line. These valves were a 3/4-in. taper plug valve in parallel with a 1/4-in. needle valve for fine control.

The equilibrium distribution data used in this investigation were obtained by Garner, Ellis and Fosbury (*5*) and Wehn and Franke (*23*). As these limiting-solubility data had been determined at 20°C., it was necessary to adjust the incoming feed liquids to this temperature by circulating water at a suitably controlled temperature through jackets surrounding the constant-head standpipe between the feed pumps and overflows. The temperatures of the incoming phases were read at phase-separating pots and those of the outgoing phases at the head and base cover plates.

The extraction column is shown in more detail in Figure 1. The toluene inlet came to within 1 1/2 in. of the underside of the lower plate. The entering continuous lighter phase was thus admitted to the column as though it came from another plate below the bottom one. The heavier water phase flowed over the 3-in. weir down the wall of the column until the top plate was reached, where it formed a layer on the uppermost side. The water phase was thus acting in a similar manner to that of a wetted-wall heavier phase for the first 7 in. of its passage down the column.

Details of the Perforated Plate. The perforated plate, a plan view of which is given in Figure 2, was of similar design to plates used in the previous investigation (*5*). The polyethylene plates and the metal ones were of the same dimensions, but the plastic plates were 1/8 in. thick and the metal plates were made from 16-gauge tinned-steel plates; each contained fifty-nine 1/8-in. holes representing 6.02% of column cross-sectional area. The upcomer diameter in both cases was 1 in. and represented 5.35% of the column cross-sectional area. The upcomers in the polyethylene plates were made "push fits" instead of being soldered in position. Metal plates were made with 4 1/2-in.-high upcomers but the polyethylene plates could be fitted with either 4 1/2- or 2-in.-high upcomers.

Eight plates were suspended at 6-in. spacings on a 1/4-in. central rod. Because of a constriction in the column diameter at each butt weld, the plates were cut to 3 15/16 in. and fitted with overlap gaskets in order to seal the gaps between the plates and the column wall.

The height of the upcomer assigned to each plate, together with the details of each group of runs, can be seen from Table 2.

RUN PROCEDURE

Most of the runs were carried out at the same low continuous toluene rate of approximately 21.0 cu.ft./(sq.ft.)(hr.), or 12.3 lb.moles/(sq.ft.)(hr.), with the exception of the *E*, *F*, and *J* runs, which were at higher toluene rates (*see* Table 2). This low rate of continuous phase was chosen so that a usual study of droplet release with variations in dispersed-phase flow rate might be made, and at the same time a variation in H.T.U.$_{OC}$ and E_A as a result of changing L_C was avoided, as observed by Garner, Ellis and Fosbury (*5*).

The following liquids were used: toluene of nitration grade, diethylamine of 97% purity, and distilled water. This system has previously been used in packed columns by Morello and Beckmann (*15*), Leibson and Beckmann (*10*), and Wehn and Franke (*23*), and in earlier work by Garner, Ellis, and Fosbury (*5*), using the same 4-in. column. The equilibrium data of the latter two groups of workers have been used.

Before each run the phase containing the solute was made up to approximately 1.0% diethylamine by weight, and after the run about 10 to 15 gal. of extracting phase were replaced by an equal quantity of solute free phase.

With toluene as the continuous phase, water was admitted until a sufficient layer had collected at the base of the column to provide an interface reading, and then the column was filled with the continuous phase. After the interface valve was closed, the desired water rate was set, while the interface steadily rose. On opening of the interface valve, water was released until no further

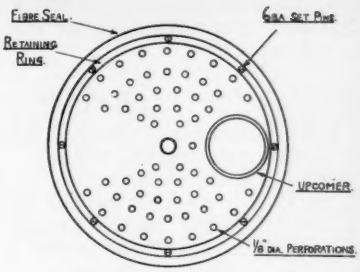

FIG. 2. PLAN VIEW OF THE PERFORATED PLATE.

toluene was pushed out of the column. The desired toluene rate was then set and the interface accurately adjusted.

After the elapse of sufficient time for two to three changes of continuous phase to take place, samples of each phase entering and leaving the column were taken, and again at intervals of 15 min. for the next 1/2 hr. Outlet flow rates were measured at points immediately after the weir vessels twice during this period. The time taken for each run was between 1 1/2 and 2 hr.

The three sets of samples of the inlet and outlet phases were bulked and analyzed for solute content using N/15 HCl. The density of the phases at 20°C. was determined by use of a Westphal balance. The average of the flow checks was used to determine the flow rates during the runs.

CONTROLLING RESISTANCE AND EXTRACTION FACTOR

When the equilibrium distribution for this system is plotted on a mole fraction basis at 20°C., the solute favors the toluene phase with the partition coefficient, $\frac{dC_T}{dC_W}$, having a value of 3.18. The equilibrium line is straight at low solute concentrations.

If y refers to the dispersed phase and x to the continuous phase, then $\frac{dy^*}{dx} = m$

When toluene is dispersed, $m = \frac{dC_D}{dC_C} = 3.18$. When, however, the water phase is dispersed, $m = \frac{dC_D}{dC_C} = 0.314$, with the solute still favoring the toluene phase.

Thus if the water phase is dispersed, the factor $\frac{1}{mk_D}$ in Equation (1), relating the over-all continuous mass transfer coefficient to the film values, is relatively high and the dispersed-water-phase resistance is controlling.

$$\frac{1}{K_{OC}} = \frac{1}{k_C} + \frac{1}{mk_D} \qquad (1)$$

The extraction factor, which is an indication of economic opera-

tion, has been defined by Treybal (*21*) and other workers in the following manner:

$$\text{Extraction factor} = \frac{dC_E}{dC_R} \cdot \frac{E}{R}$$ where

E = the extracting phase — the phase receiving the solute

R = the raffinate phase

C_E and C_R = the concentrations of solute in the extract and raffinate phases

As indicated by Pike(*16*), the extraction factor will change according to the conditions existing in the column:

1. *Toluene dispersed.* a. Transfer $T \rightarrow W$ (water the extracting phase)

$$\text{Extraction factor} = \frac{dC_W}{dC_T} \cdot \frac{V_W}{V_T} = \frac{dC_C}{dC_D} \cdot \frac{V_C}{V_D} = \frac{L_C}{mL_D}$$

b. Transfer $W \rightarrow T$ (toluene the extracting phase)

$$\text{Extraction factor} = \frac{dC_T}{dC_W} \cdot \frac{V_T}{V_W} = \frac{dC_D}{dC_C} \cdot \frac{V_D}{V_C} = m\frac{L_D}{L_C}$$

2. *Water dispersed.* a. Transfer $T \rightarrow W$

$$\text{Extraction factor} = \frac{dC_W}{dC_T} \cdot \frac{V_W}{V_T} = \frac{dC_D}{dC_C} \cdot \frac{V_D}{V_C} = m\frac{L_D}{L_C}$$

b. Transfer $W \rightarrow T$

$$\text{Extraction factor} = \frac{dC_T}{dC_W} \cdot \frac{V_T}{V_W} = \frac{dC_C}{dC_D} \cdot \frac{V_C}{V_D} = \frac{L_C}{mL_D}$$

Hence the magnitude of the extraction factor will depend not only on the individual flow rates but also on the direction of transfer and on which phase is dispersed. The range of extraction factor used in this work was 0.1–2.0 with transfer $D \rightarrow C$, and 2.0–12.0 with transfer $C \rightarrow D$, the water phase being dispersed.

CALCULATION OF MASS TRANSFER DATA

For low solute concentrations and immiscibility of the two phases, the operating line can be expressed in the form of a linear equation:

$$y = \frac{L_C}{L_D}x + \left(y - \frac{L_C}{L_D}x\right)_{avg} \quad (2)$$

where $\left(y - \frac{L_C}{L_D}x\right)_{avg}$ is the arithmetic average of $y_1 - \frac{L_C}{L_D}x_1$ and $y_2 - \frac{L_C}{L_D}x_2$.

With zero mass balance error $y_1 - \frac{L_C}{L_D}x_1$ and $y_2 - \frac{L_C}{L_D}x_2$ are equal and the operating line passes through the terminal composition points. When a mass balance error exists, the composition points lie equidistant on either side of the operating line. As the flow-rate data are believed to be more accurate than the volumetrically determined concentration data, corrected values of the terminal compositions were used for all performance calculations. The terminal compositions were obtained graphically by taking the points on the operating line nearest to the composition points and were not greatly different from the original values.

The evaluation of H.T.U. data was made by dividing the column height used by the number of transfer units, which were determined by Equations (3) and (4).

$$N_{tOD} = \frac{1}{1 - \frac{mL_D}{L_C}} \cdot \ln\left[\frac{y_1 - mx_1}{y_2 - mx_2}\right] \pm \frac{1}{2}\ln\left[\frac{1 - y_2}{1 - y_1}\right] \quad (3)$$

Interterm sign positive when $y_1 > y_2$

$$N_{tOC} = \frac{1}{\frac{L_C}{mL_D} - 1} \cdot \ln\left[\frac{y_1 - mx_1}{y_2 - mx_2}\right] \pm \frac{1}{2}\ln\left[\frac{1 - x_2}{1 - x_1}\right] \quad (4)$$

Interterm sign positive when $x_1 > x_2$

These equations apply where $L_C/L_D \neq m$. For the case where $L_C/L_D = m$, then

$$N_{tOD} = N_{tOC} = N_A = \frac{y_1 - y_2}{\left(y - \frac{L_C}{L_D}x\right)_{avg}}$$

Equations (1) and (2) are Colburn's equations simplified by Wiegand to apply to dilute solutions. In most runs the correction terms to Equations (3) and (4) were less than 0.008. From the foregoing equations it can be seen that

$$H_{tOC} = \left(\frac{L_C}{mL_D}\right) H_{tOD} \quad (5)$$

The efficiency of column performance has been expressed in a number of ways. Mayfield and Church(*13*) used the McCabe-Thiele type of plot(*14*) to obtain a continuous- or dispersed-phase efficiency, whereas Pyle, Colburn, and Duffey(*17*) used the Baker-Stockhardt modification to give an average efficiency based on either phase. The efficiency E_A used in this work was evaluated from the number of theoretical stages, determined by Equation (6), and the actual number of plates in the column. The H.E.T.S. was evaluated from the effective height and N_A. The number of theoretical stages is determined by

$$N_A = \frac{\ln\left[\frac{y_1 - mx_1}{y_2 - mx_2}\right]}{\ln\frac{L_C}{mL_D}} \quad (6)$$

This equation was obtained from a stepwise analysis(*5*) of the theoretical concentration changes in a column containing N_A theoretical stages and is not dependent on either of the phases.

The over-all volume mass transfer coefficient K_Da and K_Ca were calculated from the H.T.U. data by use of the simplified relations for dilute solutions:

$$K_Ca = \frac{V_C}{H_{tOC}} \text{ and } K_Da = \frac{V_D}{H_{tOD}} \quad (7)$$

For the purposes of calculation the phase concentrations were converted to mole fraction units by use of the average phase molecular weights, which were not significantly different from 18.1 for the water phase and 91.8 for the toluene phase. The average phase temperatures were all within the range 20 ± 1°C.

RESULTS

The results obtained experimentally from the operation of the column are presented in Table 3 together with the calculated performance data. The phase flow rates are given in pound moles per square feet per hour and also cubic feet per square feet per hour and the phase solute concentrations for the entering and leaving liquids in pound moles per square feet. The column height, as shown in Table 3, is the distance between the top of the inlet weir and the two-phase interface. The percentage mass balance error, also in Table 3, is defined by (solute out—solute in)/solute in. The over-all H.T.U. and over-all volume mass transfer coefficient based on the dispersed and continuous phases are also given. The efficiency, as calculated from Equation (6) and the number of plates in the column, is included in Table 3.

TABLE 3.—EXPERIMENTAL RESULTS AND PERFORMANCE DATA

Phase flow rates

TABLE 3.—EXPERIMENTAL RESULTS AND PERFORMANCE DATA

Run	Phase flow rates: Cu. ft./(sq. ft.) (hr.) Toluene V_T	Water V_W	Lb. moles/(sq. ft.) (hr.) Toluene L_T	Water L_W	Column height used, ft.	Phase solute concentrations, lb. moles/cu. ft. Toluene In	Toluene Out	Water In	Water Out	Solute mass balance error, %	$\frac{L_C}{mL_D}$	H.T.U.$_{OD}$ ft.	K_Ca, hr.$^{-1}$	E_A, %
*E*1	56.01	30.59	32.88	104.1	5.73	0.00197	0.00243	0.00885	0.00795	+0.9	1.004	30.3	1.85	2.4
2	56.89	16.37	33.48	55.2	5.83	0.00236	0.00269	0.00956	0.00849	−0.4	1.924	20.5	1.44	2.6
3	56.23	24.01	33.01	82.4	5.83	0.00267	0.00301	0.00936	0.00860	−0.1	1.275	25.5	1.74	2.5
*L*1	21.20	50.15	12.39	171.4	5.80	0.00240	0.00387	0.00880	0.00817	+0.2	0.2300	23.8	3.88	7.0
2	21.28	105.60	12.43	360.1	5.73	0.00234	0.00452	0.00943	0.00900	+0.9	0.1098	33.0	5.88	8.0
3	21.29	128.50	12.45	439.8	5.79	0.00232	0.00392	0.00789	0.00764	−0.1	0.0900	36.9	6.39	8.2
4	21.00	72.10	12.27	246.0	5.47	0.00360	0.00474	0.00991	0.00955	+0.3	0.1573	27.0	4.90	7.3
*K*1	21.04	84.91	12.30	292.2	5.36	0.00867	0.00256	0.00127	0.00283	−1.5	0.1338	25.2	6.21	8.6
2	20.83	44.86	12.17	154.3	5.37	0.00856	0.00417	0.00161	0.00362	+0.5	0.2509	23.1	3.60	6.3
3	21.32	29.01	12.46	99.8	5.40	0.00851	0.00514	0.00139	0.00386	0.0	0.3969	21.6	2.49	5.2
4	21.42	150.02	12.52	517.1	5.62	0.00913	0.00112	0.00057	0.00181	−5.0	0.0770	29.1	9.54	11.3
5	21.51	108.90	12.57	374.9	5.55	0.00907	0.00225	0.00162	0.00302	−1.7	0.1066	26.8	7.52	9.7
*F*1	56.23	15.44	32.88	52.8	5.94	0.00284	0.00306	0.00939	0.00875	−0.7	1.980	29.0	0.98	1.9
2	57.29	21.80	33.52	74.5	5.95	0.00306	0.00328	0.00909	0.00858	−0.3	1.435	25.3	1.58	2.5
3	21.28	47.40	12.42	161.9	5.88	0.00313	0.00364	0.00881	0.00856	0.0	0.244	61.4	1.42	2.6
4	21.26	76.79	12.43	262.9	5.71	0.00331	0.00376	0.00866	0.00851	+1.6	0.1504	94.4	1.50	2.3
*I*1	20.82	40.72	12.17	140.3	5.51	0.00906	0.00361	0.00010	0.00307	−4.0	0.2758	18.1	4.16	7.8
2	21.26	92.90	12.41	319.6	5.55	0.00898	0.00177	0.00115	0.00284	−1.3	0.1235	20.6	8.40	11.5
3	20.81	66.44	12.16	228.5	5.38	0.00870	0.00275	0.00168	0.00360	−1.6	0.1692	19.5	6.28	9.5
4	21.00	143.60	12.27	494.0	5.58	0.01031	0.00105	0.00101	0.00243	−2.6	0.0790	21.6	12.30	14.9
*J*1	75.36	139.60	44.05	480.0	5.68	0.01018	0.00480	0.00128	0.00429	−1.7	0.2925	20.3	12.70	6.9
*G*1	20.78	49.73	12.15	170.1	5.51	0.000761	0.00291	0.00858	0.00768	+0.1	0.2271	28.2	3.25	5.6
2	20.78	97.47	12.14	332.9	5.67	0.00152	0.00398	0.00956	0.00902	+0.2	0.1159	41.4	4.33	6.1
3	20.84	53.89	12.18	184.1	5.60	0.00220	0.00367	0.00927	0.00872	−0.1	0.2104	35.2	2.81	4.8
4	20.43	65.40	11.96	223.6	5.65	0.00259	0.00378	0.00901	0.00862	+4.0	0.1700	39.4	3.05	4.9
5	21.10	68.49	12.34	234.2	5.63	0.00296	0.00400	0.00930	0.00901	−0.3	0.1676	48.6	2.59	4.0
6	20.80	89.91	12.15	306.8	5.67	0.00326	0.00450	0.01031	0.00996	+0.4	0.1259	53.8	3.07	4.4
7	21.21	88.66	12.38	303.0	5.58	0.00295	0.00428	0.00997	0.00965	+0.7	0.1299	53.5	3.05	4.3
8	17.63	85.91	10.30	293.1	5.57	0.00326	0.00421	0.00952	0.00935	−0.2	0.1065	76.0	2.06	3.3
9	21.48	107.90	12.54	368.0	5.48	0.00289	0.00414	0.00935	0.00909	0.0	0.1083	57.6	3.44	4.4
10	20.93	82.12	12.22	280.3	5.51	0.00327	0.00441	0.01008	0.00978	+0.1	0.1387	53.3	2.84	4.1
11	21.88	99.24	12.78	338.9	5.53	0.00304	0.00392	0.00875	0.00857	−0.8	0.1199	55.7	3.28	4.3
12	21.49	31.48	12.55	107.6	5.14	0.00328	0.00389	0.00941	0.00897	+0.3	0.3711	29.6	1.95	3.7
13	21.08	57.55	12.32	196.2	5.77	0.00354	0.00433	0.00989	0.00964	−0.3	0.1996	47.9	2.21	3.9
14	21.49	29.52	12.32	100.7	5.58	0.00344	0.00437	0.00970	0.00906	−0.2	0.3889	17.3	3.19	6.7
15	20.47	55.54	11.96	189.6	5.65	0.00326	0.00446	0.00925	0.00885	−0.3	0.2006	32.4	3.14	5.4
*H*1	20.93	59.11	12.24	203.1	5.57	0.00894	0.00226	0.00374	0.00256	+5.4	0.1915	19.6	5.55	9.1
2	21.52	29.19	12.57	100.3	5.30	0.00855	0.00474	0.00167	0.00457	−1.3	0.3985	16.5	3.28	6.6
3	21.10	43.84	12.34	150.7	5.33	0.00904	0.00390	0.00190	0.00438	−0.5	0.2604	18.4	4.47	7.8
4	21.12	68.88	12.35	236.6	5.33	0.00940	0.00300	0.00218	0.00419	−1.1	0.1660	18.9	6.68	9.8
5	20.83	96.12	12.18	330.2	5.63	0.00802	0.00247	0.00336	0.00457	−0.4	0.1172	19.4	9.15	12.8
6	21.83	77.17	12.76	265.0	5.65	0.00958	0.00330	0.00352	0.00535	−1.1	0.1531	19.2	7.18	10.8
7	21.18	123.70	12.38	424.9	5.62	0.00946	0.00252	0.00372	0.00493	−0.6	0.0927	20.7	10.97	14.0

The results for the G runs in Figures 9 and 11, with solute transfer from the dispersed water phase to the continuous phase, show a lack of reproducibility in contrast to all the other curves, although the mass balance errors for all the runs are quite low.

Effect of the Plate Surface. If the I and K runs are compared (both have 4 1/2-in.-high upcomers and transfer direction continuous to dispersed, but the I runs were with the polyethylene plates and the K runs with mild-steel plates), it can be seen from Figure 10, showing efficiency E_A vs. V_D, that the efficiency at the same dispersed flow rate is about 25 to 30% higher for the runs with the polyethylene plates than with the metal plates. This increase in efficiency would probably be higher if a system had been used in which the droplets circulated; it has been shown (*6*) that the system toluene-diethylamine-water does not circulate under any conditions.

Typical photographs showing the performance of the polyethylene plates in the G and I runs and the mild-steel plates in the L and K runs are presented in Figures 3 to 8. The photographs are enlargements taken from 16-mm. cine film shots of the conditions existing during a particular run on the sixth plate from the base of the column.

It was not possible to determine accurately the number and size of the droplets in the column at any one time because the surface through which they were photographed was the curved column wall, which undoubtedly gave rise to distortion.

In Figures 3 to 8, the polyethylene plates give a continuous stream of relatively small droplets of fairly uniform size, but the metal plates produce "blobs of dispersed phase at regular intervals"; between these intervals a few droplets were formed, but they were quite irregular in size (*see* Figure 6, run K 4). Figures 3, 4, and 5 are with polyethylene plates and Figures 6, 7, and 8 with metal plates. The blobs of water phase that occurred with the metal plate underwent considerable turbulence as they fell from plate to plate. Some of the dispersed phase adhered to the central supporting rod and some fell down the column wall as a falling film. This unfortunately cannot be observed in the photographs as the continuous toluene phase at times became quite cloudy owing to the presence of water.

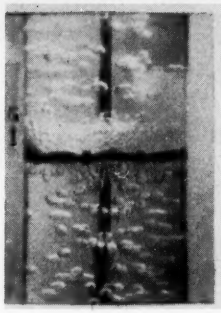

FIG. 3.

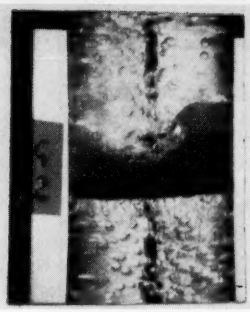

FIG. 4.

FIG. 5.

Effect of Transfer Direction. The direction of solute transfer will affect the resistance of the water film under certain conditions. Figure 11 shows a plot of the over-all volume mass transfer coefficient for the continuous toluene phase vs. the dispersed phase flow rate; the continuous rate was constant throughout except for run J 1. A similar plot can be drawn for K_Da as K_Da/K_Ca equals the distribution coefficient in volume units. The higher the value of K_Ca, the less the resistance of the controlling film. Both the polyethylene and metal plates show higher values of K_Ca for transfer from continuous to dispersed than in the opposite direction for the same upcomer size, the polyethylene plates having a higher K_Ca than the metal plates. The metal plates, however, appear more efficient than the polyethylene plates when the solute transfer is from the dispersed water phase to the continuous toluene phase as more turbulence and breakup of the dispersed phase is present with the metal plates, and this assists transfer although the area of contact is reduced. The plot of E_A vs. mL_D/L_C in Figure 9 also shows that the polyethylene plates are more suitable for water dispersion when the solute transfer is to the water phase.

Licht and Conway (*11*) have suggested that considerable hydrogen bonding exists between the solute molecule and the water molecules and that hence when the solute is put in the water phase (extraction W to T) orientation-and-hydrogen bonding takes place with the NH end of the diethylamine molecule in the water phase. When the solute is extracted from the water phase, the final break comes between the NH linkage and the OH groups of the water. If however the diethylamine is placed in the toluene phase (extraction T to W), no orientation occurs and the final separation involves overcoming of the Van der Waals forces between the organic part of the solute molecule and the toluene. As the forces of adhesion due to hydrogen bonding are more intense than those holding the organic end of the solute molecule and the organic phase together, transfer will be easier when water is the extracting phase. This is in agreement with the foregoing observations.

The Dispersed Phase. The work of Johnson and Blias (*8*) with a spray tower indicates that the phase receiving the solute should be dispersed for efficient operation. It will therefore be advantageous to operate the column at a high extraction factor by dispersing the water phase efficiently, with the use of polyethylene plates, and transferring the solute to the water phase. This results in higher solute transfer, as seen in the previous

FIG. 6.

FIG. 7.

FIG. 8.

section on the direction of transfer.

Although droplet release was extremely good with the polyethylene plates in the *G* runs (*see* Figures 3 and 4), with transfer from the dispersed to the continuous phase, the metal-plate runs with the same transfer direction (*L* runs) exhibited higher efficiencies. The extraction factor was unfavorable for high solute transfer, and consequently the greater turbulence and not so noticeable at the lower rates. This increase in efficiency is irrespective of transfer direction (*see* Figure 9 for transfer in the opposite direction with polyethylene plates). No comparisons were made for metal plates, as only one upcomer size was available. In Figures 9 and 10 run *H* 7 was on the verge of flooding, and hence the fall off in efficiency at high dispersed rates for the 2-in. upcomer with polyethylene plates.

than vertically up the column. On these grounds it would be expected that a short upcomer would give more efficient operation than a large one.

H.T.U. DATA

As a matter of further interest the H.T.U.$_{OC}$ data for the runs are plotted in Figure 12 in the manner adopted by most workers (*1, 9, 15, 18, 22*).

A set of straight lines is ob-

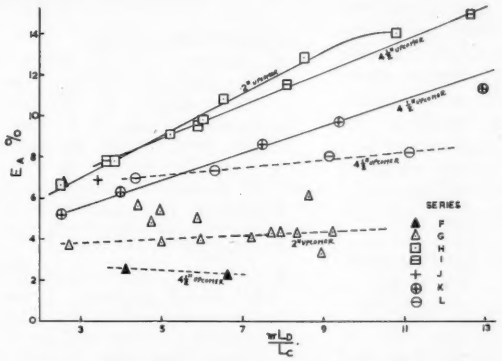

FIG. 9. EFFECT OF UPCOMER SIZE AND TRANSFER DIRECTION ON E_A ($L_C = 21$ FT./HR. EXCEPT *J*).

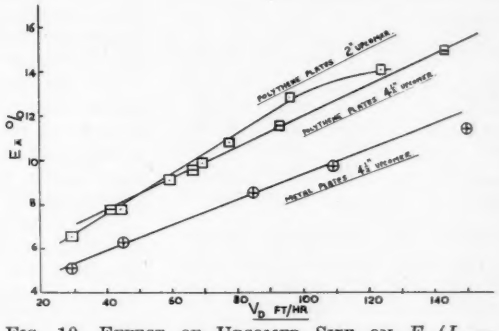

FIG. 10. EFFECT OF UPCOMER SIZE ON E_A ($L_C =$ 21 FT./HR.; WATER EXTRACTING).

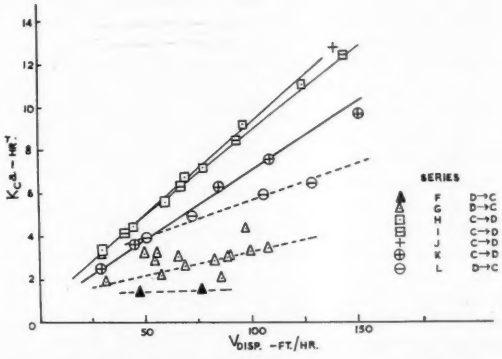

FIG. 11. EFFECT OF TRANSFER DIRECTION ON K_Oa AS A FUNCTION OF WATER RATE ($L_C = 21$ FT./HR. EXCEPT *J*).

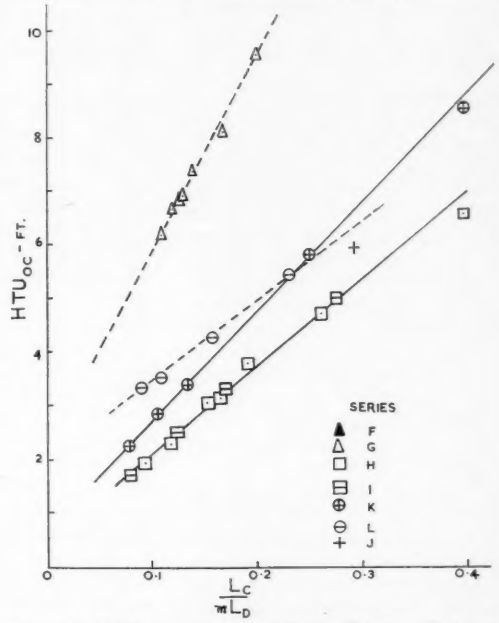

FIG. 12. H.T.U.$_{OC}$ VS. EXTRACTION FACTOR L_C/m_{LD} ($L_C = 21$ FT./HR. EXCEPT *J*).

shear of the water phase (in the *L* runs) due to the breakup of the blobs was more effective than the higher interfacial area obtained with good droplet release in the *G* runs.

Effect of Upcomer Height. Figure 10 indicates that the 2-in.-high upcomer is more efficient than the 4 1/2-in.-high one at high dispersed phase flow rates, but the effect is

The height of the upcomer has a direct bearing on the amount of turbulence and contact in the zone of free fall of dispersed phase between each plate. A short upcomer results in better counter current contact than does a large upcomer where the movement of continuous phase is nearly at right angles to the flow of dispersed phase; that is, the continuous phase moves across from plate to plate rather

tained. For the *G* runs the line was selected from the line shown in Figure 11 in order to avoid scatter.

It has been the usual practice in the past to identify the slope and intercept of this line with the film values in accordance with the equation

$$\text{H.T.U.}_{OC} = \text{H.T.U.}_C + \text{H.T.U.}_D\left(\frac{L_C}{L_D}\cdot\frac{1}{m}\right) \qquad (8)$$

In some instances however negative intercepts have been obtained (*9, 15, 18*), and the identification of the slope and intercept with the film values has been discussed (*5*).

It is interesting to note from Figure 12 that similar intercepts are obtained for different plate surfaces. For both polyethylene and metal plates the direction of mass transfer does influence the intercept and slope of the H.T.U.$_{OC}$ plot. Table 4 includes the slope and intercept data extrapolated from Figure 12.

TABLE 4

Plate type, water dispersed	Intercept	Slope	Transfer direction
Polyethylene..	0.55	15.6	$T \rightarrow W$
Metal.....	0.70	20.1	$T \rightarrow W$
Polyethylene..	2.15	36.2	$W \rightarrow T$
Metal.....	2.00	14.8	$W \rightarrow T$

Because the continuous phase flow rate was constant, both the slope and intercept appear to be independent of the dispersed phase flow rate. Garner, Ellis and Fosbury (*5*) found that the effects of the dispersed and continuous phase flow rates on H.T.U.$_{OC}$ were equal but operated in opposite directions.

CONCLUSIONS*

Pilot plant data for the system toluene-diethylamine-water at 20°C. are given for a 4-in. perforated-plate column using metal and polyethylene plates with the water phase dispersed and solute transfer in both directions. The column was operated under varying conditions of dispersed flow and a constant continuous phase throughput of 21 cu.ft./(sq.ft.)(hr.). The range of dispersed phase flow rates covered was 15 to 150 ft./(hr.). Stage-efficiency data vary from 2 to 15% and the H.T.U.$_{OC}$ data range from 2 to 50 ft.

The contact angles made by toluene and water droplets on a number of different materials in a surrounding continuous phase have been measured by the sessile droplet method. The surface of the perforated plate has been found to have a distinct influence on the operation of the plate column. The surface used for the plate must be hydrophobic when the water phase is dispersed, to ensure production of droplets from the plate surface at regular intervals. Polyethylene is suitable for this purpose.

*Since this paper was written, another paper on the subject has come to the authors' notice. R. H. Buchanan [*Australian J. Appl. Sci.*, 3, 233 (1952)] in his qualitative study of drop formation from wetted orifices has considered the effect of velocity and varying orifice materials. He concludes that strongly hydrophobic materials cannot be used to disperse a hydrophobic liquid or strongly hydrophilic materials a hydrophilic liquid.

The system toluene-water-diethylamine is noncirculating, and therefore the increase in efficiency obtained by the use of polyethylene plates instead of metal plates, which produce poor dispersions of water phase, is not so high as that expected from a system in which the droplets circulate. It is hoped in the future to investigate such a system.

With the diethylamine system the controlling resistance lies in the water phase when mole fraction units are employed, and it has been found that the efficiency of operation is higher when solute transfer is to the dispersed water phase rather than from the water phase, because of hydrogen bonding. The direction of mass transfer has also been shown to affect the value of the extraction factor significantly.

Single-line correlations have been obtained for the H.T.U.$_{OC}$ vs. L_C/mL_D plots, the slopes and intercepts of which depend on the direction of mass transfer and the plate surface used. Although the transfer direction affects both the slope and intercepts of these correlations, the type of plate surface affects only the slopes.

NOTATION

C_T, C_W = concentration of solute in the toluene and water phases, g.moles/liter

E_A = average over-all stage efficiency, from N_A

H.T.U.$_{OD}$, H.T.U.$_{OC}$ = H_{tOD}, H_{tOC} height of over-all transfer unit, based on dispersed and continuous phases, ft.

H.T.U.$_D$, H.T.U.$_C$ = height of film transfer unit, based on dispersed and continuous phases, ft.

$K_{OC}, K_{OD}, k_C k_D$ = over-all and individual extraction coefficients, lb.moles/(cu.ft.)(hr.) (lb. moles/cu.ft.)

$K_D a, K_C a, k_D a, k_C a$ = over-all and individual volume coefficients, lb. moles/(sq.ft.)(hr.)(lb.moles/cu.ft.)

L_D, L_C = dispersed and continuous phase flow rate, lb.moles/(sq.ft.)(hr.)

m = slope of the equilibrium distribution curve dy^*/dx

N_A = number of theoretical stages

N.T.U.$_{OD}$, N.T.U.$_{OC}$ = N_{tOD}, N_{tOC} number of over-all transfer units

V_D, V_C = dispersed and continuous phase flow rate, cu.ft./sq.ft.hr.

x = concentration of solute in the continuous phase, mole fraction

y = concentration of solute in dispersed phase, mole fraction

y^* = concentration of solute in dispersed phase, at equilibrium mole fraction

Subscripts

1 and 2 = column base and top concentration terminals

LITERATURE CITED

1. Allerton, J., B. O. Strom, and R. E. Treybal, *Trans. Am. Inst. Chem. Engrs.*, 39, 361 (1943).
2. Baker, T., and J. S. Stockhardt, *Ind. Eng. Chem.*, 22, 376 (1930).
3. Burns, W. A., and W. F. Johnson, U. S. Patent 2,662,001 (1953).
4. Chilton, T. H., and A. P. Colburn, *Ind. Eng. Chem.*, 27, 255, 904 (1935).
5. Garner, F. H., S. R. M. Ellis, and D. W. F. Fosbury, *Trans. Inst. Chem. Engrs.*, 31, 348 (1953).
6. Garner, F. H., and A. R. Hale, *Chem. Eng. Sci.*, 2, 157 (1953).
7. Hill, J. W., *Birmingham University Chem. Engr.* 5, 43 (1954).
8. Johnson, H. F., and R. H. Bliss, *Trans. Am. Inst. Chem. Engrs.*, 42, 331 (1946).
9. Knight, O. S., *Trans. Am. Inst. Chem. Engrs.*, 39, 439 (1943).
10. Leibson, I., and R. B. Beckmann, *Chem. Eng. Progr.*, 49, 405 (1953).
11. Licht, W., and J. B. Conway, *Ind. Eng. Chem.* 42, 1151 (1950).
12. Livingston, M. J., U. S. Patent 2,215,359 (1940).
13. Mayfield, F. D., and W. L. Church, *Ind. Eng. Chem.*, 44, 2253 (1952).
14. McCabe, W. L., and E. W. Thiele, *Ind. Eng. Chem.*, 17, 605 (1925).
15. Morello, V. S., and R. B. Beckmann, *Ind. Eng. Chem.*, 42, 1078 (1950).
16. Pike, F. P., *U. S. Atomic Energy Com. Rpt.* ORNL 929.
17. Pyle, C., A. P. Colburn, and H. R Duffey, *Ind. Eng. Chem.*, 42, 1042 (1950).
18. Row, S. B., J. H. Koffolt, and J. R. Withrow, *Trans. Am. Inst. Chem. Engrs.*, 37, 559 (1941).
19. Talmud, D., and N. M. Lubman, *Z. physik. Chem.*, 148A, 227 (1930).
20. Teller, A. J., *Chem. Eng. Progr.*, 50, 55 (1954).
21. Treybal, R. E., "Liquid Extraction," McGraw Hill Book Company, Inc. (1951).
22. Treybal, R. E., and F. E. Dumoulin, *Ind. Eng. Chem.*, 34, 709 (1942).
23. Wehn, W. E., and N. W. Franke, *Ind Eng. Chem.*, 41, 2853 (1949).
24. Werning, J. R., and K. B. Higbie, *Ind. Eng. Chem.*, 46, 644 (1954).
25. Wiegand, J. H., *Trans. Am. Inst. Chem. Engrs.*, 36, 679 (1940).

Presented at A. I. Ch. E. New York meeting.

HEAT AND MASS TRANSFER IN PACKED BEDS

DONALD A. PLAUTZ and H. F. JOHNSTONE
University of Illinois, Urbana, Illinois

Eddy mass diffusivities, effective thermal conductivities, and wall heat transfer coefficients were measured in an 8-in. tube packed with ½- and ¾-in. glass spheres. Superficial mass velocities ranged from 110 to 1,640 lb./(hr.) (sq. ft.), corresponding to modified Reynolds numbers of 100 to 2,000. Air was the main stream fluid in all cases.

The modified Peclet group ($D_p V/E^*_{ta}$) was found to be constant at a value of about 12 in the region of fully developed turbulence. At lower Reynolds numbers this group varied with the flow rate. Effective thermal conductivities were correlated by an equation. Modified Peclet numbers for heat transfer were about 25% less than those for mass transfer. The wall heat transfer coefficient varied with the superficial mass velocity as $h_w = 0.090(G_0^{0.75})$.

An explanation is suggested for the similarity in velocity dependence between these values and those for turbulent flow in an empty tube, based on channeling at the wall.

Among the recent advances in chemical engineering has been the development of analytic methods for the rational design of nonadiabatic, fixed-bed, catalytic converters. To apply these methods, a knowledge of radial heat and mass transport rates in the system is required. Temperatures and concentrations must be known as functions of the position in the bed in order to allow for their effects on the reaction rate.

The only reported studies of lateral mass transport rates in flowing fluid-packed-bed systems are those of Bernard and Wilhelm (*2*) and Latinen(*11*). The former measured eddy-diffusion rates for 3/8-in. alumina spheres in an 8-in. column with air as the main stream fluid and for several sizes of cylinders and spheres in a 2-in. tube with water as the main stream fluid. Latinen extended the range of this work to the water-solids system. All data were taken with the bed at a uniform temperature, and the results were expressed as modified Peclet numbers.

Earlier studies (*8, 12* to *14, 17*) on heat transfer in packed beds were confined to measuring boundary temperatures, and results were reported as over-all thermal conductivities or over-all heat transfer coefficients. These values incorporate the resistance to heat transfer within the bed as well as the heat transfer resistance at the walls of the confining tube and thus do not provide a basis for predicting radial-temperature gradients.

Radial heat transfer rates have been obtained from measured radial temperature traverses by Coberly and Marshall(*5*), Felix and Neill (*6*), Campbell and Huntington(*4*), Irvin, Olson, and Smith(*9*), Bunnell, Irvin, Olson, and Smith(*3*), and Schuler, Stallings, and Smith (*15*). Results were reported in terms of effective thermal conductivities of the gas-solid bed. It was also noted that the resistance to heat transfer in a bed increased near the confining walls. Coberly and Marshall, Felix and Neill, and Campbell and Huntington account for this by assuming k_e to be constant within the bed and postulate a heat transfer coefficient at the wall. Irvin *et al.*, Bunnell *et al.*, and Schuler and Smith handle this problem by decreasing the effective thermal conductivity values near the wall.

Baron(*1*), and Latinen(*11*) analyzed turbulent diffusion in packed beds on the basis of a "random walk" theory. Their analysis indicates that when turbulence is fully developed, the Peclet numbers for heat and mass transfer should be equal and constant at a value of about 11. Results of the previous investigations, however, have shown Peclet numbers for heat transfer to be less than those for mass transfer. There has been some doubt as to whether this discrepancy arises from differences in experimental techniques or from differences in bed-temperature conditions encountered in the two types of measurements. The present investigation has been conducted with the following objectives: (1) to extend isothermal-eddy-mass-diffusion measurements for a gas-solids system and to compare these values with those measured in the presence of a temperature gradient; (2) to measure eddy-mass diffusivities and effective thermal conductivities under identical temperature, bed, and flow conditions to permit a comparison of Peclet numbers for heat and mass transfer; and (3) to study the wall effect in greater detail.

In a cylindrical nonadiabatic fixed-bed catalytic converter, heat and mass move from regions of high concentrations to regions of low concentrations through the in-

Donald A. Plautz is at present with Standard Oil Company (Indiana), Whiting, Indiana.

terstices of the bed. In the ranges of flow encountered in industrial practice, longitudinal or axial transfer occurs primarily by the mechanism of velocity transport; that is, heat and mass are carried by the net mass flow of the fluid. Since it is unlikely that there is an appreciable net mass flow of fluid in the radial direction, radial transport is believed to result primarily from interstitial fluid mixing. Evaluating lateral transport parameters from an analysis of this mixing process, however, has met with only limited success as the fluid mechanics of flow in a packed bed has not as yet been developed.

A less rigorous but more successful approach to this problem has been to treat the system as though it were a homogeneous material and incorporate all transport mechanisms except mass flow into an over-all diffusion mechanism. This assumes that the presence of the packing need be considered only insofar as it affects the numerical value of the diffusion coefficient. Although there is no theoretical basis for this procedure, it is acceptable if the over-all diffusion coefficient is assumed to be a function of all the variables that affect the actual transfer mechanisms operating in the bed.

Employing this concept, one can write a single equation to describe both heat and mass transfer in a packed bed. In cylindrical coordinates this equation is

$$V\frac{\partial f}{\partial z} = E_o^*\left(\frac{\partial^2 f}{\partial r^2} + \frac{1}{r}\cdot\frac{\partial f}{\partial r} + \frac{\partial^2 f}{\partial z^2}\right) \tag{1}$$

The assumptions inherent in Equation (1) are

1. The bed is isotropic; i.e., E_o^* in the radial direction is equal to E_o^* in the axial direction.
2. E_o^* and V do not vary with radial position or bed depth.
3. Radial symmetry prevails.
4. The velocity in the radial direction is zero.
5. The fluid properties are constant.
6. The process is at steady state.
7. No chemical reaction is occurring.

In the case of mass transfer where natural convection is negligible, the total diffusivity is the sum of two diffusion processes operating in parallel. One is molecular diffusion in the fluid phase, and the other is a diffusion process arising from turbulent mixing in the bed interstices, known as eddy diffusion.

Equation (1) has been integrated (*2*) for the case of mass diffusion from a point source into a flowing stream of infinite extent:

$$\frac{C}{C_A} = \frac{(V/E_o^*)}{4Z}R^2 \cdot \exp\frac{-(V/E_o^*)}{4Z}r^2 \tag{2}$$

This solution includes a simplification possible when $Z>5R$.

The problem of heat transfer in packed beds is complicated by the existence of transfer mechanisms other than those of diffusion and by the fact that heat is also transferred through the confining walls of the bed. The first difficulty can be circumvented by defining a total diffusivity, usually expressed as a total or effective thermal conductivity, which includes the rates of heat transfer due to molecular conduction, radiation, particle-to-fluid transfer, and natural convection, in addition to eddy conduction. Under these conditions Equation (1) becomes

$$\frac{\partial t}{\partial z} = \frac{k_e}{G_o C_p}\left(\frac{\partial^2 t}{\partial r^2} + \frac{1}{r}\cdot\frac{\partial t}{\partial r} + \frac{\partial^2 t}{\partial z^2}\right) \tag{3}$$

The term $k_e(\partial^2 t/\partial z^2)$ represents the heat transferred by diffusion in the direction of flow. Except at very low velocities this quantity is small compared with that carried by mass flow of the fluid and can be neglected. Thus

$$\frac{\partial t}{\partial z} = \frac{k_e}{G_o C_p}\left(\frac{\partial^2 t}{\partial r^2} + \frac{1}{r}\cdot\frac{\partial t}{\partial r}\right) \tag{4}$$

Radial temperature traverses have shown the existence of very steep temperature gradients next to the wall when heat is being transferred through the wall. This indicates an added resistance to heat transfer at the wall and has given rise to the concept of a wall heat transfer coefficient for a packed bed. Coberly and Marshall defined this coefficient as

TABLE 1.—PHYSICAL PROPERTIES OF GLASS SPHERES

Nominal diameter, in.	Average diameter, ft.	Absolute density, lb. mass/cu. ft.	Thermal conductivity, B.t.u./(hr.)(sq. ft.)(°F./ft.)	D_p/D_t
1/2	0.0437	151.6	0.60	0.065
3/4	0.0596	151.6	0.60	0.088

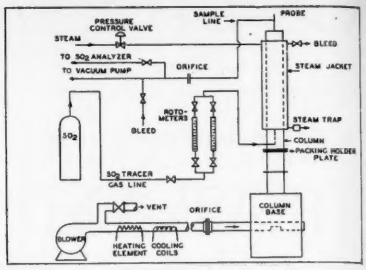

FIG. 1. FLOW DIAGRAM OF EXPERIMENTAL EQUIPMENT.

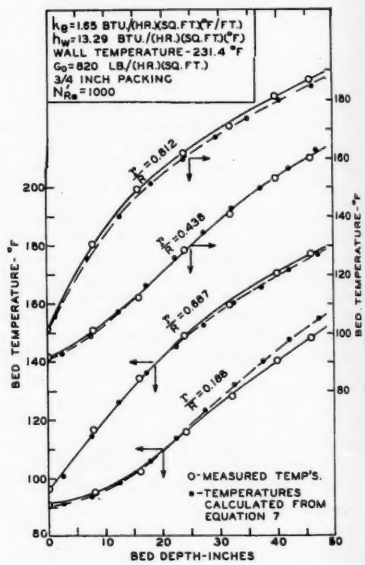

FIG. 2. COMPARISON OF MEASURED TEMPERATURE GRADIENTS WITH THOSE CALCULATED FROM EQUATION (7).

$$-k_e\left(\frac{\partial t}{\partial r}\right)_{r=R} = h_w\,(t_w - t_R) \tag{5}$$

EXPERIMENTAL EQUIPMENT

Eddy mass diffusion measurements were made by injecting a small stream of a foreign gas into the center of the fluid stream at the base of the packing and measuring the resulting concentration profiles at a given bed depth. Heat transfer measurements were made in a steam-heated, fixed-bed heat exchanger. Radial-temperature profiles were measured at several bed depths for a given flow rate by means of a high-velocity thermocouple probe placed immediately above the packing. Air was used as the main stream fluid, and sulfur dioxide as the tracer gas.

A schematic diagram of the experimental equipment is shown in Figure 1. The column was constructed from a 66-in. length of standard 8-in., Schedule-20, steel pipe, with a bolt

TABLE 2.—EFFECT OF BED DEPTH ON WALL HEAT TRANSFER COEFFICIENT

N_{Re}: 1,000
G_o'': 820 lb./(hr.) (sq. ft.)
Wall temperature: 231.4° F.
¾ in. spherical packing

Incremental bed depth, in.	h_w
0–8	11.95
8–16	14.00
16–24	13.00
24–32	13.25
32–40	14.52
40–46	11.72
Over-all	13.29

flange welded to its lower end. This was jacketed with a 4-ft. section of 12-in. pipe, starting at a point 12 in. above the column flange. The lower unjacketed portion constituted an entrance section which allowed the fluid to establish a flow pattern before entering the measuring section. Eleven equally spaced No. 24 copper-constantan thermocouples were installed in the jacketed portion of the tube wall for measuring the tube-wall temperature. Steam was admitted into the jacket through its upper jacket flange, and condensate was withdrawn through the lower jacket flange. Steam pressure in the jacket was controlled by a Fisher diaphragm controlled valve, type 57T, and an associated pilot unit. In all cases the pressure was controlled at 8 lb./sq. in. gauge.

The base of the column was a 55-gal. steel drum which had a 12-in. section of 8-in. pipe welded in the center of the top and was pierced across the midsection by the air-inlet line. To aid in emptying the column, the base was joined to the column through an easily removable 12-in. section of similar pipe bolted in place. The packing was supported by a removable grid bolted to the column flange.

Air was supplied from a 10-hp. Roots-Connorsville cycloidal blower, rated at 200 std.cu.ft./min., with a back pressure of 7 lb./sq. in. gauge. Standard 2-in. steel pipe served as the air line. The air to the column passed over an internal electrical heating coil and then over copper cooling coils to permit accurate temperature control. Metering was accomplished by means of a set of orifice flanges fitted with interchangeable orifice plates.

A modified high-velocity thermocouple probe was used to make temperature measurements. This consisted of seventeen 3/32-in. I.D. copper tubes 3 in. long; all were mounted in a header on 1/2-in. centers except the two extreme tubes, which were mounted on 3/8-in. centers. This permitted temperature measurements to within 3/16-in. of the wall. Each copper tube contained a 24-gauge copper-constantan thermocouple, the bead of which was kept from contacting the tube by means of a short length of ceramic tubing. When the probe was in operation, air was drawn through the tubes at a velocity equal to that of the air in the bed to minimize mixing effects due to drawing in air at too high a rate. The air in the tube was accelerated in the vicinity of the thermocouple bead by the constriction formed by the bead and ceramic tube. A Leeds and Northrup portable precision potentiometer was used to measure thermocouple electromotive forces.

Sulfur dioxide of 99.9% purity, was used as the tracer gas in mass diffusion runs. It was piped from the cylinder to a 1/4-in. stainless steel needle valve and then through one of two rotameters to the injection tube, an L-shape piece of 1/8-in. galvanized pipe passing through the column wall 3 in. above the flange and opening into the center of the column on a level with the lower steam-jacket flange, which constituted the beginning of the measuring section.

The mass-diffusion sampling probe consisted of nine sampling tubes, one aligned along the central axis of the column and the others spaced 3/4, 1 1/2, 2 1/4, and 3 in., respectively, from the center along one radius and 1 1/8, 1 7/8, 2 5/8, and 3 3/16 in., respectively, from the center tube along the other radius. The upper ends of the sampling tubes were connected by means of copper tubing to a bank of 1/4-in. gate valves, all of which were connected to a common sampling line. Concentrations of sulfur dioxide in the air were measured by means of a Thomas Autometer (*7, 18*).

PROCEDURE

Two sets of data were taken in the mass transfer part of the work: one with the bed at a uniform temperature and the other with a temperature gradient impressed across the bed.

For isothermal runs the bed was first packed to the desired depth and the sampling probe lowered into position. The blower was started, the barometer and air-temperature thermometer were read, and the air rate was adjusted to the proper value. Sulfur dioxide was admitted into the column at the base of the measuring section through the injection tube at a velocity just slightly less than the average linear velocity of the air in the bed interstices. The valve of the desired sampling tube was opened and the sample-line vacuum system and sulfur dioxide analyzer turned on. When steady state conditions were reached, the sulfur dioxide concentration was obtained from the Thomas Autometer. A different sampling tube was then connected in the line and the procedure repeated.

When runs were made with a temperature gradient across the bed, an identical procedure was followed except that before the tracer gas was admitted to the column the steam was turned on and the equipment allowed to attain a thermal steady state. The tracer gas was then turned on and the run proceeded as before.

For heat transfer measurements, the blower was started and the air flow adjusted to the approximate rate by means of a bleed valve. Steam was turned on and the pressure in the steam jacket adjusted to 8 lb./sq. in. gauge. The column was packed until the top of the packing was coincident with the lower steam-jacket flange. The air-line temperature was adjusted to 85°F. by means of heating and cooling coils, the barometer read, and the air rate adjusted to the exact value. The thermocouple probe was then lowered into the column until the tubes were at the level of the packing but not touching it. The vacuum system was started, and flow in the vacuum line adjusted to the proper rate. After steady state was achieved, the thermocouple readings were recorded. The probe was turned through an angle of 45° and another set of thermocouple readings taken. This was repeated twice more, giving eight readings at each radial distance, which were averaged arithmetically to give the reading at that position.

Readings were taken of the eleven thermocouples embedded in the tube wall. The probe was then removed and additional packing added. The same general sequence of operations was followed at each packing depth until the desired quantity of packing had been added.

CALCULATIONS

Mass Transfer. To apply Equation (2) to concentration-profile measurements, the equation can be written in the following form

$$\ln \frac{C}{C_A} = \frac{-(V/E_o)^*}{4Z} r^2 + \ln \frac{(V/E_o)^*}{4Z} R^2 \qquad (2A)$$

This equation is linear in $\ln(C/C_A)$ and r^2, and a plot of $\ln(C/C_A)$ vs. r^2 gives a straight line with a slope of $\frac{-(V/E_o{}^*)}{4Z}$ and an intercept of $\ln \frac{(V/E_o{}^*)}{4Z} R^2$. The value $V/E_o{}^*$

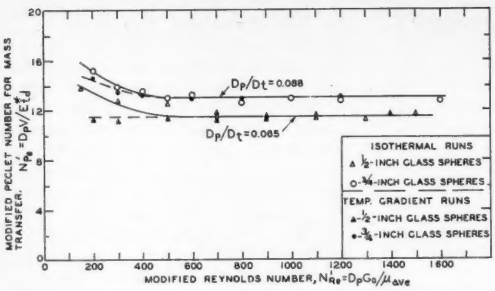

FIG. 3. CORRELATION OF MASS DIFFUSION DATA.

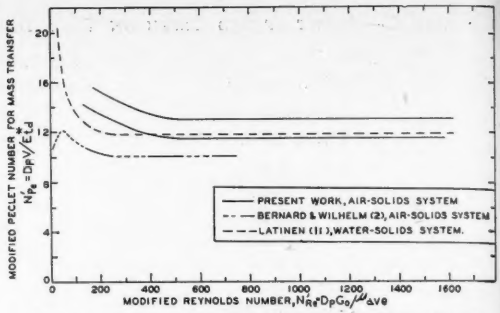
MODIFIED PECLET NUMBER FOR MASS TRANSFER, $N'_{Pe}=D_pV/E_{td}$
MODIFIED REYNOLDS NUMBER, $N_{Re}=D_pG_o/\mu_{ave}$
PRESENT WORK, AIR-SOLIDS SYSTEM
BERNARD & WILHELM (2), AIR-SOLIDS SYSTEM
LATINEN (11), WATER-SOLIDS SYSTEM.

FIG. 4. COMPARISON OF ISOTHERMAL-EDDY MASS DIFFUSION DATA.

can be calculated from either quantity. Using the intercept, however, requires taking the antilogarithm of an experimentally determined value, a procedure that magnifies small errors. More consistent results were obtained by using the slope, which can be evaluated from Equation (2A) by least squares as

$$\frac{-(V/E_o^*)}{4Z} = \frac{\Sigma r^2 \Sigma \ln(C/C_A) - a \Sigma r^2 \ln(C/C_A)}{(\Sigma r^2)^2 - a \Sigma r^4} \quad (6)$$

where a is the number of readings included in the summation.

Equations (2A) and (6) apply only to diffusion in the central core of the tube, that is, to concentration profiles in which the ratio of the maximum concentration to the concentration at the wall is 6:1 or more. Solutions for more complex cases have been presented by Bernard and Wilhelm (*2*), and Klinkenberg *et al.* (*10*).

Heat Transfer — Effective Thermal Conductivity. The values of k_e were determined by trial-and-error numerical solutions of Equation (4). If the substitution $\Gamma = \ln r$ is made, Equation (4) becomes

$$\Delta_z t = \frac{k_e}{G_o C_p} \cdot \frac{\Delta z}{(\Delta r)^2} \Delta_\Gamma{}^2 t \quad (7)$$

where $\Delta_z t$ refers to an increment of temperature in the longitudinal direction and $\Delta_r t$ represents a temperature increment in the radial direction. This equation can be solved by methods outlined in Sherwood and Reed (*16*), subject to the following boundary conditions:

1. At $z = 0$, $t = t_{inlet}$ for all values of r. It was not necessary to assume a uniform inlet temperature, as the inlet temperature distribution was measured.

TABLE 3.—EDDY MASS DIFFUSION DATA

Isothermal bed temperature: 90° F.
$D_{m_{90°F.}}$: 0.464 sq. ft./hr.

Average nonisothermal bed temperature: 140° F.
$D_{m_{140°F.}}$: 0.524 ft./hr.

Void fraction: 0.385

Modified Reynolds number, D_pG_o/μ_{avg}	Eddy mass diffusivity E_{td}^*, sq. ft./hr.	Modified Peclet number, D_pV/E_{td}^*
	1/2-in. packing—isothermal bed	
150	18.51	13.75
300	38.97	12.74
500	66.46	12.45
700	101.12	11.45
700	100.41	11.53
900	130.14	11.44
1,100	161.57	11.29
1,300	192.42	11.18
1,500	213.10	11.65
	1/2-in. packing—nonisothermal bed	
200	32.16	11.22
300	49.10	11.03
500	79.61	11.33
700	113.37	11.14
900	149.29	10.88
900	144.61	11.23
1,100	172.84	11.48
1,400	216.70	11.66
	3/4-in. packing—isothermal bed	
200	21.80	15.18
300	35.89	13.83
400	48.80	13.56
500	64.10	12.90
600	74.90	13.25
800	105.32	12.57
1,000	127.37	12.99
1,200	155.47	12.77
1,600	207.62	12.75
	3/4-in. packing—nonisothermal bed	
200	24.65	14.64
300	40.01	13.53
400	54.96	13.13
600	83.43	12.98
800	112.02	12.89
1,200	165.31	13.10

2. At $r = R$, for all values of z

$$\left(\frac{\Delta t}{\Delta \Gamma}\right)_{r=R} = \frac{(t_w - t_R)}{\frac{k_e}{h_w R}}$$

3. At $r = 0$, for all values of z

$$\left(\frac{\Delta t}{\Delta \Gamma}\right)_{r=0} = 0$$

This method presupposes a knowledge of the wall heat transfer coefficient, which can be calculated by the methods outlined below.

A value of k_e was assumed and a family of radial-temperature-gradient curves constructed by application of Equation (7), each curve being displaced from the previous one by the amount Δz. These were compared with the measured curves and the whole procedure repeated until a value of k_e was found that gave best agreement between calculated and measured temperature gradient curves. A typical plot of this type is shown in Figure 2.

Wall Heat Transfer Coefficient. Wall heat transfer coefficients were calculated by a heat balance for the column. If a uniform velocity distribution over the bed and constant fluid properties are assumed, the equation is

$$G_o (\pi R^2) C_p (t_{go} - t_{gi}) =$$

$$h_w (2\pi RZ) (t_w - t_R)_{mean} \quad (8)$$

The average inlet and outlet gas temperatures were calculated from measured temperature profiles by the equation

$$\frac{t_{avg}}{460 + t_{avg}} = \frac{2}{R^2} \int_0^R \frac{tr}{460 + t} \cdot dr \quad (9)$$

The quantity t_R, which represents the temperature at the inner boundary of the wall film, was estimated by extrapolating the measured temperature profiles to the wall. The mean temperature difference $(t_w - t_R)$ was determined by plotting $(t_w - t_R)$ at each bed depth against the bed depth and the average ordinate found by graphical integration.

MASS TRANSFER DATA

Eddy mass diffusivities were correlated in terms of modified Peclet numbers, $D_p V/E^*_{td}$, and modified Reynolds numbers, $D_p G_o/\mu$, which are symbolized as N'_{Pe} and N'_{Re}, respectively. This plot is presented in Figure 3 and all eddy mass diffusion data are given in Table 3.

From Figure 3 it would appear that the modified Peclet number is also a function of the ratio D_p/D_t. This, however, is probably due to dissimilar packing orientation. At $D_p/D_t = 0.088$, values of the Peclet numbers obtained after successive bed repackings were as much as 15% below the curve shown and agreed quite well with the lower curve. This behavior would be expected since it is not possible to reproduce accurately the orientation of packing even though the void fraction can be reproduced well. If the bed were repacked a sufficient number of times, it is probable that the upper curve would be brought closer to the lower curve. In order to discern the effect of a temperature gradient, all data shown for a given packing size were made without repacking the bed.

The curves for the different packing sizes are similar in shape and show two distinct regions. At modified Reynolds numbers above about 500 the Peclet number is constant, indicating that the eddy diffusivity is directly proportional to the fluid velocity and particle diameter. Such behavior is characteristic of fully developed turbulence and agrees well with the "random walk" analysis of Baron and Latinen.

At Reynolds numbers below 500, fully developed turbulence for mixing no longer exists and the N'_{Pe} varies with the fluid velocity. The same type of behavior was observed by Bernard and Wilhelm and by Latinen (Figure 4).

The broken line of Figure 3 represents eddy-mass-diffusion measurements made in the presence of a temperature gradient. In the region of fully developed turbulence a temperature gradient appears to make no difference. At low Reynolds numbers, however, there is a difference although the effect is much more pronounced in the case of the smaller packing. This effect might be caused by mixing due to localized natural convection currents even though the over-all conditions are not conducive to natural convection currents involving large masses of fluid. Unfortunately, the data are not sufficient to permit any general conclusions, but they show the need for further study in this area.

The eddy-mass-diffusion data of Bernard and Wilhelm (*2*) and of Latinen (*11*) are shown in Figure 4 along with the present work. The data of Latinen were obtained in a 2-in. column packed with glass spheres with water as the main stream fluid. The values of D_p/D_t ranged from 0.02 to 0.16. Bernard and Wilhelm made eddy-mass-diffusion measurements for 3/8-in. alumina spheres in an 8-in. tube $(D_p/D_t = 0.047)$, with air as the fluid. The agreement of all the data is fairly good, particularly in view of the wide divergence in properties of the systems investigated.

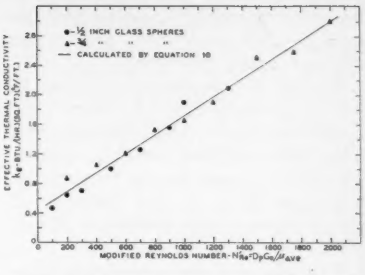

FIG. 5. CORRELATION OF EFFECTIVE THERMAL CONDUCTIVITIES.

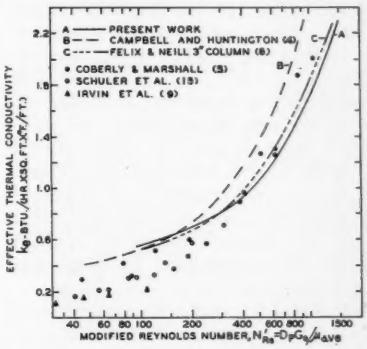
A —— PRESENT WORK
B — — CAMPBELL AND HUNTINGTON (4)
C - - - - FELIX & NEILL 3" COLUMN (8)
COBERLY & MARSHALL (5)
SCHULER ET AL. (15)
IRVIN ET AL. (9)
EFFECTIVE THERMAL CONDUCTIVITY
MODIFIED REYNOLDS NUMBER

FIG. 6. COMPARISON OF EFFECTIVE THERMAL CONDUCTIVITY DATA.

HEAT TRANSFER DATA

Effective thermal conductivity values were correlated by the equation

$$k_e = 0.439 + 0.00129 (D_p G_o/\mu_{avg}) \quad (10)$$

Figure 5 is a plot of this correlation. The average deviation of the experimental points from this line is 9.4%. All effective thermal conductivity values are summarized in Table 4.

The term μ_{avg} is the molecular viscosity of the fluid at the average bed temperature. Since the vis-

cosity varied by less than 15% it was not possible to segregate the effect of this variable, and so an average value was used.

One of the assumptions made in deriving Equation (4) was that k_e did not vary with radial position. This was checked, and in almost all cases k_e was found to vary by less than 10% up to a distance of about one particle diameter of the wall.

The effective thermal conductivities are compared in Figure 6 with the data of other investigators. The abscissa is plotted on a logarithmic scale to afford a better distribution at low Reynolds numbers, where much of the comparative data lies. Curve *A* is a plot of Equation (10) of this work. The solid points represent the data of Coberly and Marshall(*5*) for 1/8- by 1/8-, 1/4- by 1/4-, and 3/8- by 1/2-in. Celite cylinders in a 5-in. tube. Curve *C* represents the correlation obtained by Felix and Neill (*6*) for glass spheres in a 3-in. tube. The agreement in each case is quite good.

Campbell and Huntington(*4*) measured effective thermal conductivities for both cylinders and spheres of several sizes and materials in 2-, 4-, and 6-in. tubes, using both air and natural gas as the flowing fluid. Curve *B* is a plot of their final correlation when air was the fluid. They obtained k_e values by graphically differentiating temperature-profile curves at several points along the axis of the bed and taking an average. Since these values were obtained in the region of minimum packing nonuniformities, they might be expected to be somewhat larger than k_e values averaged for the entire bed. They also found k_e to be directly proportional to the molecular thermal conductivity of the fluid.

The data obtained by Schuler *et al.*(*15*) and by Irvin *et al.*(*9*) for 1/8-, 3/16-, and 1/4-in. cylindrical alumina pellets packed in a 2-in. tube fall somewhat below the other results. As mentioned before, they accounted for wall effects by decreasing k_e in the vicinity of the wall. The points of Figure 6 represent effective thermal conductivity values averaged for the whole bed. As these incorporate the wall resistance in this instance, they would be expected to be less than k_e values free of wall effects.

To compare Peclet numbers for heat and mass transfer in a packed bed, eddy thermal conductivity values (k_{td}) must be known. Since eddy diffusion results from turbulence generated in the packing interstices by the fluid flowing around the packing, the rate of transfer attributable to this mechanism would be zero at zero rate of flow, and k_{td} would also be zero. If the $k_e = N'_{Re}$ curve is extrapolated to $N'_{Re} = 0$, the intercept value of 0.439 in Equation (10) can be regarded as the approximate sum of the rates of heat transfer due to molecular conduction, radiation, possible localized natural convection, and particle-to-fluid heat transfer. This value is in reasonable agreement with the value of 0.31 reported by Campbell and Huntington and the value of 0.365 of Felix and Neill. k_{td} values can be estimated from k_e values by the equation

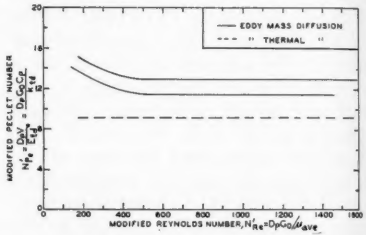

FIG. 7. COMPARISON OF PECLET NUMBERS FOR HEAT AND MASS TRANSFER.

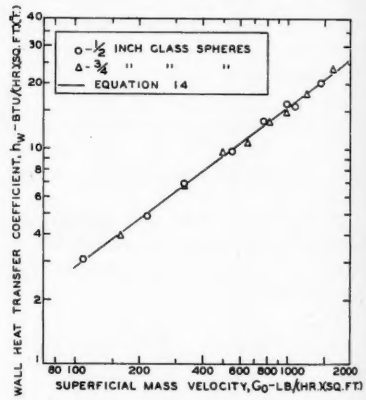

FIG. 8. CORRELATION OF WALL HEAT TRANSFER COEFFICIENTS.

$$k_{td} = k_e - 0.439 \qquad (11)$$

The modified Peclet number for heat transfer is

$$N'_{Pe_h} = \frac{D_p G_o C_p}{k_{td}} \qquad (12)$$

Substituting Equations (10) and (11) into (12) yields

$$N'_{Pe_h} = \frac{C_p \mu_{avg}}{0.00129} \qquad (13)$$

A plot of modified Peclet numbers for heat and mass transfer is

TABLE 4.—EFFECTIVE THERMAL CONDUCTIVITY AND WALL HEAT TRANSFER COEFFICIENT DATA

Average bed temperature : 150° F.

μ_{avg} $_{(150°F.)}$: 0.0488 lb./(hr.) (ft.)

Superficial mass velocity, G_o, lb./(hr.) (sq. ft.)	Modified Reynolds number, D_pG_o/μ_{avg}	Effective thermal conductivity, k_e, B.t.u./(hr.) (sq. ft.) (° F./ft.)	Wall heat transfer coefficient, h_w, B.t.u./(hr.) (sq. ft.)(°F.)
	1/2-in. packing		
109	98	0.47	3.05
218	195	0.65	4.83
327	293	0.70	6.92
545	488	1.00	9.73
764	684	1.26	13.58
982	879	1.56	16.10
1,092	978	1.90	15.74
1,420	1,272	2.09	20.10
	3/4-in. packing		
164	200	0.87	3.95
328	400	1.05	6.80
491	600	1.20	9.59
655	800	1.53	10.56
820	1,000	1.65	13.29
983	1,200	1.90	14.70
1,228	1,500	2.50	17.92
1,433	1,750	2.58	19.68
1,638	2,000	3.00	23.30

shown in Figure 7. The modified Peclet numbers for heat transfer calculated by this method are about 25% below those for mass transfer. This is not unexpected since this method of calculating modified Peclet numbers for heat transfer is based on the assumption that the rate of heat transfer due to all mechanisms except eddy diffusion is constant. It is probable that this value is not constant but increases slightly with the Reynolds number. If the assumption is made that the value is a small linear function of the Reynolds number, the agreement between Peclet numbers for heat and mass transfer would be even better.

WALL HEAT TRANSFER COEFFICIENT

Wall heat transfer coefficients were measured over a range of Reynolds numbers from 98 to 2,000. The data are given in Table 4, and the final correlation is shown in Figure 8. The equation of this curve is

$$h_w = 0.090\, G_o^{0.75} \qquad (14)$$

The average deviation of the experimental points from this line is 3.1%.

The effect of bed depth on the wall heat transfer coefficient was investigated by calculating h_w values for different incremental bed depths. The results of a typical run are given in Table 2. No trend with bed depth is apparent; instead, a constant wall heat transfer coefficient is indicated. The scattering in values may be attributed largely to the fact that for a shallow section of bed a small error in calculating the average inlet or outlet air temperature is magnified in the temperature-difference term of the heat balance and greatly affects the local wall heat transfer coefficient. When an over-all heat balance is used, however, the effect of an error of this type is considerably lessened. All h_w values were calculated from over-all heat balances.

Equation (14) shows the wall heat transfer coefficient to be proportional to the 0.75 power of the superficial mass velocity. In turbulent flow in an open channel the heat transfer coefficient is proportional to $G_o^{0.8}$. The similarity in velocity dependence is rather surprising in view of the difference in the two systems and suggests a possible similarity in flow conditions and velocity gradients near the wall.

A sphere contacts the wall at only one point, and the area of contact is small. Furthermore the portions of the spheres adjacent to the wall present little form drag to the flow of fluid along the wall. This type of arrangement would present a minimum of disturbance to the fluid flowing along the wall and would tend to promote channeling. With channeling, flow in this area would not be unlike flow in an annulus, and a similar velocity dependence of h_w might be expected.

ACKNOWLEDGMENT

The authors wish to express their appreciation to Thomas Baron and William E. Ranz for many helpful suggestions during the course of this investigation.

NOTATION

C = concentration of diffusing material, lb./cu.ft.

C_A = mixed average effluent concentration of diffusing material, lb./cu. ft.

C_p = fluid heat capacity at constant pressure, B.t.u./(lb.) (°F.)

D_m = molecular diffusivity, sq.ft./hr.

D_p = packing-particle diameter, ft.

D_t = inside diameter of containing tube, ft.

E^*_o = total diffusivity based on void area, sq.ft./hr.

E^*_{td} = eddy diffusivity based on void area, sq.ft./hr.

f = factor representing concentration of diffusing material for mass transfer and temperature in heat transfer

G_o = superficial mass velocity based on empty tube area, lb./(hr.) (sq.ft.)

h_w = wall heat transfer coefficient B.t.u./(hr.) (sq.ft.) (°F.)

k_e = effective thermal conductivity of bed based on void plus non-void area, B.t.u./(hr.) (sq.ft.) (°F./ft.)

k_{td} = eddy conductivity of the fluid phase due to turbulent mixing, B.t.u./(hr.) (sq.ft.) (°F./ft.)

N'_{Pe} = modified Peclet number for mass transfer, D_pV/E^*_{td}

N'_{Pe_h} = modified Peclet number for heat transfer, $D_pG_oC_p/k_{td}$

N'_{Re} = modified Reynolds number, D_pG_o/μ_{avg}

R = radius of containing tube, ft.

r = radial coordinate in cylindrical coordinates

t = temperature, °F.

t_{gi} = average inlet air temperature, °F.

t_{go} = average outlet air temperature, °F.

t_R = fluid temperature at inner boundary of wall film, °F.

V = local velocity in longitudinal direction, ft./hr.

Z = packing depth, ft.

z = longitudinal or axial coordinate in cylindrical coordinates

Greek Symbols

ε = void fraction

ρ = density of fluid, lb./cu.ft.

$\Gamma = \ln r$

μ_{avg} = molecular viscosity of fluid at average bed temperature, lb./(ft.) (hr.)

LITERATURE CITED

1. Baron, T., *Chem. Eng. Progr.*, 48, 118 (1952).
2. Bernard, R. A., and R. H. Wilhelm, *Chem. Eng. Progr.*, 46, 233 (1950).
3. Bunnell, D. G., H. B. Irvin, R. W. Olson, and J. M. Smith, *Ind. Eng. Chem.*, 41, 1977 (1949).
4. Campbell, J. M., and R. L. Huntington, *Petroleum Refiner*, Part I, 30, 127 (1951); Part II, 31, 123 (1952).
5. Coberly, C. A., and W. R. Marshall, Jr., *Chem. Eng. Progr.*, 47, 141 (1951).
6. Felix, J. R., and W. K. Neill, Preprints of Heat Transfer Symposium, Atlantic City, p. 125, Am. Inst. Chem. Engrs. (December, 1951).
7. Gerhard, E. R., Ph.D. thesis, Univ. Illinois (1953).
8. Hougen, J. O., and E. L. Piret, *Chem. Eng. Progr.*, 47, 295 (1951).
9. Irvin, H. B., R. W. Olson, and J. M. Smith, *Chem. Eng. Progr.*, 47, 287, (1951).
10. Klinkenberg, A., H. J. Krajenbrink, and H. A. Lauwerier, *Ind. Eng. Chem.*, 45, 1202 (1953).
11. Latinen, G. A., Ph.D. Dissertation, Princeton University (December, 1951).
12. Leva, M., *Ind. Eng. Chem.*, 39, 857 (1947).
13. Leva, M., and M. Grummer, *Ind. Chem.*, 40, 415 (1948).
14. Leva, M., M. Weintraub, M. Grummer, and E. L. Clark, *Ind. Eng. Chem.*, 40, 747 (1948).
15. Schuler, R. W., V. P. Stallings, and J. M. Smith, *Chem. Eng. Progr. Symposium Ser.* No. 4, 48, 19 (1952).
16. Sherwood, T. K., and C. E. Reed, "Applied Mathematics in Chemical Engineering," McGraw-Hill Book Company, Inc., New York (1939).
17. Singer, E., and R. H. Wilhelm, *Chem. Eng. Progr.*, 46, 343 (1950).
18. Thomas, M. D., J. O. Ivie, and C. T. Fitt, *Ind. Eng. Chem., Anal. Ed.*, 18, 383 (1946).

PERFORMANCE OF VANED-DISK ATOMIZERS

W. M. HERRING, JR., and W. R. MARSHALL, JR.
University of Wisconsin, Madison, Wisconsin

The problem of producing sprays of liquid droplets by atomization is finding increasing importance in chemical engineering processes. This is especially true for the process of spray drying, wherein one important method of producing sprays is by means of spinning disks. These atomizers produce liquid breakup by centrifugally accelerating a liquid to high velocity as it discharges from the disk periphery.

Spinning-, or centrifugal-disk, atomizers are built in a variety of designs, the simplest being a flat, smooth disk. More complicated designs may include concentric sets of vanes, two or three plates or cups separated by perforated bands, etc. Pictures and drawings of various types may be found in references *2* and *10*.

Although many designs of disk atomizers have been proposed for spray-drying applications, quantitative information on the performance characteristics of even the simplest type of atomizer is lacking. This paper is a report of an investigation of the performance characteristics of disk atomizers of the straight, radial-vaned type. The purpose of the investigation was to determine how the weight and drop-size distributions of water sprays were influenced by the diameter, speed, vane dimensions and number of the disk and by feed rate. High-speed photography was used in an effort to study the mechanism of atomization.

W. M. Herring, Jr., is at present with Standard Oil Co. (Indiana), Whiting, Indiana.

PREVIOUS WORK

Weight Distribution. Some quantitative data on the weight distributions or trajectories of sprays from vaned-disk atomizers have been reported by Adler and Marshall(*2*) and Friedman et al.(*10*). The data of Adler and Marshall were in the form of complete weight distributions, sampling being done in a plane 3 ft. below the plane of the disk. Friedman et al. reported their data in terms of the distance to which 50% of the spray was thrown before dropping 10 in. Adler and Marshall found that at low feed rates and peripheral speeds the spray was thrown farther as either feed rate or peripheral speed was increased. At higher values of the variables the spray was affected only slightly by feed rate but decreased in distance thrown with increasing peripheral speed. Friedman et al. reported that the distance to which 50% of the spray was thrown increased continuously with both peripheral speed and feed rate over the range of variables studied.

Drop-Size Distribution. Limited data on drop-size distribution for vaned disks were reported by Adler and Marshall(*2*) and by Friedman et al. (*10*). Wallman and Blyth(*18*) reported drop-size data on spray-dried sodium silicate obtained from a pilot plant spray dryer with vaned-disk atomizers.

Adler and Marshall presented drop-size-distribution data for sprays of water from (1) smooth disks, (2) one straight, radial-vaned disk, and (3) several curved-vane disks at one feed rate and disk speed. The drop-size data appeared to plot linearly on arithmetic normal probability paper. No significant differences in the drop-size distributions among these disks were observed.

Friedman et al. studying the effects of disk speed, feed rate, disk diameter, and liquid properties on drop-size distribution found that drop size decreased as disk speed increased, but increased as feed rate increased. They did not definitely establish the effect of disk diameter on drop size. Their results were correlated in terms of the Sauter mean drop diameter as a function of the operating and liquid variables in dimensionless groups as follows:

$$\frac{\bar{x}_{vs}}{r} = 0.4 \left(\frac{\Gamma}{Nr^2}\right)^{0.6} \left(\frac{\mu}{\Gamma}\right)^{0.2} \left(\frac{\sigma\rho L}{\Gamma^2}\right)^{0.1} \qquad (1)$$

where $\bar{x}_{vs}$ is the Sauter mean diameter. The uniformity of the sprays obtained was reported in terms of the

so-called Hatch dispersion coefficient defined as the ratio of x_{50} to $x_{15.87}$ where x_{50} is the mass or volume median diameter, and $x_{15.87}$ is the diameter which includes 15.87% of the mass or volume of the spray, and $x_{50} > x_{15.87}$. The Hatch dispersion coefficient, α, was correlated with $\bar{x}_{vs}$ as follows:

$$\alpha = 3.3\,(\bar{x}_{vs})^{0.1} \qquad (2)$$

This is based on only a twofold range of α. Friedman et al. also proposed a correlation for the maximum drop size, which had the same form as Equation (1) except that the coefficient 0.4 was replaced by 1.2; i.e., the maximum drop size was suggested to be three times the Sauter mean diameter.

Wallman and Blyth (*18*) studied the atomization from smooth and vaned disks by determining the particle-size distribution of spray-dried sodium silicate atomized with disk atomizers. They found particle size to decrease as centrifugal force was increased and proposed that centrifugal force, rather than peripheral speed, was the factor governing particle size. However, no correlation of drop-size distributions was proposed.

Mechanism of Atomization. The manner in which sprays are formed from a bulk of liquid has been the subject of numerous reports in the literature. The greatest amount of work on the mechanism of atomization has been done in connection with pressure nozzles (*4* to *9, 12, 13, 16*).

Since discussions of the mechanism of atomization by disks have been reviewed adequately by various investigators (*2, 3, 10, 11, 14,* and *19*), this subject will not be reviewed again here; however, the essential conclusions are presented below.

THEORETICAL CONSIDERATIONS

The practice of atomization by spinning disks is well ahead of both theory and the results of experimental studies. Theoretical predictions of drop-size distributions require a knowledge of the atomization mechanism involved. It is generally believed that three distinct factors influence the mechanism of atomization by spinning disks. Two of these involve liquid properties, and the third involves interaction with the atmosphere surrounding the atomizer.

One mechanism for spinning-disk atomization postulates that the liquid, by wetting the surface of the disk, is held to the disk by adhesion tension and flows to the disk periphery to form a torus (on smooth disks) which, because of the surface tension of the liquid, resists disintegration. Centrifugal force acting on the torus is opposed by the surface-tension force. When the centrifugal force becomes great enough (owing to either increased liquid mass or increased speed) to overcome the liquid-surface-tension force, liquid drops are torn from the torus and thrown from the disk periphery. As the liquid-feed rate increases, this mechanism goes through the regimes of direct drop formation, ligament formation, and finally film formation.

A second mechanism postulates that liquid traveling at a high velocity over the disk and along the vanes develops turbulence. At the disk periphery the liquid is discharged at high velocity and at the same time is released from the confinement of the vanes. The internal stresses in the liquid stream caused by the velocity fluctuations and turbulence produce disintegration of the liquid stream.

A third possible mechanism is that a high relative velocity between the liquid and the atmosphere creates friction, which contributes to the disintegration of the liquid.

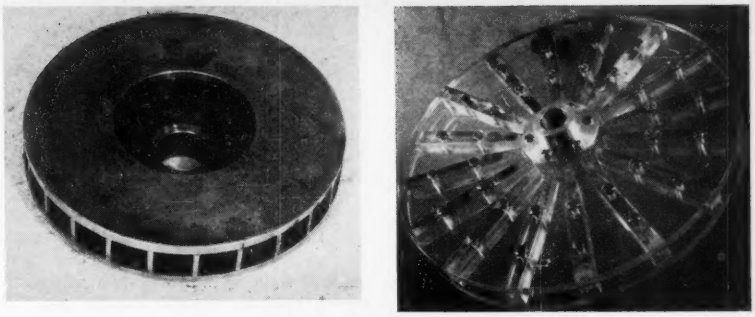

a *b*

FIG. 1. VANED DISKS: (*a*) TYPICAL VANED-DISK USED IN STUDY; (*b*) LUCITE EXPERIMENTAL VANED DISK.

Although each of these mechanisms for atomization from spinning disks is possible, in the usual industrial range of operating conditions breakup probably is due to a combination of the mechanisms. It is also probable that the controlling mechanism may change with a change in the operating conditions.

In view of the complexities involved in predicting theoretically the performance characteristics of vaned-disk atomizers, this study was restricted to an empirical correlation of weight distributions and drop-size distributions as functions of operating and disk variables. The correlations were interpreted in the light of the foregoing suggested mechanisms.

EXPERIMENTAL EQUIPMENT AND PROCEDURES

Atomization Equipment. The twelve experimental disks used in this investigation were of a simple straight-vaned design as shown in Figure 1. The ranges of disk variables were as follows: (1) diameter, 2 to 8 in.; (2) number of vanes, 8 to 24; (3) vane height, 0.22 to 1.28 in.; and (4) vane length, 0.38 to 2.5 in. Table 1 gives the dimensions of all the disks studied.

TABLE 1.—DIMENSIONS OF EXPERIMENTAL DISKS

Disk	Diameter, in.	Vane Height, in.	Vane Length, in.	Number of vanes
V-1	3.75	0.375	0.375	24
V-2	5.0	0.375	1.00	24
V-3	8.0	0.312	2.50	24
V-4	5.0	0.656	1.00	24
V-5	5.0	1.281	1.00	24
V-6	8.0	0.375	2.50	24
V-7	5.0	0.375	0.625	24
V-8	5.0	0.375	1.625	24
V-9	5.0	0.375	1.00	20
V-10	5.0	0.375	1.00	16
V-11	5.0	0.375	1.00	8
V-12	2.0	0.219	0.50	24

The experimental disks were mounted on a vertical, belt-driven shaft, Figure 2, driven by a 3 hp., 3,450 rev./min. motor. Disk speed was varied by changing the ratios of the motor and disk pulley diameters. Disk speeds ranged between 700 and 10,000 rev./min. and were measured with a Strobotac.

The feed rate ranged from 5 to 60 lb./min. The water was fed uniformly to the disk through an annular distributor, the thickness of the annular ring being 1/32 in.

The atomization equipment was located in one corner of a 12- by 16-ft. room. All sampling was done in the sector-shaped area indicated in Figure 3.

Disk V-12 was operated at speeds of from 10,000 to 35,000 rev./min. by an air turbine mounted on a frame, as shown in Figure 4, and surrounded by a barricade. The capacity of this unit was less than 1 lb./min. of water.

Weight Distribution Determinations. The weight-sampling unit consisted of a sheet metal pan in the form of an 18° section taken from a circle of 10-ft. radius. The pan was divided into compartments by arcs at radial intervals of 1 ft., each compartment being provided with a drain. The pan was mounted horizontally 3 ft. below the disk with the apex of the section plumb with the disk shaft.

Weight-distribution data were obtained by collecting and measuring the amount of spray which entered each compartment during a timed interval. The total volume of liquid atomized during this time was obtained from a rotameter reading. For a uniform spray distribution, one twentieth of the total volume fell in the 18° section. Hence from the total volume and the volumes of spray falling in the sampling compartments up to 10 ft., the volume of spray thrown further than 10 ft. was estimated. From these volumes the distribution of the spray weight in the horizontal plane 3 ft. below the atomizer was established.

Drop-Size-Distribution Determinations. Spray-droplet samples were obtained by collection in sample cells by the method discussed by Rupe(*15*) and used by Adler and Marshall(*2*) and Tate and Marshall(*17*). In this method spray droplets fell into a sample cell filled with a fluid in which all droplets settled to a common plane. The collected group of drops in each sample cell was photomicrographed and the images were counted and classified. The sample cells were fitted with optically flat glass bottoms to permit the use of transmitted light for photography.

The immersion fluid employed in this investigation was Stoddard solvent. In order to obtain completely opaque images for photography, the water was dyed black with 3% nigrosine dye. The dyed water had essentially the same physical properties as water, except for a slightly lower surface tension.

The drop samples for a particular spray were obtained by positioning ten sample cells in the horizontal plane where the spray-weight distribution was determined. From data on the previously determined weight distribution for the spray, the sample cells were positioned in the center of areas each of which included 10% by weight of the spray. Thus the sample cells were positioned at radii which included 5,15,25 . . . 95 wt. % of the spray.

The sample cells were exposed to the spray by remote control. Each cell was enclosed in a narrow, shallow box with a sliding, slotted top which acted as a shutter. The operator, on a cat-walk above the spray, exposed the cell to the spray by pulling the shutter top with a fine string.

After the ten sample cells had been exposed, they were removed to be photographed. Ten photomicrographs at 35× were taken of each sample cell without duplication of area. The photomicrographs, on 5 by 7 film, generally averaged about 100 drops/negative, although as many as 1,500 or as few as 25 drops/negative were obtained in some instances, depending on the size and concentration of the drops in the cell.

The drop images on the negatives were counted and classified according to size by means of the scanning-type drop counter developed at the University of Wisconsin(*1*). With the aid of this counter the photomicrographs were analyzed at the rate of 150/day, and for this investigation, a total of 5,200 photomicrographs were scanned and 572,000 drops counted.

CALCULATION AND CORRELATION PROCEDURES

Weight Distribution. One hundred and seventeen weight-distribution experiments were made by the procedure described above. From each of these runs the cumulative volume, or weight percentages, of spray falling within radial increments of 1 ft. were established. These cumulative percentages were then plotted as the weight distribution for that run. Typical plots of this type may be observed in Figure 18 of reference *2*.

The variables influencing weight distribution were disk speed (1,500 to 9,800 rev./min.), feed rate (10 to 50 lb./min.), and the disk dimensions listed in Table 1. It was desired to correlate the data to show how these variables influenced the cumulative weight percentage of spray falling within any given spray radius, R.

It was decided that the most useful type of generalized weight-distribution correlation would be a cumulative distribution plot on either arithmetic- or log-probability coordinates with the nonprobability coordinate involving a grouping of the spray radius and variables, and the probability coordinate representing the cumulative weight percentage of spray included within the radial distance from the disk.

This correlation was made for the entire weight distribution obtained for each experimental run. The general procedure for correlating each variable was to plot values of spray radius, R, at cumulative percentages of 20, 40, 60, and 80 as a function of the particular variable under study. From such plots, R as a function of each variable was obtained, and these functional relations are shown in Figure 5*a* and *b*.

Drop-Size Distribution. The data from each drop-size-distribution run consisted of the number of drops counted in each of twenty equal-size classes (of 30 μ each) for each of ten samples taken from the spray produced during the run (*see* Table 6 of reference *10*a). The total number of drops at each sample point averaged 1,100 or the total counted in a run was about 11,000.

The attempt was made to present the drop-size data by an overall distribution which was representative of the entire spray from which the samples were taken.

Drop-size-distribution data may be based on the number, volume, or surface area of the drops in a spray, each basis being useful for a different purpose. It was felt that volume representation would probably be most useful, and hence the drop-size distribution on a volume basis was calculated for each of the ten droplet samples. Since the samples were representative of equal volume fractions of the spray, combination of the ten individual volume distributions into an overall distribution for the entire spray was merely a matter of averaging the individual sample distributions.

The variables to be correlated with drop-size distribution were disk speed (3,000 to 9,800 rev./min.), feed rate (20 to 50 lb./min.), and disk dimensions (Table 1). The method of correlation used differed from the usual method of correlating drop-size data in terms of a mean drop size and a standard deviation or dispersion coefficient [cf., Equation (1) and (2)]; rather, a generalized correlation for all points on the distribution curves was attempted. Thus the

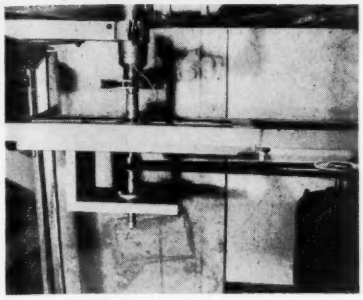

FIG. 2. ANNULAR FEEDING DEVICE: DISK IN POSITION, MOTOR, AND BELT DRIVE.

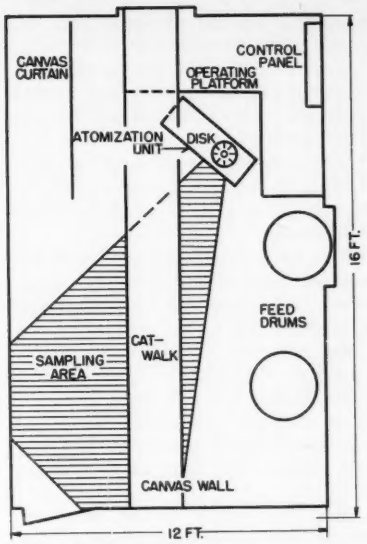

FIG. 3. LAYOUT OF EXPERIMENTAL AREA.

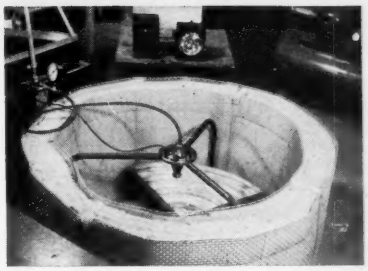

FIG. 4. AIR-DRIVEN 2-IN.-DIAM. DISK IN BARRICADE.

effects of the pertinent variables on the drop diameter, x, at cumulative volume percentages of 20, 40, 60, and 80 were correlated and then grouped to form a general correlation (Figure 11*a* and *b*).

All the drop-size distributions were found to plot very nearly as straight lines on square root–normal probability coordinates. This type of distribution was first reported by Tate and Marshall (*17*) for pressure nozzles. Distinct curvature was observed for plots on either arithmetic- or log-normal probability coordinates.

EXPERIMENTAL RESULTS

Weight Distribution. The correlation of weight-distribution data showed that the weight distribution of sprays from vaned disks, expressed as R, the radial distance of travel of the spray, was related to the pertinent variables as follows:

For disk speed, N, in the range of 1,500 to 9,800 rev./min., $R \sim N^{-0.16}$

For feed rates, w, in the ranges of 10 to 50 lb./min., $R \sim w^{0.25}$

For disk diameters, D, from 3.75 to 8 in., $R \sim D^{0.21}$

For vane heights, b, from 0.376 to 1.28 in., $R \sim b^{-0.12}$

Increasing the number of vanes from 8 to 24 showed no significant variation of spray trajectory.

A variation of vane length from 0.375 to 1.63 in. revealed no definite trend in the weight-distribution data.

On the basis of the foregoing relationships, a generalized graphical correlation involving disk speed, N, feed rate, w, and disk diameter, D, was developed by plotting the group $RN^{0.16}D^{-0.21}w^{-0.25}$ vs. the cumulative weight or volume percentage of the spray included in R on normal probability paper. This correlation is shown in Figure 5*a* and *b*. The data fell around a straight line having the constants $(RN^{0.16}D^{-0.21}w^{-0.25})_m = 7.7 =$ median value, $\sigma_w = 2.3 =$ standard deviation.

Figure 5*a* and *b* is based upon the following units for the ordinate values: $R =$ ft., $N =$ rev./min., $D =$ in., $w =$ lb./min.

Drop-Size Distribution. The drop-size-distribution data were obtained from fifty-two experimental

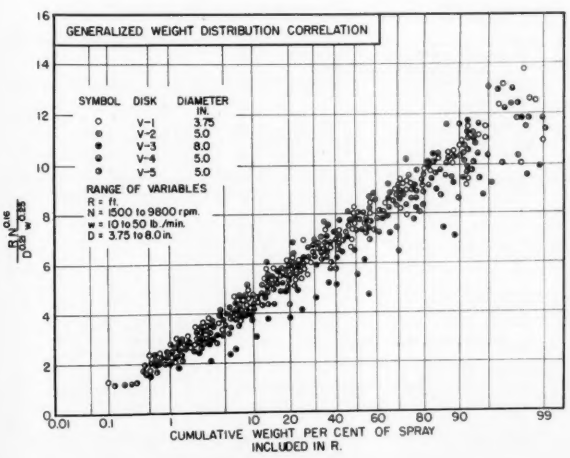

FIG. 5*a*.

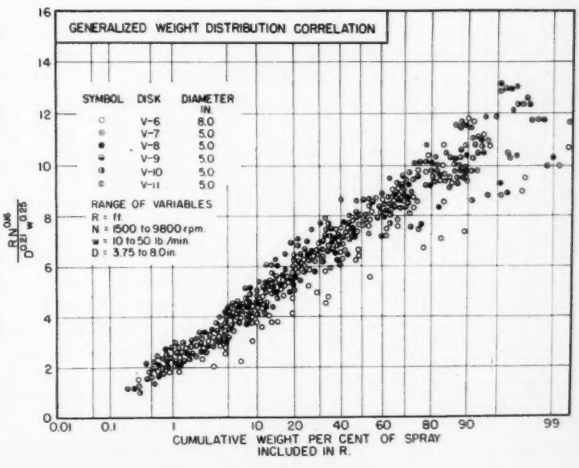

FIG. 5*b*.

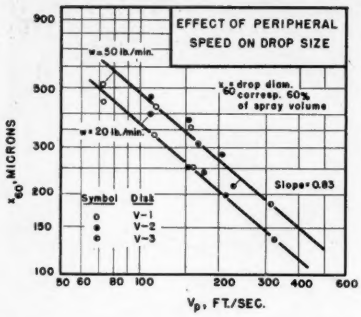

FIG. 6. TYPICAL PLOT OF EFFECT OF DISK PERIPHERAL SPEED ON DROP SIZE CORRESPONDING TO 60 CUMULATIVE PER CENT.

runs wherein about 572,000 drops were measured and counted. Analysis of the data showed that the variables affected the drop-size distribution of sprays produced by vaned disks as follows:

For a disk-speed range of 3,000 to 9,800 rev./min. drop size varied inversely with disk speed to the 0.82 power.

For disk diameters ranging from 3.75 to 8 in., drop size varied inversely with disk diameter to the 0.85 power.

The fact that disk speed and diameter had essentially the same effect on drop-size distributions suggested that the distributions were influenced by the peripheral speed of the disks. Figure 6 is a typical plot for two feed rates of drop size vs. peripheral speed for the peripheral-speed range of 50 to 300 ft./sec. The slope of the curves is –0.83.

For feed rates in the range of 20 to 50 lb./min., the drop size varied with feed rate to the 0.24 power. Figure 7 shows typical curves of the variation of drop size with feed rate. Drop diameters which include 20, 40, 60, and 80% by volume of the spray multiplied by $N^{0.82}$ are plotted vs. feed rate for three vaned disks of different diameters.

A variation of vane height from 0.375 to 1.28 in. showed that drop size varied with vane height to the –0.12 power.

Increasing the number of vanes from 8 to 20 showed that drop size varied with vane number to the –0.15 power.

Since vane height and number had essentially the same effect, it seemed reasonable to conclude that the drop-size distributions were probably influenced by the total wetted periphery for liquid discharge from the disk; however, the data on this effect scattered so much that a significant correlation cannot be proposed at this time. Therefore, the inclusion of wetted periphery in the general correlation of drop size must be regarded

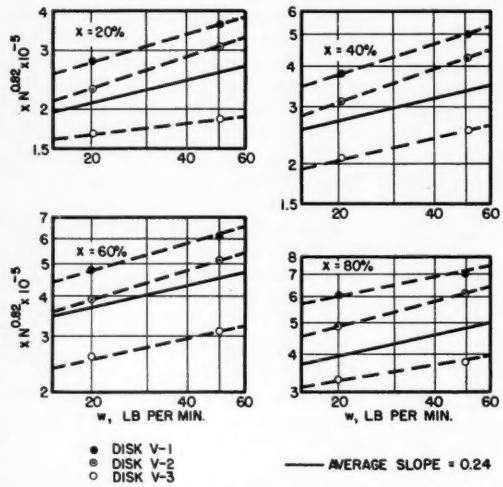

FIG. 7. TYPICAL PLOT OF EFFECT OF FEED RATE ON DROP SIZE AT VARIOUS CUMULATIVE PERCENTAGES.

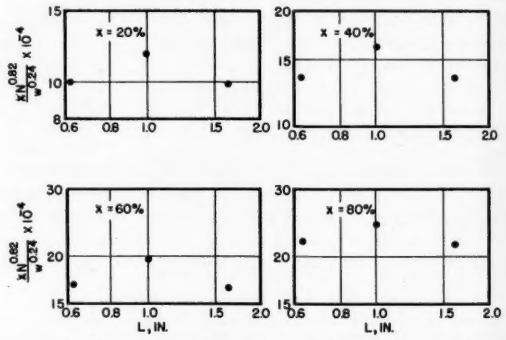

FIG. 8. EXAMPLE OF INCONCLUSIVE EFFECT OF VANE LENGTH ON DROP SIZE AT VARIOUS CUMULATIVE PERCENTAGES.

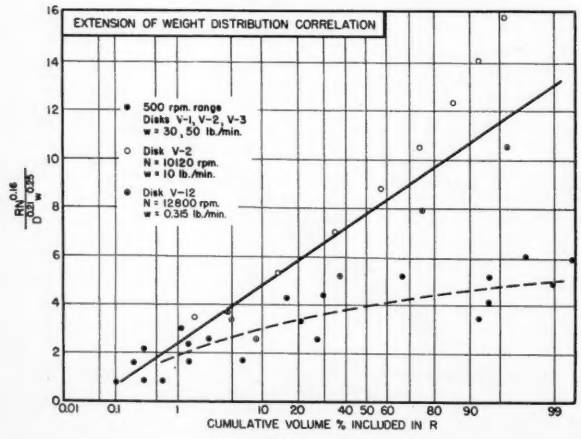

FIG. 9.

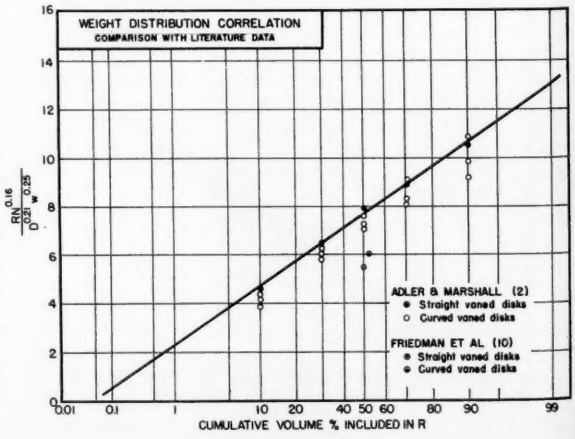

FIG. 10.

as tentative, but apparently, the effect is small.

Figure 8 shows typical plots of all the data on the effect of vane length on the drop size for a range of vane lengths from 0.376 to 1.63 in. The effect is inconclusive. Additional data involving a wider variation in vane length should be considered before a quantitative statement can be made concerning the effect of this variable on drop size.

The dimensional group of variables involving feed rate, w; peripheral speed, ND; and superficial total wetted periphery for liquid discharge, $L_p = nb$, was combined with drop diameter, x, to give the ordinate for a generalized drop-size-distribution correlation as follows:

$$y = x\,(ND)^{0.83}\,(nb)^{0.12}/w^{0.24} \quad (3)$$

The experimental data were combined into the dimensional group given by this equation and plotted on square root–normal probability coordinates as shown in Figure 11*a* and *b*. The data fell on a path about a straight line having constants

$$\left[x\,(ND)^{0.83}\,(nb)^{0.12}\,w^{-0.24}\right]_{m} = 92.5 \times 10^{2}$$

$$\sigma_v = 49.0 \times 10^{2}$$

where m refers to the median value.

The scale of the ordinate and the values of the constants for the straight line are based upon the following units for the variables: x = microns, ND = in./min., nb = in., w = lb./min.

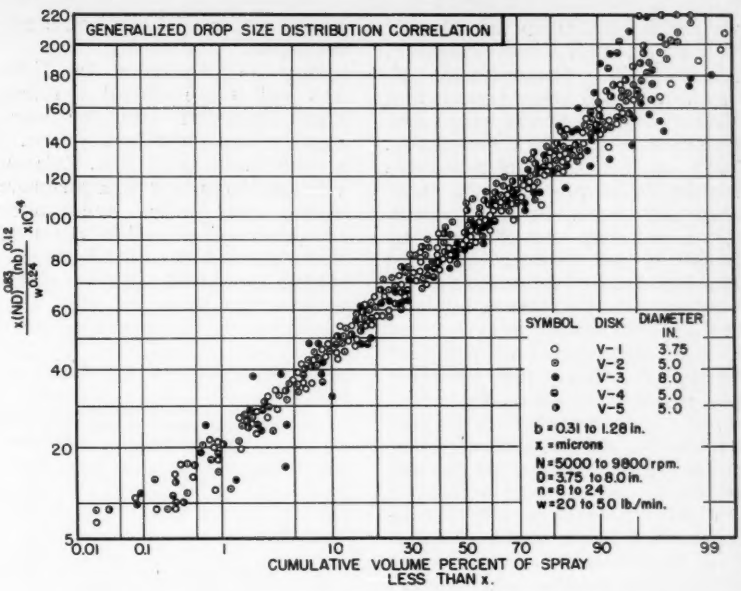
GENERALIZED DROP SIZE DISTRIBUTION CORRELATION
$\frac{x(ND)^{0.83}(nb)^{0.12}}{w^{0.24}} \times 10^{-4}$
SYMBOL DISK DIAMETER IN.
V-1 3.75
V-2 5.0
V-3 8.0
V-4 5.0
V-5 5.0
b = 0.31 to 1.28 in.
x = microns
N = 5000 to 9800 rpm.
D = 3.75 to 8.0 in.
n = 8 to 24
w = 20 to 50 lb./min.
CUMULATIVE VOLUME PERCENT OF SPRAY LESS THAN x.

FIG. 11*a*.

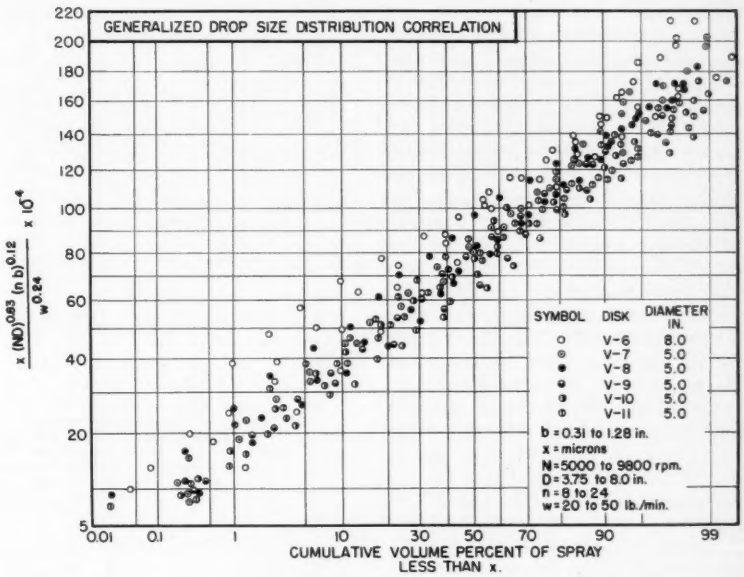
GENERALIZED DROP SIZE DISTRIBUTION CORRELATION
$\frac{x(ND)^{0.83}(nb)^{0.12}}{w^{0.24}} \times 10^{-4}$
SYMBOL DISK DIAMETER IN.
V-6 8.0
V-7 5.0
V-8 5.0
V-9 5.0
V-10 5.0
V-11 5.0
b = 0.31 to 1.28 in.
x = microns
N = 5000 to 9800 rpm.
D = 3.75 to 8.0 in.
n = 8 to 24
w = 20 to 50 lb./min.
CUMULATIVE VOLUME PERCENT OF SPRAY LESS THAN x.

FIG. 11*b*.

DISCUSSION OF RESULTS

Weight Distribution. The generalized weight-distribution correlation (shown in Figure 5*a* and *b*) indicates how disk speed, feed rate, and disk diameter influence weight distribution or spray trajectory. The correlation is valid only in the ranges of the variables studied in this investigation. Data obtained for disk speeds as low as 500 rev./min. did not follow the correlation, as Figure 10 shows. This was due to the fact that the liquid did not atomize completely and tended to pour off the disk in continuous streams. Limited data for a 2-in.-diam. disk (V-12) rotating at about 13,000 rev./min. and fed at a rate of about 0.3 lb./min. also failed to agree with the correlation (Figure 9). However, the latter condition of fine atomization made collection of the spray very difficult.

The trajectory data of Adler and Marshall (*2*) and Friedman et al. (*10*) for straight- and curved-vaned disks were plotted in terms of the generalized correlation in Figure 11. The data of the former authors for the straight-vaned disk were fitted well by the correlation; the data for the curved-vaned disks were slightly low. The fact that Friedman et al. did their weight-distribution sampling in a plane 10 in. below the atomizer instead of 36 in., as in this study, may account in part for their data for the straight-vaned disk falling below the correlation of this study.

In the investigation by Friedman et al. of the influence of variables on weight distribution, it was found that spray trajectory varied directly with disk speed, feed rate, and disk diameter all to the 0.25 power. While their results agreed with the results of this study insofar as the effects of feed rate and disk diameter are concerned, there

was no agreement on the effect of disk speed. There is no apparent reason for this disagreement. Offhand, it would seem logical that higher disk speeds also act to produce smaller drops, or a finer spray. Since small drops decelerate more rapidly than large ones, the spray trajectory should not increase with speed, but may even decrease, as found in this investigation (See also Figure 17 of reference 2).

Because air currents and objects in the spray chamber were observed to cause billowing of the spray-air mass, it is believed that the absolute values of spray trajectory which can be predicted by the generalized weight-distribution correlation may be unique for the experimental setup used in this investigation. However, the correlation should prove useful in other disk-atomization setups using straight-vaned disks for prediction of how an established weight distribution should be influenced by disk speed, feed rate, and disk diameter.

One application of the weight-distribution correlation is the prediction of the required diameter of a spray tower to perform a given operation such as spray drying. In this connection, it is evident that the correlation of Figure 5*a* and *b* is conservative; i.e., presumably the spray from a disk in a spray dryer will not travel outward as far as this correlation would predict. This is true for two reasons: (1) the drops are undergoing drying with a reduction in density which reduces their distance of travel, and (2) downward air currents in the dryer would disturb the spray trajectory. As a conservative estimate, however, it is possible to write, on the basis of the correlation in Figure 5*a* and *b*, the following empirical expression for the radial distance to which 99% of the spray will travel:

$$R_{99} = \frac{12\,D^{0.21}\,w^{0.25}}{N^{0.16}} \qquad (4)$$

R_{99} is the radial distance in feet, which includes 99% of the mass of the spray.

A comparison of this equation with an existing installation is of interest. A spray dryer atomizing 80 lb./min. from an 8-in. disk operating at 10,000 rev./min. is performing satisfactorily in a 20-ft.-diam. chamber. These data substituted in Equation (4) predict a radius, R_{99}, of about 12.5 ft. or a 25-ft.-diam. chamber confirming the conclusion that Equation (4) is conservative for spray-dryer-diameter estimates.

Drop-Size Distribution. In Figure 11*a* and *b* are plotted the drop-size-distribution data for eleven experimental disks in the form of a generalized correlation. This correlation shows how disk peripheral speed, feed rate, and wetted periphery of the disk vanes affect the drop-size distributions of sprays produced by vaned-disk atomizers.

Extension of the correlation to higher disk speeds, lower feed rates and smaller disks was indicated as feasible from drop-size data on a 2-in.-diam. disk (V-12) at feed rates of less than 1 lb./min. and at speeds up to 32,500 rev./min. This is shown in Figure 12, where the drop-size data for these conditions have been plotted to compare with the general correlation of Figure 11*a* and *b*.

This generalized correlation can

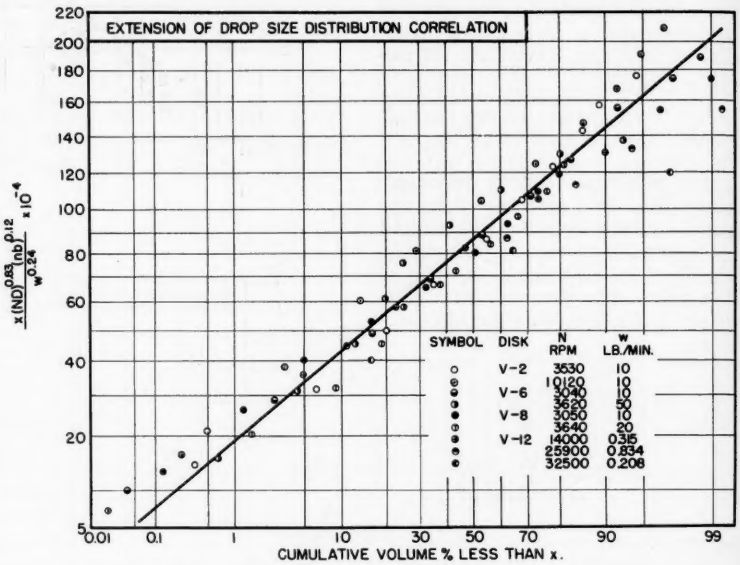

FIG. 12. EXTENSION OF DROP-SIZE CORRELATION TO HIGHER DISK SPEEDS.

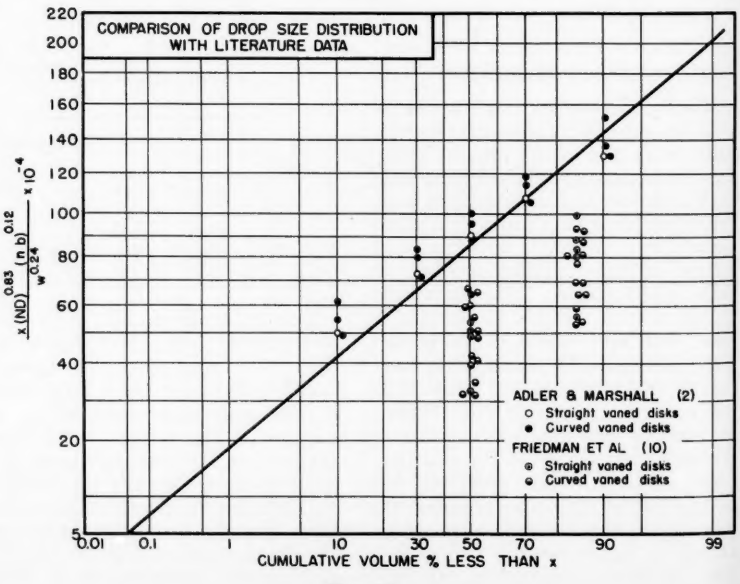
COMPARISON OF DROP SIZE DISTRIBUTION WITH LITERATURE DATA
$\frac{x\,(ND)^{0.83}\,(nb)^{0.12}}{w^{0.24}} \times 10^{-4}$
ADLER & MARSHALL (2)
Straight vaned disks
Curved vaned disks
FRIEDMAN ET AL (10)
Straight vaned disks
Curved vaned disks
CUMULATIVE VOLUME % LESS THAN x

FIG. 13.

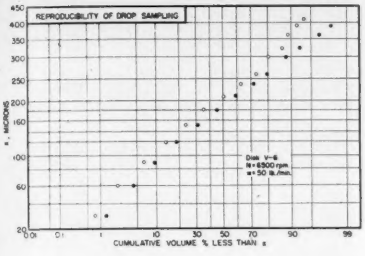

FIG. 14.

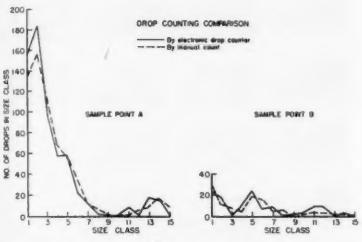

FIG. 15. COMPARISON BETWEEN DROP COUNTER AND MANUAL COUNTS.

be used within the experimental range to predict within 25% or better the drop-size distributions of sprays produced by straight-vaned disks. The correlation can also be used to determine trends in spray uniformity. The reciprocal of the difference between the drop diameter which included 84.12 volume % of the spray and that which included 50.0 volume % is a measure of spray uniformity. In terms of variables studied, uniformity may be expressed as

$$\delta = 2.04 \times 10^{-4} (\pi ND)^{0.83} (L_p)^{0.12} / w^{0.24} \qquad (5)$$

This relation shows that spray uniformity increases as peripheral speed increases, as total wetted periphery for discharge increases, and as feed rate decreases. These effects are all confirmed by experience.

Drop-size-distribution data for vaned-disk atomizers reported in the literature are meager. Only the data of Adler and Marshall (*2*) and Friedman et al. (*10*) were available for comparison with the generalized correlation. In order to determine the applicability of the correlation to the literature data, they were put in the form required by the dimensional group of Equation (3) and plotted in Figure 13.

The data supplied by Adler and Marshall for both straight- and curved-vaned disks compared well with the correlation; however, the data of Friedman et al. fell below the correlation of this study. This disagreement might be due to a number of causes, e.g., differences in drop-sampling procedures, differences in total numbers of drops counted, etc. It was believed that sufficient drops were counted in this study to ensure reliable trends of the data. Further, reproducibility of the data appeared acceptable, as Figure 14 indicates. Another factor lending confidence to the data of this study was the removal of the human error from the drop counting. The drop counter used and described in reference *1* gave consistently more reliable results than manual counting. This was checked many times. A typical comparison between a reliable manual count and the drop-counter count is shown in Figure 15.

The investigation of Friedman et al. (*10*) indicated that the effect of disk speed on drop size was in the same direction as found in this work, but to a smaller degree [cf. Equation (1)]. They reported that average drop size varied inversely with disk speed to the 0.6 power. They agreed as to direction and order of magnitude of feed rate, finding drop size to increase directly with feed rate to the 0.2 power. Because of insufficient data, they tentatively proposed that drop size varied inversely with disk diameter to the –0.2, a much smaller variation than found in this study.

In order to utilize better the drop-size-distribution correlation given in Figure 11*a* and *b*, perfomance charts (Figures 16 and 17) were prepared to show how the drop-size distribution varied with peripheral speed in one case and with feed rate in another. Figure 16 shows the drop-size distribution (volume basis) on a log-probability plot for disk peripheral speeds ranging from 50 to 300 ft./sec. These lines show how spray uniformity improves with disk speed. If plotted on square root–probability paper, the lines would be straight. A correction-factor curve for feed rate is given in the insert graph. A similar plot showing the variation of distribution with feed rate is given in Figure 17. Here a correction-factor curve for peripheral speed is included. The correction for wetted periphery is small but can be tentatively included for both charts on the basis that the drop size varies with $(nb)^{-0.12}$.

Atomization Mechanism. High-speed still and motion pictures were taken

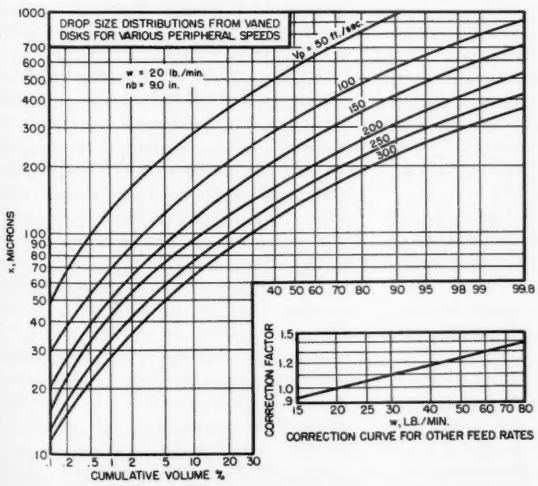
DROP SIZE DISTRIBUTIONS FROM VANED DISKS FOR VARIOUS PERIPHERAL SPEEDS
w = 20 lb./min.
nb = 9.0 in.
x, MICRONS
CUMULATIVE VOLUME %
CORRECTION FACTOR
w, LB./MIN.
CORRECTION CURVE FOR OTHER FEED RATES

FIG. 16. PERFORMANCE CHART FOR ESTIMATING THE EFFECT OF PERIPHERAL SPEED ON DROP-SIZE DISTRIBUTION FROM VANED DISKS.

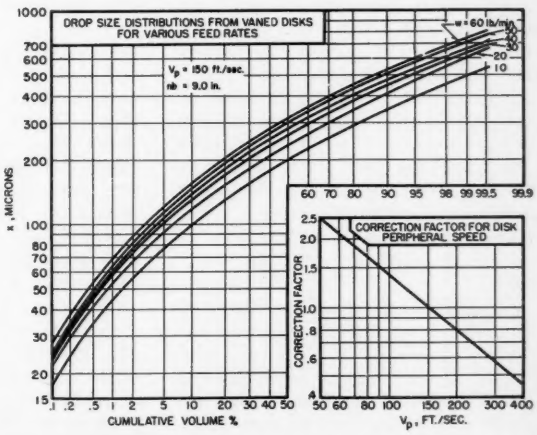
DROP SIZE DISTRIBUTIONS FROM VANED DISKS FOR VARIOUS FEED RATES
nb = 9.0 in.
x, MICRONS
CUMULATIVE VOLUME %
CORRECTION FACTOR FOR DISK PERIPHERAL SPEED
CORRECTION FACTOR
Vp, FT./SEC.

FIG. 17. PERFORMANCE CHART FOR ESTIMATING THE EFFECT OF FEED RATE ON DROP-SIZE DISTRIBUTION.

FIG. 18. HIGH-SPEED MOTION PICTURE FRAMES SHOWING COARSE LIGAMENTS FORMED AT LOW DISK SPEED; $N = 640$ REV./MIN., $w = 30$ LB./MIN.

of the atomization action at the periphery of the vaned disks in an attempt to determine what mechanisms were influencing the spray formation. Because the action above 1,500 rev./min. was too rapid to be stopped by the high-speed motion picture camera, the motion pictures were confined to shots of the disks operating at speeds of 700 and 1,500 rev./min. However, high-speed still pictures were taken of the disks operating at 5,000 rev./min.

The atomization action appeared to change as disk speed was increased from 700 to 5,000 rev./min. At the low disk speeds liquid issued from the disk in heavy streams from each vane. Part of the liquid seemed to flow along the lower disk plate as well as along the surface of the vanes. The liquid discharged from each vane retained its stream-shaped identity for some distance beyond the disk, where it then broke up. The breakup occurred as the end of the stream spread out into a sheet which flapped like a flag. Heavy ligaments extended from this sheet and also trailed from the main stream between the sheeted end and the disk periphery. From the ligaments and from the sheet itself, irregular globs and drops of varied sizes were formed as shown in the high-speed movie frames of Figure 18.

At disk speeds of 1,500 rev./min., the liquid streams issuing from the disk vanes appeared to be thinner than those at lower speeds. Liquid flow along the lower disk plate was less noticeable. The end of the discharged stream was formed into a thinner, filmlike sheet from which

FIG. 19. HIGH-SPEED MOTION PICTURE FRAMES SHOWING FILM FORMATION FOLLOWED BY LIGAMENT FORMATION AND COLLAPSE; $N = 1{,}500$ REV./MIN., $w = 30$ LB./MIN.

ligaments were torn. At several intervals between the sheeted end of the stream and the disk periphery, eruptions occurred in the stream with the resultant formation of thin-walled, balloonlike films. These balloons were laced with heavier ribs of liquid and grew until they seemed to burst to form drops, as shown in the sequence of high-speed movie frames in Figure 19 and the high-speed still in Figure 20*a*.

High-speed still photographs of atomization at disk speeds of 5,000 rev./min. showed that, instead of solid streams of liquid emerging from disk vanes, the liquid appeared to disintegrate from a film almost as soon as it was discharged (Figure 20*b*). The liquid flowed along the vertical surface of the vanes and appeared to touch the surface of the lower disk plate only to the extent of the width of the film. Disintegration appeared to be the result of the collapse of short ligaments extending from the films. No formation of globs of liquid from the films was observed.

High-speed photography at a fixed disk speed showed that an increase in feed rate resulted in larger, less filmlike streams of

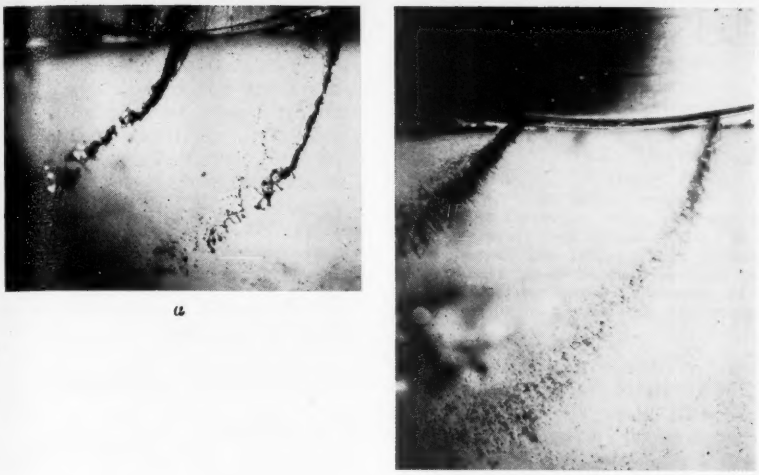

a *b*

FIG. 20. HIGH-SPEED PHOTOGRAPHS OF VANED DISKS ATOMIZING DYED WATER.

liquid being discharged from each vane. The disintegration of such streams appeared to produce more globs of liquid and larger drops. An increase in vane height resulted in thinner, more filmlike streams of liquid being discharged from each vane. Such streams disintegrated to produce fewer large masses of liquid and smaller drops.

Analysis of the high-speed photographs indicated that the atomization mechanism was to a large extent governed by liquid velocity, increases in which resulted in finer atomization. It was also observed that the quantity of liquid discharged per unit length of discharge periphery influenced atomization. The smaller the quantity of liquid, the finer the atomization. On the basis of these two observations, it is believed that the liquid disintegration was largely the result of turbulence of the high-velocity liquid stream as it left the vanes. In this respect, the mechanism is similar to pressure-nozzle atomization. The friction created by the relative velocity of the liquid stream with the surrounding air probably had some effect on the breakup, but not a major one.

The atomization mechanism for liquid disintegration from vaned-disk atomizers is reflected in the generalized drop-size-distribution correlation, which stipulates that finer, more uniform sprays are produced by an increase in peripheral speed, i.e., increased liquid velocity, and by increased wetted periphery or by decreased feed rate, both factors contributing to the formation of thinner films of liquid.

ACKNOWLEDGMENT

The authors wish to express their appreciation to the many individuals who have taken an interest in this research project. Special acknowledgement is due to Professor R. J. Parent and Dr. W. H. Darnell for their invaluable assistance in maintaining the operation of the electronic drop counter; to the University of Wisconsin Numerical Analysis Laboratory for assistance in IBM calculations of drop-size distributions; to Professor Freeman Brown, Director of the University of Wisconsin Photographic Laboratory, and W. R. Thomas for their work with the high-speed motion picture camera and for their cooperation in processing the thousands of negatives of drop images. Appreciation is also expressed to the Wisconsin Alumni Research Foundation, General Foods Corporation, and the Engineering Experiment Station for financial support.

NOTATION

b = vane height
D = disk diameter
L_p = superficial disk wetted periphery for liquid discharge = nb
L = vane length
N = rotational speed of disk
n = number of vanes for a disk
r = disk radius
R = spray radius or trajectory
R_{99} = radial distance, including 99% of mass of spray.
V_p = disk peripheral speed, ft./sec.
w = liquid feed rate, lb./min.
x = drop diameter
x_{60} = drop diameter below which 60% of the mass of the spray lies.
x_{vs} = Sauter mean drop diameter
y = ordinate value on probability plots

Greek Letters

α = Hatch dispersion coefficient
δ = measure of uniformity
Γ = feed rate of liquid atomized based on wetted periphery, lb./(min.)(ft.)
σ = surface tension
σ_w = standard deviation for generalized weight-distribution correlation
σ_v = standard deviation for generalized drop size
μ = liquid viscosity
ρ = liquid density

Subscripts

m = median value

LITERATURE CITED

1. Adler, C. R., A. M. Mark, W. R. Marshall, Jr., and R. J. Parent, *Chem. Eng. Progr.* **50**, 14 (1954).
2. Adler, C. R., and W. R. Marshall, Jr., *Chem. Eng. Progr.*, **47**, 515, 601 (1951).
3. Bär, P., doctoral dissertation, Technical College, Karlsruhe, Germany (1935).
4. Castleman, R. A., *Natl. Advisory Comm. Aeronaut, Rept.* No. 440 (1932).
5. Castleman, R. A., *Phys. Rev.*, **35**, 1014 (1930).
6. *Ibid.*, **55**, 592 (1939).
7. Castleman, R. A., *U. S. Bur. Standards J. Res.* **6**, No. 3, 369 (1931).
8. De Juhasz, K. L., *Trans. Am. Soc. Mech. Engrs.*, **53**, 65 (1931).
9. De Juhasz, K. L., O. F. Jahn, and P. H. Schweitzer, *Penn State Coll. Eng. Expt. Sta. Ser., Bull.* No. 40 (1932).
10. Friedman, S. J., F. A. Gluckert, and W. R. Marshall, Jr., *Chem. Eng. Progr.*, **48**, 181 (1952).

10a. Herring, W. M., Jr., Ph.D. thesis, Univ. Wisconsin (1953).

11. Hinze, J. O., and H. Milborn, *J. Appl. Mechanics*, **17**, 145 (1950).
12. Lee, D. W., *Natl. Advisory Comm. Aeronaut. Eighteenth Annual Report, Rept.* No. 425, 505 (1932).
13. *Ibid.*, Rept. No. 438, 703 (1932).
14. May, K. R., *J. Appl. Phys.*, **20**, 932 (1949).
15. Rupe, J. H., "Third Symposium on Combustion" (University of Wisconsin, 1948), Williams and Wilkins Company, Baltimore (1949).
16. Schweitzer, P. H., *J. Appl. Phys.*, **8**, 513 (1937).
17. Tate, R. W., and W. R. Marshall, Jr., *Chem. Eng. Progr.*, **49**, 169, 226 (1953).
18. Wallman, H., and H. A. Blyth, *Ind. Eng. Chem.*, **43**, 1480 (1951).
19. Walton, W. H., and W. C. Prewett, *Proc. Phys. Soc.* (*London*), **62B**, Part 6, 341 (1949).

Presented at the A. I. Ch. E. St. Louis meeting

THERMODYNAMIC PROPERTIES OF 1-BUTENE

JAMES H. WEBER

University of Nebraska, Lincoln, Nebraska

The thermodynamic properties of 1-butene have been calculated over a temperature range of 32° to 480°F. and at pressures up to 1,000 lb./sq. in. abs. These properties were determined from vapor-pressure, volumetric, heat-capacity, and latent-heat of vaporization data through the application of rigorous thermodynamic relationships. The calculated data have been found to be internally consistent. The enthalpy values are believed to be accurate to within ±0.5 B.t.u./lb. and the entropy values to ±0.0005 B.t.u./(lb.)(°R.).

Thermodynamic data are available for a number of paraffinic compounds but are limited to ethylene (*16*) and propene (*10*) in the olefinic series. It is the purpose of this paper to present thermodynamic data for 1-butene, one of the C_4H_8 olefins, important as a compound resulting from the dehydrogenation of *n*-butane, a step in the manufacture of 1, 3-butadiene.

AVAILABLE DATA

Volumetric data for 1-butene have been measured by three groups of investigators. The earliest work, that of Roper (*13*), covers the temperature range of —22° to +140°F. with the upper pressure limit of 16.5 lb./sq.in. abs. These data are correlated by an equation of state in the virial form

$$PV_M = RT + \frac{\beta}{V_M} \qquad (1)$$

where β is the second viral coefficient and a function of temperature only. Roper expressed this function as

$$\beta = f + \frac{g}{T} + \frac{h}{T^2} \qquad (2)$$

where f, g, and h, are constants. A more extensive investigation of the volumetric behavior was made by Olds, Sage, and Lacey (*12*), whose investigation covered the temperature range of 100° to 340°F. at pressures up to 10,000 lb./sq.in. abs. Liquid as well as vapor volumetric data are reported, including data for the liquid at the bubble point and the vapor at the dew point.

Beattie and Marple (*8, 9*) made two investigations of the behavior of 1-butene. The initial report (*8*) gives orthobaric liquid densities from 50° to 125°C. and the critical properties. The second investigation of Beattie and Marple (*9*) reports volumetric data from 150° to 250°C. and from densities of 1 to 8 moles/liter. The results, up to densities of 4 moles/liter, were fitted to the Beattie-Bridgman equation of state, and the constants are given.

Difficulties due to the polymerization of the 1-butene are reported by Olds, Sage, and Lacey (*12*) and Beattie and Marple (*9*). The former report that their sample apparently deteriorated after several hours' exposure to a temperature of 340° F., and the latter report slow polymerization at 200°C. (392°F.) and rapid deterioration at 250°C. (482°F.) The phenomenon limits somewhat the accuracy of the results at the higher temperatures.

Since there is very little overlap in the various sets of volumetric data, comparison of the results is impossible over most of the temperature and pressure range. Some comparison can be made of the data of Olds, Sage, and Lacey (*12*) with those of Beattie and Marple (*9*), but a double interpolation is necessary. This shows good agreement between the sets of data. Also, since the Beattie-Bridgman equation of state was fitted to the data of Beattie and Marple, volumetric data may be calculated at even values of temperature and pressure and compared with those of Olds, Sage and Lacey. Again this shows good agreement between the two sets of volumetric data over the limited range for which comparison is possible. Volumetric data for the saturated liquid from 30° to 77°F. have been reported (*1*).

Several studies have been made of the vapor pressure-temperature relationship of 1-butene. Lamb and Roper (*11*) report data up to 32°F.; Olds, Sage and Lacey (*12*), data from 132.7°F. to the critical point; Beattie and Marple (*8*), data from –75° to 125°C.; and the A.P.I. Research Project 44 (*2*) from 30° to 55°F. Olds, Sage, and Lacey fitted an equation,

$$\log P\,(\text{lb./sq. in. abs.}) = 6.18466 - \frac{2285.22}{T} - 0.00054633T$$

to their results. Beattie and Marple fitted the equation

$$\log P\,(\text{atm.}) = 5.196066 - \frac{1298.1722}{T\,(^\circ\text{K.})} - 0.00124829T$$

to their data. A.P.I. 44 gives the constants for the Antoine equation for the range of data reported. As can be seen, the vapor pressure-temperature relationship has been well described. With the exception of the temperature range of 122° to 167°F. (50° to 75°C.), the data of Olds, Sage, and Lacey and of Beattie and Marple are in excellent agreement. In this temperature range, the vapor pressures determined by Olds, Sage, and Lacey are lower than those reported by Beattie and Marple by 1/2 to 1/4%. The data of Lamb and Roper and Beattie and Marple are in excellent agreement.

There is some question about the critical properties of 1-butene. Olds, Sage, and Lacey (*12*) report conditions at the critical as t_c = 297°F., P_c = 588 lb./sq.in. abs., and V_c = 3.85 cu.ft./lb. mole; Beattie and Marple (*8*) report t_c = 295.6°F. (146.4°C.), P = 583 lb./sq.in. abs. (39.7 atm.), and V_c = 3.67 cu.ft./lb. mole (0.241 liter/mole). These latter values have apparently been accepted by the A.P.I. project (*3*) and have been used for this work.

Thermal data available include isobaric heat capacities of the liquid at the bubble point, measured by Schlinger and Sage (*15*); latent heat of vaporization information at the normal boiling point, 20.73° F., and 77°F., reported by A.P.I. 44 (*4*); and heat capacities of the ideal gas at unit fugacity, reported by A.P.I. 44 (*5*). These latest listed data were used to calculate enthalpies and entropies of the ideal gas at unit fugacity up to 2,200°F. Additional constants used in the calculations were, molecular weight of 1-butene, 56.104; gas-law constant, R, 10.730 (lb./sq.in. abs.) (cu. ft./lb. mole) (°R.); ice point, 491.69°R.

METHOD OF CALCULATIONS

The specific volume of the saturated liquid over the complete range of temperatures, from the literature sources cited, were plotted against temperature on a largescale graph and values at even 10°F. increments read; these values are reported in Table 1. The specific volumes of the saturated vapor were, in the main, obtained directly from the literature references given above. At temperatures below 100°F., however, values were obtained by use of the Clapeyron equation, since accurate latent-heat-of-vaporization and vapor-pressure data were available below this temperature. The residual volumes, α's, were determined and smoothed on a plot of α vs. temperature. The specific volume data of the saturated vapor are reported in Table 1.

The specific volume data of the superheated vapor were obtained from the references cited above. The Beattie-Bridgman equation, with constants reported by Beattie and Marple(*9*), was used to determine the data above 340°F. and pressure above 500 lb./sq.in. abs. The volumetric data were smoothed with the aid of large-scale plots of α vs. temperature with pressure parameters.

A region for which data were not available lay above the 340°F. isotherm and between the 14.7 and 500 lb./sq.in. abs. isobars. To complete the data, the Berthelot equation of state was used to calculate the volumetric data below 100 lb./sq.in. abs. It was felt this could be done without error, since the equation was tested at lower temperatures than 340°F. and below 100 lb./sq.in. abs. pressure, and excellent agreement with the experimental data was obtained. A plot of α vs. pressure with temperature parameters was then drawn. The isotherms above 340°F. were completed without difficulty, for the residuals changed very little up to 500 lb./sq. in. abs. at the high temperature involved. Also, the interpolation was facilitated by use of the completed isotherm at 340°F. as a guide.

Fugacity. The fugacity of the saturated and superheated vapor was determined from the graphical integration of a plot of α at constant temperature vs. pressure or mathematically,

$$\ln \frac{f}{P} = -\frac{1}{RT} \int_0^P \alpha \, dP \qquad (3)$$

The results of this operation are reported in Tables 1 and 2. The fugacity data up to temperatures of 340°F. have been reported by Sage and Lacey(*14*); their values agree very well with those reported in this work, as may be expected, since the same set of volumetric data was used in both cases.

Selection of the Datum Plane. The enthalpy and entropy of the saturated liquid at 32°F. were arbitrarily set equal to zero. This required that the enthalpy and entropy data for 1-butene in the ideal gas state, unit fugacity, reported in A.P.I. 44(*6, 7*) be changed to the datum plane used in this work.

Latent Heat of Vaporization. With the exception of the two values given in A.P.I. 44(*4*), all the latent-heat-of-vaporization data were calculated by the Calpeyron equation,

$$\frac{dP}{dT} = \frac{\Delta H_V}{T \Delta V} \qquad (4)$$

Vapor-pressure and volumetric data were obtained from literature sources cited above.

Saturated Liquid and Vapor Phases. The heat capacity data of liquid 1-butene at its bubble point reported by Schlinger and Sage(*15*) enabled the evaluation of the enthalpy and entropy of the saturated liquid phase up to 220°F. Above this temperature these properties were determined by subtracting the enthalpy or entropy of vaporization from their respective values in the saturated vapor phase; this was necessary since there were no heat-capacity data above 220°F. The thermodynamic properties of the saturated vapor phase below 220°F. were obtained by adding the enthalpy or entropy of vaporization to their respective values in the saturated liquid phase. Above 220°F. the isobars on enthalpy-temperature and temperature-entropy plots were extrapo-

TABLE 1.—THERMODYNAMIC PROPERTIES OF SATURATED 1-BUTENE

Temperature, °F.	Pressure lb./sq. in., abs.	Fugacity pressure, f/P	Volume		Enthalpy			Entropy		
			Liquid, cu. ft./lb.	Vapor, cu. ft./lb.	Liquid, B.t.u./lb.	Vaporization, B.t.u./lb.	Vapor, B.t.u./lb.	Liquid, B.t.u. (lb.) (°R.)	Vaporization, B.t.u./ (lb.) (°R.)	Vapor, B.t.u./ (lb.) (°R.)
32	18.64	0.961	0.02588	4.79	0.0	166.1	166.1	0.0000	0.3378	0.3378
40	21.91	0.954	0.02610	4.19	3.4	164.9	168.3	0.0068	0.3300	0.3368
50	26.60	0.944	0.02638	3.52	8.4	163.0	171.4	0.0167	0.3198	0.3365
60	32.0	0.935	0.02667	2.89	13.6	160.8	174.4	0.0268	0.3094	0.3365
70	38.2	0.926	0.02698	2.41	19.2	158.3	177.5	0.0375	0.2988	0.3365
80	45.2	0.917	0.02730	2.25	25.4	155.1	180.5	0.0491	0.2874	0.3365
90	53.1	0.909	0.02770	1.76	31.2	152.5	183.7	0.0597	0.2774	0.3371
100	62.5	0.900	0.02811	1.52	37.0	149.7	186.7	0.0702	0.2675	0.3377
110	72.1	0.890	0.02852	1.33	42.9	146.7	189.6	0.0806	0.2575	0.3381
120	83.5	0.881	0.02898	1.16	48.7	143.8	192.5	0.0907	0.2481	0.3388
130	96.3	0.872	0.02943	1.01	54.4	140.8	195.2	0.1007	0.2388	0.3395
140	110.2	0.862	0.02992	0.875	60.5	138.0	198.5	0.1107	0.2301	0.3408
150	125.5	0.852	0.03042	0.768	66.6	134.9	201.5	0.1207	0.2213	0.3420
160	142.4	0.843	0.03091	0.676	72.7	131.7	204.4	0.1307	0.2125	0.3432
170	161.3	0.831	0.03145	0.595	79.0	128.5	207.5	0.1409	0.2041	0.3450
180	182.0	0.820	0.03202	0.524	85.5	124.9	210.4	0.1511	0.1952	0.3463
190	204.7	0.807	0.03261	0.463	92.2	120.9	213.1	0.1615	0.1861	0.3476
200	228.6	0.795	0.03328	0.409	99.1	116.8	215.9	0.1721	0.1771	0.3492
210	254.6	0.783	0.03399	0.364	106.4	112.2	218.6	.01831	0.1675	0.3506
220	282.8	0.770	0.03477	0.324	114.1	107.1	221.2	0.1944	0.1576	0.3520
230	313.4	0.758	0.03567	0.286	122.0	101.4	223.4	0.2059	0.1470	0.3529
240	346.4	0.744	0.03671	0.251	130.0	95.2	225.2	0.2174	0.1361	0.3535
250	382.5	0.731	0.03800	0.219	138.4	88.3	226.7	0.2293	0.1244	0.3537
260	421.3	0.717	0.03962	0.189	147.1	79.4	226.5	0.2415	0.1103	0.3518
270	462.2	0.703	0.04180	0.161	158.5	67.9	226.4	0.2572	0.0931	0.3503
280	505.0	0.688	0.04488	0.134	173.4	52.0	225.4	0.2748	0.0703	0.3451

TABLE 2.—THERMODYNAMIC PROPERTIES OF SUPERHEATED 1-BUTENE

Temperature °F.	Volume cu. ft./lb.	Enthalpy B.t.u./lb.	Entropy B.t.u./(lb.) (°R.)	Fugacity pressure f/P	Volume cu. ft./lb.	Enthalpy B.t.u./lb.	Entropy B.t.u./(lb.) (°R.)	Fugacity pressure f/P
	14.696 lb./sq. in. abs. (20.73°)*				25 lb./sq. in. abs. (46.7°)*			
(at satn.)	.....	.....	.....	.....	3.657	170.5	0.3366	0.948
32	6.156	166.7	0.3469	0.964				
40	6.272	169.4	0.3526	0.966				
60	6.557	176.5	0.3665	0.970	3.772	175.3	0.3484	0.952
80	6.830	183.8	0.3803	0.974	3.940	182.6	0.3622	0.956
100	7.110	191.3	0.3940	0.977	4.103	190.2	0.3758	0.960
120	7.384	199.4	0.4077	0.979	4.275	198.4	0.3894	0.964
140	7.657	207.6	0.4213	0.982	4.441	206.7	0.4029	0.969
160	7.928	215.9	0.4347	0.983	4.605	215.0	0.4163	0.971
180	8.199	224.2	0.4480	0.985	4.767	223.4	0.4296	0.975
200	8.468	232.2	0.4613	0.986	4.925	231.5	0.4428	0.977
220	8.737	241.2	0.4745	0.988	5.086	240.5	0.4560	0.980
240	9.006	250.1	0.4876	0.989	5.246	249.4	0.4691	0.982
260	9.274	259.0	0.5005	0.990	5.407	258.4	0.4820	0.983
280	9.541	268.2	0.5134	0.991	5.565	267.6	0.4948	0.984
300	9.807	278.3	0.5263	0.991	5.726	277.7	0.5077	0.985
320	10.08	288.4	0.5390	0.992	5.882	287.9	0.5204	0.987
340	10.34	298.6	0.5517	0.993	6.045	298.1	0.5331	0.988
360	10.59	308.9	0.5643	0.993	6.198	308.4	0.5457	0.989
380	10.86	319.5	0.5769	0.994	6.355	319.0	0.5582	0.990
400	11.12	329.8	0.5893	0.994	6.513	329.6	0.5706	0.991
420	11.38	340.6	0.6017	0.995	6.668	340.2	0.5831	0.992
440	11.65	351.6	0.6141	0.995	6.825	351.3	0.5954	0.992
460	11.91	362.8	0.6263	0.996	6.980	362.4	0.6076	0.993
480	12.17	373.9	0.6384	0.996	7.135	373.5	0.6197	0.993
	50 lb./sq. in. abs. (86.2°)*				75 lb./sq. in. abs. (112.7°)*			
(at satn.)	1.891	182.5	0.3367	0.912	1.280	190.4	0.3383	0.888
100	1.957	187.7	0.3481	0.921				
120	2.049	196.0	0.3620	0.929	1.305	193.0	0.3444	0.894
140	2.140	204.5	0.3758	0.938	1.371	201.7	0.3586	0.907
160	2.229	213.0	0.3894	0.944	1.436	210.5	0.3725	0.916
180	2.308	221.4	0.4029	0.950	1.499	219.1	0.3863	0.926
200	2.402	229.7	0.4163	0.955	1.560	227.5	0.3999	0.932
220	2.488	238.8	0.4296	0.959	1.620	236.2	0.4134	0.939
240	2.571	247.8	0.4428	0.963	1.679	245.9	0.4267	0.944
260	2.653	256.9	0.4559	0.966	1.737	255.1	0.4400	0.949
280	2.737	266.1	0.4689	0.969	1.795	264.2	0.4521	0.953
300	2.819	276.4	0.4818	0.971	1.860	274.8	0.4662	0.956
320	2.901	286.6	0.4947	0.973	1.909	285.1	0.4791	0.960
340	2.981	296.9	0.5074	0.976	1.964	295.5	0.4920	0.964
360	3.063	307.3	0.5201	0.978	2.019	306.0	0.5047	0.966
380	3.143	317.9	0.5327	0.980	2.074	316.7	0.5175	0.969
400	3.225	328.5	0.5452	0.981	2.129	327.3	0.5300	0.972
420	3.306	339.1	0.5577	0.983	2.183	338.1	0.5426	0.974
440	3.386	350.3	0.5700	0.984	2.236	349.3	0.5550	0.976
460	3.464	361.5	0.5823	0.986	2.292	360.5	0.5673	0.978
480	3.544	372.7	0.5945	0.986	2.347	371.9	0.5795	0.979
	100 lb./sq. in. abs. (132.7°)*				150 lb./sq. in. abs. (164.0°)*			
(at satn.)	0.964	196.3	0.3399	0.869	0.642	205.6	0.3438	0.839
140	0.984	198.8	0.3448	0.876				
160	1.038	207.9	0.3592	0.888				
180	1.089	216.7	0.3733	0.901	0.672	212.7	0.3545	0.851
200	1.138	225.3	0.3872	0.911	0.713	220.5	0.3671	0.867
220	1.187	234.2	0.4010	0.919	0.749	229.9	0.3815	0.879
240	1.233	244.0	0.4145	0.926	0.782	240.1	0.3956	0.889
260	1.278	253.3	0.4280	0.932	0.818	249.7	0.4096	0.899
280	1.324	362.5	0.4403	0.938	0.866	259.4	0.4229	0.908
300	1.362	273.2	0.4545	0.943	0.881	270.0	0.4369	0.915
320	1.411	283.6	0.4675	0.947	0.912	280.6	0.4502	0.922
340	1.455	294.1	0.4805	0.953	0.944	291.3	0.4635	0.930
360	1.496	304.7	0.4933	0.956	0.972	302.0	0.4765	0.934
380	1.537	315.5	0.5063	0.959	1.002	313.0	0.4898	0.939
400	1.580	326.1	0.5188	0.962	1.031	323.8	0.5025	0.943
420	1.621	337.0	0.5315	0.965	1.059	334.8	0.5153	0.948
440	1.663	348.3	0.5440	0.967	1.089	346.2	0.5280	0.952
460	1.705	359.6	0.5563	0.971	1.118	357.7	0.5404	0.956
480	1.747	371.0	0.5686	0.973	1.129	369.2	0.5529	0.959
	200 lb./sq. in. abs. (188.0°)*				300 lb./sq. in. abs. (225.8°)*			
(at satn.)	0.4738	212.6	0.3476	0.812	0.2997	222.6	0.3522	0.764
200	0.4965	216.9	0.3530	0.823				
220	0.5278	225.5	0.3654	0.840				
240	0.5556	236.1	0.3803	0.853	0.3206	228.0	0.3591	0.781
260	0.5836	245.9	0.3948	0.867	0.3454	237.6	0.3719	0.801
280	0.6112	255.8	0.4086	0.878	0.3683	248.5	0.3868	0.819
300	0.638	266.7	0.4230	0.888	0.3903	259.4	0.4009	0.834
320	0.664	277.5	0.4368	0.897	0.4121	270.8	0.4158	0.849
340	0.690	288.4	0.4504	0.908	0.4309	282.2	0.4302	0.864

*Saturation temperature.

TABLE 2.—THERMODYNAMIC PROPERTIES OF SUPERHEATED 1-BUTENE (*continued*)

Temperature, °F.	Volume, cu. ft./lb.	Enthalpy, B.t.u./lb.	Entropy, B.t.u./(lb.) (°R.)	Fugacity, Pressure f/P	Volume, cu. ft./lb.	Enthalpy, B.t.u./lb.	Entropy, B.t.u./(lb.) (°R.)	Fugacity, pressure f/P
	200 lb./sq. in. abs. (188.0°)*				300 lb./sq. in. abs. (225.8°)*			
360	0.712	299.3	0.4637	0.914	0.449	293.6	0.4441	0.872
380	0.733	310.4	0.4772	0.920	0.466	305.1	0.4582	0.881
400	0.758	321.4	0.4901	0.925	0.483	316.5	0.4716	0.889
420	0.781	332.6	0.5031	0.931	0.500	328.0	0.4850	0.897
440	0.803	344.1	0.5160	0.936	0.516	339.9	0.4983	0.904
460	0.827	355.7	0.5285	0.942	0.532	351.7	0.5111	0.912
480	0.848	367.4	0.5412	0.946	0.549	363.8	0.5241	0.920
	400 lb./sq. in. abs. (254.8°)*				500 lb./sq. in. abs. (278.6°)*			
(at satn.)	0.2042	226.5	0.3524	0.726	0.1367	226.0	0.3460	0.691
260	0.2133	228.9	3.3551	0.734				
280	0.2388	238.8	0.3674	0.759	0.1408	226.4	0.3471	0.694
300	0.2596	249.9	0.3816	0.779	0.1755	238.5	0.3630	0.722
320	0.2791	262.6	0.3971	0.800	0.1982	252.1	0.3799	0.749
340	0.2974	275.0	0.4127	0.821	0.2154	266.1	0.3968	0.776
360	0.315	287.2	0.4278	0.832	0.2317	279.7	0.4125	0.791
380	0.329	299.4	0.4427	0.844	0.2461	293.0	0.4287	0.807
400	0.344	311.2	0.4567	0.853	0.2595	305.2	0.4434	0.820
420	0.357	323.0	0.4705	0.864	0.2726	317.3	0.4576	0.835
440	0.371	335.3	0.4842	0.874	0.2848	330.1	0.4715	0.847
460	0.385	347.5	0.4972	0.885	0.2967	342.7	0.4848	0.859
480	0.399	359.9	0.5105	0.895	0.3090	355.4	0.4985	0.871
	600 lb./sq. in. abs.				700 lb./sq. in. abs.			
320	0.1354	240.2	0.3611	0.698	0.0857	222.4	0.3335	0.642
340	0.1571	256.5	0.3811	0.731	0.1098	242.0	0.3581	0.683
360	0.175	270.9	0.3972	0.749	0.1311	260.5	0.3811	0.707
380	0.189	285.6	0.4152	0.769	0.1475	277.1	0.4015	0.732
400	0.202	298.5	0.4305	0.786	0.1617	291.1	0.4177	0.752
420	0.214	311.0	0.4448	0.803	0.1724	303.6	0.4322	0.772
440	0.225	324.2	0.4600	0.817	0.1827	318.3	0.4483	0.789
460	0.236	337.5	0.4737	0.832	0.1931	331.9	0.4635	0.805
480	0.246	350.5	0.4877	0.846	0.2031	345.3	0.4779	0.821
	800 lb./sq. in. abs.				900 lb./sq. in. abs.			
340	0.0752	226.8	0.3373	0.634	0.0569	211.7	0.3182	0.588
360	0.0969	248.3	0.3638	0.665	0.0748	235.8	0.3474	0.624
380	0.1144	267.1	0.3871	0.695	0.0900	256.9	0.3728	0.658
400	0.1286	283.0	0.4050	0.718	0.1042	274.6	0.3928	0.682
420	0.1409	297.2	0.4222	0.741	0.1167	290.0	0.4115	0.706
440	0.1516	312.1	0.4392	0.760	0.1271	305.6	0.4295	0.730
460	0.1617	326.1	0.4540	0.779	0.1370	320.0	0.4448	0.753
480	0.1711	339.8	0.4689	0.797	0.1459	334.0	0.4603	0.773
	1,000 lb./sq. in. abs.							
340	0.0500	199.5	0.3033	0.548				
360	0.0625	225.4	0.3340	0.587				
380	0.0748	247.9	0.3605	0.623				
400	0.0867	266.7	0.3828	0.650				
420	0.0981	282.8	0.4011	0.678				
440	0.1085	298.9	0.4198	0.704				
460	0.1176	313.7	0.4355	0.728				
480	0.1264	328.0	0.4515	0.750				

* Saturation temperature.

lated to the vaporization temperature. The enthalpy and entropy were then obtained directly from the plots. In all cases the extrapolations were over short ranges of temperature, and the final results were smoothed on an enthalpy-entropy plot. Table 1 lists the properties of the saturated liquid and vapor phases.

Entropy and Enthalpy. The change of entropy with pressure under isothermal conditions was determined through the use of the equation

$$M\,(S_P - S^o)_T = -\int_{P^o}^{P} \frac{R}{P}\,dP + \int_{P^o}^{P} \left(\frac{\partial \alpha}{\partial T}\right)_P dP \qquad (5)$$

the second term in the right-hand member of the equation being determined by graphical integration. The changes calculated from this equation were then added to the entropy of the ideal gas at the same temperature. The change in enthalpy of the superheated vapor with pressure under isothermal conditions was determined by use of the equation

$$M\,(H_P - H^o)_T = -\int_{P^o}^{P} \left[\alpha - T\left(\frac{\partial \alpha}{\partial T}\right)_P\right] dP \qquad (6)$$

In this case the entire right-hand member of the equation was evaluated by graphical integration. The changes in enthalpy thus calculated were then added to the enthalpy of the ideal gas at the same temperature, and the results were plotted on a large-scale graph as

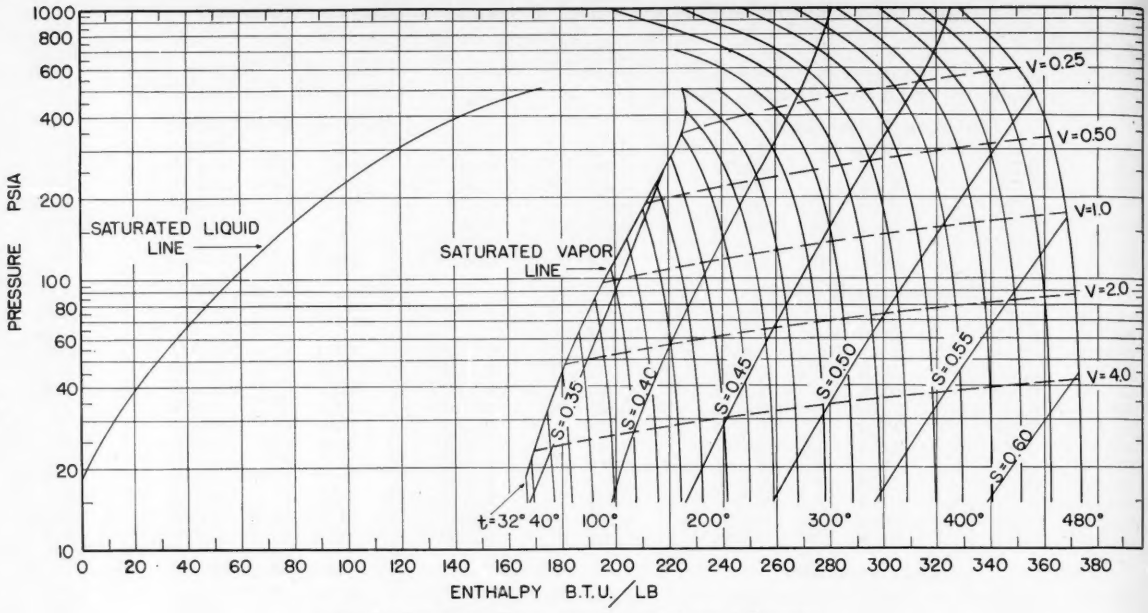

FIG. 1. PRESSURE-ENTHALPY DIAGRAM FOR 1-BUTENE.

temperature - entropy, enthalpy-temperature, and enthalpy-entropy and smoothed. The final results are presented in tabular form in Table 2. The complete results, for both saturated and superheated conditions, are presented in graphical form in Figure 1.

INTERNAL CONSISTENCY OF THE RESULTS

One method to check the internal consistency of thermodynamic data of this type is through the use of the equation:

$$dH = TdS + VdP \qquad (7)$$

which is a statement of the first two laws of thermodynamics. Setting the value of the entropy at a constant reduces the equation to

$$dH = VdP \qquad (8)$$

Multiplying the right-hand member by P/P and integrating results in the equation

$$H_2 - H_1 = PV\int_{P_1}^{P_2} d\ln P \qquad (9)$$

The right-hand member can then be evaluated by graphical integration and compared with enthalpy differences obtained from the calculated data. Such consistency checks were made on the thermodynamic data presented in this paper, and good agreement was obtained in all instances.

Since there are not enough thermal data to check the results by an independent method, the accuracy of the data presented here cannot be stated with certainty. However, it is believed that the enthalpy values are accurate within ±0.5 B.t.u./lb. and the entropy values, within ±0.0005 B.t.u./(lb.)(°R).

CONCLUSIONS

The thermodynamic properties of 1-butene, using fundamental relationships, have been calculated over the temperature range 32° to 480°F. and up to pressures of 1,000 lb./sq.in. abs. The data have been found to be internally consistent and are presented in graphical and tabular form.

NOTATION

H = enthalpy, B.t.u./lb.
M = molecular weight
P = pressure, lb./sq.in. abs., unless otherwise specified
R = gas-law constant
S = entropy, B.t.u./lb.
T = absolute temperature, °R. unless specified as °K.
V = specific volume, cu.ft./lb.
f = fugacity, same units as pressure
t = temperature, °F.
α = residual volume, cu.ft./lb. mole, $\alpha = \frac{RT}{P} - V_M$
β = second virial coefficient, defined in Equation (1)

Subscripts

c = critical property
M = molal quantity
V = vaporization

Superscripts

o = property in ideal gas state at unit fugacity

LITERATURE CITED

1. *Am. Petroleum Inst. Research Project* 44, Table 24-E, Nat. Bur. Standards.
2. *Ibid.*, Table 24 K-E.
3. *Ibid.*, Table 8i.
4. *Ibid.*, Table 8m.
5. *Ibid.*, Table 7 v-E.
6. *Ibid.*, Table 24 u-E.
7. *Ibid.*, Table 24t.
8. Beattie, J. A., and S. Marple, Jr., *J. Am. Chem. Soc.*, **72**, 1449-52 (1950).
9. *Ibid.*, 4143-5 (1950).
10. Canjar, L. N., M. Goldman, and H. Marchman, *Ind. Eng. Chem.*, **43**, 1186-93 (1951).
11. Lamb, A. B., and L. B. Roper, *J. Am. Chem. Soc.*, **62**, 806-14 (1940).
12. Olds, R. H., B. F. Sage, and W. N. Lacey., *Ind. Eng. Chem.*, **38**, 301-3 (1946).
13. Roper, E. E., *J. Phys. Chem.*, **44**, 835-47 (1940).
14. Sage, B. H., and W. W. Lacey, *Pet. Refiner*, **29**, No. 10, 123-7 (1950).
15. Schlinger, W. G., and B. H. Sage, *Ind. Eng. Chem.*, **41**, 1779-82 (1949).
16. York, R., Jr., and E. R. White, Jr., *Trans. Am. Inst. Chem. Engrs.*, **40**, 227-50 (1944).

MEMBRANE SEPARATIONS IN THE LIQUID PHASE

KARL KAMMERMEYER and D. H. HAGERBAUMER

State University of Iowa, Iowa City, Iowa

Solutions can be separated in the liquid phase by means of membranes with processes utilizing osmosis, ion exchange resins incorporated in the membranes, electric potentials across membranes, and ultrafiltration. The published literature in this field is extensive. A rather comprehensive treatise on the subject of ultrafiltration was presented by Erschler (*5*), and some very interesting findings on solute retention were reported by McBain and Stuewer (*11*). The subject matter of ion exchange has been ably summarized in a recent publication by Juda, Marinsky, and Rosenberg (*9*) with an extensive bibliography. Separation of ionic from nonionic components by means of ion exclusion has been reported by Wheaton and Bauman (*14*), who also published a treatise covering nonionic separation with ion exchange resins (*15*). A recent discussion on electrochemical properties of synthetic ion exchange membranes was presented by Winger, Bodamer and Kunin (*16*). All the studies that have been reported are concerned with aqueous solutions, and in a few instances it has been stated that polar solvents other than water should be suitable.

There appears to be no published literature on the separation of homogeneous liquid mixtures of organic compounds solely by means of permeation through microporous membranes; therefore, it should be of considerable interest that experiments have been carried out which gave such separations by what might be called "fractional filtration" through a membrane having an average pore diameter of about 40×10^{-8} cm. In comparison, ultrafiltration is generally considered as taking place with pore sizes in the range of 10^{-4} cm.

The separations were accomplished with porous glass (*7, 12*), an intermediate glass state in the manufacture of Vycor-Brand glass. This material has been investigated as a medium for gas and vapor separations and was found to be an almost ideal molecular filter in such separations (*1, 6, 8*). It possesses a rather uniform pore diameter between 20 and 60 Å., with an average diameter of about 40 Å. (*4, 12*) and approximately 1.34×10^{12} pores/sq.cm. (*13*).

A publication by Nordberg (*12*) on properties of some Vycor-Brand glasses contains data on the flow of liquid water and acetone (liquid permeabilities) through porous glass. In combination with gas- and vapor-separation studies it was a logical extension of thought to conceive the possibility of separation in the liquid phase. Furthermore, work on the separation of azeotropic mixtures in the vapor phase (*6*) had shown that separation increased as the temperature of operation approached the boiling point of the mixture. Some support of the idea was also derived from publications by Manegold and Hofmann (*10*) where the contention is made that a filter which is suitable for ultrafiltration should act not only as a barrier on a go or no-go basis for molecules of different sizes, but should also exhibit partial inhibition to the movement of the larger molecules.

For the sake of convenience, the studies in liquid separation were then carried out with some of the same azectropic mixtures which had been used for the vapor-phase separation study (*6*). These mixtures corresponded to constant boiling compositions at atmospheric pressure and the respective boiling points. They therefore did not represent azeotropic compositions at the temperature of liquid permeation.

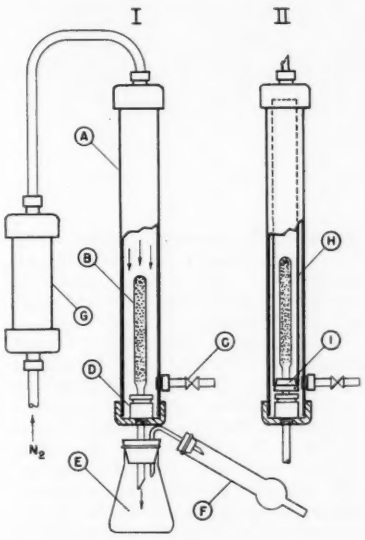

FIG. 1. SCHEMATIC DIAGRAM OF LIQUID-SEPARATION APPARATUS.

A, 1½- by 18-in.-long standard pipe; *B*, porous-glass membrane; *C*, ⅛-in. stainless steel needle valve; *D*, brass packing-gland assembly; *E*, 50-ml. collection flask; *F*, drying tube; *G*, 1½- by 10-in.-long standard pipe, silica-gel-filled gas-drying unit; *H*, 34-mm. I.D. by 16-in.-long inner glass tube; *I*, No. 7 rubber stopper.

EQUIPMENT AND PROCEDURE

The membrane was a porous glass cell in the form of a test tube provided with a capillary connection at the open end. One such specimen, having a wall thickness of about 1 mm., was subjected to a pressure drop of 600 lb./sq.in. (high pressure on outside) without fracture.

As the work was actually a pioneering study to establish the possibility of liquid-phase separation, the apparatus (Figure 1) was built as simply as possible. Cells I and II differ in that a floating glass liner is used in Cell II, to accommodate corrosive liquids. The area of the membrane used for the liquid-liquid separation experiments was 90.40 sq. cm. and the thickness was 1.0 ± 0.05 mm.

D. H. Hagerbaumer is with The Chemstrand Corporation, Decatur, Alabama.

TABLE 1.—SEPARATION OF ORGANIC LIQUID MIXTURES BY MEANS OF A POROUS GLASS BARRIER

Separation data and rates of permeation
(1) Average, (2) standard deviation

N_2 pressure, lb./sq. in. gauge		Rate perm. g./(sq. cm.) (min.) $\times 10^5$	Weight % A Perm. product	Feed	Component enriched Δconcentration increase in permeated product	System $A-B$	Number of runs
60	(1)	5.16	44.31	43.30	A 1.01	EtAc*–CCl_4	10
	(2)	0.35	0.32	.....	A 0.10		
125		10.62	45.36	43.64	A 1.72	EtAc*–CCl_4	10
		0.10	0.10	0.20	A 0.15		
200		16.15	45.06	42.95	A 2.11	EtAc*–CCl_4	10
		0.47	0.06	0.06	A 0.18		
60		1.606	63.16	69.0	B 5.84	C_6H_{12}–EtOH†	5
		0.05	0.30	.....	B 0.27		
125		4.00	62.24	69.0	B 6.76	C_6H_{12}–EtOH†	5
		0.21	0.14		B 0.13		
200		6.57	62.4	69.0	B 6.6	C_6H_{12}–EtOH†	5
		0.19	0.25	.....	B 0.26		
60		1.465	93.49	93.54	Essentially A (−0.05) no change	EtOH†H_2O	5
		0.003	0.10				
125		2.84	93.41	93.54	Essentially A (−0.13) no change	EtOH†H_2O	5
		0.003	0.25				
200		4.48	93.25	93.54	Essentially A (−0.29) no change	EtOH†H_2O	5
		0.19	0.28				
60		3.87	59.25	60.40	B 1.15	C_6H_6–MeOH‡	5
		0.24	0.05	0.05	B 0.06		
125		7.74	57.95	60.56	B 2.61	C_6H_6–MeOH‡	5
		0.20	0.03	0.18	B 0.15		
200		12.57	56.28	60.11	B 3.83	C_6H_6–MeOH‡	5
		0.22	0.47	0.10	B 0.16		
60		3.15	67.00	67.4	B 0.4	C_6H_6–EtOH†	5
		0.06	0.25	.....	B 0.18		
125		6.97	67.0	67.4	B 0.4	C_6H_6–EtOH†	5
		0.06	0.32	.....	B 0.10		
200		11.29	66.6	67.4	B 0.8	C_6H_6–EtOH†	5
		0.16	0.05	.....	B 0.05		

*EtAc–ethyl acetate.
†EtOH–ethyl alcohol.
‡MeOH–methyl alcohol.

Before the membrane was installed, it was "normalized" in an oven at 510°C. for 12 hr. to remove adsorbed organic vapors and water vapor. This procedure was rigorously followed before each new mixture and each pure component was studied. All separation runs were made at room temperature (25° to 30°C.), which is considerably removed from the 510°C. normalizing temperature. As porous glass is normally consolidated to Vycor at much higher temperatures, the pores were assumed not to be altered during the normalizing operation.

The upstream pressure on the liquid was produced by high-pressure nitrogen from a commercial cylinder. The nitrogen was oil-pumped and was quoted by the supplier as being 99% pure, but as an added precaution to exclude moisture, it was passed through the silica-gel-filled drying unit (G).

The cell was completely filled by introducing the liquid to be studied through the brass fitting at the top. After a liquid of known composition was introduced, all fittings were secured and nitrogen was admitted at the desired pressure. When fresh liquid was placed in the unit, the downstream side of the membrane was flushed with about 25 cc. of product before the first run was made.

To minimize vaporization losses from flask (E), the glass tube leading from the flask to the drying tube (F) was drawn to a fine capillary. Samples of known concentration were placed in flask (E) by use of another stopper with only the fine capillary tube opening available to the atmosphere. Various test samples showed no detectable change in concentration after standing 2 or 3 days. When a sufficient quantity (5 to 10 cc.) of liquid permeated the membrane, the collection flask (E) was removed and the sample analyzed. A sample was also withdrawn from the upstream side through the needle valve (C).

In experiments the feed was in intimate contact with the walls of the galvanized-iron pipe. To check the possibility of any metal effect, several liquid mixtures were kept in the closed unit for at least a week. Refractive-index measurements revealed that there were no detectable effects of the pipe on feed liquids.

MATERIALS

The mixtures studied and a summary of the enrichments obtained are shown in Table 1.

All liquid mixtures were analyzed with a Zeiss Pulfrich refractometer. Refractive-index data, the method used for purifying the pure components, and the procedure for preparing the azeotropes studied have been reported in reference *6*.

RESULTS AND DISCUSSION

It has been established that certain liquids can be separated by diffusion through porous membranes. Five different liquid systems have been studied at 60, 125, and 200 lb./sq.in. gauge upstream pressure and atmospheric downstream pressure in this preliminary investigation. Separation data and rates of permeation in grams per square centimeter per minute for the five mixtures studied are presented in Figures 2 through 6.

The separation data for ethyl acetate–carbon tetrachloride show

that ethyl acetate permeated the porous glass membrane faster than did carbon tetrachloride and that greater separation was obtained the higher the upstream pressure. The difference in concentration between the feed samples and permeated samples varied from 1.01 wt. % ethyl acetate at 60 lb./sq.in. gauge upstream pressure to 2.11 wt. % ethyl acetate at 200 lb./sq.in. gauge upstream pressure. The analyses were estimated to be accurate within ±0.1 wt. %.

Although an extended study was made of the rates of permeation of the ethyl acetate–carbon tetrachloride system, it was not satisfactorily determined whether the mixture permeated the membrane faster or more slowly than did ethyl acetate or whether the rates of permeation curves actually did cross as shown in Figure 2. If the mixture is faster than either pure component, then it is possible that there is decided variation in the viscosity of the mixture at various pressures, or there may be some other change in physical properties which is unaccounted for. Blocking of the pores, difference in molecular size, association and adsorption characteristics are other possibilities which should be considered. At this stage of the investigation, one can only speculate as to the reason for the decided difference between the observed rates of permeation for the mixtures compared with the pure components because of the incomplete picture of the liquid state.

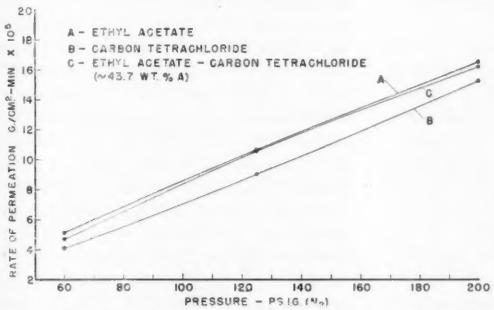
A - ETHYL ACETATE
B - CARBON TETRACHLORIDE
C - ETHYL ACETATE - CARBON TETRACHLORIDE (~43.7 WT. % A)
RATE OF PERMEATION G./CM²-MIN X 10⁵
PRESSURE - P.S.I.G. (N₂)

FIG. 2. ETHYL ACETATE–CARBON TETRACHLORIDE RATES OF PERMEATION THROUGH POROUS GLASS AT VARIOUS PRESSURES.

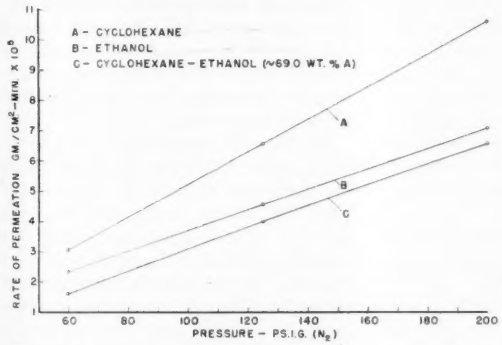

FIG. 3. CYCLOHEXANE-ETHANOL RATES OF PERMEATION THROUGH POROUS GLASS AT VARIOUS PRESSURES.

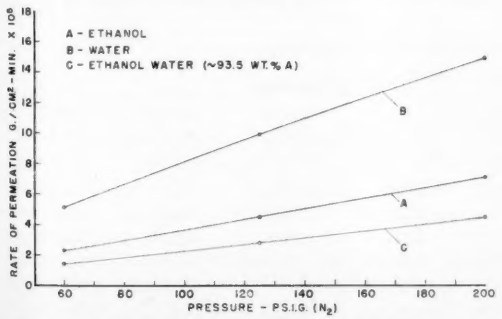

FIG. 4. ETHANOL-WATER RATES OF PERMEATION THROUGH POROUS GLASS AT VARIOUS PRESSURES.

The separation data for the cyclohexane-ethanol system show that ethanol permeates porous glass considerably faster than does cyclohexane. The effect of upstream pressure on separation is somewhat inconclusive when the data for individual runs are compared; however, in general it appears that better separation is obtained at the higher upstream pressures. About the same average degree of separation was obtained at 125 and 200 lb./sq.in. gauge upstream pressure. The analyses were estimated to be accurate within ±0.2 wt. %. The rates of permeation for the cyclohexane-ethanol system and the pure components are presented in Figure 3. It was interesting to observe that the mixture passed through the membrane more slowly than did either of the pure components, but still the degree of separation was quite large.

The separation results for the ethanol-water system presented were somewhat disappointing, for no separation was detected which was considered reliable. Of course, it may be significant that the feed was so rich in ethanol that some separation was obtained but escaped detection because of analysis limitations. Analysis of the ethanol-water system refractometrically was estimated to be within ±0.5 wt. %. Although no separation was reported for this system, it is believed that a more refined method of analysis may reveal separation even though it is quite concentrated in ethanol. The rates of permeation for ethanol-water and the pure components are shown in Figure 4. Comparison of Figures 3, 4, and 5 revealed that ethanol-water, cyclohexane-ethanol, and the benzene-methanol systems were analogous in that all the mixtures permeated the membrane at slower rates than did the pure components.

The separation results for the benzene-methanol system show that methanol permeates porous glass faster than does benzene. Furthermore, the degree of separation was noted to more than triple when the upstream pressure increased from 60 to 200 lb./sq.in. gauge. The accuracy of the analyses was established to be within ±0.2 wt. %. The rates of permeation for the benzene-methanol system and the pure components are presented in Figure 5. Unlike those for the other systems studied, the rates of permeation of the pure components

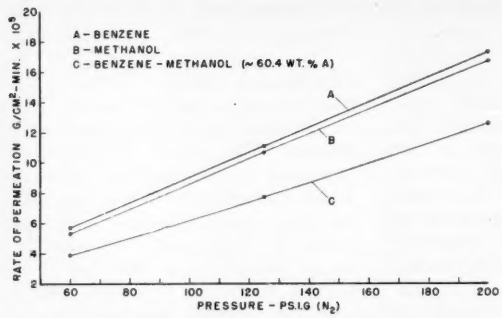

FIG. 5. BENZENE-METHANOL RATES OF PERMEATION THROUGH POROUS GLASS AT VARIOUS PRESSURES.

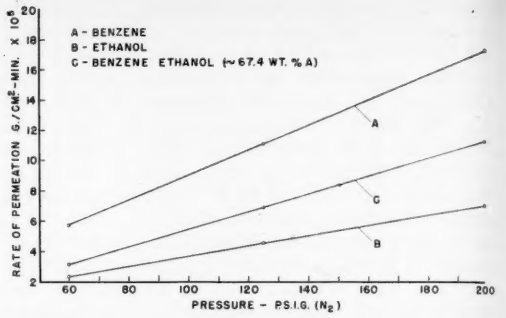

FIG. 6. BENZENE-ETHANOL RATES OF PERMEATION THROUGH POROUS GLASS AT VARIOUS PRESSURES.

were found to be very close to each other, and the curve for the mixture was relatively far removed from that for the pure components.

The separation results for the benzene-ethanol system indicate that ethanol permeates the membrane faster than benzene. It cannot be stated with any degree of confidence that increased upstream pressure results in an increase in the degree of separation for this system; however, when the data for 200 lb./sq.in. gauge upstream pressure are compared with the separation results at the lower upstream pressure, one might speculate that the degree of separation tends to be enhanced at higher upstream pressures. The analyses were estimated to be accurate within ±0.2 wt. %. The rates of permeation for the benezene-ethanol system were also unlike the other systems studied (except possibly the ethyl acetate–carbon tetrachloride system) because the curve for the rates of permeation of the mixture fell between the curves for the pure components. The decided contrast between the curves for the rates of permeation shown in Figure 5 and 6 for the benzene-methanol and benzene-ethanol systems, respectively, is rather perplexing. Benzene is common to both systems; however, the addition of a methylene group to the alcohol certainly appears to alter the permeation characteristics of the two systems. Then again, it should be recalled that methanol is the border compound between the alcohols and a seemingly unpredictable compound, water.

The rates-of-permeation curve for water (Figure 4) was the only curve which deviated from a linear form. Actually, it is believed that the rates of permeation for water may be found to fall on a straight line. Water was the only pure liquid which was found difficult to collect because it would not drain from the Vycor capillary tube on the membrane. Consequently, the validity of the water rates is somewhat questionable.

It is interesting to compare the direction of the liquid-liquid separation data with the azeotropic vapor separation data reported in reference *6* and to speculate on a possible explanation of the separation mechanism. Table 2 shows the direction of separation together with compilations of some physical properties which might be considered as having a bearing on the process.

The possibilities of interpretation of the results are numerous, particularly so as the data are so few in number. The only two properties which line up consistently with the direction of enrichment are molecular weight and dipole moment. It happens, however, that all the binary systems which were investigated in a quantitative manner contained a more polar component which also had the lower molecular weight. Thus this agreement may be entirely coincidental; nevertheless, it is possible that a more highly polar compound might more easily permeate a siliceous membrane, which certainly possesses some polarity itself, than would a compound of lower polarity. Although the less polar compound probably would not be retarded, it might not be able to pass the polar network of the membrane so easily as a highly polar compound. If the qualitative separation results for the system acetone–methyl alcohol are given some consideration, then the only property which corresponds to the direction of separation is the dipole moment. As a matter of fact, the latter system is one where the higher molecular weight compound also possesses the greater dipole moment.

It is well known that in liquid-solid interface systems there may be competition between the solvent and the solute molecules for the surface of the adsorbent, that the relative extent of adsorption may depend on a number of variables including polarity and hydrogen-bonding ability, and that solubility as well as many other physical properties of either the adsorbent or the adsorptive can have a major

TABLE 2.—SEPARATION IN LIQUID PHASE AND RELATED PROPERTIES

	Component enriched		Component having					
System	In liquid phase	In vapor phase	Lower mol. wt.	Higher dipole moment	Lower viscosity	Smaller collision diameter	Greater surface tension	Lower critical temp.
CCl_4 – EtAc	EtAc	EtAc	EtAc	EtAc	EtAc	CCl_4	CCl_4	EtAc
C_6H_{12} – EtOH	EtOH	C_6H_{12}	EtOH	EtOH	C_6H_{12}	EtOH	C_6H_{12}	EtOH
EtOH – H_2O	H_2O	EtOH	H_2O	H_2O	H_2O	H_2O	H_2O	EtOH
C_6H_6 – MeOH	MeOH	C_6H_6	MeOH	MeOH	MeOH	MeOH	C_6H_6	MeOH
C_6H_6 – EtOH	EtOH	C_6H_6	EtOH	EtOH	C_6H_6	EtOH	C_6H_6	EtOH
*Me_2CO–MeOH	Me_2CO	Me_2CO	MeOH	Me_2CO	Me_2CO	MeOH	Me_2CO	Me_2CO

*Qualitative separation results only.

effect (*2*). Considering the relative complexity of a permeation process, in which a liquid mixture passes over and in part through an active capillary system, such as a barrier, and where the components of the mixture may differ radically in their properties, it is not surprising that an explanation of the mechanism of the process is not readily available. A promising attack of the problem, not involving an adsorption mechanism, has been suggested by Drickamer (*3*). This is by way of the thermodynamic pressure effect, a phenomenon which so far has received little attention because a pressure gradient normally is dissipated into turbulence. In the small pores of the porous glass barrier, however, this may not be the case, and the pressure effect, through the pressure gradient, may be the cause of the observed separations.

It is not known whether the barrier adsorbed any components selectively, although this possibility does, of course, exist. However, about 25 cc. of permeated liquid was always collected before any runs were made. In addition, as much as 160 cc. was collected during a series of runs (CCl_4-EtAc) without any definite trend in concentration changes being shown for ten runs. In view of these facts it is believed that selective adsorption, if at all present, did not have any pronounced effect on the process.

Any strict evaluation of the experimental data must first of all take into account that the work was of a pioneering nature. The data are valid, but they should at this time be considered semiquantitative rather than strictly quantitative. The fact has been established that separation in the liquid phase by means of a microporous membrane is possible. In addition, the results give a very good indication of the magnitude of the attainable separation and of the approximate rates for the particular membrane and the range of pressures which were employed.

LIMITATIONS AND EXTENSIONS OF FINDINGS

It is readily apparent that the study was concerned mainly with the question of whether liquid mixtures could be separated by permeation through a microporous membrane. Consequently, the experimental apparatus and the procedure were as simple as possible, the installation of a continuous flow system not being warranted. Although the actual system was really a batch type, involving concentration changes in the residual liquid, the proportion of permeated product liquid to the bulk of the residual liquid was so small that the separation data are still valid. As a matter of fact, depletion in the residual liquid takes place in the faster permeating component therefore, the concentration changes are based on a higher concentration of the faster component than should actually have been present in the unpermeated liquid, and the reported results are for this reason on the conservative side.

Probably the most serious limitation of the present study was the fact that only one type of membrane was investigated. Undoubtedly other types of membranes will work. Of particular interest will be porous metal membranes, which should have a much less adsorptive character than a siliceous membrane. Likewise, combination-type membranes, which might contain hydrophilic or hydrophobic components, will be of great interest. Furthermore, the question of whether more bulky molecules can be separated by membranes having correspondingly larger pore sizes is of paramount importance.

All these problems are now being investigated. In addition, the use of higher pressures and elevated temperatures is contemplated. Some specific applications which are under consideration are the study of desalting of saline waters, waste-water purification, and separation of salt melts and of liquefied compound mixtures.

Only a very limited amount of work was done with separation of ionic compounds in aqueous solution, but it can be stated that sufficient evidence was obtained to permit the conclusion that the process may work with ionic mixtures.

CONCLUSIONS

It has been established that separations in the liquid phase can be accomplished by straightforward pressure permeation through microporous membranes. The reported results indicate what may be expected of such a process.

Industrial applications will largely depend on the rates of permeation which can ultimately be obtained. While the process suffers from the basic disadvantage of all membrane processes, that is, inherently low rates, it is entirely possible that the use of high pressures combined with membrane-development studies will result in favorable economic possibilities. A definite advantage is in the saving of thermal costs over processes which require vaporization. Future work has to some extent already been indicated. The most pressing need will be for studies of operating factors, investigation of available membranes, and improvement of promising membranes.

ACKNOWLEDGMENT

This study was sponsored by the United States Atomic Energy Commission and the support of the work is gratefully acknowledged, as is the generosity of the Corning Glass Works in supplying many of the porous glass membranes. The authors are greatly indebted to Dr. D. W. Brubaker of The Chemstrand Corporation, who participated in this work and whose suggestions contributed materially to the success of the study.

LITERATURE CITED

1. Brubaker, D. W., and Karl Kammermeyer, *"Proceedings of 1953 Conference on Nuclear Engineering."* Univ. Calif., Berkeley (Sept. 9-11, 1953).
2. Cassidy, H. G., in "Technique of Organic Chemistry," vol. 5, A. Weissberger, ed., Interscience Publishers, Inc., New York (1951).
3. Drickamer, H. G., Univ. Illinois, private communication.
4. Emmett, P. H., and M. Cines, *J. Phys. & Colloid Chem.*, **51**, 1248-62 (1947).
5. Erschler, B., *Kolloid-Z* **68**, 289-98 (1934).
6. Hagerbaumer, D. H., and Karl Kammermeyer, *Chem. Eng. Progr. Symposium Series No. 10*, **50**, 25-44 (1954).
7. Hood, H. P., and M. E. Nordberg, U. S. Patent 2,106,744 (1938).
8. Huckins, H. E., and Karl Kammermeyer, *Chem. Eng. Progr.*, **49**, 180-4, 294-8 (1953).
9. Juda, W., J. A. Marinsky, and N. W. Rosenberg, *Ann. Rev. Phys. Chem.*, **4**, 373-98 (1953).
10. Manegold, E., and R. Hofmann, *Kolloid-Z.*, **51**, 220-30, 308-15 (1930); **52**, 19-24 (1930).
11. McBain, J. W., and R. F. Stuewer, *J. Phys. Chem.*, **40**, 1157-68 (1936).
12. Nordberg, M. E., *J. Am. Ceram. Soc.*, **27**, 299-305 (1944).
13. Schwertz, F. A., *loc. cit.*, **32**, 390 (1949).
14. Wheaton, R. M., and W. C. Bauman, *Ann. N. Y. Acad. Sci.*, **57**, 159 (1953).
15. ———, *Ind.Eng. Chem.*, **45**, 228-33 (1953).
16. Winger, A. G., G. W. Bodamer, and R. Kunin, *J. Electrochem. Soc.*, **100**, 178-84 (1953).

DEHYDRATION OF HYDRAZINE BY AZEOTROPIC DISTILLATION

R. Q. WILSON, W. H. MINK, H. P. MUNGER, and J. W. CLEGG
Battelle Memorial Institute, Columbus, Ohio

A process was developed for dehydrating aqueous solutions of hydrazine by azeotropic distillation with aniline as an entrainer. The ternary system hydrazine-water-aniline, which contains the minimum-boiling aniline-water azeotrope and the maximum-boiling hydrazine-water azeotrope, was studied by fractionation analysis to determine the position of the ridge or distillation barrier in the vapor and liquid surface. The studies showed that the position and curvature of this ridge were favorable for the production, by rectification, of a solution richer in hydrazine than the azeotropic proportions. The process comprised three operations. Approximately 70% of the hydrazine charged to the system was dehydrated.

Entrainers that form binary minimum-boiling azeotropes with both hydrazine and water are discussed. Ternary systems with these entrainers have saddlepoint azeotropes that boil intermediate with respect to the other invariant components in the system.

Hydrazine is currently being produced by modifications of the German Raschig process, in which it is obtained in a low-concentration (1 to 3%) aqueous solution (*1*). Because of the maximum-boiling hydrazine-water azeotrope, sometimes called hydrazine hydrate, conventional distillation methods cannot be used to concentrate this solution to more than about 70 wt. % hydrazine and 30% water.(*6*). In the past, anhydrous hydrazine has been produced chemically through the formation of inorganic or organic derivatives which must be subjected to further treatment to yield the dehydrated product(*2*). Since these methods are costly, exploratory work was undertaken to determine whether an aqueous hydrazine solution could be dehydrated by distilling the solution in the presence of a third component that formed a minimum-boiling azeotrope with water. Of the numerous materials tested initially, aniline was the first to show real promise as an effective entrainer, and the process described is based on its use.

THE HYDRAZINE-WATER-ANILINE SYSTEM

The ternary system hydrazine-water-aniline was studied by fractionation analysis to determine the principal features of the vapor-liquid equilibrium surfaces. The basic principle of this method is that when an invariant component, i.e., a pure compound or azeotrope, is distilled from a mixture, the composition of the remaining solution moves rectilinearly in the opposite direction from the invariant component. This method was used by Ewell and Welch (*3*) for studying ternary systems with binary azeotropes, and by Lecat(*4*) for determining the composition of azeotropes in binary systems. The Todd precise fractionation assembly was used for the present analysis.

The Todd fractionating column consisted of a 1/2-in. glass column packed 36-in. high with 1/16-in. glass helices. The pot had an opening for a standard-taper thermometer and one for the entrance of nitrogen. All the vapors were condensed in the column head and the reflux was varied by adjusting a valve on the take-off line. Rubber tubing connecting the receiver vent to a bubbler provided a nitrogen seal and assured operation under a slight positive pressure of nitrogen. Vapor temperatures were measured by a thermometer in the reflux head. The column was shielded with glass and was heated with resistance wires to minimize heat losses. Both the heat load to the pot and the column heaters were controlled by variable resistors.

Two-hundred-gram samples of various ternary mixtures were distilled at a reflux ratio of 4 to 1 (reflux to distillate). Samples of the overhead vapors were collected at each temperature change of more than 2°C. during the distillations, or more often where large amounts of material came over at one temperature. Each sample was weighed and analyzed. All analyses for hydrazine were made by the method of iodate titration described by Penneman and Audrieth (*5*). The composition of a ternary mixture was then established from the analysis for hydrazine and a measurement of the refractive index.

Two typical distillation curves for ternary mixtures which yielded initial overhead vapors of different compositions are shown in Figure 1 to illustrate the method of determining vapor-liquid–equilibrium surface features on a ternary temperature-composition diagram. One curve is for a ternary mixture containing 29.5% hydrazine, 20.5% water, and 50% aniline (run 1) and the other is for a mixture containing 72% hydrazine, 7% water, and 21% aniline (run 2).

The curve for run 1 shows that the first 7.5 g. to distill over was the aniline-water azeotrope at 98.5°C. The next 23.5 g. came over in a temperature range between 116 and 118°C. Analyses of three fractions in this range showed the presence of aniline and water with increasing amounts of hydrazine as the distillation proceeded. After this point (31 g. distilled) the distillate came over at 118.0° to 118.5°C., near boiling point of the hydrazine-water azeotrope, until all the hydrazine and water were distilled. The temperature then rose toward the boiling point of aniline. All cuts except one taken in this third temperature range analyzed more than 73% hydrazine and from 15 to 18% water. Thus complete dehydration did not occur, as is expected in usual azeotropic-distillation practice, an indication that there was some distillation barrier in the system.

The curve for run 2 shows that the first material to distill over was hydrazine, B.P. 113.5°C. About 40 g. came over at this tem-

perature. The overhead temperature then rose to 116°C. and after about 58 g. had distilled, dropped to 114°C. After an additional 12 g. of vapor was collected, the temperature rose to 117°C. The fractions between 40 and 70 g. distilled contained between 86 and 90% hydrazine and the balance was water. These results also indicated the presence of a distillation barrier in the system.

Figure 2 is a plot of the ternary diagram of hydrazine-water-aniline showing the boiling temperatures of the pure compounds and the two azeotropic mixtures. An inspection of this diagram, together with the results of the distillations described above, suggested the presence of a ridge in the vapor-liquid surface of this ternary system between the hydrazine-water azeotrope and aniline, similar to those present in other ternary systems containing azeotropes, as described by Ewell and Welch(*3*). Additional distillation experiments, to be described later, confirmed this, and the position and curvature of the ridge were determined. These ridges are usually curved and form a distillation barrier, but they can be crossed from the concave side by rectification. They cannot be crossed, however, from the convex side. In the region of these ridges the vapor and liquid surfaces are rather flat and therefore cannot be represented by a sharp line as shown in the figure. Their effect as a distillation barrier occurs over a narrow area across the diagram depicted by the ridge boundaries in the figure.

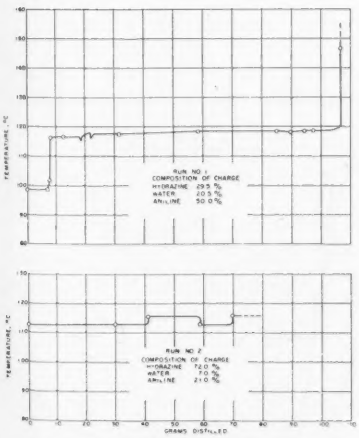

FIG. 1. DISTILLATION CURVES FOR SYSTEM HYDRAZINE - WATER - ANILINE; POINTS REPRESENT QUANTITATIVE DATA; THE SHAPES OF THE CURVES, QUALITATIVE OBSERVATIONS MADE DURING EXPERIMENTS.

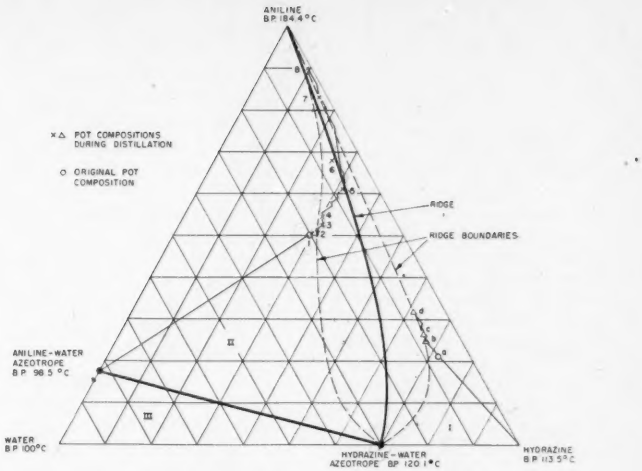

FIG. 2. HYDRAZINE-WATER-ANILINE SYSTEM.

In Figure 2 a line has been drawn connecting the invariant compositions of the azeotropes. This, together with the ridge area, divides the diagram into three fractionation areas. Any ternary mixture lying in area I will, when fractionated, give pure hydrazine in the first overhead vapors because it is the most volatile component in this particular region. A mixture with a composition falling in area II will give the low-boiling aniline-water azeotrope as the first fraction, and likewise a mixture with a composition lying in area III will give the aniline-water azeotrope in the first fraction. A mixture with a composition falling on or near the ridge, where aniline and the hydrazine-water azeotrope may be said to be in equilibrium, will, when fractionated, yield the hydrazine-water azeotrope first.

The mechanism of the two distillations described above can be followed on the diagram in Figure 2 by calculating and plotting the pot compositions throughout the experiments. In the first system (run 1) the original composition (point 1) lies in area II, where the first material to distill over should be the aniline-water azeotrope. Inspection of the distillation curve (Figure 1) shows that this was the case. As long as the pure aniline-water azeotrope came over, the composition of the pot shifted rectilinearly in the opposite direction. After a few grams of this material had distilled, the overhead vapor temperature started to rise rapidly, indicating a change in composition. The composition of the pot at this time is shown by point 2. There was no hydrazine present in the initial overhead fraction. The next three fractions showed increasing amounts of hydrazine by analysis and came over in a fluctuating temperature range close to the boiling point of the hydrazine-water azeotrope. The pot compositions at the end of these fractions (points 3, 4, and 5) were still in area II on the diagram with respect to the crown of the ridge, as indicated by the presence of aniline in the distillate. When the composition of the pot reached point 2, it approached the ridge area, where aniline and the hydrazine-water azeotrope were in equilibrium. Since the hydrazine-water azeotrope was the lower boiling, it appeared in the overhead vapors. While this material was distilling, the pot composition shifted rectilinearly in the opposite direction until its composition moved off the ridge into the area where again the aniline-water azeotrope was the lowest boiling component. After a small amount of the aniline-water azeotrope came over, the pot composition moved back upon the ridge, and the hydrazine-water azeotrope again appeared in the overhead vapors. This stepwise shifting of distillate composition continued until the crown of the ridge was crossed, shortly after the end of the fifth cut (point 5).

Once the crown of the ridge was crossed, the pot composition fell in area I, where it was under the influence of the convex side of the ridge and where pure hydrazine was the most volatile component. However, the material to distill over immediately after the crown of the ridge was crossed was the hydrazine-water azeotrope because the composition of the pot was

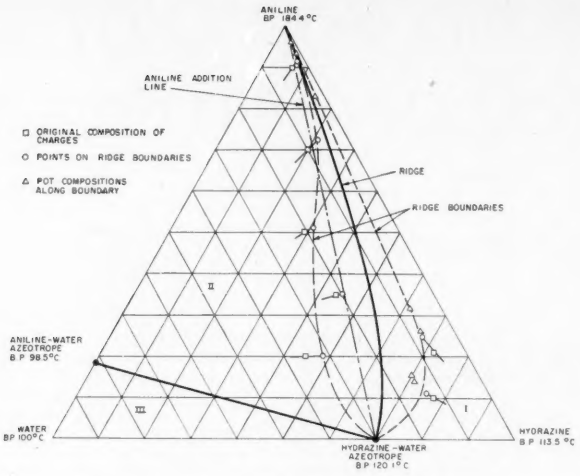

FIG. 3. HYDRAZINE-WATER-ANILINE SYSTEM.

within the ridge boundary. This shifted the pot composition further into area I, and soon pure hydrazine started to come overhead. Hydrazine continued to distill over until the pot composition shifted back to the ridge boundary, where the hydrazine-water azeotrope distilled over again. The distillation from this point on consisted of infinitesimal steps along the ridge boundary, owing to the shifting of the distillate composition, until all the hydrazine and water had been removed.

The temperature of the overhead vapors that came off after the crown of the ridge had been crossed was in the 118 to 118.5°C. range, showing that some of the hydrazine-water azeotrope was present. The composited distillate contained much more hydrazine than the azeotropic proportions. Therefore aniline could be used to increase the concentration of hydrazine in an aqueous solution beyond the azeotrope.

The original pot composition (point *a* in Figure 2) for run 2 was in area I, where hydrazine was the most volatile component, and the first fraction to distill overhead was nearly pure hydrazine. After about 40 g. of over 95% hydrazine had distilled over, the pot composition shifted to the area within the ridge boundary (point *b*) and material with the composition of the hydrazine-water azeotrope started to come overhead. After a few grams of this material came over, the pot shifted past the boundary back into area I. Since in this case the ridge was approached from the convex side, it could not be crossed and the remainder of the distillation was comprised of a continual shifting of the overhead composition between pure hydrazine and the hydrazine-water azeotrope. The pot composition moved along the ridge boundary (points *c* and *d*) toward the point represented by the composition of pure aniline.

LOCATION OF THE RIDGE

Optimum recoveries of high-purity hydrazine depend upon the location and curvature of the ridge and ridge boundaries. To find these quantitatively, several distillation experiments were made in the Todd column with varying amounts of hydrazine, water, and aniline. These are shown in Figure 3.

The straight line between the compositions of aniline and the hydrazine-water azeotrope, called the "aniline-addition line" in Figure 3, represents all possible ternary mixtures obtainable by adding aniline to the azeotrope. In the region of low aniline concentrations, the aniline-addition line was inside the ridge boundary, where very little water could be removed before the distillate became contaminated with hydrazine. Although this area could be narrowed by use of higher reflux ratios, at any reasonable reflux ratio there would be a wide area at low aniline concentrations that would act as an effective distillation barrier. At high aniline concentrations, both the ridge and the ridge boundary were some distance from the aniline-addition line. Since the primary objective was to remove water, the optimum recovery of anhydrous hydrazine would be obtained by distilling a charge farthest removed from the ridge boundary. This would be a charge that contained between 60 and 90% aniline. Additional experiments were made with aniline concentrations above this value, therefore, to determine more precisely the optimum conditions for maximum water removal.

A maximum of about 68% of the water was removed from the hydrazine-water azeotrope at an aniline concentration of 70%. This meant that when the enriched hydrazine solution was separated

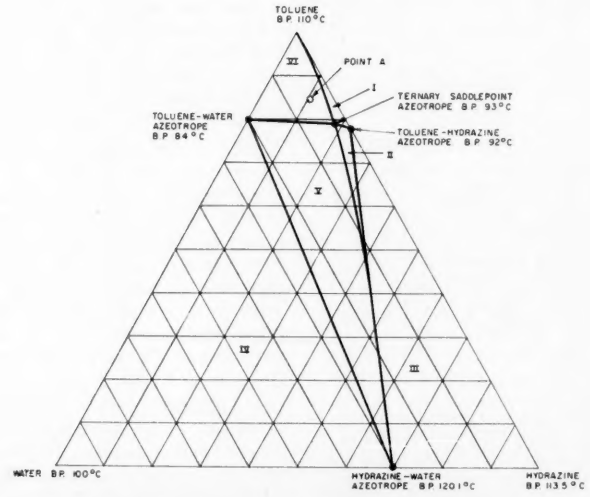

FIG. 4. HYDRAZINE-WATER-TOLUENE SYSTEM.

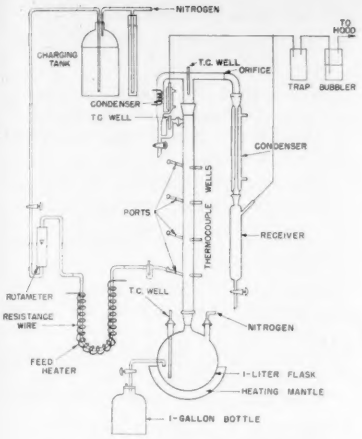

FIG. 5. TWO-INCH DISTILLING COLUMN.

from the entrainer and redistilled, approximately 68% of the original hydrazine could be recovered as anhydrous material. The balance would have to be recycled.

TERNARY SYSTEMS WITH THREE BINARY AZEOTROPES

In the search for a suitable entrainer, cursory experiments were made with materials that formed binary azeotropes with both water and hydrazine. Benzene, toluene, and xylene are representative of this group. These systems have ridges in their vapor and liquid surface similar to the one in the hydrazine-aniline-water system, but they also contain saddlepoint azeotropes, which are azeotropes that boil intermediate to the other invariant components in the system.

Figure 4 is a ternary diagram for the hydrazine - water - toluene system showing the location and boiling points of the binary and saddlepoint azeotropes. Lines connecting the invariant compositions with the ridge divide this system into six fractionation areas. Advantage can be taken of the position of the saddlepoint azeotrope to effect the dehydration of hydrazine if the charge is chosen within the ridge boundary (not shown in the figure), to ensure that the saddlepoint azeotrope is the first fraction to come overhead. For a reasonable recovery, it is also necessary that the composition of the charge be chosen so that when the pot composition shifts rectilinearly in the opposite direction from the ternary azeotrope, it remains within the ridge boundary for a maximum length of time.

A ternary mixture that satisfied these conditions was fractioned to yield a hydrazine solution richer in hydrazine than the azeotropic proportions. The starting ternary feed mixture contained 10.9% hydrazine, 4.7% water, and 84.4% toluene. Point *A* on the diagram represents this composition. About 33% of the hydrazine in the charge came over in a ternary mixture containing 18% hydrazine, 3% water, and 79% toluene. The phases were separated and the aqueous portion, which contained approximately 85% hydrazine, was redistilled to produce an anhydrous product.

DEVELOPMENT OF THE PROCESS

A 2-in. column (*see* Figure 5) that could be operated continuously was built to study the process on a larger scale. This column was packed 37 in. with 1/4-in. glass Raschig rings. There were thermocouple wells equally spaced in the packed section. Opposite each thermocouple well was an opening which could be used either for the entrance of feed or as a sampling port. The reflux head was designed to split the overhead vapors into reflux and product in the vapor phase. An orifice in the product line maintained an 8 to 1 reflux ratio (reflux to distillate), which was very nearly independent of the boil-up rate. The insulation on the column was heated with resistance windings to reduce the heat losses. The still pot was a 5-liter three-necked flask fitted with a thermocouple well and a nitrogen inlet. For continuous operations, an opening in the side of the flask provided for gravity flow out of the pot. The feed flowed to the column from a storage tank through a rotameter and a heater which was made of stainless steel tubing wrapped with resistance wire. A 10-point Micromax (Leeds and Northrup) recorder measured and recorded temperatures throughout the system.

One possible arrangement of distillation equipment for the process comprised three columns in series for the following steps:

1. Removal of about 70% of the water as the aniline-water azeotrope.
2. Separation of the resulting enriched hydrazine solution from the entrainer.
3. Distillation of anhydrous hydrazine from the enriched hydrazine solution.

Each of these steps was performed both batchwise and continuously in the 2-in. column. In continuous distillations made on the first, or water-removal step, and average of 69% of the water charged to the column was removed as the aniline-water azeotrope. The bottoms from step 1 were then fed continuously to the same column to separate the enriched hydrazine solution from the entrainer (step 2). The overhead product from this step averaged 87% hydrazine and the balance water. In step 3 the 87% hydrazine solution was fed continuously to the 2-in. column to produce anhydrous hydrazine. The overhead from this step analyzed 99.9% hydrazine.

PROCESS DESCRIPTION

Figure 6 is a line drawing of a three-column distillation for carrying out the process. The feed to column 1 contains 30% of the hydrazine-water azeotrope and 70% aniline. All the aniline charged is recycled, except a small quantity lost owing to its solubility in water. The first column removes about 70% of the water charged to the column as overhead in the form of the aniline-water azeotrope. The water is separated from the aniline in a phase separator and discarded. The aniline is recycled. The balance of the hydrazine, water, and aniline is taken off as bottoms

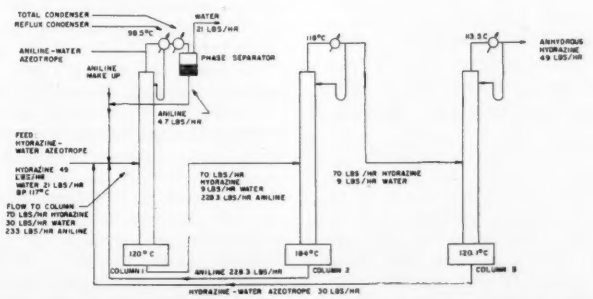

FIG. 6. PROCESS FOR DEHYDRATING HYDRAZINE HYDRATE BY AZEOTROPIC DISTILLATION WITH ANILINE AS AN ENTRAINER.

and charged to column 2. This column separates the entrainer (aniline) from the 88.6% aqueous hydrazine solution, which is taken overhead, the aniline bottoms being recycled to make up part of the feed to the first column. The enriched hydrazine solution from the second column is fed to column 3, where it is separated into anhydrous hydrazine as overhead and the hydrazine-water azeotrope as bottoms. The bottoms, which contain about 30% of the hydrazine feed to the first column, are recycled.

CONCLUSIONS

Aqueous solutions of hydrazine can be economically dehydrated by azeotropic distillation in a multicolumn distillation system with aniline as an entrainer. Although the ridge in the vapor-liquid surface of the ternary system necessitates some recycle of the hydrazine, under optimum operating conditions about 70% of the hydrazine charged to the system can be recovered in one pass through the columns as essentially anhydrous material. The process is patented (*7*).

ACKNOWLEDGMENT

This research was sponsored by the Mathieson Chemical Corporation at Battelle Memorial Institute. The authors wish to thank them for their permission to publish the results of this work.

LITERATURE CITED

1. Anonymous, *Chem. Week*, p. 77 (Dec. 12, 1953).
2. Audrieth, L. F., and B. Ackerson, "The Chemistry of Hydrazine," John Wiley and Sons, Inc., New York (1951).
3. Ewell, R. H., and L. M. Welch, *Ind. Eng. Chem.*, **37**, 1224 (1945).
4. Lecat, M., "L'Azeotropisme," Lamertin, Brussels (1918).
5. Penneman, R. A., and L. F. Audrieth, *Anal. Chem.*, **20**, 1058 (1948).
6. Wilson, R. Q., H. P. Munger, and J. W. Clegg, *Chem. Eng. Progr., Symposium Ser.* 3, 48, 115 (1952).
7. Bircher, J. R., Jr., U. S. patent 2,698,286 (Dec. 28, 1954).

Presented at A. I. Ch. E. Louisville meeting

GAS ABSORPTION IN BEDS OF RINGS AND SADDLES

MAX LEVA

Consulting Chemical Engineer

New data are presented for the system carbon dioxide—sodium hydroxide. The effect of $CO_3^=$ build-up upon K_Ga values was investigated first and the data were then used to construct a curve by means of which all data were corrected to an arbitrarily chosen reference state of 25% $CO_3^=$ concentration. K_Ga values increased with increasing liquid rate but were not dependent on gas rate if the packings were operated below loading. For some packings examined in the loading range, however, K_Ga values increased with increasing gas rate.

***K_Ga* values examined in relation to specific surface area were found to be very irregular in connection with rings. The surface-area utilization pattern of the saddles was considerably more uniform. The ring and saddle data for the carbon dioxide–sodium hydroxide system were in good qualitative agreement with the ammonia absorption data of Fellinger and the water–water vapor data of Mehta and Parekh.**

The object of this paper is to describe the behavior of rings and saddles in gas absorption. Capacity data have been observed for a wide range of conditions, and conclusions on surface-area utilization are presented. Another object of the paper is to ascertain the data level of capacity coefficients for the new Intalox saddle packing. The carbon dioxide–sodium hydroxide system was chosen for the comparison because equilibrium conditions are established quickly in the column, the analytical procedure is simple, and the liquid film seems to offer the controlling resistance. Since data sufficiently complete to permit a packing-behavior comparison are already available for the systems NH_3-H_2O (partly gas-film controlled and $(H_2O)_l$ — $(H_2O)_g$ (wholly gas-film controlled), procurement of the present liquid-film–controlled data will permit a general packing-performance analysis.

Leva Engineering Research Laboratories, 808 Beaver Avenue, Pittsburgh 33, Pennsylvania.

LITERATURE

In a study of this kind, where the relative merits of packings are to be evaluated, careful attention must be given to the construction of the experimental tower, to the analytical procedure adopted, and to the range of variables explored. Above all, it must be shown that for the system considered, the broad findings of others and the corresponding new results are in substantial agreement. A summary of the principal experimental conditions and results of earlier reported work for the carbon dioxide–sodium hydroxide system is given in Table 1. The data of Blum, Stutzman and Dodds (*2*) are of only general interest, since the columns and packings were small. Of greater interest is the work of Stutzman and Dodds (*11*); although they reported cocurrent flow data, having worked with liquid and gas rates far in excess of the present flows, some of their quantitative effects of carbonate build-up upon the data level have been noted and incorporated. The tower of Greenwood and Pearce (*6*) was suitably large, but their operating pressure (5.4 atm.) was sub-

stantially above the present atmospheric pressure and for this reason a direct comparison with the present data is not feasible. The Greenwood and Pearce work corresponds rather closely to that of Spector and Dodge (*10*), but whereas the latter report that capacity data are both liquid- and gas-film controlled, Greenwood and Pearce conclude that the gas-film alone offers appreciable resistance to mass transfer. Except for column height, the experimental conditions of Tepe and Dodge (*12*) correspond most closely to the conditions of the present work. Consequently most of their conclusions as well as the data level of their capacity data could be confirmed.

EXPERIMENTAL

The pilot plant unit is shown in Figure 1. The standard 8-in. pipe was charged in all cases with 9 1/2 ft. of packing. Before charging the tower was filled to 70% of its height with water and the packings were slowly poured from the container. Resulting packing densities and other properties are given in Table 2. The distributor was a sprinkler head, with holes sufficiently small to assure "full spread," even with the lowest irrigation rate. It was placed about 8 in. above the packing, and only the packing (not the wall) was thus initially irrigated. A series of strainers placed ahead of the distributor kept it clean.

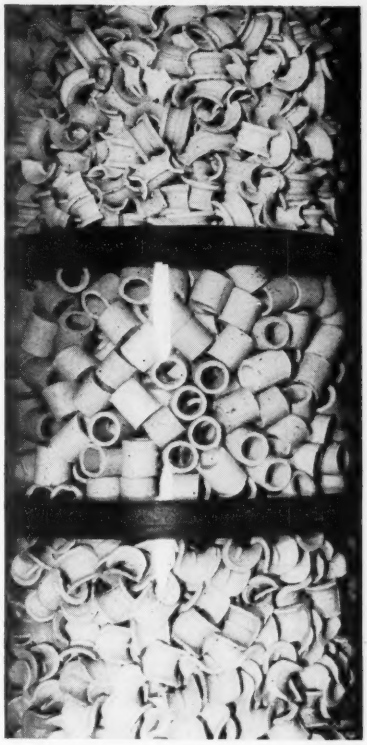

FIG. 2. TWELVE-INCH-DIAMETER TOWER SECTION PACKED WITH ONE-INCH RINGS AND SADDLES.

FIG. 3. A FEW MUTUAL COMBINATIONS OF INTALOX SADDLES.

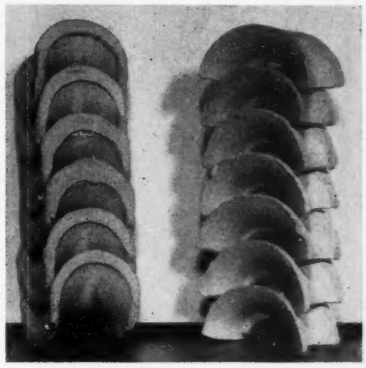

FIG. 4. STACKED BERL AND INTALOX SADDLES.

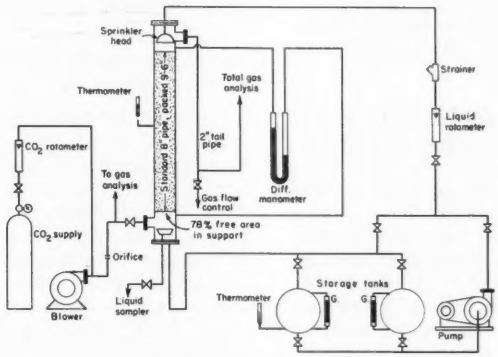

FIG. 1. EXPERIMENTAL UNIT.

The carbon dioxide content of the gas was usually about 1.5%. In some instances (when gas mass velocities were low and carbon dioxide removal was sometimes 95% or more complete), 4 to 6% carbon dioxide was required in the inlet gas, so that the exit carbon dioxide concentration would still be measurable with the chosen analytical procedure. The sodium hydroxide concentration was always close to 1.0 *N* (4% sodium hydroxide). The solution was frequently renewed to prevent high carbonate build-up, the only exception being one series of runs where with 1-in. Intalox saddles the same solution was used virtually to complete carbonation. The object was to ascertain the effect of carbonate build-up on the coefficients. Solution temperatures ranged from 75 to 81°F. During absorption no appreciable temperature rise was noted.

The liquor sampler was a shallow trough communicating with the outside by way of a 1/4-in. pipe and valve. The trough extended virtually over the entire column diameter and thus representative liquid samples were collected. The carbon dioxide gas, preliminarily metered by a small rotameter, was conducted into the air on the up-stream side of the metering orifice. Gas rate through the column was controlled by manipulation of a 2-in. slide valve at the end of the 2-in. tail pipe. Solution storage was sufficient to permit operation for at least 30 min. before collection of gas and liquid samples was begun. This was more than ample time to establish steady state conditions.

The gas samples were analyzed with a Haldane gas burette (*1*). Analytical results could easily be duplicated within ±3%, which was better than the reproducibility of the tower operation. Check runs, made frequently, were always better than ±10%. Material balances ranged between 93 and 111%. The liquor was analyzed for total alkalinity by use of methyl orange as indicator. Carbonate was determined by precipitation with an excess $BaCl_2$ and titration of the free sodium hydroxide, with phenolphthalein as indicator.

PACKINGS

Packing characteristics pertaining to the 8-in. pilot plant unit are

TABLE 1.—SUMMARY OF LITERATURE—CARBON DIOXIDE—SODIUM HYDROXIDE

Authors	Tower diameter, in.	Packed height, ft.	Packings investigated	Working pressure, atm.	Liquor normalities	Liquid rates, lb./(sq. ft.) (hr.)	Gas rates, lb./(sq. ft.) (hr.)	Approx. CO_2 inlet conc.
(2)	2.8–4.0	2.8–4.33	¼ to ½-in. rings (ceramic)	1	.....	.....	.....	3–28%
(6)	8	up to 4	¾-in. metal Lessing rings, ½ and 1-in. Raschig rings	5.4	2–2.5	600–22,000	150–700	300 p.p.m.
(10)	12	10–16	¾-in. Raschig rings and 1-in. Berl saddles	1–6	2.5	800–14,000	270–950	300 p.p.m.
(11)	18	10–15	1- , 1½-in. ceramic Berl saddles, 2-in. metal rings	1				
(12)	6	3	½-in. carbon rings	1	0.75–4.0	700–9,600	100–440	1–5%
This work	8	9.5	1-in. metal rings, 1, ¾, ½-in. Raschig rings, Berl saddles, Intalox saddles	1	1.0	380–3,200	215–1,000	1–6%

given in Table 2. The data are as expected and in satisfactory accord with large-scale commercial-tower observations. Probably of most immediate interest is the considerably higher packing population that prevails in a bed of saddles as compared with a bed of rings of equivalent size. It is believed that this property, yielding to the generally larger specific packing surface of the saddles, is responsible for the fundamentally different behavior of the saddle packings as compared with the ring packings. The difference in packing arrangement between rings and saddles is apparent from Figure 2, which shows sections of a 12-in.-diam. glass column, packed with 1-in. nominal-size Intalox saddles (top), Berl saddles (bottom), and Raschig rings (center). The rings show predominant pattern packing, both "in parallel" as well as "in series." The Berl saddles show practically no in-parallel pattern packings, though stacking and series packing is observed. The Intalox saddles exhibit no pattern packing of any kind. An essential packing difference between saddles and the rings is achieved because saddles represent an open shape, whereas

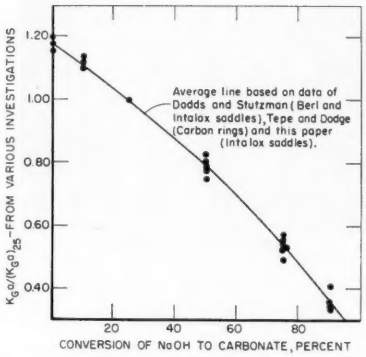

FIG. 5. EFFECT OF CARBONATE BUILD-UP ON $K_G a$.

rings, being closed packings, do not have mutual interlocking features. As far as saddle characteristics are concerned, the packing population in Intalox saddle beds is substantially higher than in Berl saddle beds of comparable nominal size, as reported in Table 2, because of the difference in the two saddle shapes. Intalox saddles, being of a more irregular shape (7), will permit a large number of mutual combinations with each other. A few such combinations, shown in Figure 3, represent the basic arrangements in the Intalox saddle bed. Since Berl saddles are of a more regular shape, their combinations are fewer and the tendency to pack in patterns is encouraged. This is the more true since the prevalent packing pattern that Berl saddles tend to assume possesses a high degree of mechanical stability. Stacked saddles, both Berl as well as Intalox, are shown in Figure 4. The more labile arrangement of the Intalox saddles and the ready area accessibility between pieces are apparent.

VARIABLES AND DATA EVALUATION

Packings investigated were 1/2-, 3/4-, and 1-in. ceramic Raschig rings and Berl and Intalox saddles. A few results, observed with 1-in. steel Raschig rings, were also reported. Since mass transfer rates will decrease as the carbonate ion concentration in the liquor increases, and because with the relatively high tower a substantial carbonate build-up in the descending liquor can result, a series of tests was desirable that would permit recognition of this fact and

TABLE 2.—PACKING CHARACTERISTICS

Packings	Number of pieces/cu. ft.	Percentage voids	Weight/cu. ft., lbs.	Specific surface area, sq. ft./ft.^{3}
1-in. metal rings	1,290	93	36	56
1-in. Raschig rings	1,440	73	39	62
1-in. Berl saddles	1,770	72	43	61
1-in. Intalox saddles	2,270 (2,160)	78 (79)	32 (30.5)	74 (71)
¾-in. Raschig rings	3,300 (3,450)	72 (71)	47 (49)	84 (88)
¾-in. Berl saddles	4,410	70	46	73
¾-in. Intalox saddles	6,930	75	37	109
½-in. Raschig rings	10,800	64	55	125
½-in. Berl saddles	13,300	67	50	117
½-in. Intalox saddles	17,100	76	33	157

possible adjustment of the capacity coefficients to a standard state. The carbonate concentration build-up in the liquor could of course be minimized by resorting to shorter packed heights, which would, however, lead to questionable results because of the then pronounced end effects and also because of possible insufficient opportunity for the liquid flow pattern to develop. Thus the data may not embody one of the characteristic packing features (namely the establishment of the internal liquid distribution pattern). Another objection to

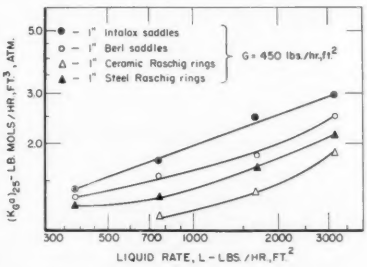
● – 1" Intalox saddles
○ – 1" Berl saddles
△ – 1" Ceramic Raschig rings
▲ – 1" Steel Raschig rings
G = 450 lbs./hr.,ft.²
$(K_G a)_{25}$ – LB. MOLS/HR.,FT.³,ATM.
LIQUID RATE, L – LBS./HR.,FT.²

FIG. 6. CORRECTED 1-IN. PACKING DATA FOR SYSTEM CARBON DIOXIDE–SODIUM HYDROXIDE; GAS RATE CONSTANT.

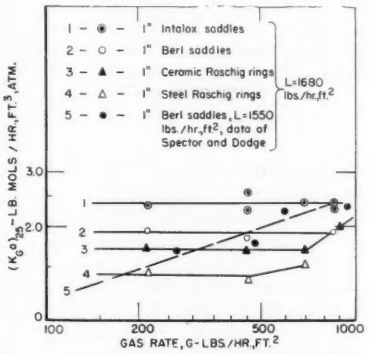
1 – ● – 1" Intalox saddles
2 – ○ – 1" Berl saddles
3 – ▲ – 1" Ceramic Raschig rings
4 – △ – 1" Steel Raschig rings
5 – ● – 1" Berl saddles, L=1550 lbs./hr.,ft², data of Spector and Dodge
L=1680 lbs./hr.,ft.²
$(K_G a)_{25}$ – LB. MOLS / HR.,FT.³,ATM.
GAS RATE, G-LBS./HR.,FT.²

FIG. 7. CORRECTED 1-IN. PACKING DATA FOR SYSTEM CARBON DIOXIDE–SODIUM HYDROXIDE. LIQUID RATE CONSTANT.

smaller heights would be the reduced accuracy of the data, caused by small concentration differences of carbon dioxide in the gas streams; on the other hand, the more concentrated the liquor the smaller will be the rate of carbonate build-up. But here too difficulties will arise, caused primarily by the higher liquor viscosity, which has a bearing on initial liquor distribution to the top of the packing. In consideration of these factors it was decided to work with a normal sodium hydroxide solution (4%) and an inlet gas stream that contained ordinarily about 1 to 2% carbon dioxide.

The effect of carbonate build-up upon the coefficients was noted first.* Since the liquor, carrying CO_3 ions exerts no appreciable CO_2 partial pressure(*3*), over-all coefficients were calculated from the equation

$$K_G a = \frac{N}{h \times A \times \Delta p_{lm}}.$$

In this equation the symbols are as follows:

N = lb.-moles of solute gas transferred/hr

h = packed height, ft.

A = tower cross-sectional area, sq. ft.

Δp_{lm} = logarithmic mean partial pressure of solute in gas stream

$K_G a$ = over-all capacity coefficient, lb.-moles/(hr.)(cu.ft.)(atm.)

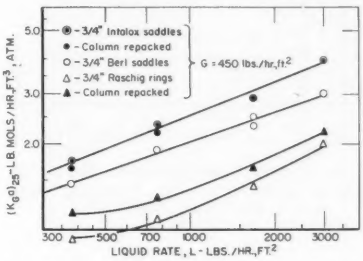
● – 3/4" Intalox saddles
● – Column repacked
○ – 3/4" Berl saddles
△ – 3/4" Raschig rings
▲ – Column repacked
G = 450 lbs./hr.,ft.²
$(K_G a)_{25}$ – LB. MOLS/HR.,FT.³,ATM.
LIQUID RATE, L – LBS./HR.,FT.²

FIG. 8. CORRECTED ¾-IN. PACKING DATA FOR SYSTEM CARBON DIOXIDE–SODIUM HYDROXIDE; GAS RATE CONSTANT.

For the purpose of ascertaining the carbonate ion effect, liquor and gas rates were kept constant and the arithmetic-average carbonate concentration was calculated between top and bottom. The resulting graph served as basis for preparation of Figure 5. $K_G a$ at 25% conversion to carbonate, $(K_G a)_{25}$, was arbitrarily chosen as reference state. The course of the curve of Figure 5 is also supported by some data of Stutzman and Dodds(*11*), as well as of Tepe and Dodge(*12*). As expected, the effect of carbonate concentration build-up, being essentially a saturation-diffusion phenomenon in the liquor, is not dependent on packing. Hence the curve of Figure 5 was used to refer all the data to the 25% carbonate reference state.

Effect of solution rates on the capacity coefficients is obtained from Figures 6, 8, and 10. In Figures 7, 9, and 11, capacity data are shown in relation to gas rate. The effect of repacking the column and the reproducibility of the performance both for Intalox saddles and rings may be observed from Figure 8. As the loading state of the packings is approached, capacity data will increase, as may be observed from Figure 12.

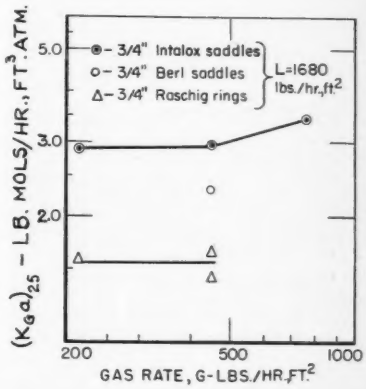

FIG. 9. CORRECTED ¾-IN. PACKING DATA FOR SYSTEM CARBON DIOXIDE–SODIUM HYDROXIDE; LIQUID RATE CONSTANT.

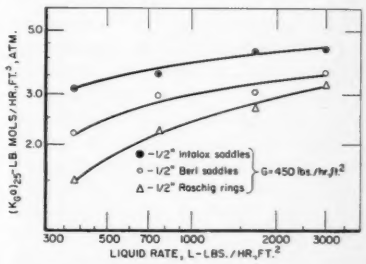

FIG. 10. CORRECTED ½-IN. PACKING DATA FOR SYSTEM CARBON DIOXIDE–SODIUM HYDROXIDE; GAS RATE CONSTANT.

DISCUSSION

Irrigation Rate Dependence. Consideration of the effect of liquid rate on the coefficients indicates that for all packing and sizes, $K_G a$ increases as the irrigation rate increases. The relationship may be approximated by $(K_G a) \propto L^n$, where n is the slope of the individual data. It is found to vary from approximately 0.35 for the large to 0.18

*Complete original data may be ordered from the Photoduplication Service, American Institute of Documentation, Library of Congress, Washington 25, D.C., as document 4564 for $1.25 for microfilm or photoprints.

for the small packings. For the larger size rings $K_G a$ is almost independent of irrigation rate when the latter is low. These variations of the slope value are doubtlessly associated with area utilization in the packed bed. No definite conclusion may be formulated, though, because irrigation rate will influence not only area utilization but the K_G portion in the capacity data as well. Since it is doubtful whether the effect of liquid rate upon K_G can be accurately determined in a packed bed, the data of Figures 6, 8, and 10 are not helpful to give a definite indication as to surface-area utilization.

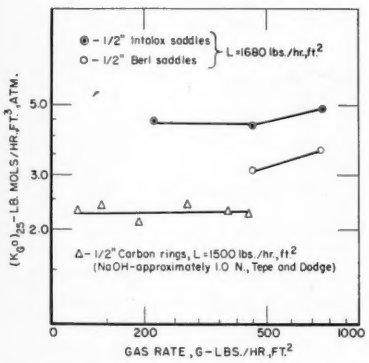
● - 1/2" Intalox saddles
○ - 1/2" Berl saddles
L = 1680 lbs./hr.,ft²
Δ - 1/2" Carbon rings, L = 1500 lbs./hr.,ft²
(NaOH - approximately 1.0 N., Tepe and Dodge)
(K_G a)_av - LB. MOLS/HR.,FT³,ATM.
GAS RATE, G - LBS./HR.,FT²

FIG. 11. CORRECTED ½-IN. PACKING DATA FOR SYSTEM CARBON DIOXIDE–SODIUM HYDROXIDE; LIQUID RATE CONSTANT.

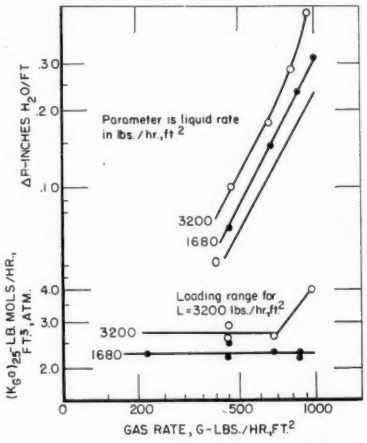
Parameter is liquid rate in lbs./hr.,ft²
3200
1680
0
Loading range for L = 3200 lbs./hr.,ft²
ΔP - INCHES H₂O/FT
(K_G a)_av - LB. MOLS/HR., FT³, ATM.
GAS RATE, G - LBS./HR.,FT²

FIG. 12. ABSORPTION AND PRESSURE DROP DATA FOR 1-IN. INTALOX SADDLES.

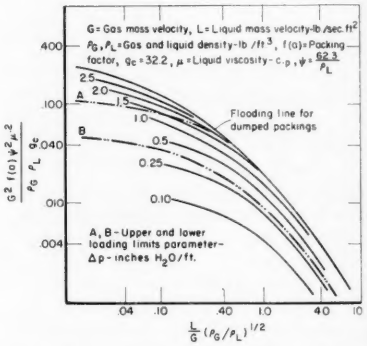
G = Gas mass velocity, L = Liquid mass velocity-lb./sec.ft²
Flooding line for dumped packings
A, B - Upper and lower loading limits parameter - Δp - inches H₂O/ft.

FIG. 13. GENERALIZED PRESSURE DROP FLOODING CORRELATION FOR DUMPED PACKINGS.

In all instances it is found that Intalox saddles give the highest capacity data; Berl saddles are next; and Raschig rings are lowest. Except for the 3/4-in. packings, the difference between Intalox and Berl saddles is equivalent to the difference between the latter and Raschig rings. It is of interest to note that the order of magnitude of the coefficients does not conform with the surface area offered by the individual packings.

The 1-in.-metal-ring data are significantly lower than the 1-in.-ceramic-ring data. The difference may be due to a number of reasons, of which the following may be the most likely. Since the metal rings have a considerably thinner wall than the ceramic rings, the free space in the metal-ring bed is much greater than in the ceramic-ring bed. Therefore, the metal rings will, for given liquid and gas rates, be in a lower state of loading than the ceramic rings. Aside from the state of loading, surface characteristics, as caused by material of construction, may be involved. Thus it is conceivable that the aqueous liquor will spread into films more readily over a ceramic than over a metal body.

The effect of repacking the column is observed from Figure 8. Table 2 shows the packing densities for the two Intalox charges and the two Raschig ring charges. The reproducibility observed with Intalox saddles is very satisfactory. Since Intalox saddles have virtually no tendency to pattern pack this is to be expected. The rings, on the other hand, show that the process of repacking (floating into water in both cases) causes a significant variation in the capacity data. This is obviously due to pattern-packing tendencies which are not controllable in ordinary packing operations. Severe differences in performance have been reported both in the field as well as in research (*4a*).

Gas-Rate Dependence. From Figures 7, 9, and 11, it may be concluded that $K_G a$ data are independent of gas rates when the latter are low. At higher gas rates $K_G a$ will increase with G sooner as one progresses from Intalox saddles to Berl saddles and finally to Raschig rings. This trend is caused by the effect which gas rate exerts on the holdup in the packing. As the loading range is approached (through an increase in gas rate) the packing-surface area will be utilized to a greater extent. Approach to loading is indicated by the pressure-drop data of Figure 12. Thus for a gas rate of, say 900, and a water rate of 3,200, lb./(hr.)(sq.ft.) the coordinates for Figure 13 (*8*) become 0.0404 and 0.123. Location of the point on the graph discloses that operation occurs in the loading range with a pressure drop of about 0.5 in. of water/ft., in agreement with the experimental value.

The gas-rate dependence of the Spector and Dodge (*10*) 1-in. Berl-saddle data, shown in Figure 7, is not due to approach to the loading range; it is a genuine gas-rate dependence, probably caused by the very dilute carbon dioxide concentration in the gas. At a solute concentration of only 300 p.p.m., absorption from the gas film may be rapid when compared with a possibly slower step of diffusion of carbon dioxide from the main body of the gas through the film. The carbon-ring data of Tepe and Dodge (*12*), shown in Figure 11, are not gas-rate dependent. For their highest gas rate of 430 and a liquid rate of 1,500 lb./(sq.ft)(hr.), the coordinates for Figure 13 become 0.0257 (packing factor 270) and 0.120, a location well below the loading range. The present study is not only in agreement with the Tepe and Dodge work on the matter of singular liquid film control, but the general data level of the two studies are also in satisfactory agreement. The present data may, therefore, be used for a further comparison of ring and saddle behavior.

$K_G a$ vs. Specific Surface Area. Specific surface-area evaluations of the packings tested are given in Table 2. In Figure 14 corrected coeffi-

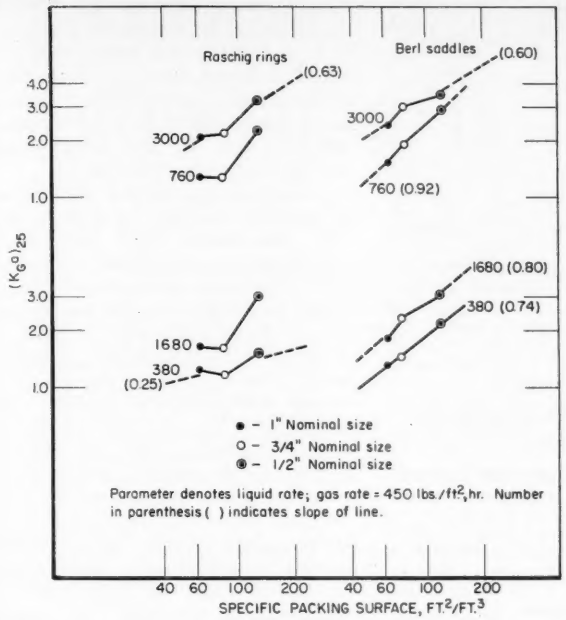

FIG. 14. RASCHIG AND BERL SADDLE DATA FOR SYSTEM CARBON DIOXIDE–SODIUM HYDROXIDE.

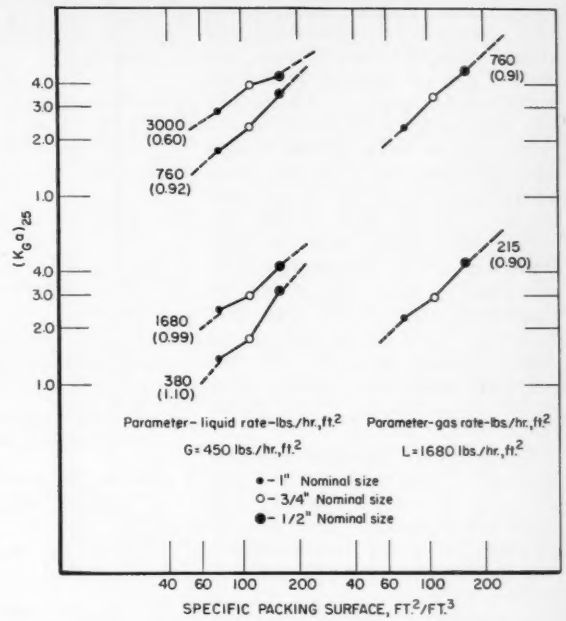

FIG. 15. INTALOX SADDLE DATA FOR THE SYSTEM CARBON DIOXIDE–SODIUM HYDROXIDE.

cients have been related to specific surface areas for Raschig rings and Berl saddles. The same type of data are given in Figure 15 for Intalox saddles. Gas rate is constant for all the data [450 lb./(sq. ft.)(hr.)]. For each set liquid rate is constant, as indicated; hence the data for the various nominal-size rings and saddles may now be compared with each other. The fundamentally different behavior of rings and saddles is immediately apparent. Proceeding from 1-in. saddles to the 1/2-in. size, there results a relatively steady increase in the coefficients. The rings, on the other hand, show no increase in coefficients between the 1-in. and 3/4-in. size. In fact, at the lowest liquid rate the coefficient for the 3/4-in. Raschig ring is actually lower than for the 1-in. ring. This retrograde result is surprising, especially because the total specific surface area of 3/4-in. Raschig rings is substantially higher than that of 1-in. rings. Even for the highest flow rate the coefficients do not recover sufficiently to rise convincingly above the 1-in.-size level. The conclusion which must be drawn from this observation is that, although with the 1-in. rings a certain modest fraction of the inside surface area of the packing may be effective contacting area, the value of the inside surface area of the 3/4-in. size is very small. This observation is supported by the fact that there is an approximate numerical equality between the total outside surface area of the 3/4-in. rings and the combined outside and inside surface areas of the 1-in. size. The foregoing retrograde phenomenon, observed at low liquid rates, points to the possibility that there may be preferential liquid flow through the inside of the packing and preferential gas flow on the outside or vice versa. The two streams would thereby be well separated from each other, a result that should lead to low coefficients. In view of such possibilities one may well wonder whether it is at all significant to measure surface-area utilization in rings (and perhaps in packings in general) by mechanical means alone, that is, in the absence of mass transfer. When the Raschig-ring data are considered further, the rapid increase in the coefficients as one proceeds to the 1/2-in. size is understandable from the very large accompanying surface-area increase. The outside 1/2-in. ring area is significantly in excess of the total 3/4-in. ring area. The inside-surface-area contribution of 1/2-in. rings is probably nil.

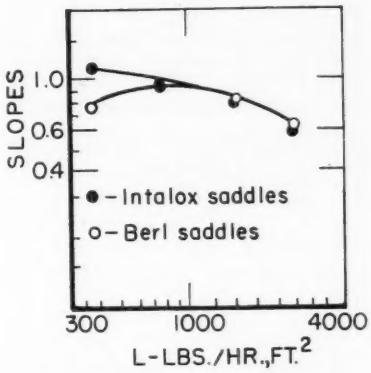

FIG. 16. SLOPE VALUES FROM FIGURES 14 AND 15.

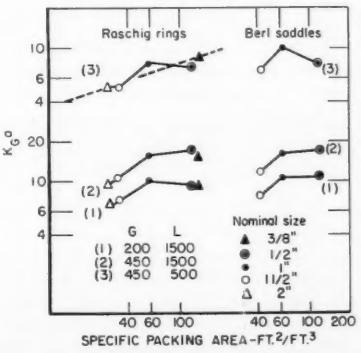

FIG. 17. DATA OF FELLINGER (NH_3-H_2O).

The saddles, being open packings, do not show a retrograde effect. The slopes of the data are an indication of the area utilization. Slopes have been evaluated for the four liquid rates and plotted in Figure 16. For flows beyond 1,000 lb./(sq.ft.)(hr.) area utilization in both Intalox and Berl saddles seems

equally good. At low flows, such as are observed in distillation columns, Intalox slope values are higher, and the packing utilizes its surface area more effectively than do Berl saddles. At high liquid rates and in beds of small packings, surface-area utilization drops off for both packings. At the particular limiting rate (3,000 lb./(sq.ft.)(hr.) when water is used) individual small streams and rivulets form in the column and become sufficiently heavy that they may no longer be broken up by small packing elements. At this point cascading flow begins, causing a reduction in effective gas-liquid contact area.

From Figure 15 it is apparent that only liquid rate has an effect on area utilization. The two sets of data for gas rates, 760 and 215 lb./sq.ft.)(hr.) and the accompanying liquid rate of 1,680 are conditions sufficiently below loading that no effect on the coefficients is observed.

Essentially all the observations made so far on surface-area utilization may be substantiated by the extensive data of Fellinger—NH_3-H_2O system—(*5*) and Mehta and Parekh — H_2O_l-H_2O_g — (*9*). Their data are reproduced in Figure 17 and 18. Fellinger observes retrograde effects with 1/2-in. and 3/8-in. Raschig rings. The retrograde effects disappear at elevated liquid rates. In general, surface-area utilization in rings improves as irrigation rate increases. Gas rate affects the over-all data level, but not significantly the extent of area utilization for the various sizes. The ring data are in reasonable agreement with the finding of Dodge and Dwyer(*4*), who report that in ammonia absorption K_Ga varies as the 0.45 power of the specific surface area. The behavior of the Berl saddles is similar, as already described. The Mehta and Parekh data lead essentially to the same observations. Retrograde effects are observed with rings. These effects are minimized and may wholly disappear as flows increase. The Berl-saddle behavior is strictly analogous to the present CO_2-NaOH results and the NH_3-H_2O data of Fellinger. The approach to cascading flow is apparent as the irrigation rate increases.

The difference between ring and saddle behavior is reflected in the character of the holdup data (Figure 19). As expected, holdup increases for all packing as irrigation rate increases. Slopes reveal

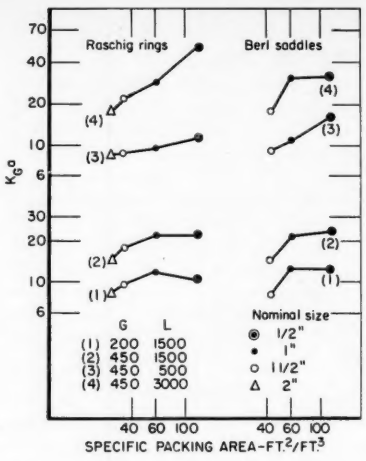

FIG. 18. DATA OF MEHTA AND PAREKH (H_2O GAS–H_2O LIQUID).

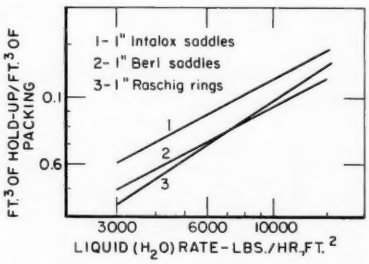

FIG. 19. HOLDUP DATA FOR RINGS AND SADDLES.

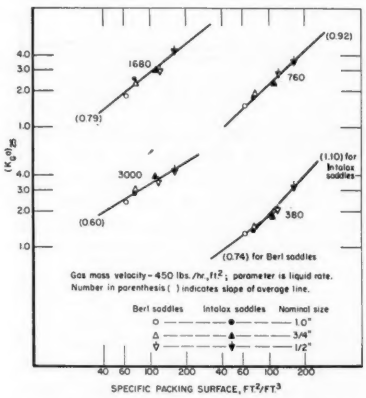

FIG. 20. COMPARISON OF SADDLE DATA FOR THE SYSTEM CARBON DIOXIDE–SODIUM HYDROXIDE.

that for the two kinds of saddles the rate of increase is the same, but is considerably higher for the Raschig rings. Significantly, at low irrigation rates the holdup is lower in rings than in saddles. The situation tends to reverse at higher liquid rates. One possible explanation is that at the low irrigation rate the liquid flows preferentially at the outside of the rings; whereas at higher rates, an ever increasing fraction of the inside-ring voidage becomes effective.

A comparison of the two types of saddles is shown in Figure 20. The observation that both Berl and Intalox-saddle data correlate (for the high irrigation rates) along one singular line indicates that at these rates area utilization in beds of both packings is about equal. The higher coefficients observed with Intalox saddles (as compared with the same nominal-size Berl saddles) are due chiefly to the higher surface area that is provided by the Intalox-saddle bed. At the low irrigation rate the higher slope of the Intalox data reveals improved area utilization. As far as order of magnitude is concerned, it is noted [in accord with Stutzman and Dodds(*11*)] that as a rule Berl saddles will give the same coefficients as the next larger nominal size of Intalox saddles.

LITERATURE CITED

1. Berger, L. B., and H. H. Schrenk, *U. S. Bur. Mines Inform. Circ.*, 7017 (1938).
2. Blum, H. A., L. F. Stutzman, and W. S. Dodds, *Ind. Eng. Chem.*, **44**, 12, 2969 (1952).
3. Dee, T. P., *Trans. Soc. Chem. Ind.*, 1 (1945).
4. Dodge, B. F., and O. E. Dwyer, *Ind. Eng. Chem.*, **33**, 485 (1941).

4a. Dell, F. R., and H. R. C. Pratt, *Trans. Inst. Chem. Engrs. (London)*, **29**, 89-109 (1951).

5. Fellinger, L., Sc.D. thesis, Mass. Inst. Technol. (1941).
6. Greenwood, K., and M. Pearce, *Trans. Inst. Chem. Engineers (London)*, **31**, 201-7 (1953).
7. Leva, Max, U. S. patent 2639909 (May 26, 1953).
8. Leva, Max, "Tower Packings and Packed Tower Design," 2 ed., The U. S. Stoneware Company, Akron, Ohio (1953).
9. Mehta, J. J., and R. H. Parekh, S.M. thesis, Mass. Inst. Technol. (1939).
10. Spector, N. A., and B. F. Dodge, *Trans Am. Inst. Chem. Engrs.*, **42**, 827-48 (1946).
11. Stutzman, L. F., and W. S. Dodds, Paper presented at A.I.Ch.E. in Springfield meeting (1954).
12. Tepe, J. B., and B. F. Dodge, *Trans. Am. Inst. Chem. Engrs.*, **39**, 255-76 (1943).

Presented at A.I.Ch.E. New York meeting.

LIQUID FILMS IN VISCOUS FLOW

A trace of radioactive material dissolved in a liquid enables the thickness of a moving film to be determined by measurement of the radiation emitted. The method is rapid and accurate and an average thickness is obtained directly even though the surface of the film may be irregular. Six liquids, having viscosities ranging from 0.5 to 20 centipoises were observed in flow down the inner wall of a vertical tube. Liquids having viscosities of about 1 centipoise or less exhibit typical viscous behavior with respect to film thickness even when waves are present. Liquids having larger viscosities give values of the film thickness which are less than for true viscous flow. The departure from normal behavior increases with increasing viscosity and occurs only over the region where the liquid moves in wave flow. Surface tension is not a factor in either wave formation or wave flow.

The wave motion appears at flow rates well within the viscous region and occurs when the Froude number exceeds unity. Equations derived for the viscous flow of liquid films on the inner wall of a vertical tube would be required where tube diameter is small or liquid viscosity large. Ordinarily the less complex equations for flow down a flat plate may be used. A theory of flow in the viscous region with waves present is suggested.

MELBOURNE L. JACKSON
University of Colorado, Boulder

Liquid films are encountered in some types of heat and mass transfer equipment, both industrial and experimental, and are of general interest to hydrodynamical theory. The importance of the mechanics of film flow to the analysis of performance of industrial equipment has recently been discussed(*4*). Several different approaches have been employed in measuring film thicknesses, a procedure that is complicated by the fact that the liquid may assume a wave motion at flow rates well within the viscous flow region.

Kirkbride(*12*) made direct measurements with a micrometer and reported that the thickness at the wave peak was several times the thickness of the film expected for normal laminar flow. Others(*3, 5*) obtained average film thickness by measuring drainage after stopping the flow of liquid simultaneously at the top and bottom of a vertical tube. This method gave satisfactory results at moderate flow rates but was subject to timing errors at high rates. It was reported that in spite of the considerable height of the wave crests, the flow behavior was that expected for true viscous flow. However, recent work has shown that when waves are present the apparent surface velocity is greater than normal(*6, 10*), and for the mass transfer process in a wetted-wall column(*9, 11, 16*) liquid-film resistances are negligibly small, possibly because of a mixing action occurring in the film.

Heat transfer to and through liquid films on column walls has been observed, particularly in the case of condensing vapors(*2*), and the heat transfer rate is above that which would be expected from viscous theory. A portion of the viscous region for flow with a free surface thus exhibits an anomalous behavior and additional information was desired. The use of radioactive tracers offers an excellent method of observing film thickness without disturbing the flow pattern.

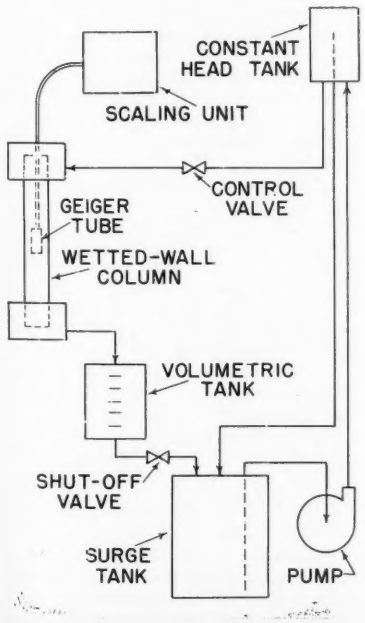

FIG. 1. FLOW DIAGRAM FOR THE MEASUREMENT OF FILM THICKNESS BY USE OF RADIOACTIVE ISOTOPES.

METHOD OF USING RADIOACTIVE TRACERS

A trace of a radioactive isotope is dissolved in a liquid which is made to flow as a film down the inner wall of a vertical tube. A Geiger-Mueller tube positioned at the center of the vertical tube registers the radioactivity emitted by the liquid. The activity observed depends on the thickness of the liquid film. Samples of the liquid must be analyzed for the concentration of radioactivity because absorption may cause changes in

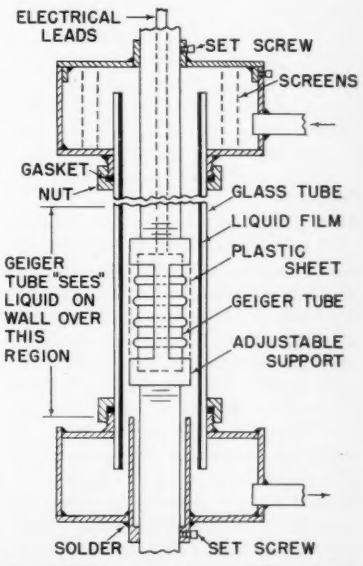

FIG. 2. DETAILS OF COLUMN CONSTRUCTION AND GEIGER-TUBE PLACEMENT.

Dr. Jackson is now with the University of Idaho, Moscow, Idaho.

concentration during the course of a run. Also, because of the trace quantities employed, it is not feasible to introduce the same concentration of activity into each liquid.

Equations Relating Radioactivity and Film Thickness. The isotope used was yttrium 91, which emits only beta radiation (1.53 mev.) and has a half life of 57 days. A linear relation does not exist between observed activity and thickness of the liquid film because beta radiation is partially absorbed by the liquid. However, corrections may be made and all observations reduced to a common basis by the following expressions:

$$m = C \times A_c \tag{1}$$

$$A_c = A_o P_a P_c \tag{2}$$

The term A_o is the activity registered by the scaling unit for flow of the liquid film down the vertical tube. The factor P_a corrects for the adsorption of the liquid film and is the ratio of the activity that the film would show without absorption to the activity observed with absorption. The factor P_c corrects the observed activity for the concentration of isotope. It is the ratio of the activity of a liquid sample to the activity of some liquid selected arbitrarily as a basis. These factors are determined by analytical methods described later. The activity of a liquid sample on the date of analysis (A) must be corrected for radioactive decay to the activity the sample had on the date of its evaluation in the flow apparatus (A'). The following expression is used for this:

$$A/A' = e^{-\lambda t} \tag{3}$$

For Y^{91}, $A/A' = 1/2$ at $t = 57$ days and $\lambda = 0.01216$ (day)$^{-1}$. The term A_o is therefore the activity that the counting apparatus would register if each liquid had zero absorption and the same concentration of radioactive isotope. The constant C is the proportionality factor between corrected activity and the film thickness. It depends on the geometry and counting efficiency of the Geiger tube and is determined by operating the flow equipment in a region where the film thickness can be calculated from viscous theory. Thus a film thickness determined by the use of a radioactive tracer is not measured directly but is computed from the ratio of an unknown to a known condition of flow.

Equations of Flow. Equations for the viscous flow of a liquid film down a vertical flat plate have been established (5) and are given below:

$$m = \left[\frac{3\,\mu\,Q}{g_c\,\rho_a}\right]^{1/3} \tag{4}$$

$$v = \frac{\rho_a\,g_c}{\mu}\left(mx - \frac{x^2}{2}\right)^{1/2} \tag{5}$$

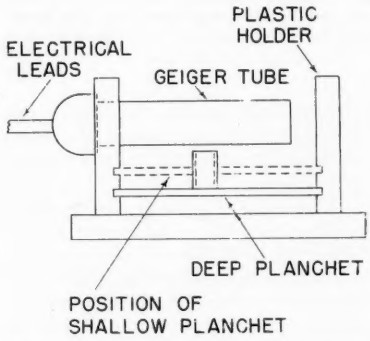

FIG. 3. ARRANGEMENT OF PLANCHETS AND GEIGER TUBE FOR THE DETERMINATION OF SAMPLE ACTIVITY.

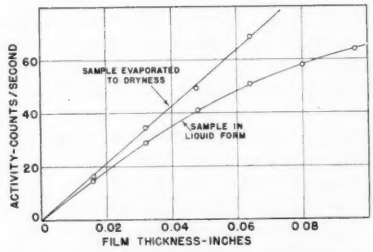

FIG. 4. TYPICAL DATA FOR THE SELF-ABSORPTION OF BETA RADIATION BY A LIQUID (70.4% GLYCEROL SOLUTION).

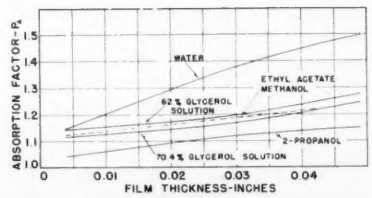

FIG. 5. DEPENDENCE OF THE ABSORPTION FACTOR P_A ON FILM THICKNESS.

$$V_s = \frac{\rho_a\,g_c\,m^2}{2\mu} \tag{6}$$

$$V = \frac{\rho_a\,g_c\,m^2}{3\mu} \tag{7}$$

$$V_s/V = 1.5 \tag{8}$$

EXPERIMENTAL EQUIPMENT AND PROCEDURE

Apparatus. The equipment consisted of a device for rigidly supporting a removable glass tube in a vertical position and for supplying the inner wall of the tube with liquid. This equipment is represented diagrammatically in Figure 1. Liquid at a constant rate was provided by a constant head tank. Glass, copper, and copper alloys were used throughout to prevent contamination by solid corrosion products which would absorb radioactive ions and deposit in the wetted-wall tube. Liquid-flow rate was measured by means of a calibrated glass vessel inserted in the drainage line between the vertical tube and the surge tank. This method gave accurate results for extreme ranges of flow rate and viscosity.

The vertical glass tube had an inside diameter of 1.423 ± 0.010 in. The upper end of the glass tube was ground to an angle of 90° with the walls and the upper edge of the inside wall was roughened slightly to ensure uniform wetting. The tube was brought into vertical alignment by use of a precision square and level. Any deviation from the vertical was of the same order of magnitude as the variation in straightness of the glass walls. The tube could be readily removed for cleaning, as was done prior to each run to reduce the background count to a minimum. Before overflowing the top of the glass tube, liquid entered an enlarged cylindrical well containing two screens concentric with the tube. No liquid disturbance in this well was apparent except at the very highest flow rates used.

Figure 2 shows the column construction details. The Geiger-Mueller tube for determining the activity of the liquid flowing on the walls was a Victoreen Model 1B85 and was held concentric with the glass tube. The holder shielded the Geiger tube to limit the area it could "see" to the immediate vicinity. This eliminated the influence of radiation from the upper and lower portions of the glass tube, where the flow pattern is not typical. The top of the Geiger tube was 12 in. below the top of the glass tube.

Procedure. A Nuclear model 165 scaler supplying 850 volts to the Geiger-Mueller tube was used for counting. The same counting tube and apparatus were used for all determinations. In most cases the number of counts obtained was 10,000 or

more, which gave a standard deviation of 100 or less. The flow rate was established simultaneously with the counting period. The background employed was that at the beginning of a run since some residual activity remained after a run due to liquid holdup and subsequent evaporation. The entire flow range was covered several times during a series of determinations to ensure that the data were representative.

The isotope Y^{91} was received as YCl_3 in 6*N* HCl acid. A stock solution of 2 mcuries of Y^{91} in 8 liters of isopropyl alcohol was prepared. Portions of this (500 to 2,000 ml.) were evaporated to a solid residue, which was then taken up by a portion of the liquid under test. In the case of methanol and ethyl acetate the residue was insoluble, and for these a portion of the original Y^{91} acid solution was placed directly in the liquid. For each flow determination 8 liters of liquid was used and 2g. of anhydrous aluminum chloride was added as a carrier to reduce loss of radioactive isotope by adsorption on the walls of the apparatus.

Because evaporation and adsorption may cause the activity to change during the course of a run, and because a solution may not easily be prepared to have a predetermined concentration of isotope, a method of analysis of liquid activity was necessary. As dip counting was not satisfactory, a method using planchets was developed. The planchets were constructed of short sections of 1/2-in. copper tubing held to the backing plate by solder, litharge-glycerin, or wax depending on the liquid under test and the type of backing used.

For comparing samples of the same liquid a deep planchet was used, 2 ml. of liquid being added to the planchet and the activity determined by the apparatus shown in Figure 3. For comparing the activity of different liquids, 0.100 ml. of the sample was placed in a shallow planchet and was then evaporated to dryness before counting. This method could have been used for all samples, but the process of analysis was speeded considerably by using the deep planchet for a series of samples of the same liquid, and the evaporative technique for only one sample of each series. The procedure is further illustrated by the sample calculation given later.

To establish values for the factor P_a it was necessary to determine the absorption of beta radiation as a function of film thickness. For this, shallow planchets having a backing plate of glass were used. This was necessary to simulate the conditions of the liquid on the wall of the glass tube because the use of a copper backing material gave results appreciably different from those for the glass. Small increments of liquid were added by micropipet and the corresponding activity was measured. Film thickness was calculated from liquid volume and planchet diameter. Surface-tension effects were reduced in the case of water and glycerol solutions by adding a small quantity of a surface-active agent. Activity values at zero absorption were obtained by evaporation. A typical absorption curve is shown in Figure 4, and values of the absorption factor as a function of film thickness are given in Figure 5.

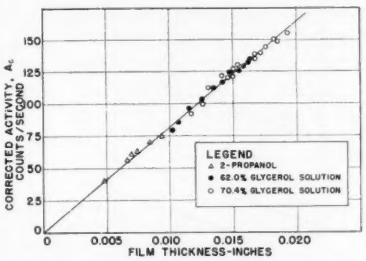

FIG. 6. CORRECTED ACTIVITY VS. CALCULATED THICKNESS FOR FLOW WITHOUT WAVES.

Materials. Six different liquids were employed in the test apparatus: ethyl acetate, methanol, water, 2-propanol, 62.0% glycerol solution, and 70.4% glycerol solution. These provided a viscosity range of 0.5 to 20 centipoises. The following grades of materials were employed: distilled water, U.S.P. glycerol, Shell 2-propanol (98-99%), Carbide and Carbon Corporation commercial-grade ethyl acetate (87-89%), which analyzed 88.0%, and methanol of unknown source. The glycerol solutions were analyzed by density measurements (*17*) and viscosities were determined from compositions (*21*). Experimental measurements of viscosity for 2-propanol, ethyl acetate, and methanol were made by use of an Ostwald drip-type viscosimeter (Fisher). Values obtained checked handbook values closely and the methanol was indicated to be of high purity. For some of the water and glycerol series, 0.1% by weight of Ethomeen C/15 (Armour) was added to reduce the surface tension of these liquids to more than one half the normal values and provide an excellent method of observing surface-tension effects without change in kinematic viscosity. It was also necessary to add about 0.1% octyl and *n*-butyl alcohols to reduce foaming.

EXPERIMENTAL RESULTS

It was necessary first to establish the value of the constant, *C*, in Equation (1). This was done by operating the vertical-tube apparatus under conditions of flow where film thickness could be calculated from flow rate using Equation (4). This may be done for the region where the flow is truly viscous and waves are absent. It was not possible to secure uniform coverage of the wall at the low flow rates required except for the more vicious liquids. The value of the constant was determined by plotting corrected activity vs. calculated thickness, as shown in Figure 6. The best line though the data points and the origin gives $C = 0.0000\text{-}1010$.

TABLE 1.—WAVE INCEPTION AS A FUNCTION OF COLUMN POSITION AND REYNOLDS NUMBER

Liquid (in order of increasing viscosity)	Distance below top of wetted-wall column, in.			
	0*	4	8	12†
Ethyl acetate	<66	880	1,670	
Methanol	<60	760	1,470	
Water	15	530	1,030	1,540
2-Propanol	15	340	660	970
62.0% Glycerol solution	18	180	330	
70.4% Glycerol solution	12	130	230	

*The distance for initial appearance of the waves was small and was assumed zero.
†This distance coincided with the top of the Geiger tube.

Calculations. A sample calculation will serve most conveniently to illustrate the method. The concentration of activity for a sample of I-52 (70.4% glycerol series) as determined by the deep planchet method for example, was 5.27 counts/sec. compared to 5.17 ct./sec. for a sample of I-8. The latter was selected as the sample for the series to be analyzed by evaporation and gave $A = 2.65$ ct./sec. Hence the activity that sample I-52 would have shown on evaporation is

$$A = \frac{5.27}{5.17} \times 2.65 = 2.70 \text{ ct./sec.}$$

These analyses were made 12 days after observations were taken in the flow apparatus, and by Equation (3) the activity corrected to the date of the run is

$$\frac{A}{A'} = e^{-0.01216 \times 12} = 0.864$$

$$A' = 2.70/0.864 = 3.11 \text{ ct./sec.}$$

A sample from the water series, G-2 was selected as the activity basis for all determinations and this sample analyzed $A' = 4.50$ct./sec. The value of the correction factor, P_c, for sample I-52 is therefore $P_c = 4.50/3.11 = 1.450$
This signifies that at the time the flow determination for the glycerol solution was made the concentration of radioactivity was less than that of sample G-2 by this ratio. Hence the activity indicated by the Geiger tube in the flow apparatus for run I-52 ($A_o = 162.0$ ct./sec.) must be increased by 1.450 so that the two series of determinations may be directly compared. In practice the value of P_c was not determined for each point because it changed only little if at all for most liquids. Four or five samples were taken over a series of determinations, and P_c was interpolated with respect to time.

The factor P_a must be obtained by trial since this depends on the film thickness, which is yet unknown. A first approximation of thickness is obtained from Equation (4) for true viscous flow. For I-52 this is

$$m = \left[\frac{3 \times 0.449 \times 16.29}{4.17 \times 10^8}\right]^{1/3} =$$

0.00374 ft. (0.0449 in.)

From Figure 5, $P_a = 1.23$, which signifies that the flow activity observed would have been greater by this factor if absorption of radiation by the film had not occurred. By Equation (2) the corrected flow activity is

$$A_c = 162.0 \times 1.450 \times 1.23 =$$

288 ct./sec.

and by Equation (1) the film thickness is
$m = 0.00001010 \times 288 = 0.00291$ ft. (0.0345 in.)

Since the calculated film thickness does not check the assumed value, a new value of $P_a = 1.19$ is selected corresponding to the calculated thickness. A recalculation gives $m = 0.00282$ ft. (0.0334 in.) and no further refinement in the value of P_a is necessary. It may be noted that large variations in film thickness result in only small changes of the factor P_a. Therefore, the use of this factor based on average thickness results in only a small error even though waves of considerable height are present.

Characteristics of Wave Flow. Flow rates, corresponding to Reynolds numbers of 4 to 5,000, were employed and covered the entire region of viscous flow although it was not possible to obtain this range with each liquid. The surface of the liquid film assumes a wave motion at very low flow rates. For the lighter liquids it was not possible to operate the apparatus in a nonwave region because of incomplete coverage of the wall. The initial formation of the waves was sharply defined and the appearance or disappearance of the waves could be effected by only a

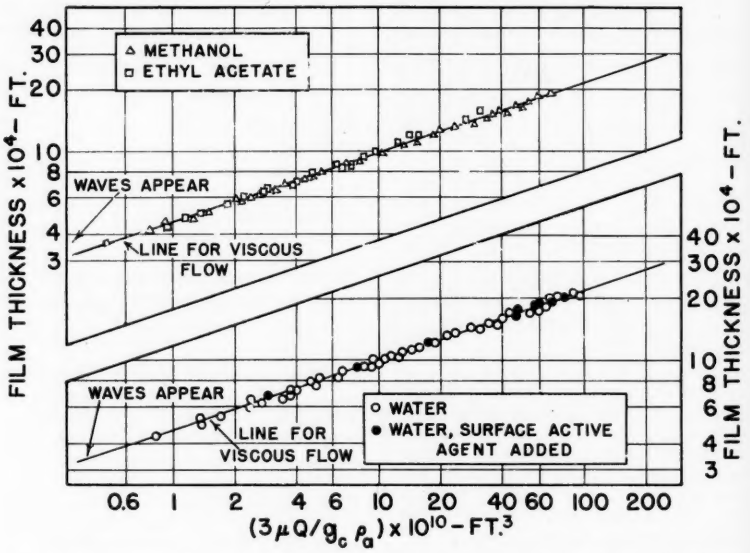

FIG. 7. FILM THICKNESS FOR WATER AND LIQUIDS LESS VISCOUS THAN WATER.

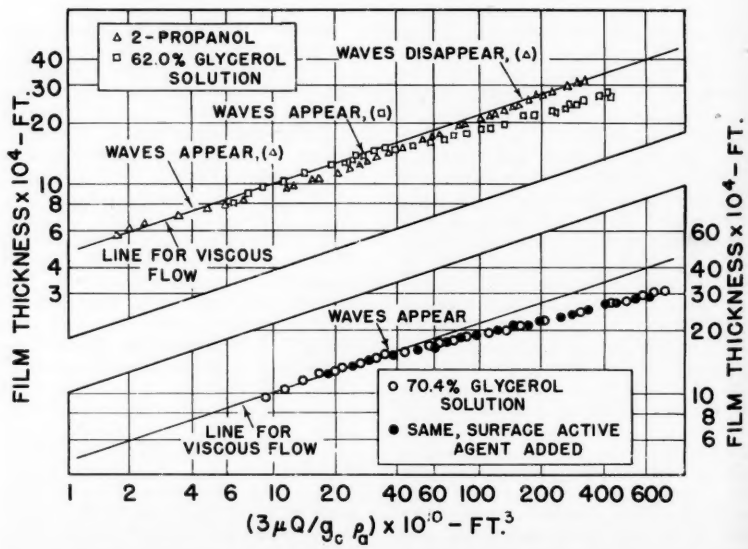

FIG. 8. FILM THICKNESS FOR LIQUIDS MORE VISCOUS THAN WATER.

small change in the flow rate. At inception the waves appeared over the entire column except for a very short distance at the top. As the flow rate increased, the point of wave formation progressed down the column, evidently because the liquid was accelerating in the upper portion. Table 1 shows this type of behavior and it is seen that a certain distance is required to establish the wave motion. This distance increases linearly with the flow rate over the range observed (the values given in Table 1 were read from the best lines through the experimental points) and increases with the viscosity. The spacing between waves was estimated at 1.25 to 1.50 in. at inception. This spacing decreased as the rate of flow increased and rapidly reached a condition where it could no longer be followed easily with the eye.

Film Thickness. Typical data are given in Table 2 for each of the liquids employed. Because of the behavior obtained, the data are conveniently placed into one of two groups according to whether the liquid is more viscous or less viscous than water. Figure 7 shows experimental film thickness plotted against a grouping of terms suggested by Equation (4). For liquids of viscosity equal to water or less, the agreement between observed and theoretical is good even though most of the flow lies in the region where waves are present.

Figure 8 shows the behavior of liquids having viscosities greater than the viscosity of water. Film thickness departs from that for true viscous flow at the point of wave inception and is less than theory predicts. In the case of 2-propanol film thicknesses are observed to return to the expected values when the waves disappear. The magnitude of the difference between experimental and theoretical thickness increases with viscosity for the region of wave flow. Sufficiently high flow rates could not be obtained to observe the behavior of the more viscous liquids near the turbulent region.

Effect of Surface Tension. The activities and flow rates of several liquids were determined before and after the addition of a surface-active agent, which was estimated to reduce the surface tension by at least one half. The surface tension of water and the 70.4% glycerol solution thus approached that for the organic liquids and permitted a direct observation of the effect of surface tension without change in viscosity or density. Inspection of Figures 7 and 8 shows that the decrease of surface tension caused no change in film thickness. It was also determined by independent observations that the point of wave inception did not change upon the addition of the surface-active agent.

TABLE 2.—TYPICAL FLOW AND ACTIVITY DATA

Determination	Q, cu. ft. / (ft.) (hr.)	Temperature, °C.	μ/ρ_a, sq. ft./hr.	$\left[\frac{3\,\mu\,Q}{g_c\,\rho_a}\right]$ ft.$\times 10^9$	A_o, ct./sec.	P_a	P_c	A_c, ct./sec.	m, ft.$\times 10^3$	Re
K series	Ethyl acetate									
9	0.338	26.8	0.01940	0.0471	16.2	1.06	2.36	36.2	0.366	66
19	5.29	26.0	0.01948	0.742	31.5	1.09	2.88	88.6	0.895	1,085
1	18.72	26.1	0.01946	2.62	66.1	1.11	2.34	146.9	1.484	3,850
L series	Methanol									
18	0.399	29.0	0.0265	0.0763	37.3	1.11	1.009	41.8	0.422	60
1	15.25	28.8	0.0266	2.92	118.5	1.15	1.009	137.6	1.390	2,240
27	30.3	29.5	0.0264	5.76	155.7	1.16	1.009	182.2	1.840	4,590
G series	Water									
13	0.642	33.0	0.0295	0.1363	26.8	1.16	1.677	52.2	0.527	87
15	21.2	33.0	0.0295	4.52	76.3	1.30	1.722	170.8	1.725	2,880
2	27.8	31.8	0.0302	6.04	88.4	1.30	1.522	174.9	1.767	3,690
G series	Water, surface-active agent added									
40	1.357	33.0	0.0295	0.288	28.8	1.20	1.980	68.5	0.693	184
39	22.2	33.0	0.0295	4.71	68.9	1.30	1.975	177.0	1.788	3,010
47	32.1	32.2	0.0300	6.93	75.0	1.31	2.010	199.5	2.01	4,280
J series	2-Propanol									
17	0.261	28.0	0.0920	0.1724	65.9	1.12	0.774	57.1	0.576	11.3
5	12.13	26.8	0.0950	8.29	220	1.17	0.736	189.5	1.920	512
42	43.7	25.6	0.0982	30.8	305	1.21	0.832	307	3.10	1,780
H series	62.0% Glycerol solution									
13	0.767	32.5	0.0253	1.395	140.6	1.16	0.693	113.1	1.142	12.1
34	6.63	34.0	0.238	11.34	221	1.18	0.693	180.9	1.827	111.3
40	18.08	34.0	0.238	31.0	290	1.20	0.693	241	2.44	304
I series	70.4% Glycerol solution									
24	0.461	34.0	0.415	1.374	68.6	1.14	1.455	113.8	1.149	4.4
7	15.29	32.0	0.453	49.7	159.1	1.19	1.455	275	2.78	142.0
45	25.2	32.7	0.439	79.3	178.5	1.21	1.450	312	3.15	229
I series	70.4% Glycerol solution, surface-active agent added									
78	0.818	32.0	0.453	2.66	80.4	1.14	1.464	134.2	1.356	7.2
56	5.38	32.2	0.449	17.37	124.2	1.17	1.450	211	2.14	47.8
52	16.29	32.2	0.449	52.6	162.0	1.19	1.450	276	2.82	145.0

DISCUSSION OF EXPERIMENTAL RESULTS

The use of radioactive tracers for the measurement of liquid film is a satisfactory technique. Determinations may be made without disturbing the flow of liquid, and a series of values over a wide range of flow rate may be obtained rapid-

ly. The correction for absorption of beta radiation by the liquid and the calibration of the apparatus by observing flow in a region of true viscous flow both provide a procedure for relating radioactivity of the dissolved isotope to the film thickness. The method appears capable of measuring film thickness with a precision of 0.0005 in. or better but the accuracy can only be inferred because an absolute measurement is not possible. The method also has possible application for flow-rate measurement in experimental work involving films.

It is not feasible to calibrate the apparatus by directly relating activity to thickness by use of the planchet technique. Inaccuracies arise from surface-tension effects and reflection of radiation from the planchet walls; also, the geometry of counting a sample in a planchet is different from that in the flow apparatus.

Beta radiation was employed because it is effectively shielded by the walls of the glass and copper tubing, and no other precautions are necessary. An alternate procedure would be to use an isotope emitting gamma radiation, which would be much more penetrating. The absorption would be zero for the thickness of films usually encountered and a linear relation between observed activity and thickness would result; however, this would require additional shielding to reduce the hazard of exposure and to eliminate radiation being recorded from undesired regions of the apparatus. Isotopes emitting beta radiation may be used only where the films being observed are not so thick that absorption effects predominate. A source of gamma radiation could be used where the absorption of beta radiation is large. The choice of isotope is limited to those which are soluble in the liquid under test, or at least to those which can be prepared as a colloidal solution or suspension and preferably to those emitting only one type of radiation.

Statements appearing in the literature(*3, 5, 6*) that liquid films in wave flow exhibit true streamline behavior with respect to thickness have been based on observations for liquids of low viscosity. For liquids more viscous than water the theoretical relations do not hold and the discrepancy can be large. Contrary to a previous report(*8*) the surface tension is not a significant factor in either wave inception or flow pattern when waves are present.

The data permit few conclusions concerning the inception of turbulence. For water and the lighter liquids, no significant departure from viscous behavior is indicated up to Reynolds numbers of 5,000 although greater scattering of the data is observed above $Re = 2{,}000$. Flow rates well up into the turbulent region could not be obtained with the equipment as originally designed.

Equations for Flow Down a Circular Tube. Equations (4) through (8) were derived for flow down a flat plate, and the validity of their use for a circular tube may be assessed by deriving equations for the tube. With reference to Figure 9, for a tube of height h the forces acting on a section of liquid toward the center of the tube at radius r are F_1, the force of gravity acting on the mass of the film; F_2, the force due to viscous shear of the liquid; F_3, the frictional force exerted by the core stream on the liquid surface (flow assumed countercurrent to wall film). Under steady state conditions these forces may be equated as follows:

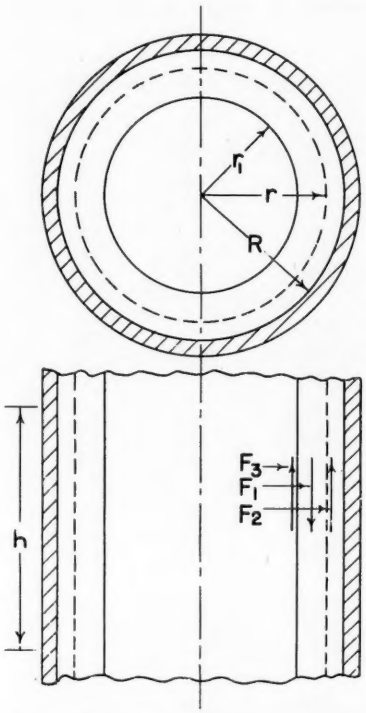

FIG. 9. SKETCH SHOWING DISTANCES AND FORCES FOR THE DERIVATION OF EQUATIONS FOR FLOW OF FILMS DOWN A VERTICAL TUBE.

$$F_1 = F_2 + F_3 \tag{9}$$

where

$$F_1 = \pi (r^2 - r_1^2) h \rho_a g_c \tag{10}$$

$$F_2 = -(2\pi rh)\,\mu\,(dv/dr) \tag{11}$$

$$F_3 = -(\Delta P \pi r_1^2)\, g_c \tag{12}$$

It has been shown(*10*) for a gas core moving at a moderate flow rate that F_3 is small in magnitude compared with the other forces and may therefore be neglected for this condition.

With this assumption, $F_1 = F_2$ and

$$\frac{dv}{dr} = -\frac{\rho_a g_c}{2\mu}\left(r - \frac{r_1^2}{r}\right) \tag{13}$$

Integrating

$$v = \frac{-\rho_a g_c}{2\mu}\left[\frac{r^2}{2} - r_1^2 \ln r\right] + C_1 \tag{14}$$

The constant of integration may be evaluated by imposing the condition that at

$$r = R, v = 0, \text{ or } C_1 = \frac{\rho_a g_c}{2\mu}\left[\frac{R^2}{2} - r_1^2 \ln R\right] \text{ and } v = \frac{\rho_a g_c}{4\mu}\left[R^2 - r^2 + 2r_1^2 \ln \frac{r}{R}\right] \tag{15}$$

Equation (15) gives the velocity of a liquid layer at any point r in the film. The liquid surface velocity is given by $v = V_s$ at $r = r_1$, or

$$V_s = \frac{\rho_a g_c}{4\mu}\left[R^2 - r_1^2 + 2r_1^2 \ln \frac{r_1}{R}\right] \tag{16}$$

The mean liquid velocity may be obtained from

$$V = \frac{Q}{\pi (R^2 - r_1^2)} \tag{17}$$

where

$$Q = \int_{r_1}^{R} v\,(2\pi r)\,dr \tag{18}$$

Combining Equations (15), (17), and (18) and integrating give

$$V = \frac{\rho_a g_c}{8\mu}\left[R^2 - 3r_1^2 - \frac{4r_1^4}{(R^2 - r_1^2)} \ln \frac{r_1}{R}\right] \tag{19}$$

Dividing Equation (16) by Equation (18)

$$\frac{V_s}{V} = 2\left[\frac{R^2 - r_1^2 + 2r_1^2 \ln \frac{r_1}{R}}{R_2 - 3r_1^2 - \frac{4r_1^4}{R^2 - r_1^2} \ln \frac{r_1}{R}}\right] \quad (20)$$

The value of this ratio for the limiting conditions of a full and empty pipe may be obtained in each case by applying L'Hopital's rule (*20*). This consists of successively differentiating the numerator and denominator until a determinate value for the ratio is obtained on substitution of limiting conditions. For an empty pipe $r_1 = R$ and $V_s/V = 1.5$, which is the same result as obtained for the flat plate. For a completely full pipe in viscous flow $r_1 = 0$ and $V_s/V = 2$, which is the expected result (V_s in this case is the velocity at the center of the pipe). It is evident that the value of V_s/V will vary continuously between these limits depending on the thickness of the film and the curvature of the pipe wall.

For liquids of medium or low viscosity and for tube radii large in comparison with film thickness, the velocity ratio may be assumed to be 1.5 for most purposes. For instance, water at 25°C. in viscous flow down the wall of a 1.5-in.-diam. tube at a Reynolds number of 2,100 would have a film thickness of 0.020 in. For these conditions the value of the ratio from Equation (20) is 1.505.

Equations (16), (19), and (20) would be required in the case of very viscous liquids, tubes of small diameter, and liquid-liquid systems where film thicknesses are much larger. The less complicated equations for flow down a flat plate would be preferred where applicable.

No quantitative relationship is readily apparent between film thickness and flow characteristics for the region of viscous flow with waves present. The development of a theoretical or empirical description of the flow pattern requires further information at point conditions because of the irregular and constantly changing surface of the film. A qualitative flow pattern and certain quantitative characteristics of wave flow are discussed below.

CRITERION FOR WAVE INCEPTION

In contemplating the behavior of films in wave flow it is apparent that factors other than those for closed conduits must be considered because of the free surface exposed. A means of predicting the conditions under which wave flow occurs is desired.

The Weber number may be used to characterize the flow under conditions where surface tension is a factor; however, the results reported show that surface tension is not a variable in either wave inception or film thickness.

The Froude number may be used to characterize the flow when density or gravity is a factor. It may be defined as the ratio of average velocity of the liquid stream to the velocity of propagation of a shallow wave*, or

$$F = V/(g_c m)^{1/2} \quad (21)$$

The velocity of propagation of a wave where the depth of liquid is small is dependent only on the depth and is independent of such factors as viscosity and surface tension (*18*). A Froude number of unity represents a critical condition at which the average liquid velocity is equal to the velocity of wave propagation; it might be expected therefore that this condition would be a critical point for the appearance of waves in film flow. This criterion will first be applied to the available data on surface velocities of liquid layers on vertical tubes.

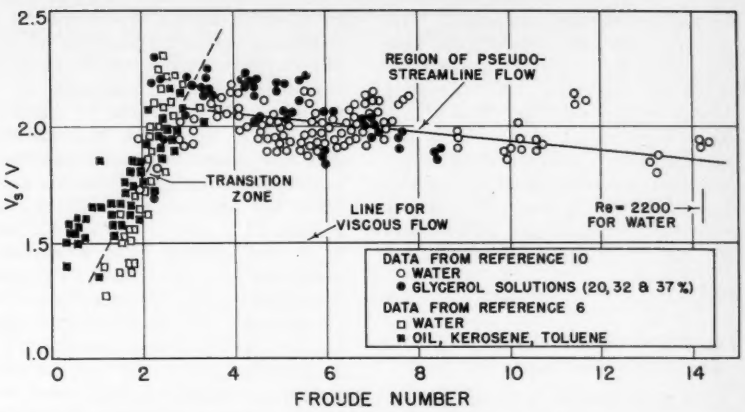

FIG. 10. RATIO OF SURFACE VELOCITY TO AVERAGE VELOCITY AS A FUNCTION OF FROUDE NUMBER FOR THE REGION OF VISCOUS FLOW.

Surface Velocities. Figure 10 shows the ratio of apparent surface velocity to average velocity plotted vs. Froude number calculated for data from two sources. The method of reference *6* timed the travel of an indicator dye (injected into the film) between two points on the column wall; it was suggested that the region of wave flow be termed pseudostreamline. The method of reference *10* used the pressure drop of a moving air phase in contact with the liquid film to determine surface velocities. The latter method is inapplicable at low liquid flow rates because of the small effect of the film on the air core and the former method is inapplicable at high flow rates because of diffusion and errors in timing. Agreement is evident where the two methods overlap.

Figure 10 shows a region where true viscous behavior is followed, a transition region where the velocity ratio continually increases, and finally a region where the ratio becomes stabilized but shows a small decrease as the limit for viscous flow is approached. The best line for the transition region intersects the line for viscous flow at a value of $F = 1.3$. It was reported (*6*) that more rapid diffusion of the dye was observed in the region where waves were present, which would result in errors of timing. The departure of apparent surface velocities from normal would appear to occur at Froude numbers approximating unity.

Data for Wave Inception. The Froude numbers for wave inception were calculated for four of the systems studied and for data reported by Fallah, Hunter, and Nash (*5*), Grimley (*8*), and Kirkbride (*12*). Results are given in Table 3, where it may be observed that the Froude number for wave

*The Froude number is sometimes used as the square of this ratio.

formation centers on unity. The data for the two liquid-liquid systems are of particular interest because of the very low apparent density of the wall film. The points given correspond to the first departure from viscous flow and were interpreted by the authors as the beginning of turbulence. The waves were quite pronounced, which may, in fact, lead to a condition of turbulence.

PROBABLE FLOW PATTERN IN WAVE FLOW

The flow pattern assumed by the liquid in the pseudostreamline region must explain a contradictory type of behavior. Except for the more viscous liquids, the film thickness is that for streamline flow; yet the apparent surface velocity is higher than normal. Further, there is the evidence cited for a mixing action in mass and heat transfer processes. Quantitative data have been given(*16*) for the same system in a wetted-wall column where the gas-film resistance was 90 to 100% of the total, compared with a packed tower, where it was only 50%. Visual observations(*6*) by means of a dye technique showed that the color thinned out more rapidly with waves present.

A qualitative explanation for flow with waves is probably somewhat as follows. Waves appear when the Froude number exceeds unity. The wave peak attains such a great height that it becomes a localized point of turbulence. The wave, which moves downward with a velocity greater than that of the laminar film because of the greater thickness, causes a disturbance in the film, which returns to laminar flow when the wave has passed. The film never becomes completely turbulent because the laminar sublayer has appreciable thickness. In Figure 11 the wave crest is likened to a rod rolling over a surface covered with a thin layer of liquid. In support of this picture it must be shown that (1) the wave crest can be in turbulent flow as the criterion is usually applied, (2) the laminar sublayer is relatively thick, and (3) wave volume is small compared with the bulk of the film for liquids of low viscosity but becomes greater as the viscosity increases. Some evidence can be cited.

The data of Kirkbride(*12*) show that at an average Reynolds number of 640 for the film, the Reynolds number based on the wave height would be 8,800, a maximum height for the liquid observed. Reynolds numbers for other flow conditions can be judged by the equation

$$Re = \frac{4 g_c m^3 (\rho_a/\mu)^{1/3}}{3} \qquad (22)$$

where the Reynolds number varies as the cube of the thickness. It is usually accepted that the beginning of turbulence in films corresponds to Reynolds numbers of 1,000 to 2,000(*2, 4, 5, 12*).

Even though the bulk of a stream may be in turbulent flow, the portion near a solid boundary remains

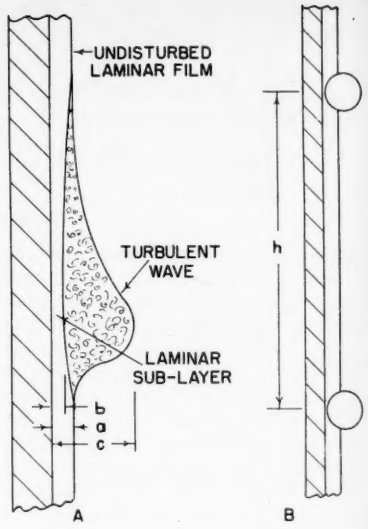

FIG. 11. SKETCH SHOWING PROBABLE PATTERN FOR WAVE FLOW.

in laminar motion(*14*). Discrepancies have been shown to exist in the generalized velocity-distance relationships as first proposed(*15*), but these may be used to illustrate the nature of the laminar sublayer in a semiqualitative manner. As pointed out by Colburn(*2*) there exists a value of the Reynolds number below which the flow will be all viscous. For higher flow rates the laminar sublayer has a minimum thickness corresponding to this limiting condition, and the remaining portion of the film need not necessarily be all viscous. In the presence of an external force acting on the film (in this case the weight of the turbulent wave) the limiting Reynolds number was calculated to be 270. Reference to Figure 11A and an example will make this clear.

For water flowing as a film down a vertical tube at an average Reynolds number of 640 (room temperature) the undisturbed thickness a would be 0.012 in., the sublayer b would be 0.009 in., and the height of the wave crest c from Kirkbride's data would be 0.029 in. These figures, though only approximate, serve to show that the disturbance caused by the passing wave is smaller than might be expected.

The laminar sublayer is probably not strictly viscous in all respects. Lin(*13*) has pointed out that disturbances in the transition zone (between turbulent and laminar layers) may propagate sidewise into the laminar layer and that a small mixing action may result.

TABLE 3.—FROUDE NUMBER FOR WAVE INCEPTION CALCULATED FROM THE DATA OF SEVERAL INVESTIGATORS

Investigator	System*	Properties of wall liquid: μ, centipoises	Properties of wall liquid: ρ_a, g./cu. cm.	Froude number for wave inception
This paper	Water-air	0.894	0.997	1.12 (avg.)
	2-propanol-air	2.02	0.782	0.92 (avg.)
	62.0% glycerol-air	10.15	1.157	1.23 (avg.)
	70.4% glycerol-air	18.64	1.179	1.06 (avg.)
(*8*)	Glycerol *A*-air	26.4	1.203	0.82
	Glycerol *B*-air	12.1	1.184	0.87
	38.7% Ethanol-air	2.84	0.942	0.87
	92% Ethanol-air	1.52	0.817	0.90
	62% Ethanol-air	2.60	0.891	1.01
	Carbontetrachloride-air	2.62	1.6	0.74
	Benzene-air	0.70	0.874	1.17
	Water-air	1.12	1.0	1.44
(*12*)	Oil 1-air	17.6	0.88	0.70
	Oil 3-Air	1.95	0.82	1.08
(*5*)	Oil-water	1.31	0.128	0.83
	Kerosene-water	1.31	0.183	1.29

*Wall liquid given first

No accurate data are available for wave volume but a simple assumption permits an estimate of the relative volume of wave and film. If the wave volume is assumed to be equal to that of a cylinder of diameter equal to wave height, and if wave spacings of 1 1/4 in. for water and 1 1/2 in. for the more viscous liquids at low flow rates are assumed, the ratio of film volume to wave volume for water would be 62, but only about 5 for the more viscous glycerol solutions. As the flow rate increases, the ratio decreases for either case but would be more pronounced with the viscous liquids, as observed experimentally.

A quantitative explanation of the flow behavior requires data on wave velocity, profile, and spacing, which may be obtained by a recently developed technique (*4*). The complexity of the problem is indicated by the highly irregular and changing character of the waves (references *4* and *8* show some excellent photographs) and the ultimate solution may require a statistical treatment. It is possible that the flow pattern of falling films in the turbulent region may also involve wave flow and that basic information for the viscous region can be applied in describing flow in the turbulent zone.

APPLICATIONS

The increase of surface velocity for the wave-flow region arises because of the increased velocity of the waves. The weight of the wave exerts a force on the boundary of the laminar sublayer and causes the normal parabolic velocity gradient [Equation (5)] to become more nearly linear. Thus the local velocity of fluid in the laminar sublayer is greater than normal and the velocity of the wave must be determined to some extent by the velocity at the boundary. The ratio of surface velocity to average film velocity is 1.5 for the parabolic gradient but 2.0 for a linear gradient and Figure 10 shows the ratio for the pseudostreamline region to be about 2.0. However, the assumption of a linear gradient for the bulk of the film is inconsistent with the observed thicknesses, and the surface velocities observed are only apparent and represent an average effect of wave flow and surface roughness. It is also possible that the interfacial area exposed with wave flow is significantly greater than for undisturbed laminar flow (*4*).

A useful form for the Froude number may be obtained by substituting the value of V from Equation (7) in Equation (21) and eliminating m by Equation (4):

$$F = \left[\frac{Q\ \rho_a}{3\mu}\right]^{1/2} \qquad (23)$$

With the condition imposed that at wave inception $F = 1$, the flow rate at which waves appear depends only on the kinematic viscosity, or $Q(\text{for wave inception}) = 3(\mu/\rho_a)$ Thus waves will form at low rates for low viscosity liquids, but higher rates are necessary to establish wave flow as the viscosity increases. This behavior was observed for the liquids employed. For liquid-liquid systems, where the ratio of (μ/ρ_a) is large, waves will appear in the wall liquid at a flow rate greater than that for a corresponding liquid-gas system. Nevertheless, the point of wave inception for liquid-liquid systems probably lies well within the usual operating range.

The Froude number is used as a criterion for vortex formation in mixing problems (*19*) and as a means of predicting particulate or aggregative fluidization in fluid-solid systems (*23*). It thus becomes an additional parameter in the fluid mechanics of processes important to the field of chemical engineering.

In correlating mass transfer coefficients with fluid properties for two phase systems, the effect of each phase on the fluid mechanics of the other must be considered. For instance, in liquid-gas systems the Reynolds number of the gas phase must be that relative to the liquid surface, and the velocity of the gas stream calculated from the mass rate of flow must be increased (if countercurrent) by an amount equal to the liquid surface velocity. This correction can amount to 25% or more for rectification (*9*) and for air-water (*10*). Figure 10 may be used to determine the apparent surface velocities of low-viscosity liquids in the pseudostreamline region and as a first approximation for more viscous liquids. It is possible that the behavior shown in Figure 10 is not typical for high-viscosity liquids or liquid-liquid systems or for the case where the force, F_3, at the interface is not negligible.

The behavior pattern of liquid films where the drag force at the interface is not negligible would depend on the magnitude and direction of this force. For countercurrent flow (*see* Figure 9) the average liquid rate would be decreased; for cocurrent flow the drag force and gravity would act in the same direction, thus speeding the flow of the wall liquid. The point of wave formation and the velocity gradient in the film would be influenced. The presence of a finite force, no matter how small, can easily be demonstrated by blowing smoke across the top of a column of liquid which exposes a free surface. A portion of the smoke is rapidly transported to the bottom of the column. Data have been presented (*10*) which show that the drag force can be neglected for moderate gas velocities. The magnitude of the force can be calculated from the pressure drop if this is known and if the geometry of the flow channel is simple. Colburn (*2*) has described the unusual behavior of the liquid film for a system where the vapor is moving at very high velocities.

In translating the behavior of films in the pseudostreamline region to the flow of liquids in packed columns it should be pointed out that the free fall necessary to establish wave flow may not occur in this type of equipment because of the discontinuous flow path. It was shown earlier that waves did not appear for some distance below the inlet for a wetted-wall column. The absence of wave flow in a packed column, or the extent to which it does occur, should be verified. It was observed (*9*) for rectification in a wetted-wall column that discontinuities in the height of a transfer unit occurred in the upper part of the column, indicating that some liquid-film resistance was present where wave flow was not established. Peck and Wagner (*16*) showed that liquid-film resistances were small for a wetted-wall column but comprised half the total resistance for packed columns.

Industrial process equipment could be designed to take advantage of the low liquid side resistances of falling films in the pseudostreamline and turbulent regions. The use of a bank of vertical wetted-wall tubes was reported to be unsatisfactory because of inadequate liquid distribution, but it is conceivable that a series of vertical plates, each with an independent supply of liquid, would provide a large surface area and would permit large quantities of liquid and gas to be brought into contact. Such a system would be particularly attractive for gas-absorption systems because of the low pres-

sure loss in the gas phase. The use of a falling film inside a vertical tube with an external supply of heat has been used for a stripping operation. A new technique in gas-separation processes, "sweep diffusion" (*1*), provides a recent application of the use of liquid film for component separation.

SUMMARY AND CONCLUSIONS

Equipment and a method are described for the measurement of thickness of liquid films by the use of a radioactive tracer dissolved in the liquid. The method has a precision of 0.0005 in. and could be applied for the further study of liquid films in gas-liquid or liquid-liquid systems. Six liquids with viscosities ranging from 0.5 to 20 centipoises were observed in flow down the inner wall of a vertical tube.

Wave motion appears at low flow rates well within the viscous region, which results in departure from true viscous flow. The waves are shown to appear when the Froude number exceeds unity. Liquids having a viscosity less than that of water exhibit the film thicknesses expected for true viscous flow even though waves are present. Liquids with a viscosity greater than that of water show film thicknesses less than for viscous flow. The departure from normal behavior increases with increasing viscosity. Surface tension is not a factor in either wave inception or flow behavior with waves present.

Equations for the flow of viscous films inside tubes (without waves) are derived and would be required for small-diameter tubes or very viscous liquids. In many situations, particularly those involving low-viscosity liquids, the less complex equations for flow down a flat plate may be used.

A qualitative theory is proposed which accounts for the presence of a pronounced mixing action even though the basic flow is essentially streamline. The waves attain a condition at low average flow rates where turbulence can begin locally. The bulk of the film and the sublayer beneath the wave remain in streamline flow. The turbulent wave moves downward at a velocity greater than that of the film and creates a disturbance and mixing action in passing. The ratio of wave volume to film volume is small except in the case of liquids more viscous than water.

ACKNOWLEDGMENT

The assistance of Dr. Orville J. Sweeting, Isotopes Laboratory, and of the Council on Research and Creative Work, University of Colorado, is gratefully acknowledged, as is the assistance of personnel at the U. S Naval Ordnance Test Station, China Lake, California.

NOTATION

A, A' = activity of a sample of liquid as analyzed and as corrected to a given date, counts/sec.

A_o, A_c = activity of liquid film on vertical-tube apparatus as observed and as corrected for absorption and sample activity, counts/sec.

C = constant relating corrected activity to film thickness, ft./(counts/sec.)

F = Froude number, dimensionless, equal to $V/(g_c m)^{\frac{1}{2}}$ for a liquid film

F_1, F_2, F_3 = forces acting on an isolated portion of film, lb. force

g_c = dimensional constant, 4.170×10^8, (lb. mass) (ft.)/(lb. force) (hr.^{2})

h = height of column section, also spacing between successive waves, ft.

m = film thickness, ft.

ΔP = pressure drop over height h of column, lb. force/sq.ft.

P_a, P_c = absorption and concentration factors, defined in the text

Q = volumetric rate of liquid flow per unit of wetted periphery, cu.ft./(ft.) (hr.)

r, r_1 = radius from center of tube to point within film and to the inner surface of the film, ft.

R = radius of tube and outer boundary of film, ft.

Re = Reynolds number $= 4Q\rho_a/\mu$ for a liquid film

t = time of radioactive decay, days

v, V, V_s = point, average, and surface velocity, ft./hr.

x = distance from wall to point within film, ft.

λ = constant for radioactive decay, days^{-1}

μ = liquid viscosity, lb. mass/(ft.) (hr.) unless given otherwise

ρ_a = apparent film density, equal to liquid density minus fluid density of core (the latter is negligible for a gas core), lb. mass/cu.ft. unless given otherwise

LITERATURE CITED

1. Cichelli, M. T., W. D. Weatherford, Jr., and J. R. Bowman, *Chem. Eng. Progr.*, 47, 63 (1951).
2. Colburn, A. P., and F. G. Carpenter, "Heat Transfer Lectures," Vol. II (N.E.P.A.-979-IER-13), p. 96, Fairchild Engineer and Airplane Corp., Oak Ridge, Tenn. (1949).
3. Cooper, C. M., T. B. Drew, and W. H. McAdams, *Trans. Am. Inst. Chem. Engrs.*, 30, 158 (1934); *Ind. Eng. Chem.*, 26, 428 (1934).
4. Dukler, A. E., and O. P. Bergelin, *Chem. Eng. Progr.*, 48, 557 (1952).
5. Fallah, R., T. G. Hunter, and A. W. Nash, *J. Soc. Chem. Ind.*, 53, 369T (1934)
6. Friedman, S. J., and C. O. Miller, *Ind. Eng. Chem.*, 33, 885 (1941).
7. Greenewalt, C. H., *loc. cit.* 18, 1291 (1926).
8. Grimley, S. S., *Trans. Inst. Chem. Engrs. (London)*, 23, 228 (1945).
9. Jackson, M. L., and N. H. Ceaglske, *Ind. Eng. Chem.*, 42, 1188 (1950).
10. Jackson, M. L., R. T. Johnson, and N. H. Ceaglske, "Proceedings of the First Mid-Western Conference on Fluid Dynamics," p. 226, Edwards Brothers, Inc., Ann Arbor, Mich. (1951).
11. Johnstone, H. F., and R. L. Pigford, *Trans. Am. Inst. Chem. Engrs.*, 38, 25 (1942).
12. Kirkbride, C. G., *Trans. Am. Inst. Chem. Engrs.*, 30, 170 (1934).
13. Lin, C. C., *Quart. App. Math.*, 3, 277 (1945-46).
14. McAdams, W. H., "Heat Transmission," 2 ed., p. 99, McGraw-Hill Book Company, Inc., New York (1942).
15. Miller, B., "Heat Transfer Lectures," Vol. I (NEPA-804-IER-10), p. 93, Fairchild Engine and Airplane Corp., Oak Ridge, Tenn. (1948).
16. Peck, R. E., and E. F. Wagner, *Trans. Am. Inst. Chem. Engrs.*, 41, 737 (1945).
17. Perry, J. H., "Chemical Engineers' Handbook," 3 ed., pp. 191, 372, McGraw-Hill Book Company, Inc. New York (1950).
18. Rouse, H., "Fluid Mechanics for Hydraulic Engineers," p. 369, McGraw-Hill Book Company, Inc., New York (1938).
19. Rushton, J. H., "Proceedings of the First Mid-Western Conference on Fluid Dynamics," Edwards Brother, Inc., Ann Arbor, Mich. (1951).
20. Sherwood, T. K., and C. E. Reed, "Applied Mathematics in Chemical Engineering," p. 20, McGraw-Hill Book Company, Inc., New York (1939).
21. Sheely, M. L., *Ind. Eng. Chem.*, 24, 1060 (1932).
22. Westhaver, J. W., *Ind. Eng. Chem.*, 34, 126 (1942).
23. Wilhelm, R. H., and M. Kwauk, *Chem. Eng. Progr.* 44, 201 (1948).

Presented at A.I.Ch.E. San Francisco meeting

VAPOR-LIQUID EQUILIBRIUM RELATIONS PREDICTED BY THERMODYNAMIC EXAMINATION OF ACTIVITY COEFFICIENTS

ALBERT H. WEHE and JESSE COATES

Louisiana State University, Baton Rouge, Louisiana

Data on vapor-liquid equilibria are of considerable importance from a theoretical point of view and from the standpoint of industry. For ideal solutions these data can be readily calculated, but unfortunately most solutions are nonideal in behavior. Although many data are available on nonideal solutions, there is no way, in the absence of experimental data, at present to predict quantitatively the deviations from nonideality.

It is possible to define thermodynamically certain functions, such as activity coefficients, which measure the degree of departure from ideality. The ideal situation would be one in which these activity coefficients could be predicted from properties of the pure components of the solution. Such a prediction, however, would have to be consistent with rigorous thermodynamic relations. The most promising concentration range in which to work, if the activity coefficients are to be related to the properties of pure compounds, is the dilute region. In this study most attention has been paid to collection of data and to thermodynamic analysis in this region. Work is described which, it is felt, contributes to the solution of the problem of prediction of activity coefficients, and the way is pointed for future work.

A discussion of the fundamental concept of activity coefficients and other thermodynamic quantities will be helpful in making this analysis. Also, an understanding of activity coefficients at infinite dilution will be important in developing a method of correlation of these coefficients for binary systems.

FUGACITY, ACTIVITY, ACTIVITY COEFFICIENT

Activity is defined as the ratio of the fugacity of a component in a given state to the fugacity of the pure component in some arbitrarily chosen standard state at the same temperature T. The given state may be taken as the component in solution, and the standard state as the pure component at the temperature and pressure of the solution. Thus the activity expresses the variation of fugacity with composition and for nonideal solutions shows the deviation from ideality. This deviation is more clearly expressed by activity coefficients, the ratio of the activity of one component to the mole fraction of that component in solution. For ideal solutions this ratio equals unity. In nonideal solutions the ratio becomes some value other than unity, expressing the deviation from ideality.

For liquid solutions the activity coefficient may be expressed by

$$\gamma_1 = \frac{(f_1)_L}{x_1 (f_1^\circ)_L} \qquad (1)$$

where subscript L designates the liquid state, $x_1 =$ mole fraction of component 1 in the liquid, and $(f_1^\circ)_L =$ fugacity of pure component 1 as a liquid at the temperature and pressure of the solution. at low pressures

$$(f_1^\circ)_L = P_1^* \qquad (2)$$

where $P_1^* =$ vapor pressure of pure component 1 at the temperature of the solution.

At equilibrium, assuming fugacity rule holds for the vapors,

$$(f_1)_L = (f_1)_V = y_1 (f_1^\circ)_V \qquad (3)$$

where subscript V designates the vapor state, $y_1 =$ mole fraction of component 1 in the vapor, and $(f_1^\circ)_V =$ fugacity of pure component 1 as a vapor at the temperature and pressure of the solution.

At low pressures and temperatures, such that the fugacity coefficient equals unity,

$$(f_1^\circ)_V = \pi \qquad (4)$$

and

$$(f_1)_V = y_1 \pi = p_1 \qquad (5)$$

where $\pi =$ total pressure on the system and $p_1 =$ partial pressure of component 1 in the vapor.

Under these conditions Equation (1) reduces to

$$\gamma_1 = \frac{p_1}{x_1 P_1^*} = \frac{y_1 \pi}{x_1 P_1^*} \qquad (6)$$

The ratio y/x is the equilibrium vaporization constant, K, and an expression for this constant may be derived in terms of activity coefficients.

$$\frac{y_1}{x_1} = K_1 = \frac{\gamma_1 P_1^*}{\pi} \qquad (7)$$

For high pressures the relationship becomes

$$\frac{y_1}{x_1} = K_1 = \frac{\gamma_1 (f_1^\circ)_L}{(f_1^\circ)_V} \qquad (8)$$

Equation (8) is the more exact expression, although Equation (7) may be used where the ideal-gas law and the fugacity rule for the gas phase are applicable. For ideal solutions, that is, when the activity coefficient is unity, the equilibrium constant becomes equal to the ratio of the fugacity of the pure component in the liquids to that in the vapor.

$$K_1^* = \frac{(f_1^\circ)^*_L}{(f_1^\circ)^*_V} \qquad (9)$$

where the superscript* designates the ideal-solution condition.

For a given nonideal solution there are two equilibrium vaporization constants which may be evaluated: one for the nonideal system and one for the same system considered as an ideal system. The symbol K^* will indicate the ideal-equilibrium vaporization constant. An expression for activity coefficient may now be written in terms of K and K^*.

$$\gamma_1 = K_1/K_1^* \qquad (10)$$

For nonideal solutions

$$\gamma_1 (f_1^\circ)_L = (f_1)_L/x_1 \qquad (11)$$

For ideal solutions

$$(f_1^\circ)^*_L = (f_1)^*_L/x_1 \qquad (12)$$

Combining Equations (8) through (12) gives

$$\gamma_1 = \frac{K_1}{K_1^*} = \frac{(f_1)_L/(f_1^\circ)_V}{(f_1)^*_L/(f_1^\circ)^*_V} \qquad (13)$$

At very low concentrations such that the boiling point of the nonideal solution approaches that of the ideal solution

$$(f_1^\circ)_V = (f_1^\circ)^*_V \qquad (14)$$

Equation (13) now becomes

$$\gamma_1 = \frac{K_1}{K_1^*} = \frac{(f_1)_L}{(f_1)^*_L} \qquad (15)$$

If the temperature and pressure are so low that the fugacity coefficients are equal to unity, Equation (15) may be written as

$$\gamma_1 = \frac{K_1}{K_1^*} = \frac{P_1}{P_1^*} \qquad (16)$$

where $P_1 = p_1/x_1$ = "nonideal" vapor pressure of *pure* component 1. P_1^* = "ideal" vapor pressure of pure component 1, or the actual vapor pressure of pure component 1 at the temperature of the solution.

The assumptions involved in Equation (16) restated are (1) that the temperature and pressure of the solution are so low that the fugacity coefficients are substantially equal to unity, (2) that the concentrations of the solution are so dilute that the differences in boiling points of the ideal and nonideal solutions are negligible, and (3) that the total pressures of the solutions are equal. Similar expressions may be written for component 2 expressing the nonideal vapor pressure of this component. These nonideal vapor pressures will be useful in correlating the activity coefficients at infinite dilution for different systems.

ACTIVITY COEFFICIENTS AT INFINITE DILUTION

Carlson and Colburn (*4*) suggest a method for finding the deviations from Raoult's law for systems composed of a member of a homologous series of compounds and another compound. This method is based on equations derived by Scatchard (*12*) for systems in which the change of entropy on mixing is the same as that for an ideal mixture. This assumption is not justified in many cases of nonideal solutions.

Another method of handling the activity coefficients of the components in dilute solution has been to relate them to the constants in equations such as the van Laar equations given by Carlson and Colburn in the following forms:

$$\log \gamma_1 = \frac{A x_2^2}{[(A/B)x_1 + x_2]^2} \qquad (17)$$

$$\log \gamma_2 = \frac{B x_1^2}{[x_1 + (B/A)x_2]^2} \qquad (18)$$

Since A is the terminal value of log γ_1, where $x_1 = 0$, and B is the terminal value of log γ_2, where $x_2 = 0$, it has been suggested that these constants be obtained by plotting the logarithm of the activity coefficient against the mole fraction and extrapolating the curves to zero concentration. These extrapolations, however, are of very uncertain accuracy. Also, the van Laar equations are restricted to constant temperature, and this extrapolation is usually made from data obtained at constant pressure. The van Laar and other two-constant equations are frequently used for correlating vapor-liquid equilibrium data for nonideal solutions. The equations involve certain assumptions, and generally when one equation fails, the other two-constant equations fail.

Butler and Harrower (*3*) have considered the quantity p/x, which is called the nonideal vapor pressure in this work, and its variation in systems of homologous series of compounds and another type of compound. The free energies of solution from the vapor, $RT \ln p/x$, at a constant temperature have been related to the number of carbon atoms in compounds of the homologous series, even though the solutions showed large deviations from ideality. These free energies of solution were found to change regularly as the number of carbon atoms in the molecule was increased or decreased in the cases studied, specifically alcohols and alkyl halides in benzene, carbon tetrachloride, and cyclohexane. Use of the nonideal vapor pressure in the present work avoids an anomaly of the quantity p/x, tending to become indeterminate as the solution becomes very dilute, that is, as x approaches zero.

An understanding of the significance of activity coefficients at infinite dilution requires a recognition of certain facts concerning the familiar x-y diagram. It follows, from Equation (8), that at $x_1 = 0$

$$\left[\frac{\partial y_1}{\partial x_1}\right]_{x_1=0} = (K_1)_{x_1=0} = (\gamma_1)_{x_1=0}\left[\frac{(f_1^\circ)_L}{(f_1^\circ)_V}\right]_{x_1=0} \qquad (19)$$

Necessarily, $(f_1^\circ)_L$ and $(f_1^\circ)_V$ are evaluated at the temperature and pressure conditions existing at $x_1 = 0$, that is, the boiling point and pressure of component 2. Similarly, for component 2, at $x_2 = 0$

$$\left[\frac{\partial y_1}{\partial x_1}\right]_{x_1=1} = \left[\frac{\partial y_2}{\partial x_2}\right]_{x_2=0} = (K_2)_{x_2=0} = (\gamma_2)_{x_2=0}\left[\frac{(f_2^\circ)_L}{(f_2^\circ)_V}\right]_{x_1=0} \qquad (20)$$

Here $(f_2^\circ)_L$ and $(f_2^\circ)_V$ are the fugacities of component 2 evaluated at the boiling point and pressure of component 1. If the system were acting ideally, the activity coefficients would be unity and the slopes at infinite dilution of the ideal system would be

$$(\partial y_1/\partial x_1)^*_{x_1=0} = (K_1^*)_{x_1=0} = \left[\frac{(f_1^\circ)_L}{(f_1^\circ)_V}\right]_{x_1=0} \qquad (21)$$

$$(\partial y_1/\partial x_1)^*_{x_1=1} = (K_2^*)_{x_2=0} = \left[\frac{(f_2^\circ)_L}{(f_2^\circ)_V}\right]_{x_1=1} \qquad (22)$$

If Equation (19) is divided by Equation (21), a relationship is obtained which expresses the activity coefficient at infinite dilution. This points out the fact that the nonideality of a system is indicated by the deviation of the slope of the x-y diagram at infinite dilution from the slope for the same system acting ideally.

At low pressures and temperatures, $(f_1^\circ)_L$ becomes P_1^* and $(f_1^\circ)_V$ becomes π. The slopes at infinite dilution of the x-y diagram for the nonideal system and for the ideal system become

TABLE 1.—TYPICAL EXPERIMENTAL RESULTS, VAPOR-LIQUID EQUILIBRIUM DATA

System: benzene-ethanol

x_1	y_1	Temp., °C.	Pressure, mm. Hg	γ_1	γ_2	$\ln\gamma_1$	$\ln\gamma_2$
0.0000	0.0000	80.10	760.5	10.48*	1.0007	2.350*	0.00070
0.0048	0.0400	78.60	760.0	8.2427	1.0128	2.10933	0.01272
0.0085	0.0790	77.11	760.5	9.7542	1.0219	2.27770	0.02166
0.1720	0.3560	68.90	760.0	3.0351	1.1219	1.11024	0.11502
0.3085	0.4040	67.98	760.0	1.9898	1.2789	0.68803	0.24600
0.4855	0.4490	67.67	760.0	1.4230	1.6051	0.35277	0.47319
0.7545	0.5720	69.18	760.0	1.0956	2.4838	0.09130	0.90979
0.8815	0.7030	71.86	760.0	1.0324	3.2668	0.03189	1.18381
0.9870	0.9545	77.51	760.0	0.9983	3.7125	−.00170	1.31171
0.9910	0.9685	77.75	760.0	0.9994	3.6771	−.00060	1.30212
1.0000	1.0000	78.32	760.3	1.0004	3.568*	0.00040	1.272*

Component 1 is ethanol; *extrapolated values.

TABLE 2.—TYPICAL EXPERIMENTAL RESULTS, VAPOR-LIQUID EQUILIBRIUM DATA

System: benzene–*n*–propanol

x_1	y_1	Temp., °C.	Pressure, mm. Hg	γ_1	γ_2	$\ln\gamma_1$	$\ln\gamma_2$
0.0000	0.0000	80.10	759.7	5.165*	0.9996	1.642*	−.0004
0.0270	0.0590	79.23	759.7	4.5723	0.9935	1.52002	−.0065
0.0445	0.0870	78.68	760.0	4.1908	0.9849	1.43298	−.0150
0.0980	0.1475	77.69	759.7	3.2813	1.0196	1.18824	0.01941
0.2300	0.2170	77.21	760.0	2.1561	1.1440	0.76830	0.13453
0.5015	0.3075	78.19	760.0	1.3426	1.4756	0.29461	0.38907
0.6725	0.3900	81.10	760.3	1.1206	1.8059	0.11386	0.59106
0.8540	0.5705	86.50	760.3	1.0285	2.4157	0.02811	0.88199
0.9375	0.7490	91.39	761.5	1.0086	2.8538	0.00857	1.04865
0.9560	0.8060	92.29	760.3	1.0249	3.0464	0.02459	1.11396
0.9730	0.8640	94.11	760.3	1.0037	3.3003	0.00370	1.19401
0.9760	0.8775	94.23	760.3	1.0114	3.3325	0.01134	1.20372
0.9800	0.8830	94.37	760.3	1.0080	3.8041	0.00797	1.33608
0.9885	0.9380	95.70	760.0	1.0067	3.3690	0.00668	1.21462
1.0000	1.0000	97.20	760.0	1.0003	4.031*	0.00030	1.394*

Component 1 is *n*-propanol; *extrapolated values.

$$(\partial y_1/\partial x_1)_{x_1=0} = (P_1^*/\pi)_{x_1=0}$$

$$(\gamma_1)_{x_1=0} = (P_1/\pi)_{x_1=0} \quad (23)$$

$$(\partial y_1/\partial x_1)^*_{x_1=0} = (P_1^*/\pi)_{x_1=0} \quad (24)$$

Consider the conditions existing at the point $x_2 = 0$ in a series of systems such as the benzene-alcohol series. Here the subscript 1 indicates the alcohol and 2, the benzene. At constant total pressure π, the temperature of the solution at $x_2 = 0$ will be the boiling point of the alcohol. The ideal slopes of the x-y diagram of the solutions of the various alcohols in benzene will vary as the vapor pressure of benzene varies with temperature. This follows from Equation (24) written in terms of component 2. This variation will be a straight line on a log P_2^* vs. $1/T$ plot, where P_2^* is the vapor pressure of pure benzene and T is the absolute temperature. This suggests a method of correlating the nonideal slopes, that is, by plotting the logarithm of the nonideal slope vs. the reciprocal of the absolute temperature. This nonideal slope is proportional to the nonideal vapor pressure of the pure component as shown in Equation (23).

At the point $x_1 = 0$ the conditions at constant total pressure are similar to those described above with one important difference. The temperature is constant at the boiling point of benzene, component 2, and the ideal slopes for the different systems now vary as the vapor pressures of the different alcohols at this constant temperature. The vapor pressure of the methanol at this temperature is higher than that of ethanol, of *n*-propanol, and of other higher alcohols in the series. It is possible to relate the ideal vapor pressures of these different compounds by use of the boiling points; therefore, slopes $(\partial y_1/\partial x_1)^*_{x_1=0}$ can be related to temperature for the different systems. A plot of log P_1^* vs. $1/T$ is usually satisfactory and this suggests that a similar correlation for the nonideal vapor pressure and therefore, the nonideal slopes, should be used.

The net result of these correlations as presented above may be shown mathematically as follows:

$$\log (P_1/\pi)_{x_1=0} = (M/T) + N \quad (25)$$

$$\log (P_1^*/\pi)_{x_1=0} = (M^*/T) + N^* \quad (26)$$

where M, N, M^*, and N^* are constants and T is the absolute temperature. By subtraction

$$\log (P_1/P_1^*)_{x_1=0} = (M - M^*)/T + (N - N^*) \quad (27)$$

Since by Equation (19)

$$(\gamma_1)_{x_1=0} = (P_1/P_1^*)_{x_1=0} \quad (28)$$

$$\log (\gamma_1)_{x_1=0} = (A'/T) \times B' \quad (29)$$

Similarly,

$$\log (\gamma_2)_{x_2=0} = (A''/T) + B'' \quad (30)$$

where T = absolute temperature. Equations (25) and (26) permit estimation of $(\partial y_1/\partial x_1)_{x_1=0}$ and $(\partial y_1/\partial x_1)_{x_1=1}$ for higher alcohols in the series by extrapolation, provided these slopes are known for lower members in the series. From these nonideal slopes, activity coefficients at infinite dilution may be calculated and used in equations such as those of van Laar for determining the vapor-liquid equilibria of the system.

CALCULATION PROCEDURE

By use of the data in Tables 1 and 2, which were collected on benzene-ethanol and benzene–*n*-propanol, and those of Gautreaux

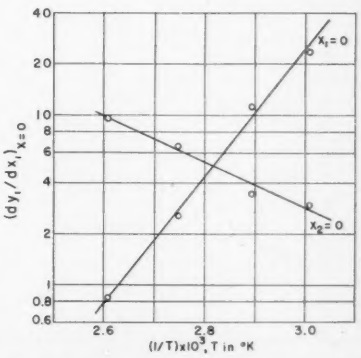

FIG. 1. NONIDEAL SLOPE OF x-y DIAGRAM VS. $1/T$ BENZENE ALCOHOLS.

(6) on benzene-methanol the x-y diagrams were constructed and the initial slopes $\partial y/\partial x$ were determined. These are tabulated in Table 3 and plotted in Figure 1 vs. the reciprocal of the absolute temperature. A straight line resulted. The lines were extended to the benzene-butanol range and extrapolated values of the slopes $\partial y/\partial x$ for this system were read. Later data were collected on the benzene-butanol system and compared with the predicted results obtained by the method shown below.

An example of this type of calculation, for the benzene–n-butanol system, follows. The Van Laar equations are used in this example but any two-constant equation might be used.

At $T = 117.50°C. = 390.50°K.$ the normal boiling point of n-butanol $1/T = 0.002560/°K.$

$$(\partial y_1/\partial x_1)_{x_1=0} = 0.840, \text{ from Figure 1}$$

$$(\partial y_1/\partial x_1)_{x_2=0} = 9.70, \text{ from Figure 1}$$

$$(\partial y_1/\partial x_1)^*_{x_1=0} = \frac{(f_1^\circ)_L}{(f_1^\circ)_V} =$$

$$\frac{(vP_1^*)\ P_1^*\, e^{V_1(\pi - P_1)/RT}}{(v_\pi)_1\ \pi} =$$

0.2189 (at boiling point of benzene)

$$(\partial y_1/\partial x_1)^*_{x_2=0} = \frac{(f_2^\circ)_L}{(f_2^\circ)_V} =$$

$$\frac{(vP_2^*)\ P_2^*\, e^{V_2(\pi - P_2)/RT}}{(v_\pi)_2\ \pi} =$$

2.7752 (at boiling point of n-butanol)

$$(\gamma_1)_{x_1=0} = 0.840/0.2189 = 3.837$$

$$(\gamma_2)_{x_2=0} = 9.70/2.7752 = 3.495$$

$$A = \log(\gamma_1)_{x_1=0} = \log 3.837 = 0.58399$$

$$B = \log(\gamma_2)_{x_2=0} = \log 3.495 = 0.54345$$

Activity coefficients over the entire concentration range may be determined by substitution in the van Laar equations (4).

The following procedure permits calculation of x and y from the activity coefficients (8).

1. Assume a boiling point for the solution of composition x_1.

2. Determine P_1*and P_2* at this temperature.

3. Calculate y by the following equation:

$$y_1 = \frac{x_1 P_1^* \gamma_1}{x_1 P_1^* + x_2 P_2^* \gamma_2}$$

4. Check the assumed temperature by calculating P_1*:

$$P_1^* = \frac{y_1 \pi}{\gamma_1 x_1}$$

This procedure is repeated until a satisfactory check is obtained. The second assumption usually provides an adequate check.

Figure 2 shows a plot which was prepared for the system benzene–n-butanol by this procedure. Experimental points collected on this same system are also shown, and the agreement is good. Bonauguri et al. (2) report data, collected at 740 mm., which is in general agreement with these data when allowance for the difference in pressure is made. Similar calculations were made on the system benzene–n-amyl alcohol and good agreement was obtained between the calculated and experimental results.

EXPERIMENTAL METHODS

The reagents used were benzene, ethyl alcohol, n-propyl alcohol, n-butyl alcohol and n-amyl alcohol.

The benzene was purchased from Merck and Company and purified by redistillation. The fraction used in this work had a refractive index n_D^{25} of 1.4979, in agreement with values reported in International Critical Tables (14). The ethanol was purchased from U. S. Industrial Chemicals, the n-propanol from Fisher Scientific Company. Both of these were treated with magnesium by the method of Fieser (5) to remove any water present. The refractive index n_D^{25} of the purified ethanol was 1.3595, compared with literature values (12) of 1.3594 to 1.3596; that of n-propanol was 1.3938, compared with literature values (9) of 1.3834.

The n-butanol and n-amyl alcohols were obtained from the Fisher Scientific Company. These were purified by redistillation in an Oldershaw column. The purified n-butanol had a refractive index n_D^{25} of 1.3992, compared with a literature value (7) of 1.3993; the purified n-amyl alcohol had a refractive index n_D^{25} of 1.4082, compared with a literature value (13) of 1.4084.

Densities were also determined and good agreement was obtained with literature values. Refractive indices were determined with a Bausch and Lomb precision refractometer, model 33-45-01.

TABLE 3.—SLOPE AT INFINITE DILUTION OF x-y DIAGRAMS FOR BENZENE-ALCOHOL SYSTEMS

System	$\left(\frac{\partial y_1}{\partial x_1}\right)^*_{x_1=0}$	$\left(\frac{\partial y_1}{\partial x_1}\right)_{x_1=0}$	$(\gamma_1)_{x_1=0}$	T, °K.
Benzene-methanol	1.7808	23.605	13.255	337.9
Benzene-ethanol	1.0677	11.189	10.48	351.5
Benzene–n-propanol	0.5008	2.587	5.165	370.4
Benzene–n-butanol	0.2189	0.840†	3.837	390.7

System	$\left(\frac{\partial y_1}{\partial x_1}\right)^*_{x_2=0}$	$\left(\frac{\partial y_1}{\partial x_1}\right)_{x_2=0}$	$(\gamma_2)_{x_2=0}$	T, °K.
Benzene-methanol	0.6099	2.9551	4.845	337.9
Benzene-ethanol	0.9684	3.4552	3.568	351.5
Benzene–n-propanol	1.6400	6.6108	4.031	370.4
Benzene–n-butanol	2.7752	9.70†	3.495	390.7

The values of $(\partial y_1/\partial x_1)_{x=0}$ were obtained by calculation from $(\gamma)_{x=0}$ and $(\partial y_1/\partial x_1)^*_{x=0}$.

†Extrapolated values.

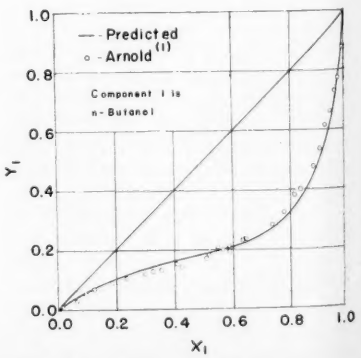

FIG. 2. x-y DIAGRAM FOR BENZENE–n-BUTANOL; PRESSURE: 760 MM. HG.

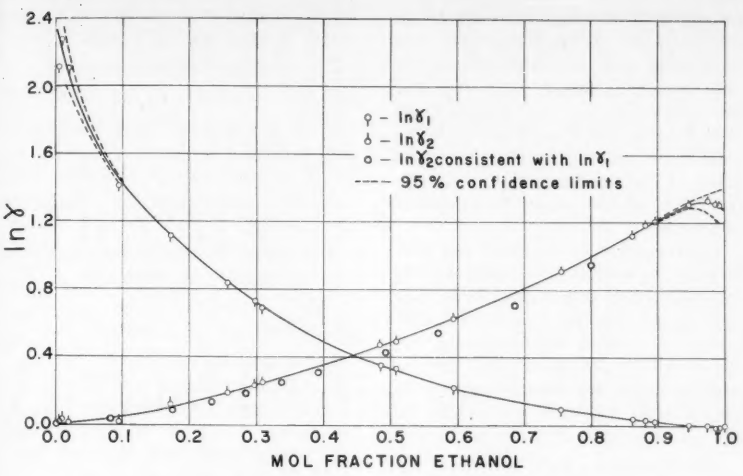

FIG. 3. LOGARITHM ACTIVITY COEFFICIENT VS. MOLE FRACTION ETHANOL, BENZENE-ETHANOL SYSTEM.

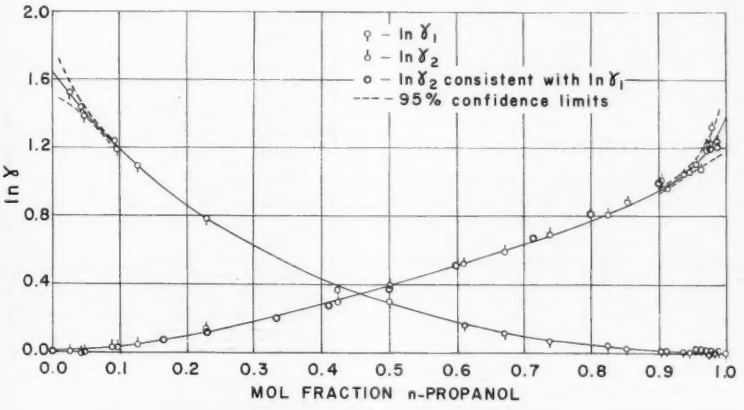

FIG. 4. LOGARITHM ACTIVITY COEFFICIENT VS. MOLE FRACTION *n*-PROPANOL, BENZENE–*n*-PROPANOL SYSTEM.

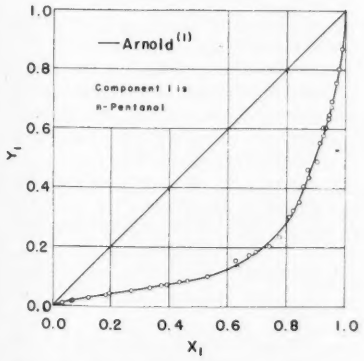

FIG. 5. *x-y* DIAGRAM FOR BENZENE–*n*-PENTANOL; PRESSURE: 760 MM. HG.

APPARATUS AND PROCEDURE

The apparatus used in collecting the present data was an equilibrium still designed by Jones, Schoenborn, and Colburn(*10*). The still had a capacity of about 65 ml. The contents of the still were protected at all times from atmospheric moisture by means of a silica gel drying tube.

Copper - constantan thermocouples were used to measure the temperatures, with an insulated ice bath to maintain a constant reference temperature. A Leeds and Northrup type *K* potentiometer capable of measuring voltages of 0.001 mv. was used to measure the thermocouple e.m.f. The null point was indicated by a suspended-coil D'Arsonval-type galvanometer, with which a bracket 0.004 mv. wide could be obtained around the correct e.m.f. reading. This is equivalent to a bracket of 0.09°C. around the correct temperature over the temperature range of these experiments.

A Cartesian-type manostat was used to regulate the pressure in the still to 760 mm. Hg and to keep pressure fluctuations to within ±2 mm. of water or ±0.1474 mm. Hg. The difference between atmospheric pressure and the still pressure was indicated by a differential water manometer. The slight vacuum was maintained by means of an aspirator.

Atmospheric pressure was measured with a mercury barometer which could be read to the nearest 0.01 Hg or 0.3 mm. Hg. Thus, any temperature fluctuations due to the variation of pressure from 760 mm. Hg were small and could be assumed negligible.

The condensed vapor and liquid samples were analyzed for composition with a Bausch and Lomb refractometer. With this instrument the refractive index could be read to the nearest 0.0001 and estimated to the nearest 0.00001. The calibration of the instrument was checked with a test glass of known refractive index supplied with the instrument.

The temperature of the instrument was held to 25°C. ± 0.2° by means of water circulation from a constant-temperature water bath. Before any vapor-liquid equilibrium data were collected, the thermocouples were calibrated. Charts relating the composition to the refractive index were prepared for each system.

The vapor-liquid equilibrium data were collected at a total pressure of 760 mm. Hg and over the entire range of concentrations.

EXPERIMENTAL DATA*

The experimental results obtained by the present authors consist of vapor-liquid equilibrium data for the two binary systems, benzene-ethanol and benzene–*n*-propanol, shown in Tables 1 and 2. In addition, the results of Gautreaux(*6*) on benzene-methanol and of Arnold(*1*), on benzene–*n*-butanol, and benzene–*n*-amyl alcohol have been included. These men worked on this same general project in the same laboratories as the authors.

Activity coefficients (*see* Figures 3 and 4) for component 2, which are thermodynamically consistent with activity coefficients for component 1, have been calculated by the Gibbs-Duhem equation to show the consistency of the data. Ninety-five per cent confidence limits, indicated by dashed lines in the figures, were also calculated for these experimental data.

Benzene-methanol data are reported by Gautreaux(*6*) at 766.4 mm. Hg total pressure.

Temperature measurements have been corrected to a total pressure of 760.0 mm. Hg by means of approximate relationships. These tempera-

* Complete tables of the author's experimental data and also those of Gautreaux (*6*) and Arnold (*1*) are on file with the Photoduplication Service, American Documentation Institute, Library of Congress, Washington 25, D. C., as document 4561 and may be ordered for $1.25 for microfilm or photoprints.

ture corrections were between 0.2 and 0.3°C.

DISCUSSION OF RESULTS

The suggested method for correlation of activity coefficients has been applied to the benzene–*n*-butanol system, the results being plotted in Figure 2. It is pointed out that these vapor-liquid equilibrium data were calculated on the nonideal system benzene–*n*-butanol without the aid of any experimental data on this system.

The results of this calculation are considered to be good. Reference to Figure 2 shows that the greatest disagreement between the calculated and experimental data is between the liquid concentration ranges of 0.2 to 0.8 mole fraction. In this range the predicted line is somewhat higher than the experimental points between 0.2 and 0.5 mole fraction and is somewhat lower than the experimental points between 0.5 and 0.8 mole fraction in the liquid. The difference between the experimental and predicted values are rather small over the entire range. Similar results were obtained when this method was tried on the benzene–*n*-amyl-alcohol system.

An examination of Figure 2 shows that the calculated and experimental curves agree closely in the dilute regions, and it is therefore seen that the calculated and experimental nonideal slopes in the x-y diagram at infinite dilution also agree closely. This is evidence that the proposed correlations of these slopes at infinite dilution is reasonably satisfactory and that the differences between the calculated and experimental curves in Figure 2 are not caused by an inadequacy of the proposed correlation.

The van Laar equations were used in the example presented in this paper. One reason for the difference between the predicted and experimental data may lie in inadequacies in this equation, as has been previously mentioned. It should be borne in mind that the present method allows the prediction of the constants in any two-constant equation for activity coefficients and that the use of the van Laar equations, as such, is not part of the method. Another two-constant equation could have been used. If a three-constant equation for activity coefficients is considered necessary, then the present method should be useful in the prediction of two of the constants.

SUMMARY

The concept of the nonideal vapor pressure of a component in dilute solution has been developed and explained, and the relation between the nonideal vapor pressure and the slope of the y-x equilibrium diagram has been derived. In addition, an equation relating the nonideal vapor pressure and the boiling point of the pure component is presented.

A procedure is outlined for predicting the entire y-x diagram from these nonideal vapor pressures. The method allows data taken on systems for which experimental results are available to be used to predict those for other systems on which only the boiling points of the pure components are available.

Vapor-liquid equilibrium data were collected on the systems benzene-methanol, benzene-ethanol, and benzene–*n*-propanol. These were used to predict the y-x diagram for benzene–*n*-butanol, and the agreement with experimental values was found to be good. Experimental data are also presented on the system benzene–*n*-butanol and benzene–*n*-pentanol (Figure 5).

ACKNOWLEDGMENT

The authors wish to acknowledge assistance of T. H. Arnold, Ethyl research fellow in chemical engineering for 1952-54 at Louisiana State University, for the graphs and for data on benzene–*n*-butanol and benzene–*n*-amyl alcohol. The work described in this paper is part of a continuing research program on vapor-liquid equilibrium being conducted at Louisiana State University under a grant from the Ethyl Corporation.

NOTATION

f = fugacity of component in solution

f° = fugacity of pure component at the temperature and total pressure of the solution

y = mole fraction of component in the vapor

x = mole fraction of component in the liquid

π = total pressure

p = partial pressure of component in the vapor

γ = activity coefficient of component in solution

P^* = vapor pressure of pure component at the temperature of the solution

$K = y/x$ = equilibrium vaporization constant of component

P = nonideal vapor pressure of pure component, defined by Equation (16) at low pressures and concentrations

A, B = constants in the van Laar Equations (17) and (18)

T = absolute temperature, °K.

M, N = constants in Equation (25)

M^*, N^* = constants in Equation (26)

A', B' = constants in Equation (29)

A'', B'' = constants in Equation (30)

ν = fugacity coefficient—ratio of fugacity to pressure

Subscripts

V = vapor state

L = liquid state

1, 2 = component number

P^* or π = pressure at which fugacity coefficient is evaluated

Superscripts

$*$ = the ideal-solution condition

LITERATURE CITED

1. Arnold, T. H., Private communication.
2. Bonauguri, E., L. Bicelli, and G. Spiller, *Chimica e industria (Milan)*, **33**, 81 (1951).
3. Butler, J. A. V., and P. Harrower, *Trans. Faraday Soc.*, **33**, 171 (1937).
4. Carlson, H. C., and A. P. Colburn, *Ind. Eng. Chem.*, **34**, 581 (1942).
5. Fieser, L. F., "Experiments in Organic Chemistry," p. 358, D. C. Heath and Co., Boston (1941).
6. Gautreaux, M. F., Thesis, Louisiana State Univ. (1951).
7. "Handbook of Chemistry and Physics," 30 ed., Chemical Rubber Publishing Co., Cleveland (1947).
8. Hougen, O. A., and K. M. Watson, "Chemical Process Principles," Part II, John Wiley and Sons, Inc., New York (1941).
9. Huntress, E. H., and S. P. Mullikin, "Identification of Pure Organic Compounds," John Wiley and Sons, Inc., New York (1941).
10. Jones, C. A., E. M. Schoenborn, and A. P. Colburn, *Ind. Eng. Chem.* **35**, 666 (1943).
11. Perry, J. H., "Chemical Engineers' Handbook," 3 ed., McGraw-Hill Book Company, Inc., New York (1950).
12. Scatchard, G., and W. J. Hamer, *J. Am. Chem. Soc.*, **57**, 1805 (1935).
13. Timmermans, J., "Physico-Chemical Constants of Pure Organic Compounds," Elsevier Publishing Co., New York (1950).
14. Washburn, E. W., "International Critical Tables," 1 ed., McCraw-Hill Book Company Inc., New York (1926).

Presented at the A.I.Ch.E. Washington meeting

PERFORMANCE OF PACKED COLUMNS

I. Total, Static, and Operating Holdups

H. L. Shulman, C. F. Ullrich, and N. Wells
Clarkson College of Technology, Potsdam, New York

Total and static holdups have been measured for ½-, and 1-in. ceramic Berl saddles, ½-, 1-, and 1½-in. ceramic Raschig rings, and 1-in. carbon Raschig rings with air rates from 100 to 1,000 lb./(hr.) (sq. ft.) and water rates from 1,000 to 10,000 lb./(hr.) (sq. ft.).

The holdup measurements and motion picture observations of the flow of dye solutions through packings provide an explanation for the great differences observed when gas-phase mass transfer rates are measured by absorption and vaporization methods. If the effective interfacial area for vaporization is assumed to be proportional to total holdup and the area for absorption is assumed proportional to operating holdup, the ratio of the two mass transfer rates should be equal to the ratio of the two holdups.

The departure from equality of the two ratios can be explained by the observation that the static holdup is displaced slowly, resulting in additional effective area for absorption over that expected from the operating holdup alone.

In recent years investigations of mass, heat, and momentum transfer in fluid-soild systems have indicated that the free space, or void fraction, ε, is an important variable in the correlation of data (*1, 4, 5, 6, 10, 12*). To apply these findings to an analysis of more complex systems such as those occurring in packed absorption and distillation columns, one must know the total liquid holdup to determine the void fraction available for gas flow under operating conditions. A knowledge of liquid holdups is also of interest in the study of batch distillation and effective interfacial areas for diffusional operations employing packed columns.

Three different types of liquid holdup have been discussed in the literature (*8, 11*). The *total holdup*, h_t, defined as the total liquid in the packing under operating conditions, is expressed as cubic feet of liquid per cubic foot of packing. The *static holdup*, h_s, as used in this work is defined as the liquid in the packing which does not drain from the packing when the liquid supply to the column is discontinued and is also expressed as cubic feet of liquid per cubic foot of packing. The *operating holdup*, h_o, defined as the difference between the total and static holdups, represents the liquid which will drain from the packing and is also a measure of the liquid flowing through the packing when the column is in operation. The relation between the three holdups is given by

$$h_t = h_s + h_o. \qquad (1)$$

Several investigators (*2, 9, 13, 15, 19, 22*) have measured or estimated liquid holdups, and two extensive studies have been reported by Elgin and coworkers (*3, 11*). Unfortunately the previous investigations have dealt with operating holdups almost exclusively and no investigation has been reported of the three types of liquid holdup in packings for which extensive mass transfer data are available, namely, Raschig rings and Berl saddles.

The object of the present work is the determination of the three types of liquid holdup for 0.5-, 1.0-, and 1.5-in. unglazed white porcelain Raschig rings, 0.5-, and 1.0-in. unglazed white porcelain Berl saddles, and 1.0-in. carbon Raschig rings. These data will be used to explain the differences observed in gas-phase mass transfer rates when vaporization and absorption techniques are used. In Part II of this paper the data will be applied to

Additional tabular material may be obtained from the Photoduplication Service, American Documentation Institute, Library of Congress, Washington 25, D.C., as document 4565 for $1.25 for microfilm or photoprints.

TABLE 1.—CHARACTERISTICS OF PACKING USED FOR HOLDUP MEASUREMENTS

Type	Raschig rings (U. S. Stoneware Co.)			Berl saddles (Maurice A. Knight Co.)		Raschig rings (National Carbon Co.)
Manufacturer						
Material	Unglazed white porcelain			Unglazed white porcelain		Carbon
Nominal size, in.	0.5	1.0	1.5	0.5	1.0	1.0
Void fraction, dry	0.605	0.726	0.715	0.660	0.695	0.700
Specific gravity, dry	2.38	2.41	2.36	2.36	2.44	1.57
Pieces/cu. ft	10,900	1,370	430	15,000	1,810	1,470
Surface area, sq. ft./cu. ft.	116	58.5	40.9	133	62.6	62.7
Surface area/piece, sq. ft.	0.01063	0.0427	0.0952	0.00888	0.0346	0.0427
Diameter of equivalent sphere, ft.	0.0582	0.1167	0.1740	0.0532	0.1050	0.1167

the problem of separating the volumetric mass transfer coefficients (k_Ga and k_La) into their components, the effective interfacial area, a, and the mass transfer coefficients, k_G and k_L.

EQUIPMENT

The equipment used for these studies, shown schematically in Figure 1, is the same as that described in detail in a recent paper by Shulman and DeGouff (*18*) except for minor modifications, which will be discussed. A water tank and pump were installed to permit adjustment of water temperature and recycling of water. Two calibrated rotameters were installed to replace the orifice meters previously used to meter the air. The 10-in.-diam. by 36-in. packed glass column was arranged so that it might be weighed with its contents while in operation. This was done by supporting the column by means of four 0.25-in. steel rods connected at the top by a yoke and at the bottom by a steel ring on which the glass column and the four legs of the packing support plate rested. In operation the glass column was suspended in air except for a few inches at the bottom which were immersed in a water seal. The column and its contents were counterbalanced by weights on a pan connected to the yoke at the top of the column by the lever arm and knife edges obtained from a platform scale. The pan of weights rested in turn on the pan of a 20-kg.-capacity platform scale which could be read to within 1 g. The weighing system was capable of detecting a change in weight of the column of as little as 3 g., and it was therefore possible to determine holdups to within 1% under the poorest conditions, i.e., static-holdup determinations of the larger packings. The column was open at the top to the atmosphere, and so a draft gauge employed for reading the pressure at the base of the column measured the pressure drop across the packing. The weighings were corrected for the buoyancy effect of the portion of the column in the water seal and for the upward thrust due to the pressure drop across the column, which was operated at all times with 28 in. of packing using water at 19° to 25°C. and saturated air of approximately the same temperature to prevent vaporization of water.

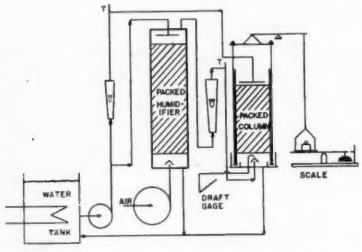

FIG. 1. SCHEMATIC DIAGRAM OF APPARATUS.

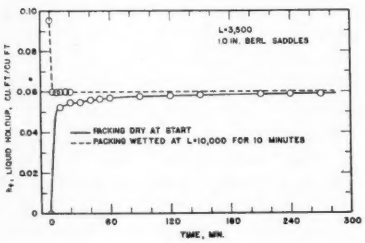

FIG. 2. TOTAL HOLDUP VS. TIME AT $L = 3{,}500$ FOR 1.0-IN. BERL SADDLES.

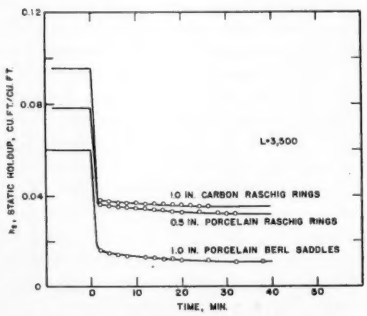
L=3,500
1.0 IN. CARBON RASCHIG RINGS
0.5 IN. PORCELAIN RASCHIG RINGS
1.0 IN. PORCELAIN BERL SADDLES
h_t, STATIC HOLDUP, CU FT/CU FT
TIME, MIN.

FIG. 3. STATIC HOLDUP VS. DRAINAGE TIME.

The water distributor, which was supported independently of the column approximately 1/2 in. above the packing, consisted of eight arms extending radially from a special fitting and was 9 in. in diameter. It had a total of 160 0.1-in. holes evenly spaced in three rows on four alternate arms and in a single row on the remaining arms. Several holes were plugged with solder as the result of tests made to ensure uniform distribution of liquid for the liquid rates employed.

PROCEDURE

Preliminary tests made possible the establishment of a procedure which gave reproducible data even when the column was emptied and repacked. When the column was packed with dry packing and the water rate was set at a fixed value, the total holdup was found to increase with time until a constant equilibrium value was reached. The same equilibrium value could be reached in a much shorter time by supplying water at a very high rate for a short time, to wet the packing thoroughly, and then running at the desired rate. Figure 2 shows the total holdup for 1.0-in. Berl saddles as a function of time when the two methods are employed. The effect of time is even more noticeable with the smaller packings, which have greater holdups. The buildup with time is believed to be due to the gradual accumulation of water in pockets at points of contact, inside rings, or on portions of the surface which are not continually covered by flowing liquid. The splashing of liquid as it falls from one piece of packing to another and the random motion of the moving liquid over the surface of the packing not only causes this gradual accumulation, until an equilibrium value is reached, but also results in a slow turnover of the liquid in what might otherwise be stagnant pockets. Observations based upon motion picture studies of the flow of dye solutions in packings will be discussed later in connection with the interpretation of mass transfer data.

The total holdup was found to vary with the density of the packed bed

TABLE 2.—VARIATION OF HOLDUP WITH PACKING DENSITY

Packing: 1.0-in. porcelain Raschig rings

Liquid rate, lb./(hr.) (sq. ft.)	3,500	3,500	3,500	3,500	3,500	3,500
Gas rate, lb./(hr.) (sq. ft.)	0	0	300	300	600	600
Void fraction, dry	0.726	0.709	0.726	0.709	0.726	0.709
Pieces/cu. ft., N	1,370	1,460	1,370	1,460	1,370	1,460
h_t, cu. ft./cu. ft.	0.0539	0.0567	0.0543	0.0574	0.0592	0.0724
$(h_t/N)\times10^5$	3.94	3.88	3.96	3.93	4.32	4.96

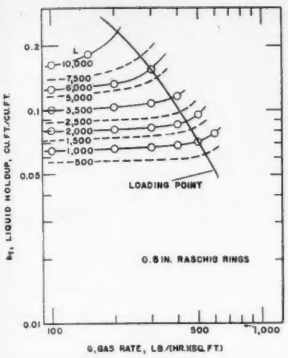

FIG. 4. TOTAL HOLDUP IN 0.5-IN. RASCHIG RINGS.

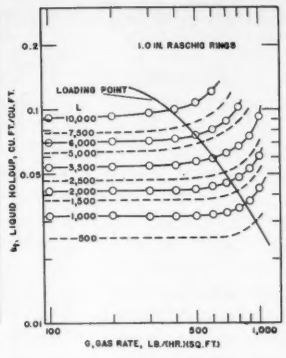

FIG. 5. TOTAL HOLDUP IN 1.0-IN. RASCHIG RINGS.

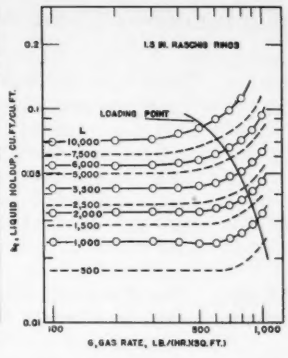

FIG. 6. TOTAL HOLDUP IN 1.5-IN. RASCHIG RINGS.

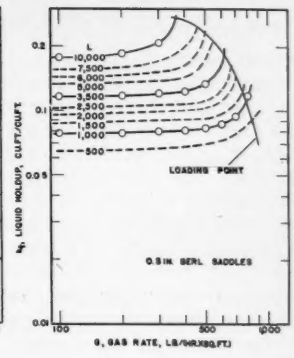

FIG. 7. TOTAL HOLDUP IN 0.5-IN. BERL SADDLES.

when the column was repacked several times with the same packing. For this reason the holdups reported apply only to packing with the characteristics listed in Table 1. The data in Table 2 show that the total holdups are approximately proportional to the number of pieces of packing per cubic foot for a given packing. This observation provides the simplest correction for packing densities other than those listed in Table 1.

To determine the static holdup, h_s, the water supply was cut off after equilibrium conditions were reached, the column was permitted to drain, and a record of column weight vs. time was made. Figure 3 illustrates several drainage curves. It will be noticed that different packings require different lengths of time to drain to fairly constant weight.

On the basis of these preliminary tests the following procedure was adopted to ensure obtaining reproducible data. The air was saturated and cooled to the temperature of the water in the tank. The weight of the column and the dry packing was obtained and the packing was thoroughly wetted by setting the water rate up to over 10,000 lb./(hr.)(sq.ft.) for a minimum of 1 hr. The water rate was then decreased to the rate to be investigated and the air rate was set at 100 lb./(hr.)(sq.ft.) When the platform scale indicated constant weight for more than 3 min. the readings of weight, pressure drop, and temperature were taken and the air rate was increased to the next higher value. For each packing a series of runs was made in this fashion at constant liquid rates with increasing gas rates. The highest liquid rate, 10,000 lb./(hr.)(sq.ft.), was used first, and the gas rate was increased up to 1,000 lb./(hr.)(sq.ft.) or the flooding point, whichever was reached first. The lowest liquid rate employed was 1,000 lb./(hr.)(sq.ft.) because it was felt that good liquid distribution could not be ensured at lower rates.

For the static holdup tests a similar procedure was followed, but the water supply was cut off when equilibrium was reached and data for a drainage curve were recorded. It was soon found that static holdup was independent of liquid and gas rates when this procedure was employed, and so it was not necessary to investigate the two ranges so thoroughly as for total holdup.

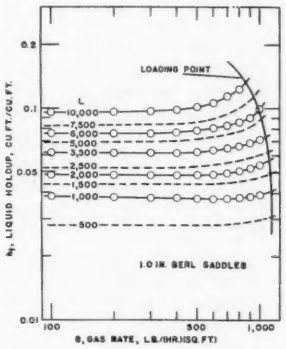

FIG. 8. TOTAL HOLDUP IN 1.0-IN. BERL SADDLES.

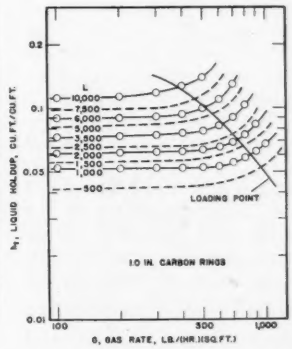

FIG. 9. TOTAL HOLDUP IN 1.0-IN. CARBON RINGS.

EXPERIMENTAL RESULTS

Total Holdup. The data obtained from the total holdup measurements are plotted in Figures 4 to 9 for the six packings studied. The experimental points are shown, and additional lines, obtained by interpolation, extrapolation, and cross plotting, have been added to make the plots more useful for estimating total holdups in the ranges of gas and liquid rates covered. The loading-point line on each plot was obtained from the data of Tillson (*21*) for the same packing. The shapes of the curves are quite similar to those obtained by Elgin and Weiss (*3*) for operating holdups. This is to be expected because the two holdups differ by a constant, the static holdup, as will be shown later. At low liquid rates the total holdup is almost independent of gas rate up to the loading point, but for higher liquid rates, especially for the smaller packings, and for gas rates at approximately the loading point the effect of gas rate cannot be ignored. This sudden increase in holdup as gas rate increases causes the break in the pressure-drop curve which has been taken as the definition of the loading point. It is interesting to note that the total holdups for 1.0-in carbon rings are greater than those for porcelain rings of the same size. This difference is accounted for by the differences in static holdup for the two packings; thus the operating holdups are of the same magnitude. Apparently the nature of the surfaces causes a greater accumulation of semistagnant water in carbon than in porcelain; therefore the total and static holdups reported here probably do not apply to surfaces other than ceramics similar to unglazed

TABLE 3.—CONSTANTS FOR EMPIRICAL EQUATIONS FOR TOTAL AND STATIC HOLDUPS

Type of packing material	Raschig rings Porcelain	Raschig rings Carbon	Saddles Porcelain	Equation
α	2.25×10^{-5}	7.90×10^{-5}	2.50×10^{-5}	2
γ	0.965	0.706	0.965	3
δ	0.00104	0.00250	0.00032	4
θ	0.376	0.376	0.376	3
λ	1.21	1.21	1.56	4
D_P, 1.5-in. packing, ft.	0.174	0.178	0.155	2, 3, 4
D_P, 2.0-in. packing, ft.	0.238	0.235	.....	2, 3, 4

porcelain. The operating holdups, however, seem to be independent of the nature of the surface.

For purposes of estimating the total holdups of rings and saddles larger than those investigated in this study the following empirical equations are recommended below the loading point:

$$h_t = \frac{\alpha L^{\beta}}{D_P^{\,2}} \qquad (2)$$

$$\beta = \gamma D_P^{\,\theta} \qquad (3)$$

The constants, α, γ, and θ, are given in Table 3. These equations fit the experimental data very well up to loading and have been found useful for estimating the holdups for 2.0-in. rings and 1.5-in. saddles.

Static Holdup. The experimental data for the static holdups, summarized in Table 4, show the holdups to be independent of varying gas and liquid rates. In Figure 10 the average value of static holdup for each packing is plotted vs. the equivalent diameter, D_p. Although an insufficient number of packings of each type have been studied to give a good correlation of the data, it is evident that the static holdup is a function of the material of construction, the shape of the packing, and the size of the packing.

The lines on Figure 10 may be used to estimate the static holdups of packings which have not been studied, or the following equation for the lines may be used.

$$h_s = \delta D_P^{\,-\lambda} \qquad (4)$$

The constants, δ and λ, are given in Table 3.

The static holdup, which is a measure of the accumulated semistagnant liquid, may play an important, but hitherto unknown, role in the interpretation of mass transfer studies in packing. It can easily be seen that this semistagnant liquid may be as effective as moving liquid for vaporization work, but relatively ineffective for absorption or desorption operations. A more detailed analysis of this problem is given in another section of this paper.

Operating Holdup. The operating holdup is determined by taking the difference between the total and the static holdups, as indicated by Equation (1). The operating holdups derived from the present studies are in fair agreement with those obtained by previous investigators. The differences may be due to the use of different materials of construction of the packing, slightly different packing dimensions, differences in methods of packing the column, and different drainage

TABLE 4.—SUMMARY OF STATIC HOLDUP DATA

Type of packing material		Static holdup, h_s, cu. ft./cu. ft. Raschig rings Unglazed porcelain			Berl saddles Unglazed porcelain		Raschig rings Carbon
Nominal size, in.		0.5	1.0	1.5	0.5	1.0	1.0
L	G						
10,000	0	0.0322	0.0150	0.00884	0.0315	0.0108	0.0358
6,000	0	0.0328	0.0149	0.00895	0.0315	0.0110	0.0357
3,500	0	0.0326	0.0150	0.00895	0.0319	0.0110	0.0359
2,000	0	0.0326	0.0149	0.00899	0.0318	0.0111	0.3539
1,000	0	0.0324	0.0148	0.00893	0.0318	0.0110	0.0359
3,500	300	.....	.....	0.00896	0.0318		
3,500	300	.....	0.0152				
3,500	600	.....	.....	0.00867			
3,500	600	.....	0.0151				
6,000	200	0.0325					
6,000	300	.....	.....	.....	.....	0.0111	0.0359
Average h_s		0.0325	0.0150	0.00890	0.0317	0.0110	0.0358

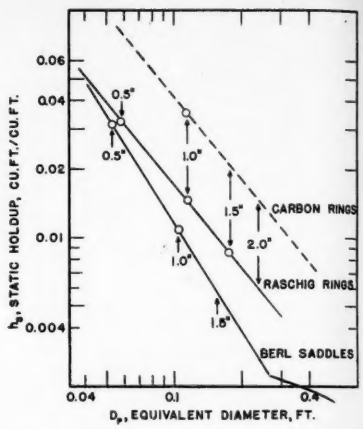

FIG. 10. STATIC HOLDUP OF PACKINGS.

times. Thus Furnas and Bellinger (*9*) drained for 3 min., Jesser and Elgin (*11*) for 10 min., and the authors for each packing to a constant weight.

Serious errors may be made in estimating operating holdups by using the methods presented by previous investigators and adopted by various texts and handbooks presenting these data. In the past it has been assumed that operating holdup is independent of gas rate up to the flooding point and so operating holdups were in many cases measured at zero gas rate. These data are then plotted as straight lines with logarithmic coordinates and extrapolated to very high liquid rates approaching 100,000 lb./(hr.)(sq.ft.) in some cases. From Figures 4 to 9 it may be seen such a procedure would give erroneous operating holdups for all but very low gas rates. It is recommended that by means of Figures 4 to 10 and Equation (1) operating holdups be determined at the actual gas and liquid rates employed.

APPLICATIONS TO MASS TRANSFER

The primary reason for obtaining the holdup data was a desire to determine the void fraction in packings under operating conditions in order to separate the mass transfer coefficients, k_G and k_L, from the volumetric transfer coefficients, k_Ga and k_La. This work is reported in Part II and will not be discussed here.

Figure 2 emphasizes a fact which has been reported occasionally by investigators on the basis of their experience: it is desirable to wet a packing thoroughly before

attempting to determine mass transfer coefficients or the equivalent. This is particularly important when small packings are employed at low liquid rates because it may take several hours of operation under such conditions before the equilibrium total holdup is reached. Failure to observe this precaution undoubtedly accounts for widely scattered data, which are difficult to interpret and impossible to reproduce. If in addition, poor liquid distribution and end effects are added to the usual analytical problems it is easy to understand why the literature contains a considerable number of investigations, the results of which may never be fully explained.

The results of the holdup studies, presented in Figures 4 to 10, may offer an explanation of several mass transfer anomalies which have arisen in recent years. The first is concerned with the differences observed when gas-phase mass transfer coefficients, $k_G a$, are determined by vaporization and absorption methods. Excellent discussions of this problem are provided by Pigford and Colburn (*14*) and Sherwood and Pigford (*17*). These authors point out that the most reliable data for $k_G a$, obtained by vaporization and absorption measurements, are in disagreement by as much as 300% and no simple explanation is available to account for such large differences. One possibility suggested by these authors is that the ammonia absorption data, which are believed to be reliable, should be interpreted as though a chemical reaction takes place when ammonia dissolves in water and the reaction rate is slow enough to cause an abnormally high liquid-phase resistance. This suggestion was based on the work of Vivian and Whitney (*23* and *24*) on the absorption of chlorine and sulfur dioxide where a mechanism of this sort seemed to explain the data; however, the same authors compared the gas-phase mass transfer coefficients obtained from the sulfur dioxide work with those obtained by ammonia absorption and found them to be in reasonable agreement, and so it is rather unlikely that the chemical reaction mechanism can explain such large differences as have been observed.

An explanation for this mass transfer problem can be offered on the basis of observations of the flow of dye solutions through packed columns. The equipment used for the holdup studies was arranged so that a concentrated dye solution might be injected into the water line several inches before the liquid distributor. With the equipment in operation at a fixed liquid rate the dye solution was injected at a continuous rate for a short period of time and then cut off. By use of 1.5-in. Raschig rings, it was possible to observe the displacement of clear water by dye solution and then the displacement of dye solution by clear water through the glass column. It was found that a considerable portion of the water was not displaced immediately; i.e., there was no sharp line of demarcation between water and dye solution as dye was added or when the dye was cut off. Instead there were pockets of what might be described as semistagnant liquid and splashing, and the random motion of liquid over the packing surface deposited or removed dye from these areas by means of a slow and random dilution process. Thus when dye was injected for about 20 sec. some of the pockets picked up dye, which was not completely washed out by the following clear water until as much as 5 min. had passed. The water in these pockets corresponds to the static holdup, and the rate at which water enters or leaves these areas can be judged qualitatively from Figure 2, which shows the buildup of total holdup when dry packing is used. It can be concluded that there exists in the packing a quantity of water, with a corresponding interfacial area, the composition of which would change rather slowly even if the composition of the liquid entering the column changed rapidly.

If a packed column is used for vaporization, the effective interfacial area consists of the surface area of the moving liquid as well as of the water in the semistagnant pockets. If the column is used for absorption the semistagnant pockets tend to become saturated in a short time, their surface area becomes ineffective, and so the effective interfacial area is substantially that of the moving liquid alone. Of course, the observed volumetric mass transfer coefficients, $k_G a$, for the two cases will be different because the effective areas are different. This explanation can be tested quantitatively if the effective area for vaporization is assumed to be proportional to the total holdup, h_t, and that for absorption proportional to the operating holdup, h_o, which represents the moving liquid.

This same line of reasoning can be extended to predict, in part, the behavior of packed columns used for absorption followed by an irreversible chemical reaction such as the absorption of ammonia in acid or of sulfur dioxide and chlorine in alkali solutions. For example, if ammonia is absorbed in water or very dilute acid, the effective area will be that of the moving liquid. As the acid concentration is increased, the semistagnant liquid, even with its slow turnover, will have an increasing capacity to absorb ammonia and at high enough acid concentrations this liquid may be as effective as the moving liquid. Thus one would predict a plot of $k_G a$ vs. acid concentration which would have the $k_G a$ value for water absorption at zero acid concentration, and then $k_G a$ would increase as acid concentration increased until the limiting value corresponding to the $k_G a$ to be expected for vaporization, corrected for diffusivity, was reached. It should be noted that this explanation provides the two extreme values of $k_G a$ but cannot, by itself, predict the shape of the intermediate portion of the curve because the relative rates of chemical reaction and diffusion must be taken into account as well as the changing effective area. For the same reason, any theory of absorption and chemical reaction in packed columns which does not take account of the variable effective area could not predict quantitatively the effect of concentrations. It should be noted that the concentration of the solute in the gas phase will influence the effectiveness of the semistagnant liquid. The greater this concentration, the lower the effectiveness because the acid in the pockets will be neutralized at a faster rate than at lower concentrations. As both acid concentration in the liquid and solute concentration in the gas must be considered when a reaction occurs with or without a changing effective area, it may be possible to take into account the effect of these concentrations on both the rates and areas at the same time. Sherwood and Pigford (*17*) provide an excellent discussion of simultaneous absorption and chemical reaction.

To test the explanations offered, as suggested, it was necessary to search the literature for reliable mass transfer data obtained with the Raschig rings and Berl saddles for which holdup data are available. Unfortunately, there is a very

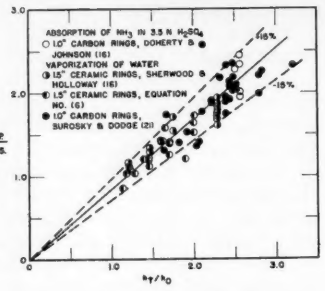
ABSORPTION OF NH3 IN 3.5 N H2SO4
○ 1.0" CARBON RINGS, DOHERTY & JOHNSON (16)
VAPORIZATION OF WATER
◑ 1.5" CERAMIC RINGS, SHERWOOD & HOLLOWAY (16)
◐ 1.5" CERAMIC RINGS, EQUATION NO. (6)
● 1.0" CARBON RINGS, SUROSKY & DODGE (21)
+15%
-15%
(kGa)VAP / (kGa)ABS.
ht/ho

FIG. 11. $(k_Ga)_{vap}/(k_Ga)_{abs}$ vs. h_t/h_o.

limited amount of data suitable for this purpose. An excellent set of data given by Fellinger(*7*) for ammonia absorption in water can be corrected for liquid-phase resistance by means of the Sherwood and Holloway(*16*) correlation and for gas diffusivity to the 2/3 power to provide k_Ga for absorption for all the comparisons desired. Reliable vaporization data are difficult to obtain because end effects are extremely important when the short packing heights required are employed. Surosky and Dodge(*20*) give water-vaporization data for 1.0-in. carbon rings which have been corrected for end effects. Sherwood and Holloway(*16*) report water vaporization data for 1.5-in. ceramic rings for which end effects are estimated to be 35 to 40%. An equation was given for the uncorrected data by Pigford and Colburn (*14*) which is equivalent to

$$k_Ga = 0.0341\,G^{0.69}\,L^{0.33} \qquad (5)$$

Applying a correction of 37.5% based on the investigators' estimate of end effects results in the corrected equation

$$\kappa_Ga = 0.0213\,G^{0.69}\,L^{0.33} \qquad (6)$$

This equation as well as the corrected experimental data can be used for the comparisons. Some data for the absorption of ammonia in sulfuric acid by use of 1.0-in. carbon rings were obtained by Doherty and Johnson and reported by Sherwood and Holloway(*16*). The experimental points of the four sources mentioned were used if the combination of liquid and gas rates fell in the regions investigated in the holdup work reported in Figures 4 to 9. It was felt that excessive extrapolation of the holdup curves was not justified because poor liquid distribution at low liquid rates and rapidly changing holdups at gas and liquid rates above loading would add to the scattering of the original data and result in an inconclusive test of the proposed explanation.

Figure 11 is a plot of the ratio $(k_Ga)_{vap}/(k_Ga)_{abs}$ vs. the holdup ratio h_t/h_o where $(k_Ga)_{vap}$ is the value obtained from the vaporization measurements and absorption runs with high acid concentrations and $(k_Ga)_{abs}$ is the corresponding value for ammonia absorption in water at the same gas and liquid rate, as obtained by Fellinger(*7*). The ammonia and water data were corrected to a common basis by correcting for gas diffusivity to the 2/3 power, employing the values of 0.236 (cm.sq.)/(sec.) for ammonia and 0.256 (cm.sq.)/(sec.) for water at 25°C. and 1 atm. It can be seen that the points fall in a band which is relatively narrow when one considers that the magnitude of some of the ratios represents otherwise unexplainable differences of well over 200%. The best line through the points can be represented by

$$\frac{(k_Ga)_{vap}}{(k_Ga)_{abs}} = 0.85\,\frac{h_t}{h_o} \qquad (7)$$

The broken lines on the diagram 15% above and below the best line indicate the magnitude of the agreement of most of the points. The average deviation from the line given by Equation (7) is ± 8%. The inequality of the two ratios may be caused by the failure of the effective areas to be directly proportional to the holdups as assumed, a different proportionality for the two areas, surface temperature variations making one area less effective than the other, and the possibility that the slow, but finite, turnover of the semistagnant liquid makes some of its area effective for absorption with water work. The departure from equality is not great, however, and it seems as if Equation (7) can be used empirically with Fellinger's data and the holdups to predict mass transfer rates for vaporization and absorption with concentrated absorbents.

A test of the ability of Equation (7) to predict the limiting values of k_Ga for a k_Ga vs. acid concentration plot is shown in Figure 12. The acid-absorption K_Ga data are plotted, and Fellinger's water-absorption value of k_Ga as well as the k_Ga obtained by multiplying it by 0.85 (h_t/h_o) are shown as limiting values. It can be seen that all the experimental data fall between the two as expected, and at high concentrations there is close agreement with the limiting value.

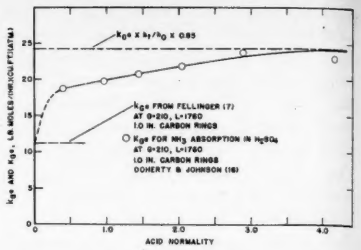
kGa x ht/ho x 0.85
kGa FROM FELLINGER (7)
AT G=210, L=1760
1.0 IN. CARBON RINGS
○ KGa FOR NH3 ABSORPTION IN H2SO4
AT G=210, L=1760
1.0 IN. CARBON RINGS
DOHERTY & JOHNSON (16)
kGa AND KGa, LB. MOLES/(HR.)(SQ.FT.)(ATM.)
ACID NORMALITY

FIG. 12. AMMONIA ABSORPTION IN SULFURIC ACID.

Another packed-column mass transfer anomaly which may be explained eventually with holdup data is the reason for the different effects of gas diffusivity obtained when vaporization and absorption techniques are employed. A large amount of mass transfer data obtained with all sorts of materials and techniques indicates that the gas-phase mass transfer rates should be proportional to gas diffusivity raised to the 2/3 power. However, two seemingly reliable sets of data obtained by vaporization techniques by Surosky and Dodge(*20*) and Mehta and Parekh as reported by Sherwood and Holloway(*16*) indicate the power to be 0.15 to 0.17. The vaporization technique assumes that the effective interfacial area is the same when different liquids wet the packing. In view of the fact that static holdups are a function of surface properties such as interfacial tensions, as illustrated by the differences obtained with carbon and porcelain, one would expect liquids with different physical and chemical properties to wet solid surfaces differently. At the present time this explanation cannot be tested; however, work underway to study the effects of surface tension, viscosity, and the nature of solid surface on holdups may provide the required data.

SUMMARY

Total, static, and operating holdups, obtained for six ring and saddle packings, are represented by Figures 4 to 10 and Equation (1). Equations (2), (3), and (4) may be used to estimate holdups up to loading conditions for rings and saddles larger than those investigated. Total holdups are approximately proportional to the number of pieces of packing per cubic foot. Static holdups are independent of gas and liquid rates but are dependent upon the nature of the surface of the packings; operating holdups are independent of the packing surface.

The holdups can be used to explain the differences between gas-phase mass transfer rates obtained by vaporization and absorption techniques and to provide the limiting mass transfer rates for low and high absorbent concentrations when absorption is followed by an irreversible chemical reaction.

NOTATION

a = effective interfacial area, sq. ft./cu.ft.
D_p = diameter of sphere possessing the same surface area as a piece of packing, ft.
G = superficial gas rate, lb./(hr.)(sq.ft.)
h_o = operating holdup, cu.ft./cu.ft.
h_s = static holdup, cu.ft./cu.ft.
h_t = total holdup, cu.ft./cu.ft.
k_G = gas-phase mass transfer coefficient, lb. moles/(hr.)(sq. ft.)(atm.)
k_L = liquid-phase mass transfer coefficient, lb. moles/(hr.)(sq. ft.)(lb. mole/cu.ft.)
L = superficial liquid rate, lb./(hr.)(sq.ft.)
N = pieces of packing/cu.ft. of packing

Subscripts

vap = obtained by vaporization or absorption in very concentrated absorbents
abs = obtained by absorption in water or extremely dilute absorbents

Greek Letters

α = constant in Equantion (2)
β = constant in Equation (2)
γ = constant in Equation (3)
δ = constant in Equation (4)
ε = void fraction, cu.ft./cu.ft.
θ = constant in Equation (3)
λ = constant in Equation (4)

LITERATURE CITED

1. Chu, J. C., J. Kalil, and W. A. Wetteroth, *Chem. Eng. Progr.*, **49**, 141 (1953).
2. Cooper, C. M., R. J. Christl, and L. C. Perry, *Trans. Am. Inst. Chem. Engrs.*, **37**, 979 (1941).
3. Elgin, J. C., and F. B. Weiss, *Ind. Eng. Chem.*, **31**, 435 (1939).
4. Ergun, S., *Chem. Eng. Progr.*, **48**, 89 (1952).
5. Ergun, S., *Chem. Eng. Progr.*, **48**, 227 (1952).
6. Evans, G. C., and C. F. Gerald, *Chem. Eng. Progr.*, **49**, 135 (1953).
7. Fellinger, L., Sc.D. thesis, Mass. Inst. Technol. (1941).
8. Fenske, M. R., C. O. Tongberg, and D. Quiggle, *Ind. Eng. Chem.*, **31**, 435 (1939).
9. Furnas, C. C., and F. M. Bellinger, *Trans. Am. Inst. Chem. Engrs.*, **34**, 251 (1938).
10. Gamson, B. W., *Chem. Eng. Progr.*, **47**, 19 (1951).
11. Jesser, B. W., and J. C. Elgin, *Trans. Am. Inst. Chem. Engrs.*, **39**, 277 (1943).
12. McCune, L. K., and R. H. Wilhelm, *Ind. Eng. Chem.*, **41**, 1124 (1949).
13. Payne, J. W., and B. F. Dodge, *Ind. Eng. Chem.*, **24**, 630 (1932).
14. Perry, J. H., "Chemical Engineers' Handbook," 3rd ed., Section 10, McGraw-Hill Book Company, Inc., New York (1950).
15. Piret, E. L., C. A. Mann, and T. Wall, *Ind. Eng. Chem.*, **32**, 861 (1940).
16. Sherwood, T. K., and F. A. L. Holloway, *Trans. Am. Inst. Chem. Engrs.*, **36**, 21 and 39 (1940).
17. Sherwood, T. K., and R. L. Pigford, "Absorption and Extraction," 2nd ed., McGraw-Hill Book Company, Inc., New York (1952).
18. Shulman, H. L., and J. J. DeGouff, *Ind. Eng. Chem.*, **44**, 1915 (1952).
20. Simmons, C. W., and H. B. Osborn, *Ind. Eng. Chem.*, **26**, 529 (1934).
21. Surosky, A. E., and B. F. Dodge, *Ind. Eng. Chem.*, **42**, 1112 (1950).
22. Tillson, P., S.M. thesis, Mass. Inst. Technol. (1939).
23. Uchida, S., and S. Fujita, *J. Soc. Chem. Ind. (Japan)*, **39**, 432 (1936); **40**, 238 (1937).
24. Vivian, J. E., and R. P. Whitney, *Chem. Eng. Progr.* **43**, 691 (1947).
25. Whitney, R. P., and J. E. Vivian, *Chem. Eng. Progr.*, **45**, 323 (1949).

II. Wetted and Effective-interfacial Areas, Gas - and Liquid-phase Mass Transfer Rates

H. L. Shulman, C. F. Ullrich, A. Z. Proulx, and J. O. Zimmerman

Clarkson College of Technology, Potsdam, New York

A study was made of separating the volumetric mass transfer coefficients, k_Ga and k_La, into their components k_G, k_L, and a so that the effects of variables might be determined separately for each component. Mass transfer rates for four packings, ½- and 1½-in. Raschig rings and ½-in. and 1-in. Berl saddles, made of naphthalene, were determined by vaporization into air at gas rates from 100 to 1,000 lb./(hr.) (sq. ft.).

The correlation for k_G was used to determine the wetted areas of those packings when irrigated with water and to calculate the effective interfacial areas, a, from Fellinger's data for ammonia absorption. These effective areas were then used to evaluate k_L from previously published k_La data, and a correlation was obtained for all packings.

The correlations for k_G and k_L and the effective-interfacial-area data make possible a more rigorous method for the design of packed columns than was heretofore available.

To predict the performance of columns employing ring and saddle packings for design purposes reliable data such as those of Fellinger(*4*) for volumetric gas-phase coefficients, k_Ga, and of Sherwood and Holloway(*8*) for volumetric liquid-phase coefficients, k_La, are used. Such coefficients can be estimated for aqueous systems from these sources of data and combined by the following relation to give for a limited number of packings the over-all mass transfer coefficients desired for design.

$$\frac{1}{K_Ga} = \frac{1}{k_Ga} + \frac{1}{Hk_La} = \frac{1}{HK_La} \quad (1)$$

Although these sources of data are

Additional tabular material may be obtained from the American Documentation Institute Auxiliary Publications Project, Photoduplication Service, Library of Congress, Washington 25, D.C., as document 4566 by remitting $2.50 for photoprints or $1.75 for microfilm.

considered reliable, they are of questionable value for predicting mass transfer rates for nonaqueous systems and for packings other than those for which data are reported. An examination of the data reveals no simple relation between packing size and performance even for one type of packing. For this reason the data must be presented in the form of plots or empirical equations which are of little value in predicting the performance of packings for which data are not available. The work of Surosky and Dodge (*11*) and Mehta and Parekh (*7*) on the vaporization of organic liquids and water in packed columns and that described in Part I of this paper, on total liquid holdup in carbon and porcelain packings, indicate that the effective interfacial area is a function of the properties of the liquids employed and the nature of the packing surface. Thus it is unlikely that data obtained with aqueous systems and a specific packing material can be used to estimate the performance in nonaqueous systems or even in aqueous systems when packing materials with different surface properties are used.

To overcome the limitations of the methods discussed, a more fundamental approach to the problem of mass transfer between phases in packed columns must be employed. As the first and most obvious step in this direction it would be desirable to separate the coefficients, k_G and k_L, from the effective interfacial area, a, in order to determine separately the effects of variables on each component of the volumetric coefficients, k_Ga and k_La.

Two attempts to separate a and k_G have been reported by Shulman and DeGouff (*9*) and Weisman and Bonilla (*14*). The methods used were equivalent to using k_G, obtained by vaporization of naphthalene or water from special Raschig rings of known transfer area, and various sources of k_Ga data to evaluate a, the effective interfacial area. As no liquid was used to irrigate the packing, no attempt was made to take into account the effect of the liquid flowing through the packing under practical operating conditions. Part I indicates that an appreciable portion of the void space in packing may be occupied by liquid, leaving a much smaller free space for gas flow than had been expected previously. In addition the recent work of Gamson (*5*), Evans and Gerald (*3*), McCune and Wilhelm (*6*), and Chu, Kalil and Wetteroth (*1*) has shown that the free space for gas flow, ε, is an important variable for correlating mass transfer data.

The present work was undertaken to separate k_G and k_L from a, to overcome the limitations of methods employed previously, and to obtain correlations for k_G and k_L in terms of all pertinent variables in order to make possible the prediction of the performance of packings for which data are not available. The method employed is outlined as follows.

1. Naphthalene packings (0.5- and 1.5-in. Raschig rings and 0.5- and 1.0-in. Berl saddles) were used to obtain k_G data which could be combined with previous work to obtain a single k_G correlation for all ring and saddle packings which would take into account the effect of liquid in the packing on k_G.

2. The k_G correlation was used in conjunction with Fellinger's (*4*) extensive k_Ga data for ammonia absorption to calculate the effective interfacial areas, a, for the five packings, 0.5-, 1.0-, and 1.5-in. Raschig rings and 0.5- and 1.0-in. Berl saddles, for which total holdup data were available.

3. The effective interfacial areas were applied to the k_La data of several investigators to obtain k_L values for the five packings which could be correlated by a single equation.

TABLE 1.—PROPERTIES OF NAPHTHALENE PACKINGS

	Raschig rings			Berl saddles	
Nominal size, in.	0.5	1.0*	1.5	0.5	1.0
Height, in.†	0.50	1.0	1.5	....	....
Outside diameter, in.†	0.50	1.0	1.5	....	....
Wall thickness, in.†	0.0938	0.125	0.250	....	....
Void fraction, dry	0.630‡	0.758†	0.688‡	0.660†	0.695†
No. of pieces/cu. ft.	10,700‡	1,220‡	366‡	15,000†	1,810†
Surface area/piece, sq. ft.	0.0105‡	0.0430‡	0.0955‡	0.00888**	0.0346**
Surface area, sq. ft./cu. ft.‡	113	52.5	35.0	133	62.6
Diam. of equivalent sphere, ft.*	0.0578	0.1167	0.174	0.0532	0.105

* From data of Shulman and DeGouff (*9*)

† From measurements.

‡ Calculated

** From data of Maurice A. Knight, Akron, Ohio

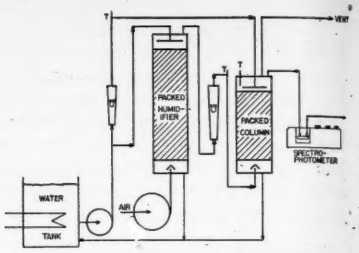

FIG. 1. SCHEMATIC DIAGRAM OF APPARATUS.

4. The correlations for k_G and k_L were tested and found satisfactory for extension to larger packings, 2.0-in. rings and 1.5-in. saddles, for which incomplete data were available.

In addition to the studies outlined, work was done on the wetted area in ring and saddle packings to supply data which may be of value in developing a method for predicting the behavior of nonaqueous liquids in packings.

APPARATUS AND PROCEDURE

The apparatus, a schematic diagram of which is given in Figure 1, has been described in detail by Shulman and DeGouff (*9*) except for several minor changes, which will be discussed. To improve control a water-storage tank with a circulating pump was installed and the air orifice meters were replaced by two calibrated rotameters. A new technique was developed to analyze the air for naphthalene. The optical density of air containing naphthalene, as measured in 10-cm. quartz cells in a Beckmann model DU photoelectric quartz spectrophotometer, was found to be proportional to the naphthalene partial pressure. This provided a very rapid and simple method of analysis for the naphthalene.

The naphthalene Raschig rings, which were prepared by means of special molds on a fast-acting hydraulic press, were held to close tolerances by weighing the feed for each 1.5-in. ring and by using a calibrated feed measure for the 0.5-in. rings. The 0.5- and 1.0-in. naphthalene Berl saddles, prepared by Maurice A. Knight, have the same dimensions as do the porcelain Berl saddles supplied commercially by this company. The characteristics of the naphthalene packings used are tabulated in Table 1. The naphthalene used for all the work was crushed refined Polar naphthalene obtained from the Barrett Division of Allied Chemical and Dye Corporation.

To determine k_G and wetted areas for a naphthalene packing the 3-ft. by 10-in. diam. Pyrex column was packed with 6 in. of porcelain packing followed by 3 to 6 in. of naphthalene packing of the same type and another 6 in. of porcelain packing. The porcelain packing above and below the naphthalene provided the

gas and liquid distribution which was characteristic of the packing used. Air and water temperatures were adjusted to the 20° to 23°C. range and held constant to within ±0.1°C. for each run. To determine k_G with a dry packing the air rate was set at the desired value and inlet and outlet air temperatures were checked for constancy for a minimum of 10 min. When equilibrium was established, a copper air-sampling line at the top of the column, which operated at a pressure slightly above atmospheric, was opened and a 10-cm. quartz cell was flushed for about 1 min. with the outlet air. The cell stopcocks were closed and the cell was placed in the spectrophotometer for analysis. The optical density of the air-naphthalene mixture was determined at three naphthalene ultraviolet absorption peaks, 221.75, 258.75, and 268.75 $m\mu$. The optical densities of air saturated with naphthalene had been measured previously at these three wavelengths at several temperatures in the 15° to 25°C. range. The k_G for the run was calculated by an equation employing these optical densities, which was derived as follows. As the inlet air was free of naphthalene and a logarithmic mean driving force was applicable because the partial pressure of naphthalene never exceeded 0.1 mm. Hg, one can write

$$k_G A \frac{[(p_s)-(p_s-p_o)]}{\ln\left[\frac{p_s}{p_s-p_o}\right]} = \frac{GSp_o}{M_M P} \quad (2)$$

and as the optical density, α, as measured by the spectrophotometer, is proportional to the partial pressure of naphthalene

$$k_G = \frac{GSp_o}{AM_M P} \frac{\ln\left[\frac{p_s}{p_s-p_o}\right]}{p_o} = \frac{GS \ln\left[\frac{\alpha_s}{\alpha_s-\alpha_o}\right]}{AM_M P} \quad (3)$$

The term containing the optical densities was evaluated for the readings at the three wavelengths and an average value was used for each run. In addition each run was duplicated, and each k_G value reported is the average value for two or more runs at the same conditions. An attempt was made to keep the outlet air naphthalene concentration in the neighborhood of 50 to 60% saturated. This was not always possible with the smaller packings at lower air rates, and these date scattered as a result. The naphthalene concentrations could be duplicated within 2%.

To determine the wetted area of the naphthalene packings when they were irrigated with water, a similar procedure was used except that Equation (3) was rearranged so that $k_G A$ was evaluated for the dry area. The corresponding k_G was calculated from the correlation of the data obtained with the dry packing so that the dry area, A, might be calculated and the wetted area found by the difference from the total surface area.

EXPERIMENTAL RESULTS

Mass Transfer in Dry Naphthalene Packings. The data obtained with the dry naphthalene packings are shown in Figure 2 with the data of Shulman and DeGouff (*9*) for 1.0-in. rings as a plot of the mass transfer factor, j_D, vs. a modified Reynolds number. The equation for the best line through the points is

$$j_D = \left[\frac{k_G M_M P_{BM}}{G}\right]\left[\frac{\mu_G}{\rho_G D_V}\right]^{2/3} = 1.195\left[\frac{D_P G}{\mu_G(1-\epsilon)}\right]^{-0.36} \quad (4)$$

Other methods of correlation were tested, such as those suggested by Gamson (*5*) and Taecker and Hougen (*11*), but the one used was found to represent the data best. The correlation includes the void fraction, ϵ, which makes it possible to take into account the effect of liquid in the packing when the total holdup is known under operating conditions. In Figure 3 the data are compared with the extensive data of Chu, Kalil, and Wetteroth (*1*) on fixed and fluidized beds of a variety of particles coated with naphthalene. The agreement is good, with the best line for Chu's data (not shown on Figure 3) lying slightly below the line recommended by the authors. The broken line on Figure 3 represents the equation

$$j_D = 1.77\left[\frac{D_P G}{\mu_G(1-\epsilon)}\right]^{-0.44} \quad (5)$$

which Chu obtained as the best line representing his data and those of numerous previous investigators of fixed and fluidized beds.

Figure 4 compares the authors' line with the data of Taecker and Hougen (*11*) obtained by vaporizing water from porous packings. There is good agreement for the Berl saddle data, but each series of data for the rings shows increasing disagreement at the higher Reynolds numbers corresponding to

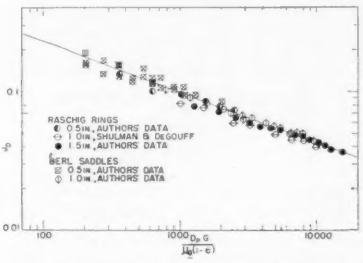

FIG. 2. MASS TRANSFER FACTORS FOR NAPHTHALENE PACKING.

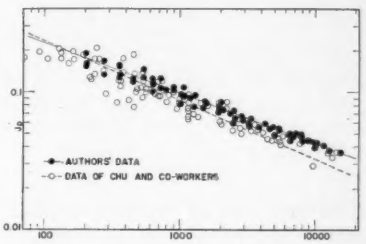

FIG. 3. COMPARISON OF AUTHOR'S DATA WITH DATA OF CHU AND CO-WORKERS.

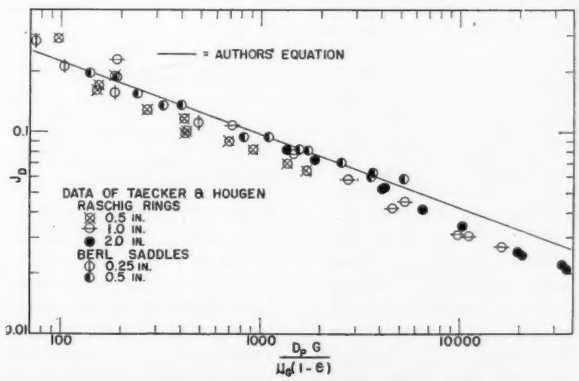

FIG. 4. COMPARISON OF AUTHOR'S EQUATION WITH DATA OF TAECKER AND HOUGEN.

high gas rates. A possible explanation of this type of behavior for wetted porous rings may be an incompletely wetted surface brought about by the inability of the water to migrate to the surface fast enough to keep the surface completely wetted. It is interesting to note that the Berl saddles used by Taecker and Hougen(*11*) were prepared by Maurice A. Knight by molding and the Raschig rings were prepared by the authors by extrusion. The differences in preparation may have resulted in porous materials with different properties. The good agreement with the Berl saddle data and the Raschig ring data at the lower gas rates is an indication that the Schmidt number to the 2/3 power is capable of correlating data of different systems.

this phenomenon as offered in the earlier work seems to be valid. It will be shown later that the effective interfacial areas also decrease at increasing gas rates for low liquid rates.

The wetted-area data obtained in this work can be correlated by a line for each type of packing, as shown in Figure 10. For some unknown reason the data of Shulman and DeGouff(*9*) for the 1.0-in. rings scatter badly on this type of plot. The equations of the two lines in Figure 10 are

$$\frac{a_w}{a_t} = 0.35\left[\frac{L}{G}\right]^{0.20} \qquad (6)$$

source of data. Part I of this paper explains the reason for the large differences between $k_G a$ obtained by vaporization and absorption techniques on the basis of total and operating holdups. On the basis of this explanation it should be emphasized that the effective interfacial areas reported here are valid for absorption work. For vaporization of water the effective area is greater by a factor equal to 0.85 times the ratio of total to operating holdup at the liquid and gas rates employed.

Fellinger's(*4*) data were corrected for liquid-phase resistance by means of the Sherwood and

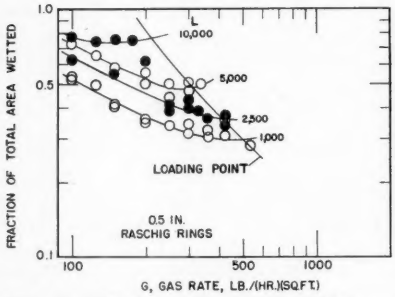

FIG. 5. WETTED AREA FOR 0.5-IN. NAPHTHALENE RASCHIG RINGS.

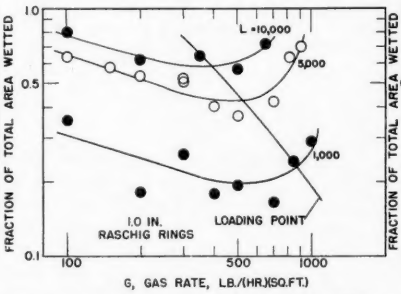

FIG. 6. WETTED AREA FOR 1.0-IN NAPHTHALENE RASCHIG RINGS CALCULATED FROM DATA OF SHULMAN AND DEGOUFF.

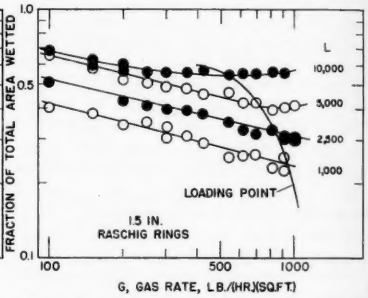

FIG. 7. WETTED AREA FOR 1.5-IN. NAPHTHALENE RASCHIG RINGS.

Wetted Area in Naphthalene Packings. The wetted areas for irrigated naphthalene packings were divided by the total surface areas, listed in Table 1, and are presented in Figgures 5, 7, 8, and 9 as the fraction of the total area wetted. Figure 6 shows the data of Shulman and DeGouff(*9*) for 1.0-in. Raschig rings recalculated by means of Equation (4) for k_G and the total holdup data obtained in Part I. The loading points shown in these figures are obtained from the work of Tillson(*12*). For all the packings the wetted areas increase with increasing liquid rate and decrease with increasing gas rate usually until the loading point is reached when the lines tend to become horizontal or even to show an increase in wetted area at still higher gas rates. The unusual effect of gas rate was first reported by Shulman and DeGouff(*9*) and was found again for the four packings used in this work. The explanation of

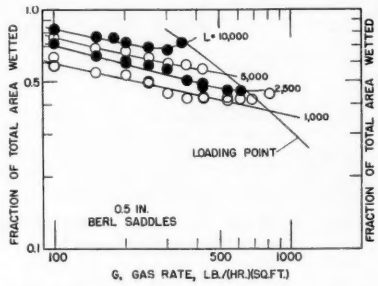

FIG. 8. WETTED AREA FOR 0.5-IN. NAPHTHALENE BERL SADDLES.

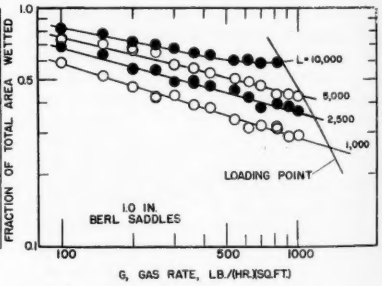

FIG. 9. WETTED AREA FOR 1.0-IN. NAPHTHALENE BERL SADDLES.

for Berl saddles and

$$\frac{a_w}{a_t} = 0.24\left[\frac{L}{G}\right]^{0.25} \qquad (7)$$

for Raschig rings.

EFFECTIVE INTERFACIAL AREA

A correlation for k_G, such as is given by Equation (4), makes it possible to calculate the effective interfacial area, a, from reliable sources of $k_G a$ data. The data of Fellinger(*4*) for ammonia absorption in water obtained by use of nine ceramic packings seem to be the most complete and reliable

Holloway(*8*) correlation and divided by the corresponding k_G obtained from Equation (4) and the

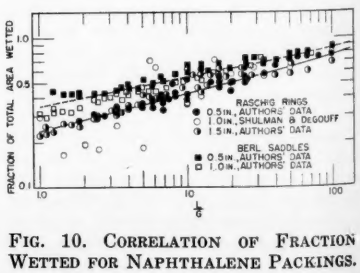

FIG. 10. CORRELATION OF FRACTION WETTED FOR NAPHTHALENE PACKINGS.

holdup data of Part I. Figures 11, 12, 13, 15, and 16 present the effective interfacial areas for the packings for which both absorption and holdup data are available. Figures 14 and 17 present these areas for 2.0-in. rings and 1.5-in. saddles employing holdups estimated by means of correlating equations given in Part I. The loading-point line on each figure was obtained from the data of Tillson (*12*).

An examination of these plots shows that the effective interfacial area increases with increasing liquid rate and is fairly independent of gas rate although in general it increases with gas rate at high liquid rates, decreases at the lower liquid rates, and is independent at the intermediate liquid rates. The behavior at low liquid rates is similar to that of the wetted area. A comparison of wetted and effective areas reveals some important differences. Wetted areas increase as packing size decreases. The effective area, however, is smallest for the smallest packings in spite of the fact that they possess the largest total surface and wetted area. The effective area seems to go through a maximum for the 1.0-in. rings and saddles although the larger packings have almost as much effective area. It may be possible to explain these results by the holdup studies in Part I. The small packings were found to have very large static holdups which exist in the packing as pockets of almost stagnant water. This water can account for the large wetted area, but it is practically useless for absorption because it comes to equilibrium with the gas very rapidly. The water which runs through the packing, corresponding to the operating holdup, flows through the numerous crevices at the points of contact in the small packing, exposing a relatively small surface area. In the larger packings there are fewer points of contact and resulting crevices, and so the water must spread out over the surface and the effective area is more closely related to the wetted area.

CORRELATION OF k_L FOR RINGS AND SADDLES

Sherwood and Holloway (*8*) have obtained k_La data for nine ceramic packings by desorption of slightly soluble gases from water. Some of this work has been checked by other investigators, for instance, Deed, Schutz, and Drew (*2*) and Vivian and Whitney (*13, 15*), with good agreement. As was pointed out earlier, there is no way to correlate the k_La data for the different packings. With the effective interfacial areas for absorption, as shown in Figures 11 to 17 inclusive, it is a simple matter to extract k_L and attempt a generalized correlation. Figure 18 shows the best correlation that could be obtained from the three sources of data cited above. For some of the packings it was possible to extrapolate with confidence the effective interfacial areas to liquid rates well above those shown in Figures 11 to 17. The line drawn in Figure 18 is the best line through the points for 0.5-, 1.0-, and 1.5-in. rings and 0.5- and 1.0-in. saddles.

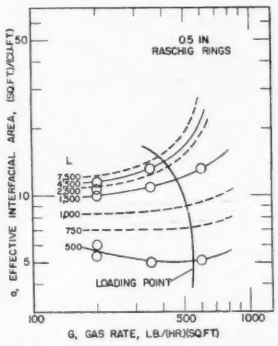

FIG. 11. EFFECTIVE INTERFACIAL AREA FOR 0.5-IN. RASCHIG RINGS BASED ON DATA OF FELLINGER.

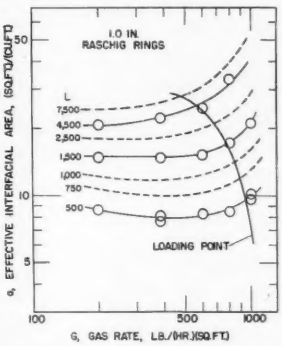

FIG. 12. EFFECTIVE INTERFACIAL AREA FOR 1.0-IN. RASCHIG RINGS BASED ON DATA OF FELLINGER.

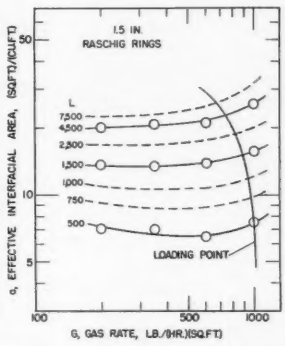

FIG. 13. EFFECTIVE INTERFACIAL AREA FOR 1.5-IN. RASCHIG RINGS BASED ON DATA OF FELLINGER.

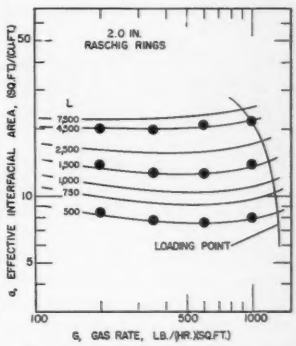

FIG. 14. EFFECTIVE INTERFACIAL AREA FOR 2.0-IN. RASCHIG RINGS BASED ON DATA OF FELLINGER USING ESTIMATED HOLDUPS.

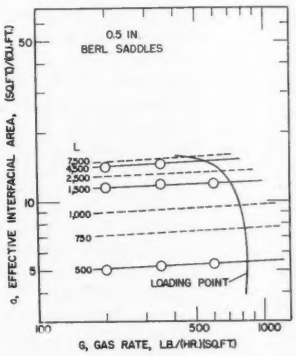

FIG. 15. EFFECTIVE INTERFACIAL AREA FOR 0.5-IN. BERL SADDLES BASED ON DATA OF FELLINGER.

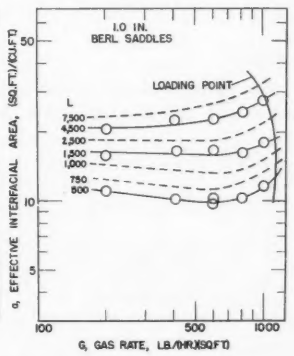

FIG. 16. EFFECTIVE INTERFACIAL AREA FOR 1.0-IN. BERL SADDLES BASFD ON DATA OF FELLINGER.

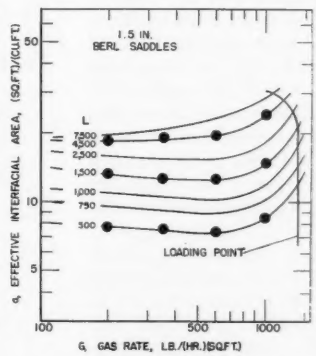

FIG. 17. EFFECTIVE INTERFACIAL AREA FOR 1.5-IN. BERL SADDLES BASED ON DATA OF FELLINGER USING ESTIMATED HOLDUPS.

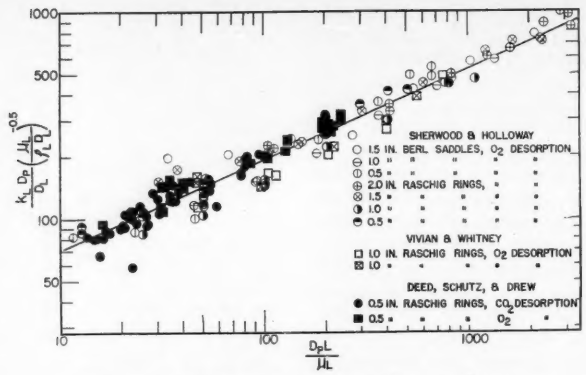
SHERWOOD & HOLLOWAY
1.5 IN. BERL SADDLES, O2 DESORPTION
1.0 " " " " " "
0.5 " " " " " "
2.0 IN. RASCHIG RINGS, " " " "
1.5 " " " " " "
1.0 " " " " " "
0.5 " " " " " "
VIVIAN & WHITNEY
1.0 IN. RASCHIG RINGS, O2 DESORPTION
1.0 " " " " " "
DEED, SCHUTZ, & DREW
0.5 IN. RASCHIG RINGS, CO2 DESORPTION
0.5 " " " O2 "
1000
500
100
50
10
100
1000

FIG. 18. CORRELATION OF LIQUID-PHASE DATA.

The points for 2.0-in. rings and 1.5-in. saddles, which are based on effective interfacial areas calculated from Fellinger's(4) data, Equation (4) for k_G, and estimated holdups, are also in good agreement with this line. This indicates that the correlations for k_G, k_L, and holdup can be used to predict the performance of packings for which complete data are not available.

The equation for the line in Figure 18 is

$$\frac{k_L D_P}{D_L} = 25.1\left[\frac{D_P L}{\mu_L}\right]^{0.45}\left[\frac{\mu_L}{\rho_L D_L}\right]^{0.5} \qquad (8)$$

It can be seen that k_L is independent of gas rate, and so $k_L a$ can be expected to vary with gas rate as a does, as shown in Figures 11 to 17 inclusive. This observation seems to contradict that of Sherwood and Holloway(8), who found $k_L a$ to be independent of gas rate up to loading. Their statement, however, seems to be based on data obtained with 1.5-in. rings at a liquid rate of 2,000 lb./(hr.)(sq.ft.). As an examination of Figure 13 shows a to be just about independent of gas rate at this liquid rate, $k_L a$ should also be independent. It should be noted that it would not be serious to neglect the effect of gas rate with large packings, but some of the small packings do show an appreciable effect at the high and low liquid rates.

Equation (8) will predict the effects of temperature and diffusivity as found by Sherwood and Holloway(8). If further work on effective interfacial areas makes possible predictions for nonaqueous systems, it will be possible to use Equations (4) and (8) to predict the performance of ring and saddle packing for all systems.

RESULTS AND CONCLUSIONS

For Raschig ring and Berl saddle packings mass transfer rates can be predicted for the gas phase by

$$j_D = \left[\frac{k_G M_M P_{BM}}{G}\right]\left[\frac{\mu_G}{\rho_G D_V}\right]^{2/3} = 1.195\left[\frac{D_P G}{\mu_G(1-\epsilon)}\right]^{-0.36} \qquad (4)$$

and for the liquid phase by

$$\frac{k_L D_P}{D_L} = 25.1\left[\frac{D_P L}{\mu_L}\right]^{0.45}\left[\frac{\mu_L}{\rho_L D_L}\right]^{0.5} \qquad (8)$$

The effective interfacial areas, a, for absorption and desorption are given for seven packings in Figures 11 to 17 inclusive, and those for vaporization can be estimated from these by applying a factor equal to 0.85 times the ratio of total holdup to operating holdup.

The wetted areas for five packings, Figures 5 to 9 inclusive, are not related in any simple manner to the effective interfacial areas.

NOTATION

A = total dry surface area, sq.ft.
a = effective interfacial area, sq. ft./cu.ft.
a_w = wetted area, sq.ft./cu.ft.
a_t = total surface area, sq.ft./cu.ft.
D_L = diffusivity of solute in liquid, sq.ft./hr.
D_P = diameter of sphere possessing the same surface area as a piece of packing, ft.
D_V = diffusivity of solute in gas, sq.ft./hr.
G = superficial gas rate, lb./(hr.)(sq.ft.)
H = Henry's law constant, lb. moles/(cu.ft.)(atm.)
j_D = mass transfer factor
K_G = over-all mass transfer coefficient, lb. moles/(hr.)(sq.ft.)(atm.)
k_G = gas-phase mass transfer coefficient, lb. moles/(hr.)(sq. ft.)(atm.)
K_L = over-all mass transfer coefficient, lb. moles/(hr.)(sq.ft.)(lb. moles/cu.ft.)
k_L = liquid-phase mass transfer coefficient, lb. moles/(hr.)(sq. ft.)(lb. moles/cu.ft.)
L = superficial liquid rate, lb./(hr.)(sq.ft.)
M_M = mean molecular weight of gas, lb./(lb. mole)
P = total pressure, atm.
p_{BM} = mean partial pressure of inert gas in the gas phase, atm.
p_o = partial pressure of naphthalene in outlet air, atm.
p_s = vapor pressure of naphthalene, atm.
S = column cross-sectional area, sq. ft.

Greek Letters

α = optical density
α_o = optical density of outlet air
α_s = optical density of air saturated with naphthalene
ϵ = void fraction, cu.ft./cu.ft.
μ_G = gas viscosity, lb./(hr.)(ft.)
μ_L = liquid viscosity, lb./(hr.)(ft.)
ρ_G = gas density, lb./cu.ft.
ρ_L = liquid density, lb./cu.ft.

LITERATURE CITED

1. Chu, J. C., J. Kalil, and W. A. Wetteroth, *Chem. Eng. Progr.*, 49, 141 (1953).
2. Deed, D. W., P. W. Schutz, and T. B. Drew, *Ind. Eng. Chem.* 39, 766 (1947).
3. Evans, G. C., and C. F. Gerald, *Chem. Eng. Progr.*, 49, 135 (1953).
4. Fellinger, L., Sc.D. thesis, Mass. Inst. Technol. (1941).
5. Gamson, B. W., *Chem. Eng. Progr.*, 47, 19 (1951).
6. McCune, L. K., and R. H. Wilhelm, *Ind. Eng. Chem.*, 41, 1124 (1949).
7. Mehta, J. J., and R. H. Parekh, S.M. thesis, Mass. Inst. Technol. (1939).
8. Sherwood, T. K., and F. A. L. Holloway, *Trans. Am. Inst. Chem. Engrs.*, 36, 21, 39 (1940).
9. Shulman, H. L., and J. J. DeGouff, *Ind. Eng. Chem.*, 44, 1915 (1952).
10. Surosky, A. E., and B. F. Dodge, *Ind. Eng. Chem.*, 42, 1112 (1950).
11. Taecker, R. G., and O. A. Hougen, *Chem. Eng. Progr.* 45, 188 (1949).
12. Tillson, P., S.M. thesis, Mass. Inst. Technol. (1939).
13. Vivian, J. E., and R. P. Whitney, *Chem. Eng. Progr.*, 49, 691 (1947).
14. Weisman, J., and C. F. Bonilla, *Ind. Eng. Chem.*, 42, 1099 (1950).
15. Whitney, R. P., and J. E. Vivian, *Chem. Eng. Progr.*, 45, 323 (1949).

III. Holdup for Aqueous and Nonaqueous Systems

H. L. Shulman, C. F. Ullrich, N. Wells, and A. Z. Proulx
Clarkson College of Technology, Potsdam, New York

Total, static, and operating holdups have been measured for 1-in porcelain and carbon Raschig rings and 1-in. porcelain Berl saddles, employing aqueous solutions of calcium chloride, sorbitol, and a wetting agent as well as pure methanol and benzene. The range of variables covered by this investigation includes liquid rate, 1,000 to 10,000 lb./(hr.) (sq. ft.); viscosity, 0.6 to 185 cp.; surface tension, 23 to 86 dynes/cm.; specific gravity, 0.8 to 1.32.

Equations and charts are presented for estimating holdups for all liquids. The application of holdups for estimating mass transfer coefficients, k_G, and effective interfacial areas, a, is discussed.

The total holdups for water, methanol, and benzene can be used to explain why mass transfer coefficients obtained by vaporization of pure liquids in packings seem to depend on gas diffusivity raised to the 0.15 power instead of the 0.67 power, as found in other mass transfer studies. The larger total holdups of nonaqueous liquids result in larger effective interfacial areas in the packing, which mask the effect of the change in gas diffusivity.

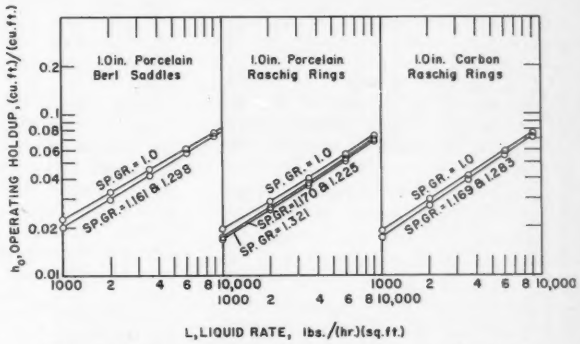

FIG. 2. OPERATING HOLDUP FOR CALCIUM CHLORIDE SOLUTIONS AND WATER AT 20°C. WITH SPECIFIC GRAVITY VARYING FROM 1.0 TO 1.321.

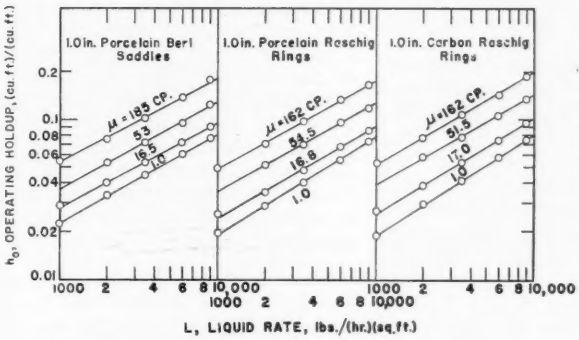

FIG. 1. OPERATING HOLDUP FOR SORBITOL SOLUTIONS AND WATER AT 20°C. WITH VISCOSITY VARYING FROM 1.0 TO 185 cp.

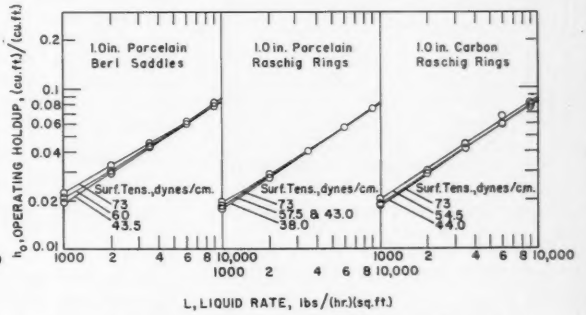

FIG. 3. OPERATING HOLDUP FOR PETROWET SOLUTIONS AND WATER AT 20°C. WITH SURFACE TENSION VARYING FROM 38 TO 73 DYNES/CM.

In the first two parts of this study of the performance of packed columns it was shown that total, static, and operating holdup data could be used in the prediction of mass transfer coefficients for absorption and vaporization in packed columns. Up to the present time mass transfer and holdup studies in packings have been limited almost exclusively to systems employing water as the liquid. For this reason the extension to nonaqueous systems of design methods developed for aqueous systems is of questionable value until appropriate data have been obtained to check the assumptions made.

Attempts have been made to study the vaporization of water and organic liquids in packed columns by Metha and Parekh (*3*) and Surosky and Dodge (*4*). The results of both of these studies indicated that the gas-phase mass transfer coefficient, $k_G a$, was proportional to the diffusivity raised to the 0.15 to 0.17 power. This conclusion is in disagreement with all the other mass transfer studies in which a much higher power, in the neighborhood of 0.67, was found to correlate the data. Surosky and Dodge noted that their assumption of a constant effective interfacial area, a, for all liquids may have been unjustified, and if the organic liquids wetted the packing surface to a greater extent than water, the effect of diffusivity may have been masked.

The object of this work is to study total, static, and operating holdups in packings to determine the effects of liquid physical properties, such as viscosity, surface tension, and density, and the shape and nature of the packing. By working with water solutions on several packings it is possible to cover a wide range of variables and to develop relationships for the prediction of holdups in aqueous and nonaqueous systems. By working with benzene and methanol on the same packings, data can be obtained to check these relationships for nonaqueous liquids. The holdup data for water, benzene, and methanol can also be used to disprove the validity of the assump-

Additional tabular material may be obtained from the American Documentation Institute Auxiliary Publications Project, Photoduplication Service, Library of Congress, Washington 25, D.C., as document 4567, by remitting $1.25 for photoprints or microfilm.

tion that the effective interfacial area, a, in packings is the same for all liquids and to help to explain the disagreement between the small effect of diffusivity found by Metha and Parekh (3) and Surosky and Dodge (4) and the large effect noted by other investigators.

APPARATUS AND PROCEDURE

The apparatus used in this work is the same as that described in Part I of this paper except for a minor modification which consisted of the addition of a gear pump and a small heat exchanger in the line leading to the liquid distributor at the top of the column. These changes made it possible to pump liquids of high

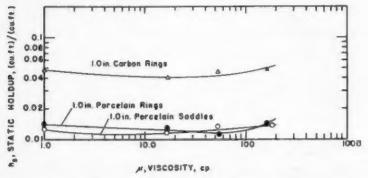

FIG. 4. STATIC HOLDUP FOR SORBITOL SOLUTIONS.

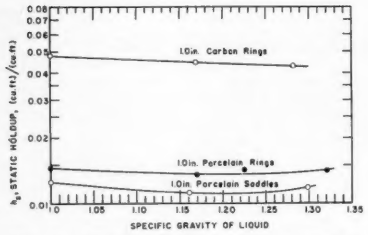

FIG. 5. STATIC HOLDUP FOR CALCIUM CHLORIDE SOLUTIONS.

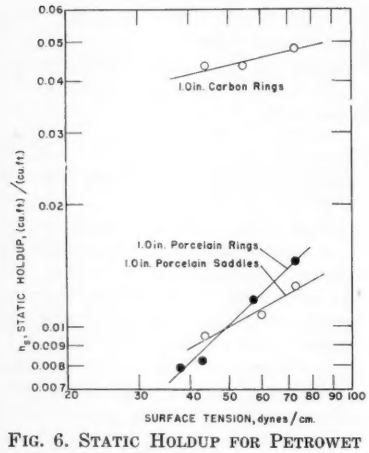

FIG. 6. STATIC HOLDUP FOR PETROWET SOLUTIONS.

viscosity and to hold entering liquid temperatures at 20.0° ± 0.1°C. for all the runs. Water solutions of varying viscosity were prepared by adding sorbitol to the water tank and recycling the solution through the apparatus until a uniform solution of the desired viscosity was obtained. Solutions with viscosities up to 185 cp. could be handled in the apparatus.

Calcium chloride was used to prepare solutions with densities up to 1.32 g./ml. The surface tension of water was decreased to as low as 38 dynes/cm. by the addition of a wetting agent, DuPont Petrowet. To reduce the tendency to foam of these solutions a small quantity of a silicone defoamer, Dow Corning Antifoam A, was added as required. Benzene and methanol served as liquids with densities, viscosities, and surface tensions lower than those attained with any of the water solutions.

Flow rates were measured with rotameters calibrated with each of the liquids employed. Viscosities were measured and controlled with a Rich-Roth Ultra-Viscoson, by use of a gold-plated probe, which was calibrated against glycerol solutions. Surface tension was measured with a Cenco-duNouy interfacial tensiometer, and densities were determined with a Precision specific-gravity balance.

The procedure used was similar to that described in Part I for measuring total, static, and operating holdups except that all runs were made at zero gas rate. One-inch unglazed-porcelain rings and saddles and carbon rings were used. The characteristics of these packings were described in Part I, and in all runs the column was packed so that the dry void fraction was within 1.0% of that reported previously.

EXPERIMENTAL RESULTS

The operating and static holdups for the three packings are shown in Figures 1 to 6 inclusive for the aqueous solutions. The methanol holdups are given in Figure 7, and the benzene holdups in Figure 8. The effects of the physical properties can be determined only qualitatively from some of these figures because it was not possible always to vary one physical property without varying another to some extent. Table I illustrates this point. A series of equations, which can be used to estimate holdups for any liquid on the three packings, was developed by the following procedure. The data for solutions with varying surface tensions were used to determine the effect of surface tension on operating and static holdups. This was possible because these solutions had constant density and viscosity. The data for the calcium chloride solutions were then corrected for the effect of surface tension and used to determine the effect of density. The viscosities of these solutions are low, although higher than the viscosity of water, but the effect of such small changes in viscosities is almost negligible, and slight adjustments could be made after the effect of viscosity had been determined. The effect of viscosity was determined by correcting the sorbitol solution data for the effect of density found previously. The resulting equations are tabulated in Table 2. For the three 1.0-in. packings employed, the operating holdups were found to be independent of the nature of the packing surface, whereas the static holdups were very dependent, as evidenced by the much higher static holdups observed with carbon rings as compared to porcelain rings. The effect of each variable will be discussed separately.

Effect of Surface Tension. The effect of surface tension was found to vary with liquid rate for operating holdup. At low liquid rates, decreasing surface tension resulted in decreasing operating holdup, whereas at high liquid rates de-

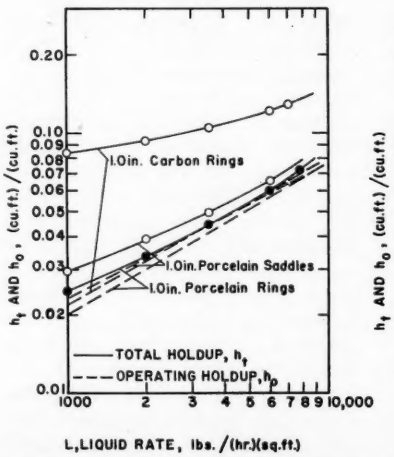

FIG. 7. TOTAL AND OPERATING HOLDUPS FOR METHANOL.

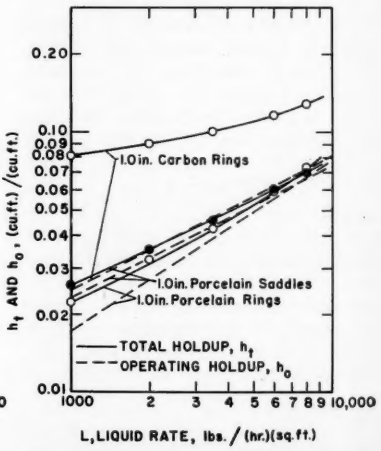

FIG. 8. TOTAL AND OPERATING HOLDUPS FOR BENZENE.

creasing surface tension increased operating holdup. Similar observations were made by Jesser and Elgin(*1*) with 1/2-in. carbon rings, although they found the point of changing effect at much lower liquid rates. The present work and that of Jesser and Elgin(*1*) may result in an erroneous conclusion as to the effect of surface tension because water solutions of wetting agents may have foaming tendencies which are not found in pure liquids of low surface tension. When the present work was started, the Petrowet solutions were found to foam and result in high holdups even at low liquid rates(*1*). The addition of a silicone defoamer, such as Dow Corning Antifoam *A*, eliminated most of the foam at the low liquid rates, but some was still present at higher liquid rates. Unfortunately, there was no way to eliminate the foam completely and so somewhat higher holdups were found than might otherwise have been obtained. Further evidence of this effect of foam formation on the equations which were developed can be obtained by using the equations to estimate the operating holdups of methanol and benzene and comparing them with the experimental values. Although good agreement is obtained in general, the calculated values tend to be high at high liquid rates and low at low liquid rates, as is to be expected if foam formation appeared at the higher liquid rates for the water solutions. The equations appear to be satisfactory, however, for estimating operating holdups of nonaqueous liquids in the range of liquid rates employed in this work, namely, 1,000 to 10,000 lb./(hr.)(sq.ft.).

Table 1.—Physical Properties of the Liquids Employed for Holdup Measurements at 20°C.

Liquid	Viscosity, cp.	Density, g./ml.	Surface tension, dynes/cm.
Sorbitol solution	185	1.299	73.0
Sorbitol solution	53	1.268	73.0
Sorbitol solution	16.5	1.215	73.0
Water	1.0	1.000	73.0
Calcium chloride solution	4.5	1.321	86.3
Calcium chloride solution	2.4	1.225	80.3
Calcium chloride solution	1.4	1.170	77.4
DuPont Petrowet solution	1.0	1.000	57.5
DuPont Petrowet solution	1.0	1.000	43.0
DuPont Petrowet solution	1.0	1.000	38.0
Methanol	0.59	0.7998	22.6
Benzene	0.65	0.8780	28.9

Table 2.—Equations for Estimating Operating and Static Holdups

1. Operating holdup for 1.0-in. Raschig rings for $\mu<12$ cp.

$$h_o = 0.00039\, L^{0.57}\, \mu^{0.13} \left(\frac{1}{\rho}\right)^{0.84} \left(\frac{\sigma}{73}\right)^{0.925 - 0.262 \log L} \tag{1}$$

for $\mu>12$ cp.

$$h_o = 0.00025\, L^{0.57}\, \mu^{0.31} \left(\frac{1}{\rho}\right)^{0.84} \left(\frac{\sigma}{73}\right)^{0.925 - 0.262 \log L} \tag{2}$$

2. Operating holdup for 1.0-in. Berl saddles for $\mu<20$ cp.

$$h_o = 0.00043\, L^{0.57}\, \mu^{0.13} \left(\frac{1}{\rho}\right)^{0.84} \left(\frac{\sigma}{73}\right)^{1.033 - 0.262 \log L} \tag{3}$$

for $\mu>20$ cp.

$$h_o = 0.00025\, L^{0.57}\, \mu^{0.31} \left(\frac{1}{\rho}\right)^{0.84} \left(\frac{\sigma}{73}\right)^{1.033 - 0.262 \log L} \tag{4}$$

3. Static holdup

$$h_s = c\, \mu^m \left(\frac{1}{\rho}\right)^{0.37} \sigma^n \tag{5}$$

where c, m, and n have the following values for each packing

Packing	c	m	n
1.0-in. carbon Raschig rings	0.0185	0.02	0.23
1.0-in. porcelain Raschig rings	0.00020	0.02	0.99
1.0-in. Berl saddles	0.00119	0.04	0.55

The effect of surface tension on static holdup is independent of liquid rate, as shown in Table 2; however, the effect is different for each packing, indicating that both the shape and nature of the packing material influence static holdup. The shape of the packing determines the number of points of contact and the horizontal or almost horizontal surfaces on which the static holdup accumulates. The nature of the packing surface will determine the interfacial tension at the liquid-gas-packing contact points and control the degree of wetting and accumulation of the liquid which makes up the static holdup. For this reason, each type of packing material may show a different effect of surface tension on static holdup. For all the packings the static holdup increases as surface tension increases, as might be predicted from an analogy to hanging drops of liquid although there is no direct proportionality for all packings. The absence of a direct proportionality is an indication that there is more than one mechanism for the accumulation and retention of water in packings.

Effect of Viscosity. For viscosities below 12 cp., operating holdups increase with increasing viscosity to the 0.13 power. This is in good agreement with the 0.1 power found by Jesser and Elgin(*1*) in the same viscosity range. For viscosities over 12 cp. for rings and 20 cp. for saddles, the effect changes and the 0.31 power on viscosity represents the data satisfactorily. There is no good reason to account for this change in the effect of viscosity at an intermediate viscosity.

Static holdups are affected very little by increases in viscosity, as shown by the 0.02 to 0.04 power on viscosity. From the definition of static holdup one might expect no effect of viscosity at all, but from an experimental point of view the slow-flowing liquids of very high viscosity can easily cause some of the operating holdup to be mistaken for static holdup.

Effect of Liquid Density. Operating holdups were found to decrease as density increased. The 0.84 power on $(1/\rho)$ is in good agreement with the 0.78 power observed by Jesser

and Elgin(*1*) over a more limited range of liquid densities.

The static holdups show a similar, although smaller, effect of density, the power on $(1/\rho)$ being 0.37.

Effect of Liquid Rate. The operating holdups were found to be proportional to L to the 0.57 power. This is in good agreement with the 0.6 power, which Leva(*2*) found as a good average value for rings and saddles.

Static holdups were found to be independent of liquid rate, as in Part I.

Effect of the Packing Surface. Operating holdups are independent of the nature of the packing surface. It is probably safe to assume that they can be estimated for any packing material by means of the equations developed from the unglazed-porcelain and carbon packings.

Static holdups, however, vary widely for different packing materials. Carbon rings have static holdups which are approximately three times as great for water, thirteen times as great for methanol, and eleven times as great for benzene as for the corresponding porcelain rings. A portion of the larger static holdups in the carbon packing may be accounted for by a porous surface. Thus the static holdup as determined with carbon rings which have been soaked in water for 2 weeks is about 25% greater than that found when dry rings are employed. When carbon rings were soaked in water, benzene, and methanol it was found that they gained several percent in weight up to about a week and the relative gain in weight was approximately proportional to the static holdup found with these liquids. It is unlikely, however, that porosity can account for more than a fraction of the total static holdup, and a better reason probably could be found in the interfacial tension which exists at the gas-liquid-solid interface, which causes increased wetting of the carbon surface and greater retention of liquid at points of contact between adjacent rings.

The static holdups reported in this work with water solutions were obtained with rings which had been kept immersed in water when not in use. The static holdup for water on carbon rings, which was reported in Part I, was obtained by starting with dry rings and is about 25% lower than holdup in this part. Under normal conditions of use in a packed column, the static holdup would probably attain some intermediate value depending upon the relative humidity of the gas passing through the column.

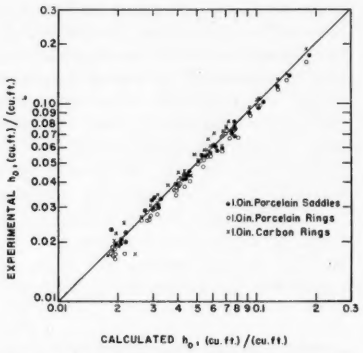

FIG. 9. COMPARISON OF EXPERIMENTAL AND CALCULATED OPERATING HOLDUPS.

APPLICATIONS

Estimation of Holdups. Although the equations tabulated in Table 2 were developed from data for one-inch packings, the good agreement as to the effects of the physical properties of the liquids with previous work on different packings makes it possible to estimate holdups for any packing for which water data are available. Extensive holdup data for six packings were reported in the first part of this study (4). Figures 13 to 16, inclusive, were prepared to supply factors to be applied to water holdups to correct for any departure from the viscosity, density, and surface tension of water at 20°C. To estimate the operating and static holdups for any liquid, at given liquid and gas rates, the corresponding water holdups are found first, as in Part I, and then multiplied by the three factors for viscosity, density, and surface tension as given in Figures 13 to 16.

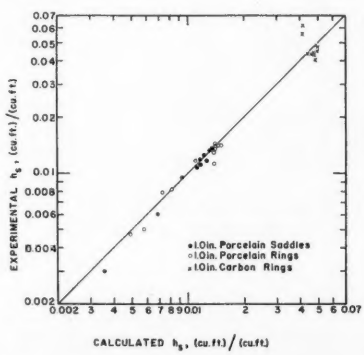

FIG. 10. COMPARISON OF EXPERIMENTAL AND CALCULATED STATIC HOLDUPS.

The use of these charts is equivalent to using the effects of the variables as given in Equations (1) to (5) in Table 2. Figures 9 and 10 show a comparison of the experimental points for water, water solutions, benzene, and methanol with values calculated from the charts or equations. It can be seen that there is good agreement between the two values.

Vaporization of Liquids in Packed Columns. In Parts I and II a design method was proposed for packed columns which consisted of determining the mass transfer coefficient, k_G, and the effective interfacial area, a, separately and combining the two to obtain the $k_G a$ required for design. The k_G is determined from the following equation:

$$\frac{k_G M_M P_{BM}}{G} = 1.195\left[\frac{D_P G}{\mu\,(1-\epsilon)}\right]^{-0.36}\left[\frac{\mu}{\rho D}\right]^{-0.67} \qquad (6)$$

It was pointed out in the introduction that Surosky and Dodge(*4*) vaporized water and several organic liquids in a column packed with 1.0-in. carbon rings and found $k_G a$ proportional to $D^{0.15}$ rather than $D^{0.67}$ as indicated by Equation(*6*). It may be possible to explain the difference if it can be shown that a is not the same for all liquids, as assumed by Surosky and Dodge(*4*) and other investigators. A comparison of the total holdups in 1.0-in. carbon rings for water, benzene, and methanol, which were three of the liquids employed, shows the organic liquids to have much greater holdups than water, as required to help explain the difference. To test this quantitatively Figure 11 shows a plot of $k_G a(\mu/\rho D)^{2/3}$ vs. G at a liquid rate of 1,600 lb./(hr.)(sq.ft.) for the vaporization of these three liquids based on the data of Surosky and Dodge. If the 2/3 power on diffusivity held and the effective interfacial areas for the three liquids were the same, the data should fall on one line. It is obvious that this is not the case. If it is assumed that a is proportional to total holdup, h_t, and the effect of different total holdups on k_G is taken into account in the $(1-\varepsilon)$ term in Equation (6), then $k_G a(\mu/\rho D)^{2/3}\ (h_t)\ (1-\varepsilon)^{0.36}$ plotted vs. G for the same data should bring the points in line. The results are shown in Figure 12, where it can be seen that the

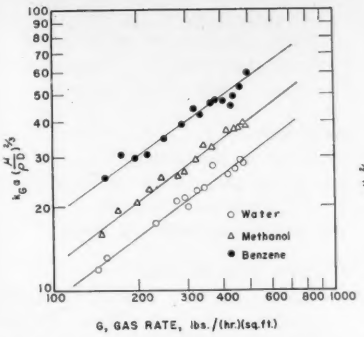

FIG. 11. VAPORIZATION MASS TRANSFER COEFFICIENTS FOR THREE SYSTEMS CORRECTED FOR DIFFUSIVITY.

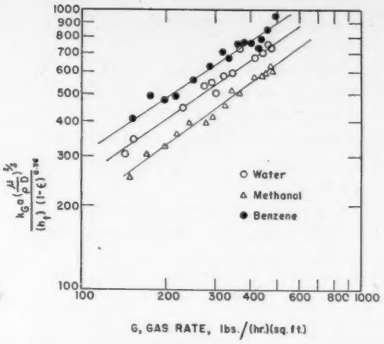

FIG. 12. VAPORIZATION MASS TRANSFER COEFFICIENTS FOR THREE SYSTEMS CORRECTED FOR DIFFUSIVITY AND HOLDUP.

points are in much better agreement than in Figure 11. There are several reasons that may be advanced to account for the disagreement that still exists. The total holdup may not be directly proportional to a or the proportionality constant may not be the same for

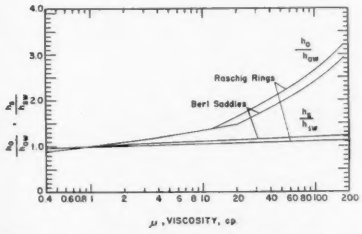

FIG. 13. FACTORS TO BE APPLIED TO WATER HOLDUPS TO ESTIMATE THE EFFECT OF VISCOSITY.

all the liquids. In addition, the vaporization data may be in error because of the difficulties encountered in obtaining good data. The data used were obtained with a packing depth of 4.0 in.; corrections were made for end effects equivalent to 2.2 in., as found by experiment for water. Errors in measuring the packing depth or in assuming the same end effect for all liquids may easily account for some of the disagreement shown in Figure 12. If one had used the water vaporization data, and all the corrections suggested, it would have been possible to estimate the data for benzene and methanol vaporization within about 15% of the experimental values. Disagreement of this magnitude can be tolerated in the design of packed columns.

Estimation of a. Holdups can be of value in estimating both k_G and a for the purposes of determining the mass transfer coefficient, $k_G a$, required for design. As was mentioned previously, the total holdup, h_t, which is the sum of the operating and static holdups, is required to evaluate the void fraction, ε, available for gas flow in the packing for use in Equation (6). This void fraction, ε, is simply the void fraction for the dry packing minus the total holdup, h_t.

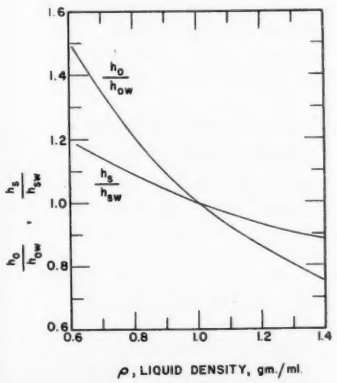

FIG. 14. FACTORS TO BE APPLIED TO WATER HOLDUPS TO DETERMINE THE EFFECT OF LIQUID DENSITY.

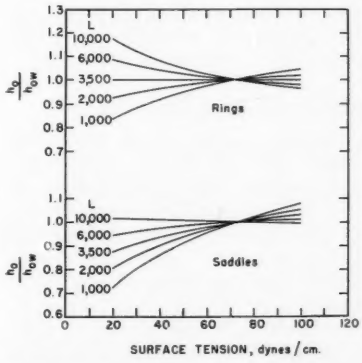

FIG. 15. FACTORS TO BE APPLIED TO WATER OPERATING HOLDUPS TO DETERMINE THE EFFECT OF SURFACE TENSION.

Total and operating holdups can be used to estimate effective interfacial areas for absorption and vaporization for any liquid from the areas presented in Part II for absorption in water. In absorption, a is proportional to operating holdup, and so it can be estimated as follows:

$$a_{abs} = (a_{abs})_w \frac{h_o}{h_{ow}} \qquad (7)$$

The ratio h_o/h_{ow} is the product of the factors obtained from Figures 13, 14, and 15 which correct for liquid physical properties different from those of water.

In vaporization, a is proportional to total holdup, and the relationship

$$\frac{a_{vap}}{a_{abs}} = 0.85 \frac{h_t}{h_o} \qquad (8)$$

which was found in Part I to hold for water, can be applied to estimate a_{vap} for any liquid from

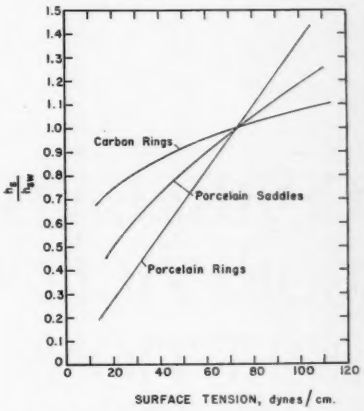

FIG. 16. FACTORS TO BE APPLIED TO WATER STATIC HOLDUPS TO DETERMINE THE EFFECT OF SURFACE TENSION.

$$a_{vap} = 0.85\,(a_{abs}) \frac{h_t}{h_o} \qquad (9)$$

or

$$a_{vap} = 0.85\,(a_{abs})_w \frac{h_t}{h_{ow}} \qquad (10)$$

The required values of $(a_{abs})_w$ and h_{ow} are available in Parts I and II for the common sizes of ring and saddle packings.

SUMMARY OF RESULTS AND CONCLUSIONS

Operating and static holdup data have been obtained for water solutions of sorbitol, calcium chloride, and a wetting agent as well as for benzene and methanol, by use of 1-in. porcelain and carbon rings and porcelain saddles.

Charts have been prepared for estimating holdups for any liquid from data available for water.

Applications of holdup data to explain the effect of diffusivity on the vaporization of liquids in packings and to estimate effective interfacial areas for mass transfer have been outlined.

ACKNOWLEDGMENT

The authors wish to acknowledge support of this work (Parts I, II, and III) under Grant G-200 of the National Science Foundation and Contract No. AT(30-1)-1463 of the Atomic Energy Commission.

NOTATION

a = effective interfacial area, sq. ft./cu.ft.
c = constant in Equation (5)
D = diffusivity of solute in gas, sq. ft./hr.
D_p = diameter of sphere possessing the same surface area as a piece of packing, ft.
G = superficial gas rate, lb./(hr.)(sq.ft.)
h_o = operating holdup, cu.ft./cu.ft.
h_s = static holdup, cu.ft./cu.ft.
h_t = total holdup, cu.ft./cu.ft.
k_G = gas-phase mass transfer coefficient, lb. moles/(hr.)(sq. ft.)(atm.)
k_Ga = gas-phase mass transfer coefficient, lb. moles/(hr.)(cu. ft.)(atm.)
L = superficial liquid rate, lb./(hr.)(sq.ft.)
m = constant in Equation (5)
M_M = mean molecular weight of gas, lb./lb. mole
n = constant in Equation (5)
P_{BM} = mean partial pressure of inert gas in the gas phase, atm.

Greek Letters

μ = liquid viscosity, centipoises
= gas viscosity, lb./(hr.)(ft.)
ρ = liquid density, g./ml.
= gas density, lb./cu.ft.
σ = surface tension, dynes/cm.
ε = void fraction, cu. ft./cu.ft.

Subscripts

w = for water systems
abs = for absorption work without a chemical reaction
vap = for vaporization work

LITERATURE CITED

1. Jesser, B. W., and J. C. Elgin, *Trans. Am. Inst. Chem. Engrs.*, **39**, 277 (1943).
2. Leva, M., "Tower Packings and Packed Tower Design," 2nd ed., The United States Stoneware Company, Akron, Ohio (1953).
3. Mehta, J. J., and R. H. Parekh, S.M. thesis, Mass. Inst. Technol. (1939).
4. Surosky, A. E., and B. F. Dodge, *Ind. Eng. Chem.*, **42**, 1112 (1950).

Parts I and II presented at the A. I. Ch. E. Springfield meeting, Part III at the New York meeting.

CORRELATION OF DIFFUSION COEFFICIENTS IN DILUTE SOLUTIONS

C. R. WILKE and PIN CHANG

University of California, Berkeley, California

The diffusion coefficient is normally defined and assumed in this study to be the proportionality constant in the rate equation written for undirectional mass transfer as follows:

$$N_A = -D\frac{dC_A}{dz} \qquad (1)$$

Equation (1) is strictly applicable in ideal dilute solutions in which convective transport due to volume changes on mixing is negligible, and in which other possible modes of mass transfer are not operative. This paper represents an attempt to generalize the relation of D to conveniently available properties of dilute solutions so as to permit estimation of diffusion coefficients for engineering purposes.

PREVIOUS CORRELATION

In the earlier paper by Wilke (*10*) a method of correlating diffusion coefficients was proposed on the basis of qualitative conclusions of the Eyring theory (*3*) and the Stokes-Einstein relation. It was shown that the group $T/D\eta$, designated as the diffusion factor F, was essentially independent of temperature for available systems. Furthermore F could be represented as a smooth function of molal volume for diffusion of various solutes in a given solvent. In general it was assumed that this function extrapolated into the Stokes-Einstein equation at very large solute molal volumes.

DEVELOPMENT OF NEW CORRELATION

Sources of Data. At the time of the previous work so few data were available for diffusion of single solutes in a variety of solvents that the effect of solvent properties could not be brought into a general correlation. In a special effort to obtain suitable data of this kind a companion experimental study (*2*) was conducted involving the diffusion of iodine and toluene in a wide variety of hydrocarbon

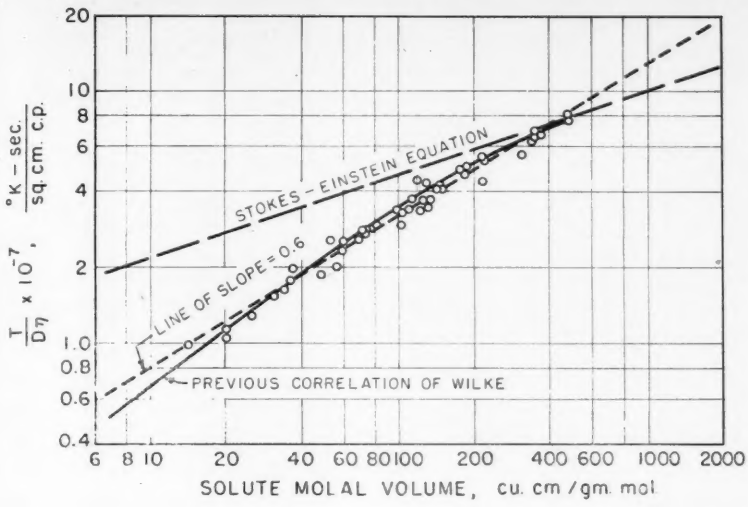

FIG. 1. DIFFUSION IN WATER.

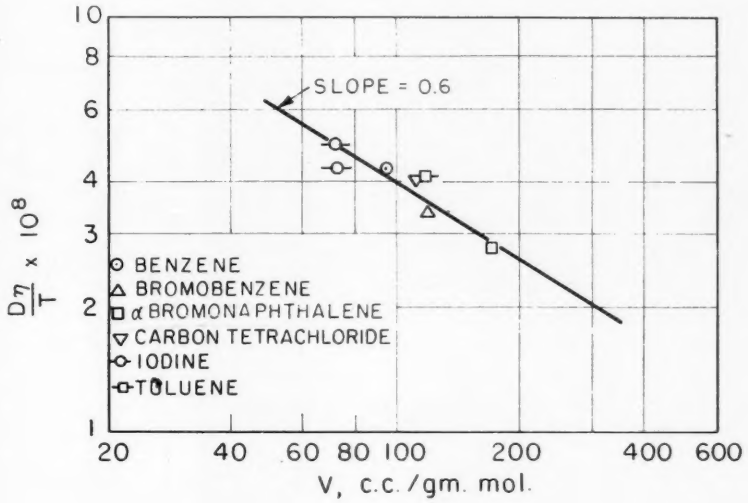

FIG. 2. DIFFUSION IN HEXANE.

solvents ranging from hexane through tetradecane. Data were also obtained for diffusion of organic acids in several solvents. These new data were supplemented by certain other data from the literature, including all the data reported in the previous paper (*10*), to provide a basis for the present development. All data which supplement those presented in Tables 2 through 5 of reference (*10*) are presented in Table 1.

Effect of Solute Molal Volume. Figure 1 shows the diffusion as a function of molal volume for various solutes in water based on data from Table 2 of reference *10*. Molal volumes used throughout this work are values at the normal boiling point estimated for complex molecules by the atomic contributions of LeBas (*1, 6*) as summarized in Table 2.

As indicated in Figure 1, F is a smooth function of molal volume having a log-log slope of about 0.7 at low molal volumes and apparently merging smoothly with the

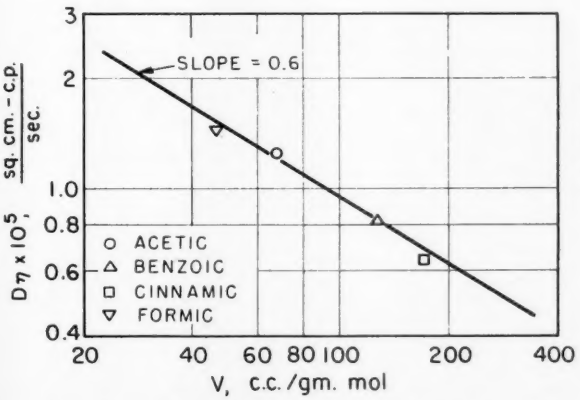

FIG. 3. DIFFUSION OF ORGANIC ACIDS IN TOLUENE.

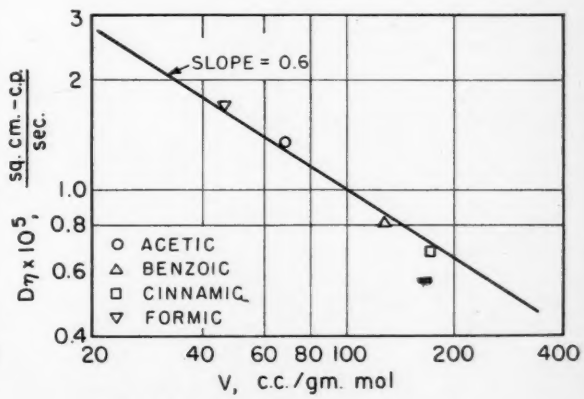

FIG. 4. DIFFUSION OF ORGANIC ACIDS IN CARBONTETRACHLORIDE.

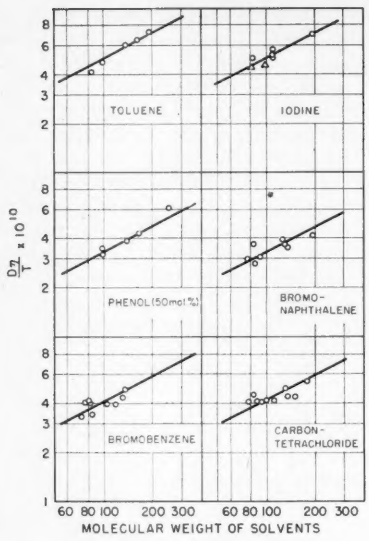

FIG. 5. EFFECT OF SOLVENT MOLECULAR WEIGHT.

Stokes-Einstein equation which requires a slope of 1/3 at high molal volumes. On the assumption that molecules are spherical with a radius equal to $(3V/4\pi N)^{1/3}$ the Stokes-Einstein equation may be written as follows:

$$\frac{T}{D\eta} = 1.004 \times 10^7 \, V^{1/3} \qquad (2)$$

Equation (2) is shown as a dotted line on Figure 1. The general behavior of the curve of Figure 1 relative to the Stokes-Einstein equation constitutes reasonable evidence in favor of the proposed method of correlation.

Over the middle range of molal volumes the curve of Figure 1 may be satisfactorily represented by a line of slope 0.6. Bearing in mind the theoretical limitations of the assumption it is convenient to assume that the diffusion factor is proportional to $V^{0.6}$ over the middle range. The proportionality of $D\eta$ to $V^{0.6}$ was used by Thakar and Othmer (*8*) in their representation of the correlation for diffusion of substances in water.

To explore the molal volume effect in nonaqueous systems several solvents were studied as shown in Figures 2 through 4. The group $D\eta/T$ may be represented satisfactorily as proportional to $V^{0.6}$. It is therefore a fair generalization that $D\eta/T$ is proportional to $V^{0.6}$ in the medium molal volume

TABLE 1.—DIFFUSION DATA FOR VARIOUS SYSTEMS

(Supplementary to Tables 2 to 5 of reference *10*)

Solute	Solvent	Temperature, °C.	$D\times10^5$ sq. cm./sec. (obs.)	$D\times10^5$ sq. cm./sec. (calc.)	Ref.
Acetic acid	Acetone	40.0	4.044	3.49	*a*
		25.0	3.309	2.85	
		15.0	2.916	2.51	
	Benzene	25.0	2.081	1.74	*a*
		5.9	1.587	1.22	
	Carbon tetrachloride	6.5	1.151	1.13	*a*
		14.8	1.267	1.32	
		25.0	1.490	1.58	
		40.0	1.780	2.04	
	Toluene	25.0	2.265	2.00	*a*
		15.0	1.905	1.72	
		6.8	1.661	1.48	
i-Amyl alcohol	Ethyl alcohol	20.0	0.78	0.85	*b*
Aniline	Ethyl alcohol	18.5	2.70	2.41	*c*
Benzene	Bromobenzene	7.5	1.02	1.20	*d*
	Chloroform	15.0	3.70	2.54	*e*
	n-Hexane	15.0	3.70	3.85	*e*
Benzoic acid	Acetone	13.2	2.368	1.66	*a*
		25.0	2.622	1.89	
		40.0	3.054	2.19	
	Benzene	15.0	1.170	0.95	*a*
		25.0	1.379	1.13	
		40.0	1.762	1.44	
	Carbon tetrachloride	14.8	0.776	0.87	*a*
		25.0	0.908	1.04	
		40.5	1.168	1.36	
	Toluene	16.0	1.289	1.16	*a*
		25.0	1.493	1.34	
		40.0	1.851	1.65	
Benzo-trichloride	Toluene	7.6	1.32	1.29	*d*
Bromobenzene	Benzene	7.3	1.41	1.29	*d*
	Cyclohexane	7.3	0.90	0.91	*d*
	m-Cymene	7.3	1.34	1.18	*d*
	Ethyl benzene	7.3	1.44	1.55	*d*
	Ethl ether	7.3	3.50	3.80	*d*
	n-Hexane	7.3	2.60	3.02	*d*
	Mesitylene	7.3	1.31	1.54	*d*
	Transdecalin	7.3	0.47	0.48	*d*
	m-Xylene	7.3	1.52	1.69	*d*
Bromform	Acetone	20.0	2.74	3.22	*f*
	Benzene	20.0	1.77	1.88	*f*
	Ethyl alcohol	20.0	0.97	0.96	*b*
Bromonaphthalene	Ethyl alcohol	20.0	0.76	0.72	*b*
a-Bromo-naphthalene	Benzene	7.3	1.04	1.05	*d*
	Cyclohexane	7.3	0.85	0.72	*d*
	Decalin	7.3	0.34	0.39	*d*
	Dibenzyl ether	7.3	0.149	0.17	*d*
	n-Hexane	7.3	2.15	2.44	*d*
	a-Methyl naphthalene	7.5	0.226	0.22	*d*
	Tetralin	7.5	0.36	0.38	
	Toluene	7.5	1.24	1.31	*d*
m-Bromotoluene	Toluene	7.4	1.52	1.48	*d*
Carbon tetrabromide	Benzene	7.3	1.12	1.27	*d*
Carbon tetrachloride	Benzene	25.0	2.00	1.87	*g*
	Carbon tetrachloride	25.0	1.41	1.74	*j*
	Cyclohexane	25.0	1.49	1.32	*g*
	Decalin	25.0	0.776	0.733	*g*
	Dioxane	25.0	1.02	1.01	*g*
	n-Heptane	25.0	3.17	3.25	*g*
	n-Hextane	25.0	3.70	3.71	*g*
	Isooctane	25.0	2.57	2.86	*g*
	Kerosene	25.0	.961	1.03	*g*
	Tetralin	25.0	0.735	.735	*g*
	Toluene	25.0	2.19	2.22	*g*
Cinnamic acid	Acetone	25.0	2.41	2.51	*a*
	Benzene	25.0	1.21	0.99	*a*
	Carbon tetrachloride	25.0	0.755	0.91	*a*
	Toluene	25.0	1.18	1.14	*a*
Ethyl benzoate	Acetone	20.0	2.47	2.29	*h*
	Benzo trichloride	20.0	0.52	0.58	*h*
	Ethyl acetate	20.0	1.85	2.01	*h*
	Nitrobenzene	20.0	0.60	0.51	*h*

Ethylene bromide	Ethylene chloride	7.3	1.11	1.31	*d*
Formic acid	Acetone	25.0	3.768	3.59	*a*
		18.5	3.274	3.12	
		6.5	3.132	2.87	
	Benzene	6.2	1.991	1.48	*a*
		13.9	2.306	1.76	
		25.0	2.577	2.14	
	Carbon tetrachloride	8.5	1.612	1.48	*a*
		25.0	1.888	2.01	
		15.0	1.673	1.67	
	Toluene	6.2	2.285	1.90	*a*
		14.1	2.463	2.32	
		25.0	2.646	2.54	
n-Heptyl bromide	Heptane	7.4	1.52	1.48	*d*
n-Hexyl bromide	Hexane	7.6	2.31	2.54	*d*
Iodine					
	Carbon tetrachloride	25.0	1.50	2.30	*i*
	Cyclohexane	15.0	1.54	1.19	*a*
	Dioxane	25.0	1.07	1.31	*i*
	Ethyl alcohol	40.0	1.772	1.72	*a*
		25.0	1.316	1.32	*a*
	Heptane	25.0	3.42	4.60	*i*
	Hexane	25.0	4.05	4.96	*i*
	n-Hexane	25.0	4.24	4.37	*a*
Iodine	Methyl cyclohexane	40.0	2.71	2.74	*i*
		30.0	2.30	2.28	*i*
	n-Octane	15.0	2.43	3.04	*a*
	n-Tetradecane	25.0	0.96	1.14	*a*
Iodobenzene	Benzene	7.3	1.35	1.31	*d*
Methyl iodide	Toluene	7.4	2.23	2.40	*d*
	Methylene chloride	7.5	2.06	2.54	*d*
Nitrobenzene	Acetone	20.0	2.94	2.83	*h*
	Ethyl benzoate	20.0	0.73	0.66	*h*
	Ethyl acetate	20.0	2.25	2.48	*h*
n-Octyl bromide	Octane	7.5	1.46	1.42	*d*
Pyridine	Ethyl alcohol	20.0	1.12	1.00	*b*
1, 2, 4, 5–Tetrachlorobenzene	Benzene	7.6	1.24	1.03	*d*
1, 2, 4–Trichlorotoluene	Benzene	7.6	1.34	1.12	*d*
Toluene	*n*-Decane	25.0	2.09	1.77	*a*
	n-Dodecane	25.0	1.38	1.19	*a*
	n-Heptane	40.0	4.33	4.08	*a*
		25.0	3.72	3.35	*a*
		6.9	2.95	2.56	*a*
	n-Hexane	25.0	4.21	4.13	*a*
	n-Tetradecane	25.0	1.02	0.86	*a*

[a]Chang, Pin, and C. R. Wilke, "Some Measurements of Diffusion in Liquids," *J. Phys. Chem.* (in press).
[b]*International Critical Tables* 5, 63-75 (1929).
[c]Muchin, G. E., and G. P. Faermann, *Z. physik. Chem.*, **121**, 180 (1926).
[d]Herzog, R. O., et al., *Z. physik. Chem.*, (A)**167**, 329 and 343 (1933).
[e]Le Monde, H., *J. phys. radium*, 7, 371-8 (1936).
[f]Oholm, L. W., *Medd. Nobelinst.*, 2, 23 (1913).
[g]Hammond, B. R., and R. H. Stokes, personal communication to J. H. Hildebrand (Sept. 21, 1954).
[h]Dummer, E., *Z. anorg. u. allgem. Chem.*, **109**, 49 (1919).
[i]Stokes, R. H., P. J. Dunlop, and J. R. Hall., *Trans. Faraday Soc.*, **49**, 886 (1953).
[j]Watts, H., B. J. Alder, and J. H. Hildebrand, *J. Phys. Chem.*, **23**, 659 (1955).

range for both aqueous and nonaqueous solvents. However, it must be recognized that special structural features of molecules and other molecular interactions may be important in certain cases and that therefore the proposed relationship is at best an oversimplification utilized to obtain a practical result.

Effect of Solvent Properties. Study of the effect of solvent properties in addition to viscosity centered on the behavior of the group $D\eta/T$ for diffusion of single solutes in a variety of solvents. A wide variety of variables such as molal volume, heat of vaporization, molecular weight, etc., were examined. Of these the solvent molecular weight appeared to correlate the data most successfully. Figure 5 shows the group $D\eta/T$ as a function of molecular weight for diffusion of given solutes in a number of solvents.

Although there is considerable scatter of the points a line of slope 1/2 on the log-log plots correlates each system moderately well. As in the case of the molal-volume effect there are obviously other factors involved so that use of solvent molecular weight is satisfactory only as a first approximation. The data of Trevoy and Drickamer (*9*) are for 0.50 mole fraction of phenol in various hydrocarbons so that the solvent molecular weight is used primarily to show the trend.

General Correlation for Unassociated Liquids. From the results of the preceding section it was concluded that an equation of the following form would express the effects of solute and solvent:

$$D = \text{const.} \frac{TM^{1/2}}{\eta V^{0.6}} \qquad (3)$$

Figure 6 shows a log-log plot of D/T vs. the group $\eta V^{0.6}/M^{1/2}$ for a wide variety of unassociated solvents embracing the data of Table 2 of this paper and Table 5 of reference *10*. The method of plotting was selected to spread the data and best illustrate the scope of the correlation. The line through the data has slope –1 as required in the assumptions of the correlation and may be expressed by the equation

$$D = 7.4 \times 10^{-8} \frac{TM^{1/2}}{\eta V^{0.6}} \qquad (4)$$

Data for 155 points among 123 different solute-solvent systems are expressed by the correlation with an average deviation of 12% between calculated and observed results.

Correlation of Associated Liquids. Associated liquids such as water and other hydrogen-bonding solvents might be expected to show deviation from the correlation of Figure 6. Figure 7 shows the plot of D/T vs. $\eta V^{0.6}/M^{1/2}$ for diffusion in water. The best line through the data falls clearly above the dotted line representing Figure 6. This deviation is in the direction corresponding to association of the solvent. By assigning a molecular weight to the solvent equal to 2.6 times the nominal molecular weight of water one can bring the data of

TABLE 2—ATOMIC VOLUMES FOR COMPLEX MOLECULES, MOLECULAR VOLUMES FOR SIMPLE SUBSTANCES

Atomic Volumes

Bromine	27.0	Nitrogen, in secondary amines	12.0
Carbon	14.8	Oxygen (except as noted below)	7.4
Chlorine	24.6	Oxygen, in methyl esters	9.1
Hydrogen	3.7	Oxygen, in methyl ethers	9.9
Iodine	37.0	Oxygen, in higher ethers and esters	11.0
Nitrogen, double bonded	15.6	Oxygen, in acids	12.0
Nitrogen, in primary amines	10.5	Sulfur	25.6

For three-membered ring, as in ethylene oxide, deduct	0.6
For four-membered ring, as in cyclobutane, deduct	8.5
For five-membered ring, as in furan, thiophene, deduct	11.5
For pyridine, deduct	15
For benzene ring, deduct	15
For naphthalene ring, deduct	30
For anthracene ring, deduct	47.5

Molecular Volumes

H_2	14.3	N_2O	36.4
O_2	25.6	NH_3	25.8
N_2	31.2	H_2O	18.9
Air	29.9	H_2S	32.9
CO	30.7	COS	51.5
CO_2	34.0	Cl_2	48.4
SO_2	44.8	Br_2	53.2
NO	23.6	I_2	71.5
D_2O*	20.0		

*Estimated value.

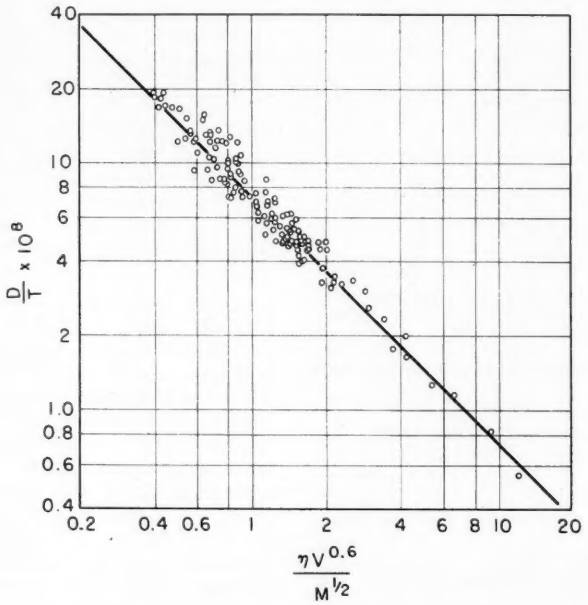

FIG. 6. DIFFUSION IN UNASSOCIATED LIQUIDS.

Figure 7 squarely onto the curve of Figure 6.

Thus the correlation for diffusion in water and also in nonassociated solvents may be expressed by the general equation

$$D = 7.4 \times 10^{-8} \frac{(xM)^{1/2}T}{\eta V^{0.6}} \quad (5)$$

The association parameter x is introduced to define the effective molecular weight of the solvent with respect to the diffusion process. For nonassociated solvents $x = 1$ and for water $x = 2.6$.

Diffusion in methyl alcohol is shown similarly in Figure 8, indicating an association parameter of 1.9, and for diffusion in ethyl alcohol, illustrated in Figure 9, x is found to be 1.5.

TABLE 3—COMPARISON OF ASSOCIATION PARAMETERS WITH ASSOCIATION NUMBERS OF JACOBSEN

Solvent	Association parameter, x	Association number*
Water	2.6	60
Methyl alcohol	1.9	3.5
Ethyl alcohol	1.5	2.7
Benzene	1.0	1.0
Ether	1.0	1.02
Heptane	1.0	1.0

*At 20°C.

It is of interest to compare the values of x with the association numbers recommended by Jacobsen (4) from intermolecular free-length relationships as given in Table 3. Although Jacobsen's association numbers are larger than the present association parameters the agreement in order of the solvents suggests that the general concept of the association effect may be valid. The results further suggest that the methods of Jacobsen might be used to select an association parameter which normally would lie between the values of 2.6 for water and 1.0 for unassociated solvents.

By use of the given association parameters the data for diffusion in water are correlated by Equation (5) with an average deviation of about 6%. Data for methyl alcohol are predicted within 11%. It should be noted that the experimental data for methyl alcohol systems are known to be of rather low precision in the original source.

DISCUSSION

General Comment. The correlation represented by Equation (5) is satisfactory for estimation of diffusion coefficients in dilute solutions with sufficient precision for most engineering purposes, i.e., about 10% average error.* It must be emphasized that the diffusion process is extremely complex and that any rigorous treatment must consider solute-solvent interaction in a more detailed manner than the present relation could possibly imply.† Although the present functional relationship of diffusion coefficient to solute molal volume rests upon some qualitative theo-

*For 285 points among 251 solute-solvent systems of this study.

†Diffusion of iodine in aromatic hydrocarbons, for example, has been excluded from the present correlation because of known complex formation.

retical foundation, the relationship to solvent molecular weight is strictly empirical. Some theoretical basis for the latter relationship or some improved correlation would be highly desirable.

Only a tenfold range of viscosity is covered by the solvents presented here. Study of the correlation and deviations from constancy of the group $D\eta/T$ over more extensive temperature and viscosity ranges is especially needed. Although deviations in constany of $D\eta/T$ have been observed and might well be expected for strongly interacting solute-solvent systems such as iodine in aromatic solvents and acetic acid in ethylene glycol, use of the group seems justified for prediction of the effect of temperature on D in absence of experimental data.

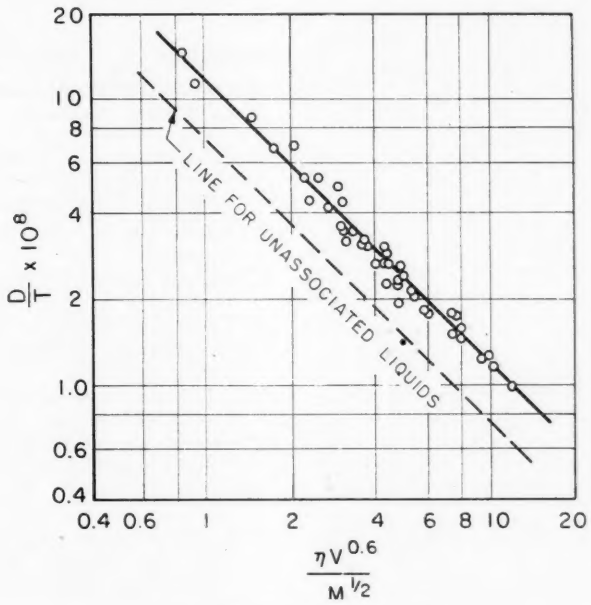

FIG. 7. DIFFUSION IN WATER.

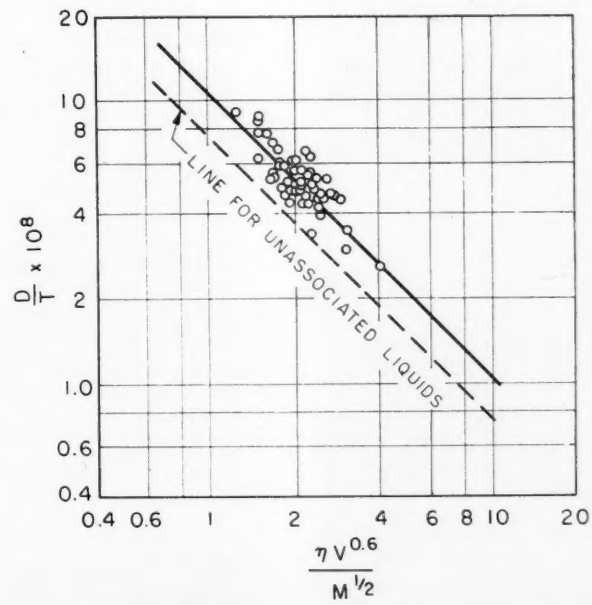

FIG. 8. DIFFUSION IN METHYL ALCOHOL.

Comparison with Other Correlations. Olson and Walton(*5*) have proposed a general form of correlation of diffusion coefficients based on surface-tension lowering of the solvent by the solute. In view of the special data required no attempt will be made to compare their method quantitatively with the present correlation.

Scheibel(*7*) has fitted the correlation of Wilke to a general equation involving the molal volumes of solute and solvent based on the curves for water, methyl alcohol, and benzene. In view of the special distinction developed above between water and methyl alcohol as associated solvents and benzene as an unassociated solvent the basic assumptions used by Scheibel are believed to be in error.

Thakar and Othmer(*8*) have proposed the following general equation developed through the reference substance method:

$$D = \frac{14 \times 10^{-5}}{\eta_s^{\circ} V^{0.6} \eta_w^{1.1} L_s/L_w} \qquad (6)$$

For diffusion in water only it was assumed that the group $D\eta^{1.1}$ fitted the temperature behavior better than did the Stokes-Einstein group $D\eta/T$. However since the ratio $[\eta^{1.1}]/[\eta/T]$ changes only 10% for water between 0° and 80°C. it is difficult to justify a choice between the two ways of representing the temperature dependence on the basis of the relatively limited data presently available.

Contrary to conclusions of the present study, for diffusion of a single solute in various solvents at 20°C. Equation (6) does not permit variation of $D\eta_s^{\circ}$ with solvent molecular weight. Application of Equation (6) to thirty-six representative systems involving diffusion of various solutes among twenty-one unassociated solvents gave rather unsatisfactory results, with an average deviation of over 30% between calculated and experimental diffusion coefficients.

CONCLUSION

It is believed that Equation (5) represents an improvement over previous correlations of diffusion coefficients in dilute solutions. Due caution of course should be observed in extending the method far beyond the range of variables and types of systems included in the present development. To facilitate use of the method a revised diffusion-factor chart is given in Figure 10 to include the association parameter and molecular weight of the solvent.

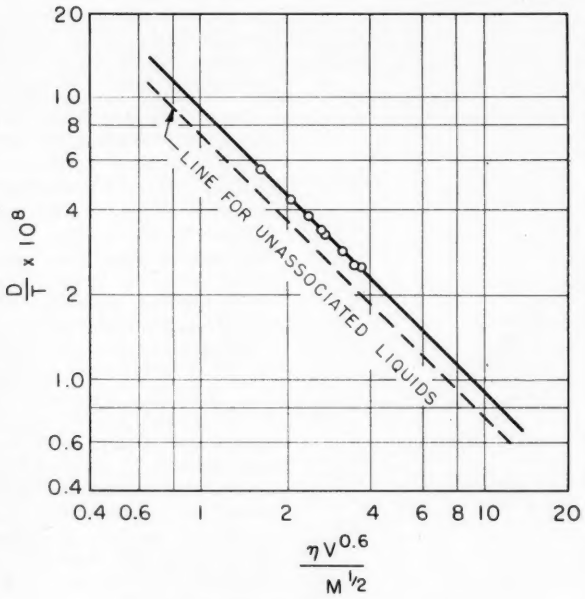

FIG. 9. DIFFUSION IN ETHYL ALCOHOL.

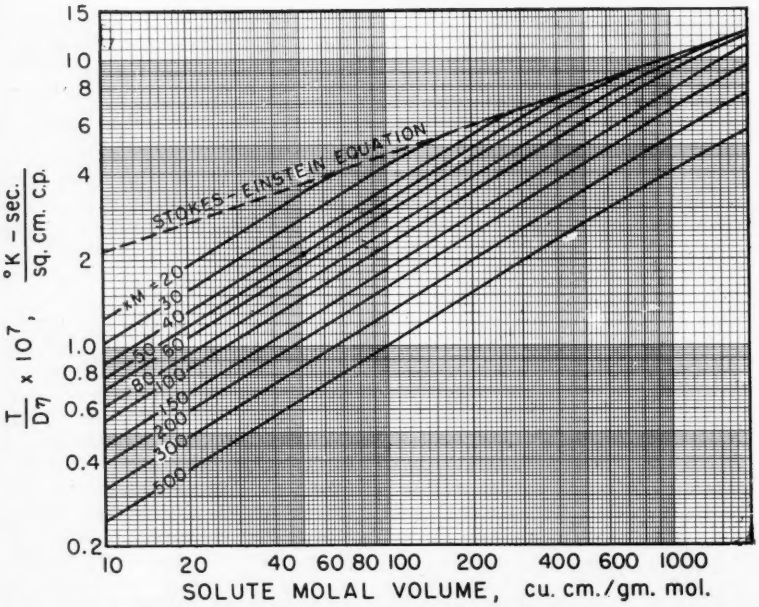

FIG. 10. GENERALIZED DIFFUSION-FACTOR CHART.

ACKNOWLEDGMENT

Assistance of Research Corporation through a grant-in-aid is gratefully acknowledged.

NOTATION

C = concentration, g. moles/cc.
D = diffusion coefficient, sq.cm./sec.
F = diffusion factor, $T/D\eta$, $\frac{(°K.)\,(sec.)}{(sq.cm.)\,(centipoise)}$
L_s = latent heat of vaporization of solvent
L_w = latent heat of vaporization of water
M = molecular weight of solvent
N = Avogadro's number, molecules per mole
N_A = diffusion rate of component A, g. moles/(sec.)(sq.cm.)
V = molal volume of solute at normal boiling point, cc./g. mole
t = temperature, °C.
T = temperature, °K.
x = association parameter, multiple of nominal molecular weight of solvent to give effective value
Z = distance in direction of diffusion
η = viscosity of solution, centipoise
η_w = viscosity of water, centipoise
η_s^o = viscosity of solvent at 20°C., centipoise

LITERATURE CITED

1. Arnold, J. H., *Ind. Eng. Chem.*, 22, 1091 (1930).
2. Chang, Pin, and C. R. Wilke, *J. Phys. Chem.* (in press).
3. Eyring, H., *J. Chem. Phys.*, 4, 283-91 (1936).
4. Jacobsen, Bertil, "Association Numbers in Liquid Systems from Intermolecular Free Length Relationships," Karolinska Institute, Stockholm (in press).
5. Olson, R. L., and J. S. Walton, *Ind. Eng. Chem.*, 43, 701 (1953).
6. Perry, J. H., "Chemical Engineers' Handbook," McGraw-Hill Book Company, Inc., New York (1950).
7. Scheibel, E. G., *Ind. Eng. Chem.*, 46, 2007 (1954).
8. Thakar, N. S., and D. F. Othmer, *Ind. Eng. Chem.*, 45, 589 (1953).
9. Trevoy, D. J., and H. G. Drickamer, *J. Chem. Phys.*, 17, 1117 (1949).
10. Wilke, C. R., *Chem. Eng. Progr.*, 45, 219 (1949).

Presented at A. I. Ch. E. New York meeting

Communications to the Editor

A Note on the Locus of the Maximum of a Distillation Line

R. M. BUTLER
Queen's University, Kingston, Ontario

In a recent paper(*1*) Lee and Kammermeyer point out that it would be desirable to derive a theoretical equation for the locus of the point of maximum concentration of the intermediate component in a distillation at total reflux for a ternary system of constant relative volatilities. The following note is a solution to this problem.

With subscripts 1, 2, and 3 referring to the components in increasing order of relative volatility, the composition in the still may be given by X_{1s}, X_{2s}, and X_{3s}. The composition of the vapor rising from the nth plate is equal to the composition of the liquid falling from the plate above and is given by Y_1, Y_2 and Y_3 in the following modified forms of Fenske's equation. In these equations the still is considered as the first plate.

$$\log Y_2 = n \log\left(\frac{\alpha_2}{\alpha_3}\right) + \log\left(\frac{X_{2s}}{X_{3s}}\right) + \log Y_3 \qquad (1)$$

$$\log Y_2 = n \log\left(\frac{\alpha_2}{\alpha_1}\right) + \log\left(\frac{X_{2s}}{X_{1s}}\right) + \log Y_1 \qquad (2)$$

Although Equations (1) and (2) have a real meaning only for integral values of n (for columns composed of theoretical plates), it is convenient for the present purpose to consider n as a continuous variable. As fractional theoretical plates frequently occur in design calculations this assumption introduces no new concept. Concentrations in a packed tower do, of course, change smoothly.

At the maximum concentration of Y_2,

$$\frac{d \log Y_2}{d n} = 0$$

Therefore when (1) and (2) are differentiated with respect to n, the still composition being constant,

$$\frac{d \log Y_3}{d n} = -\log\left(\frac{\alpha_2}{\alpha_3}\right) \qquad (3)$$

and

$$\frac{d \log Y_1}{d n} = -\log\left(\frac{\alpha_2}{\alpha_1}\right) \qquad (4)$$

If (3) is divided by (4) the result is

$$\frac{d \log Y_3}{d \log Y_1} = \frac{Y_1}{Y_3} \cdot \frac{dY_3}{dY_1} = \frac{\log(\alpha_2/\alpha_3)}{\log(\alpha_2/\alpha_1)} \qquad (5)$$

But $Y_3 + Y_2 + Y_1 = 1$

Therefore $dY_3 + dY_2 + dY_1 = 0$

at the maximum of Y_2, $dY_2 = 0$

$$\text{Therefore } \frac{dY_3}{dY_1} = -1 \qquad (6)$$

If (6) is substituted in (5) the following equation for the locus of the maximum is obtained,

$$Y_3 = \frac{\log(\alpha_2/\alpha_1)}{\log(\alpha_3/\alpha_2)} \cdot Y_1 \qquad (7)$$

As was foreseen by Lee and Kammermeyer, this is the equation of a straight line passing through the origin. Although Equation (7) represents the dotted lines drawn by Lee and Kammermeyer in their Figures 1 and 2, it is not of the same form as the empirical equation which they suggest.

LITERATURE CITED

1. Lee, Kwo-Tseng, and Karl Kammermeyer, *Chem. Eng. Progr. Symposium Series*, 49, No. 6, 99 (1953).

Commencement

Following are some of the comments received by the editor on the first issue of the Journal. Suggestions in these and other letters are much appreciated.

I have just had an opportunity to examine my copy of Vol. 1, No. 1, of the A.I.Ch.E. Journal, and I want to congratulate you on its appearing and to wish you the best of success in this new venture.

Personally, moreover, I want to felicitate you on your consistency in the application of the A.I.Ch.E. recommended system of nomenclature and abbreviations, and in general on the typographical standards exhibited throughout the pages.

THOMAS H. CHILTON
Wilmington, Delaware

Last evening I received a copy of the first issue of the A.I.Ch.E. Journal. I think it is splendid and I want to thank you and Van for an excellent job. . . .

J. H. RUSHTON
Chicago, Illinois

My hearty congratulations on the splendid first number of the A.I.Ch.E. Journal. It shows every evidence of painstaking and highly competent editorial planning and execution. In my opinion the new Journal, which has been needed for a long time, will very soon become recognized throughout the world as the leader in its field. . . .

W. B. VAN ARSDEL
Albany, California

The first issue of the A.I.Ch.E. Journal arrived this morning. Let me extend my congratulations and good wishes for the excellent job in getting together the first issue. . . .

ROBERT YORK
St. Louis, Missouri

Would you please accept my hearty congratulations for your great success in the first issue of A.I.Ch.E. Journal? I was very happy to see another excellent publication of the Institute. . . .

CHEN-JUNG HUANG
Beaumont, Texas

You and your staff are to be congratulated on the A.I.Ch.E. Journal. . . .

H. TEN BROECK
Queens Village, New York

The long-awaited debut of the A.I.Ch.E. Journal materialized in fine style. The maiden issue is certainly most impressive and I'd like to add my congratulations to you and your staff. It will certainly provide plenty of grist for any one's mill. . . .

MARCEL BOGART
New York, New York

DU MONT Multiplier Phototube REFERENCE MANUAL

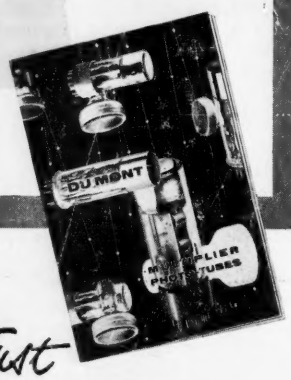

Just Available — The first comprehensive reference manual of commercially available multiplier phototubes by Du Mont.

In 64 pages, this manual gives you:

- **Design considerations**
- **Operating principles**
- **Applications**
- **Typical circuits**
- **Detailed specifications of all multiplier phototubes**

The new Du Mont multiplier phototube reference manual will be helpful not only in choosing the proper tube for a specific task, but also in obtaining the best possible results through selection of optimum operating conditions.

This manual is available by writing on your company letterhead to:

Technical Sales Department
Allen B. Du Mont Laboratories, Inc.
760 Bloomfield Avenue, Clifton, N. J.

DU MONT

BOOKS

Molecular Theory of Gases and Liquids. Joseph O. Hirschfelder, Charles F. Curtiss, and R. Byron Bird. John Wiley & Sons, Inc., New York (1954). 1219 pages. $20.

This volume, the result of studies undertaken in the Bumblebee Program of the Bureau of Ordnance, is divided into three roughly equal parts covering equilibrium properties (equation of state, vapor-liquid equilibria, surface tension), nonequilibrium or transport phenomena (viscosity, diffusion, thermal conductivity), and intermolecular forces.

The first section contains a review of equilibrium statistical mechanics and develops the equation of state in terms of the potential energy of interaction between molecules of the fluid. In principle the dependence of the potential energy of interaction on the distance between two interacting molecules and their orientation can be calculated from *a priori* quantum mechanical considerations. In practice empirical potential-energy functions containing adjustable parameters are used.

The second section is a presentation of nonequilibrium statistical mechanics and of the theory of transport phenomena. Included are hydrodynamic applications such as propagation of sound waves, detonations, and flames.

The third section is devoted to the electromagnetic and quantum mechanical theory of the forces between molecules, ions, free radicals, and atoms. The results of calculations of intermolecular forces are compared with the information obtained from bulk properties in sections one and two.

A particularly useful feature of the book is the inclusion of numerous illustrative examples giving in detail numerical examples of the calculation methods employed. Problems are given at the end of each chapter. The book concludes with about eighty pages of tables of functions required in the calculation of properties by means of potential-energy functions.

This volume will be useful and informative for the engineer who has good basic training in mathematics, physics and statistical mechanics. It will be particularly valuable in indicating logical methods for predicting properties and extrapolating, on a sound theoretical basis, into regions where no experimental data exist.

The authors are to be complimented on this work. It is a compendium of the present status of knowledge of a fundamental portion of our science.

A useful excerpt* of the work has also been published.

ERNEST SOLOMON
THE M. W. KELLOGG COMPANY

*Hirschfelder, J. O., C. F. Curtiss, and R. B. Bird, *Am. Soc. Mech. Engrs.*, **76**, 1011 (1954).

C. E. P. Monograph and Symposium Series

MONOGRAPH SERIES

(8½ by 11, paper covered)

1. **Reaction Kinetics by Olaf A. Hougen**
   (74 pages; $2.25 to members, $3.00 to nonmembers)
2. **Atomization and Spray Drying by W. R. Marshall, Jr.**
   (122 pages; $3.25 to members, $4.25 to nonmembers)

SYMPOSIUM SERIES

(8½ by 11 in., paper covered)

1. **Ultrasonics—two symposia**
   (87 pages; $2.00 to members; $2.75 to nonmembers)
2. **Phase-Equilibria—Pittsburgh and Houston**
   (138 pages; $3.75 to members, $4.75 to nonmembers)
3. **Phase-Equilibria—Minneapolis and Columbus**
   (122 pages; $3.75 to members, $4.75 to nonmembers)
4. **Reaction Kinetics and Transfer Processes**
   (125 pages; $3.75 to members, $4.75 to nonmembers)
5. **Heat Transfer—Atlantic City**
   (162 pages; $3.25 to members, $4.25 to nonmembers)
6. **Phase-Equilibria—Collected Research Papers for 1953**
   (113 pages; $3.25 to members, $4.25 to nonmembers)
7. **Applied Thermodynamics**
   (163 pages; $3.25 to members, $4.25 to nonmembers)
8. **Communications**
   (57 pages; $1.00 to members, $1.50 to nonmembers)
9. **Heat Transfer—Research Studies for 1954**
   (67 pages; $1.50 to members, $2.25 to nonmembers)
10. **Collected Research Papers—for Spring 1954**
    (142 pages; $3.25 to members, $4.25 to nonmembers)
11. **Nuclear Engineering—Part I**
    (280 pages; $3.25 to members, $4.25 to nonmembers)
12. **Nuclear Engineering—Part II**
    (250 pages; $3.25 to members, $4.25 to nonmembers)
13. **Nuclear Engineering—Part III**
    (274 pages; $3.25 to members, $4.25 to nonmembers)
14. **Ion Exchange**
    (121 pages; $3.25 to members, $4.25 to nonmembers)
15. **Mineral Engineering Techniques**
    (96 pages; $2.50 to members, $3.75 to nonmembers)
16. **Mass Transfer—Transport Properties**
    (125 pages; $3.25 to members, $4.25 to nonmembers)

Price of each volume depends on number printed. Series subscriptions, which allow a 10% discount, make possible larger runs and consequently lower prices.